Targeting cancer with small molecule pan-KRAS degraders

Johannes Popow*[,1], William Farnaby*[,2,3], Andreas Gollner*[,1], Christiane Kofink*[,1], Gerhard Fischer[1], Melanie Wurm[1], David Zollman [2,3], Andre Wijaya [2,3], Nikolai Mischerikow[1], Carina Hasenoehrl[1], Polina Prokofeva[4], Heribert Arnhof[1], Silvia Arce-Solano[1], Sammy Bell[5], Georg Boeck[1], Emelyne Diers[3], Aileen B. Frost[2,3], Jake Goodwin-Tindall[3], Jale Karolyi-Oezguer[1], Shakil Khan[2,3], Theresa Klawatsch[1], Manfred Koegl[1], Roland Kousek[1], Barbara Kratochvil[1], Katrin Kropatsch[1], Arnel A. Lauber[1], Ross McLennan [2,3], Sabine Olt[1], Daniel Peter[1], Oliver Petermann[1], Vanessa Roessler[1], Peggy Stolt-Bergner[1], Patrick Strack[1], Eva Strauss[1], Nicole Trainor[3], Vesna Vetma[2,3], Claire Whitworth[3], Siying Zhong[3], Jens Quant[1], Harald Weinstabl[1], Bernhard Kuster[4], Peter Ettmayer[#,1], Alessio Ciulli[#,2,3]

1 Boehringer Ingelheim RCV GmbH & Co KG, Dr.-Boehringer-Gasse 5-11, 1221 Vienna, Austria.

2 Centre for Targeted Protein Degradation, School of Life Sciences, University of Dundee, 1 James Lindsay Place, DD1 5JJ, Dundee, UK.

3 Division of Biological Chemistry and Drug Discovery, School of Life Sciences, James Black Centre, University of Dundee, Dow Street, DD1 5EH Dundee, Scotland, U.K.

4 Proteomics and Bioanalytics, School of Life Sciences, Technical University of Munich, 85354 Freising, Germany.

5 Boehringer Ingelheim Pharmaceuticals Inc., 900 Ridgebury Road, Ridgefield, CT 06877, USA.

* equal contribution, # corresponding authors

Abstract

Despite the high prevalence of cancers driven by KRAS mutations, to date only the G12C mutation has been clinically proven to be druggable via covalent targeting of the mutated cysteine amino acid residue[1]. However, in many cancer indications other KRAS mutations, such as G12D and -V, are far more prevalent and small molecule concepts that can address a wider variety of oncogenic KRAS alleles are in high clinical demand[2]. Here we show that a single small molecule can be used to simultaneously and potently degrade 13 out of 17 of the most prevalent oncogenic KRAS alleles, including those not yet tractable by inhibitors. Compared with inhibition, degradation of oncogenic KRAS results in more profound and sustained pathway modulation across a broad range of KRAS mutant cell lines. As a result, KRAS degraders inhibit growth of the majority of cancer cell lines driven by KRAS mutations while sparing models without genetic KRAS aberrations. Finally, we demonstrate that pharmacological degradation of oncogenic KRAS leads to tumour regression *in vivo*. Together, these findings unveil a new path towards addressing KRAS driven cancers with small molecule degraders.

Main Text

Introduction

Kirsten rat sarcoma viral oncogene homologue (KRAS) is the most commonly mutated oncogene in human cancers[3]. Variants, predominantly mutations at Glycine (G) 12 or Glutamine (Q) 61, increase the proportion of activated, GTP-loaded KRAS, enhancing RAF-MEK-ERK (MAPK) signaling and drive

tumour growth. To date, clinical advances in drugging oncogenic KRAS variants have relied on specific interactions of small molecules with the mutated amino acid residues. For example, covalent inhibitors rely on a cysteine residue available in $KRAS^{G12C}$ [1,4] while reversible inhibitors rely on interactions between basic moieties and a variant specific aspartate residue in $KRAS^{G12D}$ [5]. Indeed, beyond these variants, even pre-clinical target validation has been reliant on genetic means that lack dose, kinetic and temporal control. New concepts that can lead to single agents capable of potently and selectively addressing multiple KRAS variants stand to have major clinical impact. Recently, the first example of a KRAS inhibitor capable of engaging a broader spectrum of KRAS alleles than clinically validated inhibitors was disclosed[6].

Small molecule heterobifunctional degraders (proteolysis targeting chimeras - PROTACs) are transforming drug development for oncology, with >25 degrader drugs in clinical trials for several indications[7,8]. Early PROTACs recruiting the von Hippel-Lindau (VHL) or cereblon E3 ubiquitin ligases to $KRAS^{G12C}$ have been disclosed based on covalent KRAS binders[9,10]. However, as KRAS engagement mediated by covalent target ligands itself leads to irreversible inhibition, this approach inherently lacks key mechanistic advantages of degraders such as substoichiometric and catalytic mode of action[11]. To engage and degrade a wider range of KRAS variants beyond G12C, PROTAC degraders thus require leveraging of non-covalent KRAS binders, the discovery of which has proven inherently challenging. However, there has been recent progress in this direction, with non-covalent $KRAS^{G12D}$ degraders based on $KRAS^{G12D}$-selective inhibitors currently undergoing early clinical testing[12].

Here, we provide pre-clinical validation for a single small molecule degrader, targeting 13 of the 17 most prevalent KRAS mutants, which illuminates a new pan-KRAS degradation concept conferring potential for major clinical benefit. By employing structure-guided design we identify ACBI3, which achieves *in vivo* degradation of oncogenic KRAS, resulting in durable pathway modulation and tumour regressions in a KRAS mutant xenograft mouse model.

Identification of VHL-based KRAS Degraders Based on Non-Covalent KRAS Binders

As a starting point, we chose to use a high affinity KRAS switch II pocket ligand we have recently disclosed[6]. Analysis of co-crystal structures highlighted a solvent exposed sub-pocket formed by the amino acids His95, Glu62, and Asp92, which we deemed to be a promising position to install linkers for PROTAC design (Fig. 1a). Due to the importance of the interaction of the basic center of these substituents with the surrounding amino acids we focused our PROTAC design approach on motifs maintaining the basicity of the molecule in this region. Thorough X-ray crystallographic analysis (PDB accession code 8QUG) of the recently published BI-2865 and close analogs revealed that the homopiperazine compound **1** (dissociation constant for $KRAS^{G12V}$ by surface plasmon resonance – SPR – K_D = 25 nM, extended data table 1), provided a suitable trajectory for linker attachment (Fig. 1a). Applying an initial screening approach based on alkyl and polyethylene glycol (PEG)-based linkers in combination with VHL ligase binders based on VH032[13], we tested the resulting molecules in a biophysical screening assay based on fluorescence polarization (FP). This assay reports affinity for the VHL:EloC:EloB (VCB) complex with or without pre-incubation at saturating concentrations of $KRAS^{G12D}$. Cooperative VCB:PROTAC:$KRAS^{G12D}$ ternary complex formation is indicated by lower competitor concentrations achieving half maximal displacement (K_D) in the presence of $KRAS^{G12D}$ [14]. This highlighted compound **2** (Fig 1b) as a highly cooperative (alpha = 479, extended data table 1) and high-affinity ternary complex inducer (K_D = 7187 nM vs 15 nM in the absence or presence of $KRAS^{G12D}$, respectively) (Fig 1c, extended data table 1). We orthogonally confirmed ternary complex formation via SPR yielding a ternary complex dissociation half-life ($t_{1/2}$) of 159 s and an equilibrium dissociation constant (K_D) of 20 nM (Fig. 1d, extended data table 1). Compound **2** dose-dependently degraded $KRAS^{G12D}$ in Gp5d cells with a concentration inducing half maximal degradation (DC_{50}) at 24

h of 607 nM and a maximal extent of degradation (D_{max}) of >95 % (Figure 1e, Extended Data Fig 1a, extended data table 2). Compound **2** also degraded $KRAS^{G12V}$ in SW620 cells (DC_{50} = 1203 nM, D_{max} >95 %) indicating that KRAS degradation is not limited to $KRAS^{G12D}$ (Extended data Figure 1b, extended data table 2). To enable high throughput characterization of degraders, we set up a bioluminescence-based degradation assay in Gp5d cells expressing $KRAS^{G12D}$ with a small luminescence complementation (HiBit) tag inserted into the endogenous KRAS locus yielding comparable degradation parameters (Extended Data Fig. 1c, extended data table 2)[15]. Degradation was abolished in the presence of the NEDD8-activating enzyme inhibitor MLN4924[16] or the competing VHL ligand VH298[17] (Extended Data Figure 1d) supporting that KRAS degradation by compound **2** depends on intracellular recruitment of an active VHL ligase complex. We also detected direct KRAS ubiquitination and intracellular formation of ternary complexes by bioluminescence resonance energy transfer (BRET) based assays (Extended Data Fig. 1e and f). The cellular target engagement assays, comparing the ability of compound **2** to engage VHL in either permeabilised or live cells (IC_{50} values 5 µM and >10 µM, respectively) indicated the need to further optimise cellular permeability as well as VHL affinity (Figure 1f).

Having established compound **2** as a VHL-based KRAS degrader, we went on to synthesise a molecular matched pair, replacing the oxygen atom in the linker by a methylene group yielding compound **3** (Fig. 1b). Compound **3** still displayed positive cooperativity and long-lived ternary complex half-life (alpha = 17, K_D = 340 nM by FP, K_D = 80 nM and $t_{1/2}$ = 103 s by SPR, Fig 1c, Extended Data Fig. 1g, extended data table 1) albeit reduced compared to compound **2**. Degradation potency improved by greater than ten-fold for $KRAS^{G12D}$ (GP5d, DC_{50} = 32 nM, D_{max} = 99 %) (Fig 1e, extended data table 2) and $KRAS^{G12V}$ (SW-620, DC_{50} = 278 nM, D_{max} = 88 %) (Extended Data Fig. 1b, extended data table 2). Cellular target engagement assays, comparing the ability of compound **2** and compound **3** to engage VHL in either permeabilised or live cells showed that both improved cellular permeability as well as VHL affinity likely contributed to the superior degradation potency of compound **3** (Fig. 1f). Selective targeting of KRAS while sparing H- and NRAS has been linked to the therapeutic window of the KRAS ligand we based our design upon[6]. We therefore tested selectivity of degradation by targeted proteomics in the cell line NCI-H358. While we detected degradation of both $KRAS^{G12C}$ (D_{max} ≥ 54 %) and $KRAS^{WT}$ (D_{max} ≥ 86 %), which represents roughly one third of the KRAS pool in this cell line, we detected no significant change in H- or NRAS levels (Fig. 1g, Extended Data Figure 1h). Given that compound **3** has a poorer efficiency of degradation for $KRAS^{G12C}$ as opposed to WT (Fig. 1g), we were motivated to investigate if further improving ternary complex stability and intracellular VHL engagement could broaden the range of KRAS mutants we could potently degrade.

To understand the binding mode and enable structure-based optimization, we determined the ternary co-crystal structure of compound **3** in complex with VCB and $KRAS^{G12V}$ at 2.2 Å resolution (Fig. 1h) (PDB 8QW6). Compound **3** adopts a “fishhook” conformation, burying the VHL binder section of compound **3** in a de novo binding interface formed between $KRAS^{G12V}$ and VHL. The crystal structure contains two molecules of ternary complex in the asymmetric unit, revealing a consistent binding mode (RMSD = 0.54 Å), but a different fingerprint of protein-protein and protein-ligand interactions. This indicates that there is subtle flexibility within the compound **3** ternary complex, allowing the complex to shift between nearby networks of favourable protein-protein interactions. Together, the data establishes compound **3** as a KRAS degrader prototype based on a non-covalent target ligand amenable to structure-based optimization.

Identification of Pan-KRAS Degraders

Extending ternary complex stability (increased $t_{1/2}$) has been shown to improve rate and potency of target protein degradation[18-20] . Analysis of the VCB:compound **3**:KRAS^{G12V} co-crystal structure (Fig. 1h) highlighted an opportunity to enhance interactions within the ternary complex by improving π-stacking between the exit vector amide of the VHL ligand and Tyr112. We therefore switched the amide for an isoxazole, which has been previously reported to improve VCB affinity in this position in other contexts[21], yielding compound **4** (Figure 2a). A ternary complex co-crystal structure of VCB:compound **4:**KRAS^{G12V} (PDB 8QW7) confirmed a consistent overall binding mode to that observed for compound **3** (RMSD = 0.72 Å), with compound **4** able to engage in π-stacking interaction between the isoxazole and Tyr112 of VCB as designed (Figure 2b). As with compound **3**, the compound **4** ternary complex revealed different networks of induced protein-protein interactions within the two ternary molecules in the asymmetric unit, indicating complex flexibility. FP, SPR and cellular target engagement studies support a minor improvement in binary VHL engagement for compound **4**, with moderate cooperativity retained (Extended data figure 2a-c, extended data table 1). A larger shift in durability of ternary complex can be observed via SPR for compound **4** ($t_{1/2}$ = 230 s, extended data table 1) vs compound **3** ($t_{1/2}$ = 103 s, extended data table 1) vs. We then investigated the impact of these structural changes on degradation kinetics in live HiBit-tagged Gp5d cells (Extended Data Figure 3a-d). While maximal degradation rates (λ_{max}) did not vary significantly between compound **3** and compound **4** (approximately 0.5 h^{-1} for both compounds, extended data table 2), the concentration inducing the half maximal cellular degradation rate ($Dmax_{50}$) was three-fold lower for compound **4** ($Dmax_{50}$ = 56 nM for compound **3** vs $Dmax_{50}$ = 17 nM for compound **4**) (Fig 2c, extended data table 2). The improved $Dmax_{50}$ for compound **4** translated into drastically improved cellular degradation potencies of compound **4** vs compound **3** for endogenous KRAS^{G12D} (GP5d, DC_{50} = 1 nM, D_{max} = 99.5 %, extended data table 1) and KRAS^{G12V} (SW-620, DC_{50} = 13 nM, D_{max} = 89 %) (Figure 2d, Extended Data Figure 3e).

To gauge KRAS mutation specificity on a broader basis without contribution of potentially confounding factors, we established an isogenic series of cell lines transduced with retroviral constructs expressing the most prevalent KRAS mutants fused to a HiBit-tag in GP5d cells. Dose titration revealed that compound **4** efficiently degraded 13 of the 17 most prevalent KRAS mutant alleles and KRAS^{WT} with single digit nanomolar potency (Fig 2e). KRAS mutants with a more complete loss of GTPase activity, such as KRAS^{G12R} (DC_{50} = 45 nM, D_{max} = 59 %) and -Q61L/K/R (DC_{50} > 470 nM D_{max} < 60%), were degraded less potently, consistent with the relative binary binding affinity to these KRAS mutants of the ligand class employed in this study[6]. Together, these data are consistent with degradation of KRAS mutants with residual GTPase activity by engagement of the inactive, GDP-bound state. Compound **3** was associated with a similar degradation spectrum albeit with reduced potency for all degradable mutants suggesting that the optimised potency of compound **4** vs compound **3** affected a broad spectrum of KRAS alleles (Fig. 2f). We went on to assess the cellular selectivity of compound **4**-induced KRAS degradation by unbiased MS-proteomics in GP2d cells, using compound **5**, a VHL binding deficient stereoisomer of compound **4** as a negative control. KRAS was the only detected protein showing > 2-fold depletion (p < 0.01) (Fig 2g). Similar results were obtained in KRAS^{G12C} mutant MiaPaCa-2 cells using another VHL binding deficient isomer, compound **6** as a degradation deficient control (Extended Data Figure 3f). Together, these data establish compound **4** as a highly selective KRAS degrader acting on a broad spectrum of KRAS mutants with high prevalence in cancer patients.

KRAS Degradation Potently Suppresses Oncogenic Signaling and Proliferation.

We confirmed degradation of KRAS by compound **4** in KRAS-dependent (GP2d, SW620 and NCI-H358 expressing $KRAS^{G12D}$, -G12V or -G12C, respectively) as well as in KRAS independent (A-375, HEK293) cell lines (Fig. 3a, Extended Data Figure 4a). To compare degradation vs inhibition of KRAS, we also profiled compound **5** (VHL-binding deficient stereoisomer) which has the same overall chemical formula and close-to-identical physicochemical properties and engages KRAS non-covalently without inducing KRAS degradation Fig. 3a, Extended Data Figure 4a. Alongside, we also profiled the covalent inhibitor of $KRAS^{G12C}$ Sotorasib[22] or the non-covalent $KRAS^{G12D}$ inhibitor MRTX-1133[23] as appropriate (Fig. 3a, Extended Data Figure 4a). Both inhibition and degradation repressed the established markers of MAPK signaling pERK (Extended Data Figure 4b-d) and DUSP6 (Fig. 3b, Extended Data Figure 4e) in KRAS dependent cell lines. Both KRAS independent cell lines did not exhibit suppression of pERK or DUSP6 exceeding 50 % of control (Fig. 3b, Extended Data Figure 4b-e). Compound **4** was > 10-fold more potent in suppressing MAPK signalling in KRAS dependent cell lines compared to its VHL binding deficient stereoisomer compound **5** indicating that E3 ligase engagement and subsequent target degradation as compared to inhibition results in more potent pathway engagement (Fig. 3b, Extended data Figure 4b-e, extended data table 2). In the KRAS-dependent cell lines MAPK pathway engagement coincided with prominent inhibition of proliferation, with VHL engagement conferring a greater than 10-fold potency gain (Fig. 3c, Extended Data Figure 4f, extended data table 2). Neither degradation nor inhibition had appreciable anti-proliferative effects in the KRAS independent cell lines A-375 and HEK293 (Fig. 3c, Extended Data Figure 4f). Comparable results albeit with lower potency were obtained for compound **3** (Extended Data Figure 5, extended data table 2).

Pharmacological degradation of a target can result in target resynthesis dependent pathway engagement[24]. To test whether this applies to our KRAS degraders, we pre-treated $KRAS^{G12D}$-dependent GP2d cells with compound **4** to achieve maximal KRAS degradation or the inactive stereoisomer compound **5** at the identical concentration and 10-fold excess to achieve comparable pathway inhibition by non-covalent engagement of KRAS. After pre-incubation, the medium was exchanged to wash out compound **4** or its inactive stereoisomer and replaced by culture medium containing VH298 to compete against VHL binding of any residual compound **4**. Upon washout, $KRAS^{G12D}$ levels recovered in a time-dependent fashion in cells pre-treated with compound **4** (Fig. 3d). Both pERK and DUSP6 rapidly recovered after washout of the inactive stereoisomer compound **5** reaching control levels after 2-4 h even though the 10-fold excess of compound **5** achieved pERK and DUSP6 suppression comparable to the compound **4** pre-incubation. In contrast, cells pre-treated with compound **4** exhibited long lasting MAPK pathway suppression consistent with the delayed recovery of $KRAS^{G12D}$ after washout (Fig. 3d). Hence, KRAS degradation results in long-lasting MAPK pathway suppression with delayed recovery compared to non-covalent KRAS inhibition upon compound withdrawal. We also tested the ability of compound **4** to suppress proliferation on a wider scale in a cell line panel comprising 300 cell lines harboring a range of KRAS mutations and covering a wide range of cancer indications (Fig. 3e). Cell lines bearing KRAS mutants had lower concentrations required for half-maximal proliferation inhibition (IC_{50}) as compared to WT cell lines (geometric mean IC_{50} = 739 nM vs 4934 nM, respectively) (Extended Data Figure 4g). To characterise the effects of pan-KRAS degradation more globally on the molecular level, we performed a time-resolved (phospho-)proteomic analysis of NCI-H358 and GP2d cells in response to compound **4** or its VHL-binding deficient isomer compound **5** at the concentration of compound **4** achieving maximal degradation in each cell line (Extended Data Figure 6a). The results recapitulated KRAS (but not HRAS) degradation in both models (Extended Data Figure 6b and c), and quantification of ~20000 phosphorylation sites allowed for the comprehensive characterization of affected phosphorylation

events (Extended Data Figure 6d). Phosphorylation events detected in all treatments revealed a pronounced overlap for both compounds in either cell line, with several cell line-specific differences (Fig. 3f). While both compound **4** and compound **5** engaged the MAPK pathway, compound **4** modulated phosphorylation events detected in all treatments with greater effect size than compound **5** (Fig. 3f, Extended Data Figure 6e). Only a few phosphorylation events displayed more pronounced modulation by compound **5** as compared to compound **4** (Fig. 3f, Extended Data Figure 6e). Gene ontology enrichment analysis demonstrated reduced activity of multiple pathways, including the cell cycle, in response to compound **4** but not compound **5** (Fig. 3g, Extended Data Figure 6f and g). Hence, both inhibition and degradation of KRAS modulate largely overlapping sets of phosphorylation events albeit with distinct effect size and potency. Taken together, as compared to target inhibition achieved by compounds with comparable molecular properties, KRAS degradation enables greater than 10-fold higher potency paired with extended and more pronounced suppression of MAPK signaling.

In Vivo KRAS Degradation leads to regressions in KRAS mutant tumour-bearing mice.

Next, we wished to understand possible advantages of KRAS degradation *in vivo,* such as extending pharmacodynamic (PD) efficacy beyond the detectable pharmacokinetic (PK) presence of a degrader[24]. Pharmacokinetic profiling of compound **4** suggested insufficient exposure irrespective of the route of administration. Plasma concentrations achieved via intravenous (*i.v.*) or sub-cutaneous (*s.c.*) dosing did not cover the predicted *in vivo* DC_{50} (Fig4a extended data table 3 and 4). The latter was estimated using potency of degradation of HiBit-labeled $KRAS^{G12D}$ in assays with fetal calf serum (FCS) substituted by serum of NMRI mice or human serum. Whereas the degradation potency of compound **4** was comparable in FCS and human serum (DC_{50} = 1.4 and 1.9 nM, respectively), we noted a 24-fold potency drop in presence of 10 % mouse serum (DC_{50} = 33 nM) (Figure 4b). This yields a predicted *in vivo* DC_{50} of 851 nM for the GP2d model in NMRI mice (vs 3.6 nM in FCS) (extended data table 2).

Seeking to achieve *in vivo* active concentrations and to maintain the productive elements of ternary complex molecular recognition observed in compounds **3** and **4**, we swapped the isoxazole for a triazole and introduced a hydroxymethyl group at the benzylic position of the VHL binder to obtain compound **7,** herein referred to as ACBI3 (Fig 4c). While slightly improving solubility (4 µg/mL vs < 1 µg/mL at pH 4.5, extended data table 4) SPR, FP and intracellular nano-BRET studies revealed remarkable VHL engagement for ACBI3, with a biophysical half-life of its binary complex with VHL of > 2000 s (Extended Data Figure 7a, extended data table 1). Aiming to measure ternary complex stability, we noted that the FP assay reached the limits of quantification due to ternary K_D approaching that of the assay probe, however, by SPR, ternary complex K_D was quantifiable and 4-fold improved vs compound **4** (6 nM for ACBI3 vs 26 nM for compound **4**) (Extended Data Figure 7a, b and c, extended data table 1). Single particle cryo electron microscopic analysis of the $KRAS^{G12V}$:ACBI3:VCB:Cul2:Rbx1 complex revealed significant flexibility throughout the entire complex (Fig 4d), likely necessary for successful ubiquitin transfer. While high-resolution modelling of ACBI3 binding was limited by a high flexibility of KRAS, we clearly observed the density of the VHL-ligand, as well as the connecting density of the linker (Extended Data Figure 7d-f). Overlay with a 2.2 Å resolution ternary co-crystal structure of $KRAS^{G12V}$:ACBI3:VCB (PDB 8QVU) supports the same overall binding architecture via both techniques (Fig 4d, Extended Data Figure 7g). Details of the PROTAC binding site in the X-ray structure were resolved revealing a flexible binding mode overall consistent with those of compound **3** and compound **4** (Extended Data Figure 7h). ACBI3 maintains the triazole-Tyr112 π-stack as observed with the isoxazole of compound **4**, while being able to pick up an additional H-bond interaction between the newly incorporated benzylic hydroxy group and Gln99 in

$KRAS^{G12V}$ (Extended Data Figure 7h). Multiple strong protein-protein interactions were apparent in the crystal structure which differed between protomers, indicating that, as with compound **3** and compound **4,** ACBI3 ternary complexes can dynamically transition between different H-bond networks between VHL and $KRAS^{G12V}$.

ACBI3 exhibited potent intracellular VHL engagement, ternary complex formation and ubiquitination translating into overall E3-ligase dependent cellular degradation potency comparable to compound **4** (Extended Data Figure 8a-g, extended data table 2). Similarly, kinetic degradation parameters of ACBI3 and KRAS allele degradation specificity were comparable to compound **4** (Extended Data Figure 8h-l, extended data table 2). Testing the anti-proliferative activity in a 240 cancer cell line panel revealed that ACBI3 was broadly active on cancer cell lines bearing KRAS mutations vs KRAS WT cell lines (geometric mean IC_{50} = 478 nM vs 8.3 µM, respectively) (Extended Data Figure 8m). Similar to compound **4**, ACBI3 exhibited high efflux in the Caco-2 assay (extended data table 4). Reasoning that high efflux may result in compromised cellular activity in KRAS mutant cell lines with high expression of known drug transporters, we also tested the activity of ACBI3 in cell lines in presence of the ABCB1 inhibitor Zosuquidar[25]. While inhibition of drug efflux resulted in a 1000-fold shift in antiproliferative potency in individual cell lines with high ABCB1 expression such as LS513 (Fig 4e), the overall sensitivity pattern in the 240 cell line panel was comparable in the presence or absence of Zosuquidar (Extended Data Figure 8m and n). On a global scale, we observed an average 5-fold shift in potency attributable to efflux transporter expression in KRAS mutant cell lines (Extended Data Figure 8o). We conclude that, in addition to compromising oral bioavailability, ABCB1-mediated efflux creates the need for compensation by higher doses of ACBI3 in ABCB1 expressing tumours.

We formulated ACBI3, which lacks oral bioavailability, in PEG-400 / Transcutol / Kolliphor HS 15[26] to enable multiple *s.c.* daily dosing studies with a delayed absorption profile. *S.c.* administration of 30 mg/kg ACBI3 in this formulation resulted in a plasma concentration-time-profile (Fig. 4f) covering the *in vivo* DC_{50} of 281 nM—predicted based on degradation potency shift assays (Fig. 4g) and the degradation potency of ACBI3 in GP2d cells in 10 % FCS (DC_{50} = 3.9 nM) (extended data table 2)—for around 6 h.

Administering ACBI3 to GP2d tumour bearing mice, we observed degradation of $KRAS^{G12D}$ (44 % of untreated controls) in tumours consistent with exposures covering the DC_{50} for at least 6 h *in vivo* (Fig 4 h and i). While exposures varied 5-fold between the 6 and 24 h timepoints (Fig 4h), $KRAS^{G12D}$ levels did not recover to a notable extent consistent with extending the pharmacodynamic efficacy beyond the pharmacokinetic presence of ACBI3 at concentrations covering the predicted *in vivo* DC_{50}. In an anti-tumour efficacy study in GP2d tumour bearing mice, 30 mg/kg ACBI3 dosed daily *s.c.* for up to 14 days resulted in pronounced tumour regressions (Fig 4j) with a tumour growth inhibition of 127 % and a significant difference of control vs. treatment group ($p < 0.0001$). This demonstrates that the PROTAC mediated suppression of oncogenic KRAS observed *in vitro* translates into *in vivo* regressions in KRAS mutant tumour bearing mice. Pleasingly, we also noted no impact on body weight (extended data fig 8p) suggesting selective degradation of KRAS is systemically tolerated in mice. Together these data provide first pre-clinical therapeutic proof-of-concept for pan-KRAS degradation.

Conclusion

Activating mutations in KRAS are prevalent in patients suffering from solid tumours with unmet medical need. For example, 35 % of lung, 45 % of colorectal, and up to 90 % of pancreatic cancers are associated with KRAS mutations[2]. This amounts to an incidence of approximately 150000 new

cases in the United States for these three tumour types[27]. An inherent challenge to targeting KRAS with small molecules is the wide range of mutations leading to oncogenic activation. This in turn creates a challenge to identify small molecules that can broadly address the different mutations with potencies and exposures required for clinical efficacy. Despite intense research investment over decades, so far only allele specific inhibitors have been approved and the need for potent KRAS targeting concepts with broad mutation coverage remains high.

Here, we establish degradation of a broad spectrum of oncogenic KRAS variants with a single agent achieving deep and long-lasting suppression of oncogenic signaling *in vitro* and *in vivo*. ACBI3 is a selective, potent and *in vivo* active pan-KRAS degrader discovered via a structure-based design approach guided by optimisation of VHL:PROTAC:KRAS ternary complex stability and durability. This optimisation allowed us to achieve a degrader that effectively acts on the majority of KRAS mutants with high prevalence in cancer patients, and as a result potently inhibit proliferation in KRAS mutant cell lines covering a wide range of tumour types. KRAS degradation via ubiquitin ligase recruitment enables a greater than 10-fold higher potency compared to target inhibition and results in prolonged suppression of MAPK signaling. ACBI3 is a first example of a single agent capable of targeting simultaneously a major share of highly prevalent oncogenic KRAS variants. We also establish that ACBI3 suppresses oncogenic KRAS protein levels in vivo beyond its pharmacokinetic presence, ultimately resulting in tumour regression. ACBI3 illustrates many key features specific to degraders made of reversible target binders, such as catalytic mode of action independent of occupancy driven pharmacology. This more broadly suggests fundamental advantages for targeting a spectrum of chemically heterogenous disease-relevant protein variants by targeted protein degradation. We anticipate that pan-KRAS degradation will deliver a new path to address a broad sweep of malignancies with high unmet medical need.

Figure Legends

Fig 1 | Identification of reversible, KRAS selective degraders – a, Exit vector explored to derivatise KRAS-binders. Three-dimensional crystal structure of KRAS displayed in brown, compound **1** in green. PDB Accession code 8QUG. **b,** Chemical structures of compound **2** and -**3**. **c,** VCB FP displacement for compounds **2** and -**3** in presence or absence of saturating $KRAS^{G12D}$ concentrations (*N*=3, SD). **d,** SPR characterization of TC for VCB, $KRAS^{G12D}$:GDP and compound **2** (*N*=3, representative trace). **e,** Dose-dependent degradation of $KRAS^{G12D}$ in GP5d cells (24 h, *N*=3, SD). **f,** VHL target engagement by nanoBRET in live or permeabilised HEK293 cells for compounds **2** and -**3** (*N*=3, SD). **g,** Degradation time course of total KRAS, $KRAS^{WT}$, $KRAS^{G12C}$, H- and NRAS by 1 µM compound **3** in NCI-H358 cells (*N*=3, SD) by targeted proteomics. **h,** ternary complex co-crystal structure of VCB: compound **3**:$KRAS^{G12V}$.

Fig 2 | Targeting of all major oncogenic KRAS alleles and sustained pathway engagement with rapid degraders – a, Chemical structures of compound **4** and inactive degrader controls compound **5** (*(S)*-hydroxyproline derivative compound **4**) and **-6** (*(S)*-isopropyl). **b**, Left: superposition of TC structures of compound **3** (red):VCB (light blue):$KRAS^{G12V}$ (wheat), and compound **4** (white):VCB (teal):$KRAS^{G12V}$ (yellow) displaying conserved ternary binding orientations (RMSD = 0.72 Å). Right: views from the compound **4** ternary complex PROTAC binding sites (molecules A and B) displaying side chains of residues involved in potential strong protein:protein interactions (blue dotted lines) and Fo-Fc omit map contoured to 3 σ for compound **4**. **c,** Concentration dependency of degradation rates for compound **3** and compound **4** in Hibit-tagged Gp5d cells (*N*=6, mean±95%CI). **d,** Dose-dependent degradation of $KRAS^{G12D}$ and $KRAS^{G12V}$ in GP5d and SW260 cells, respectively (24 h, *N*=3, SD). **e,** Degradation of retrovirally transduced HiBit-tagged indicated KRAS mutants by compound **4**

(18 h, *N*=3) or **f,** compound **3** in GP5d cells (24 h, *N*=2). **g,** Whole cell proteomics MS analysis of Gp2d cells treated with 50 nM compound **4** or inactive stereoisomer compound **5** (8 h, *N*=3).

Fig 3 | Pan-KRAS degradation impacts MAPK signaling and cancer cell proliferation – a, KRAS degradation (6 and 24 h, *N*=2, range), **b,** DUSP6 modulation (6 h, *N*=3, SD), **c,** proliferation (5 days, *N*=3, SD) for compound **4**, compound **5** and MRTX1133 in $KRAS^{G12D}$ and KRAS-independent $BRAF^{V600E}$ cell lines, respectively. **d,** $KRAS^{G12D}$, pERK and DUSP6 recovery after washout and VHL competition after pre-treatment with compound **4** and compound **5** (*N*=3, SD). **e,** Proliferation inhibition data for 300 cancer cell lines by compound **4** bars represent IC_{50} per cell line(5 days, *N* =3). **f,** Heat map of phosphorylation events upon treatment with compound **4** or compound **5** in NCI-H358 ($KRAS^{G12C}$, 500 nM) and GP2d ($KRAS^{G12D}$, 100 nM) cells (8 h, *N*=3). **g,** Volcano plots of combined gene set enrichment analyses of phospho-proteome changes induced by compound **4** (upper panel) or compound **5** (lower panel) in NCI-H358 and GP2d cells at 8 h.

Fig 4 | *In vivo* efficacy associated with degradation of $KRAS^{G12D}$– a, Pharmacokinetic profile of compound **4** in mice upon *i.v.* or *s.c.* dosing (*N*=3, geometric mean and geometric SD). **b,** Degradation of HiBit-$KRAS^{G12D}$ (24 h, *N*=4, SD) by compound **4** in GP5d cells in presence of 10 % fetal calf, mouse or human serum. **c,** Chemical structure of ACBI3. **d,** Cryo-EM structure of the KRAS:ACBI3:VCB:Cul2:Rbx1 heptameric complex, major motions indicated as red arrows (Cul2 breathing, KRAS rocking and Rbx1 twisting), expected positions of the E2-ligase and ubiquitin added schematically in dotted ellipses. **e,** Proliferation of ACBI3 in LS513 cells in presence and absence of 2.5 µM Zosuquidar (5 days, *N*=3). **f,** Pharmacokinetic profile of ACBI3 in mice upon *i.v.* or *s.c.* dosing (*N*=3, geometric mean and geometric SD). **g,** Degradation of HiBit-$KRAS^{G12D}$ (24 h, *N*=4, SD) in GP5d cells in presence of 10 % fetal calf-, mouse- or human serum. **h,** *in vivo* degradation of $KRAS^{G12D}$ upon *s.c. q.d.x3* dosing of 30 mg/kg ACBI3. (N=*5*, mean and SD). **i,** ACBI3 plasma levels in subcutaneous GP2d tumour bearing mice dosed with 30 mg/kg ACBI3 *q.d.x3* (*N*=5, geometric mean and geometric SD). **j,** *In vivo* efficacy of ACBI3 in a GP2d xenograft model (*N*=10, mean and SD).

Extended Data Fig 1 | Validation of initial KRAS degraders – a, KRAS and GAPDH levels by Western blot of GP5d cells treated with compounds **2** or -**3** (24 h), numbers indicate normalised KRAS levels vs controls (*N*=3). **b,** Dose-dependent degradation of $KRAS^{G12V}$ in SW620 cells (24 h, *N*=3, SD). **c,** Dose-dependent degradation of Hibit-$KRAS^{G12D}$ in GP5d cells for compounds **2** and -**3** (24 h, *N*=3, SD). **d,** $KRAS^{G12D}$ levels in GP5d cells treated with compound **2** in presence or absence of MLN4924 or VH298 by capillary electrophoresis (24 h, *N*=3, SD). **e,** Detection of compound **2** and -**3** induced ternary complex formation for $KRAS^{G12D}$ in Gp5d cells (4 h, *N*=3, SD). **f,** $KRAS^{G12D}$ ubiquitination in Gp5d cells treated with compounds **2** or -**3** (4 h, *N*=3, SD). **g,** SPR characterization of ternary complex for VCB, $KRAS^{G12D}$:GDP and compound **3**. **h,** Data as in Figure 1g with protein abundance stated as molecules per cell.

Extended data Fig 2 | Ternary complex kinetics of compound 4 – a, VCB FP displacement for compound **4** in presence or absence of saturating $KRAS^{G12D}$ concentrations (*N*=3, SD). **b,** VHL target engagement by nanoBRET in live or permeabilised HEK293 cells for compound **4** (*N*=3, SD). **c,** SPR characterization of ternary complex for VCB, $KRAS^{G12D}$:GDP and compound **4**. **d,** KRAS and GAPDH levels by Western blot of GP5d cells treated with compound **4** (24 h), numbers indicate normalised KRAS levels vs. controls (*N*=3). **e,** KRAS levels in GP5d cells treated with compound **4** in presence or absence of MLN4924 or VH298 by Western blot (24 h), numbers indicate normalised KRAS levels vs controls (*N*=3).

Extended data Fig 3 | Degradation kinetics of KRAS degraders compound 2, -3 and -4 – a, Live cell degradation time course of Hibit-$KRAS^{G12D}$ in presence of varying concentrations of compound **2**, **b,**

compound **3** and **c,** compound **4**. **d,** Degradation rate vs concentration for compound **2** (*N*=6, 95%CI). **e,** Degradation of $KRAS^{G12D}$ by compound **4** in Hibit-tagged Gp5d cells. **f,** Whole cell proteomics MS analysis of Mia-PaCa-2 cells treated with 300 nM compound **4** or inactive stereoisomer compound **6** (8 h, *N*=3).

Extended data Fig 4 | Extended characterization of pan-KRAS degradation on MAPK signaling and cancer cell proliferation – a, KRAS degradation (6 and 24 h, N=2, range), **b,** pERK modulation (6 h, *N*=2, range) for compound **4**, compound **5**, MRTX1133 or sotorasib in $KRAS^{G12V}$, $KRAS^{G12C}$ and $KRAS^{WT}$ cell lines, respectively. **c,** pERK modulation (6 h, *N*=2, range) for compound **4**, compound **5** and MRTX1133 in GP2d cells and **d,** A375 cells. **e**, DUSP6 modulation (6 h, *N*=3, SD), **f,** proliferation (5 days, *N*=3, SD) for compound **4**, compound **5**, MRTX1133 or sotorasib in $KRAS^{G12V}$, $KRAS^{G12C}$ and $KRAS^{WT}$ cell lines, respectively. **g,** proliferation (5 days) for compound **4** in 300 cell line panel, analysis by KRAS mutation status (geometric mean, SD).

Extended data Fig 5 | KRAS degradation and inhibition of MAPK pathway and cancer cell proliferation by compound 5 – a, KRAS degradation (6 and 24 h, *N*=2, range), **b,** pERK modulation (6 h, *N*=2, range), **c,** DUSP6 modulation (6 h, *N*=3, SD) **d,** proliferation (5 days, *N*=3, SD) for compound **3** in $KRAS^{G12D}$, -V and –C and -WT cell lines, respectively.

Extended data Fig 6 | Phospho-proteomics characterization of KRAS degradation vs -inhibition – a, Experimental design for the time-course analysis of the proteome and phospho-proteome of NCI-H358 ($KRAS^{G12C}$) and GP2d ($KRAS^{G12D}$) cells in response to compound **4** or compound **5** (500 nM for NCI-H358, 100 nM for GP2d). **b,** Time course of changes in KRAS protein abundance. **c,** Time course of changes in individual peptides representing KRAS and HRAS in cell lines treated with compound **4**. **d,** Number of identified and regulated phosphorylation sites across treatments, categorization of up- or down-regulation of phosphorylation by unsupervised K-means clustering and filtering for the effect size of all identified phospho-sites. **e,** Heatmap of the regulated phospho-proteome after 24 h of compound treatment. **f,** Time-resolved changes in Tyr15 phosphorylation of CDK1/2/3. **g,** Volcano plot of gene set enrichment analysis phospho-proteomes downregulated by compound **4** (left) or compound **5** (right) at 24h (data for both cell lines combined).

Extended data Fig 7 | Biophysical and structural characterization of ACBI3 ternary complexes – a, Single-cycle kinetics of interactions between ACBI3 and VCB by SPR in presence of saturating $KRAS^{G12D}$:GDP concentrations. **b,** Single-cycle kinetics of interactions between ACBI3 and VCB by SPR. **c,** VHL FP displacement for ACBI3 in presence or absence of saturating $KRAS^{G12D}$ concentrations. **d,** Experimental density of the KRAS:ACBI3:VCB:Cul2:Rbx1:complex by cryo EM. **e,** 2D-classes obtained by cryoEM. **f,** Interface between KRAS (sand) and VHL (blue) formed by ACBI3 (red). Shown is cryoEM-density on top of a cartoon representation, with ACBI3 as stick-model. **g,** Overlay of the ACBI3 complex structures determined by cryo-EM (sand/orange/blue) – and X-ray-crystallography (grey). Alignment was performed on VHL. **h,** Left: superposition of ternary crystal structures of ACBI3 (red):VCB (light blue):$KRAS^{G12V}$ (wheat), and compound **4** (white):VCB (teal):$KRAS^{G12V}$ (yellow) displaying conserved ternary binding orientations (RMSD = 1.21 Å). Right: Views of the ACBI3 ternary complex PROTAC binding sites (molecules A and B) displaying side chains of residues involved in potential strong protein:protein interactions (blue dotted lines), Fo-Fc omit map contoured to 3 σ for ACBI3.

Extended data Fig 8 | Extended cellular profiling of ACBI3 – a, VHL engagement by nanoBRET in live or permeabilised HEK293 cells for ACBI3 (*N*=3, SD). **b,** Detection of VCB:ACBI3:$KRAS^{G12D}$ complexes in Gp5d cells (4 h, *N*=3, SD, one-way ANOVA, Dunnet correction). **c,** $KRAS^{G12D}$ ubiquitination in Gp5d cells treated with ACBI3 (4 h, *N*=3, SD, one-way ANOVA, Dunnet correction). **d,** KRAS and GAPDH

levels by Western blot of Gp5d cells treated with ACBI3 or **e,** inactive stereoisomer compound **8** (24 h), numbers indicate normalised KRAS levels vs controls (*N*=3). **f,** KRAS levels in GP5d cells treated with ACBI3 in presence or absence of MLN4924 or VH298 by Western blot (24 h), numbers indicate normalised KRAS levels vs controls (*N*=3). **g,** Degradation of $KRAS^{G12D}$ or $KRAS^{G12V}$ in GP5d, GP2d or SW620 cells by ACBI3, respectively (24h – 18 h for GP2d, *N*=3, SD). **h,** Live cell degradation time course of Hibit-$KRAS^{G12D}$ in presence of varying concentrations of ACBI3 (*N*=6). **i,** Degradation rate by live cell degradation vs concentration for ACBI3 (mean and 95% CI). **j,** Degradation timecourse of endogenous $KRAS^{G12D}$ in GP2d cells at varying concentrations of ACBI3 by capillary electrophoresis (*N*=3). **k,** Degradation rate for endogenous $KRAS^{G12D}$ vs concentration for ACBI3 (mean and 95% CI). **l,** Degradation of indicated retrovirally transduced HiBit-KRAS mutants by ACBI3 (24 h, *N*=3). **m,** Proliferation inhibition data for 240 cancer cell lines for ACBI3, bars represent IC_{50} per cell line (5 days, *N*=3). **n,** Proliferation inhibition data for 240 cancer cell lines for ACBI3 in presence of 2.5 µM Zosuquidar, bars represent IC_{50} per cell line (5 days, *N*=3). **o,** Cumulative proliferation data for ACBI3 in 240 cell line panel in presence or absence of 2.5 µM Zosuquidar for $KRAS^{WT}$ vs KRAS mutant cell lines (geometric mean, geometric SD). **p,** Effect of ACBI3 or vehicle treatment on body weight of GP2d tumour bearing mice (*N*=10, mean and SD).

Fig. 1

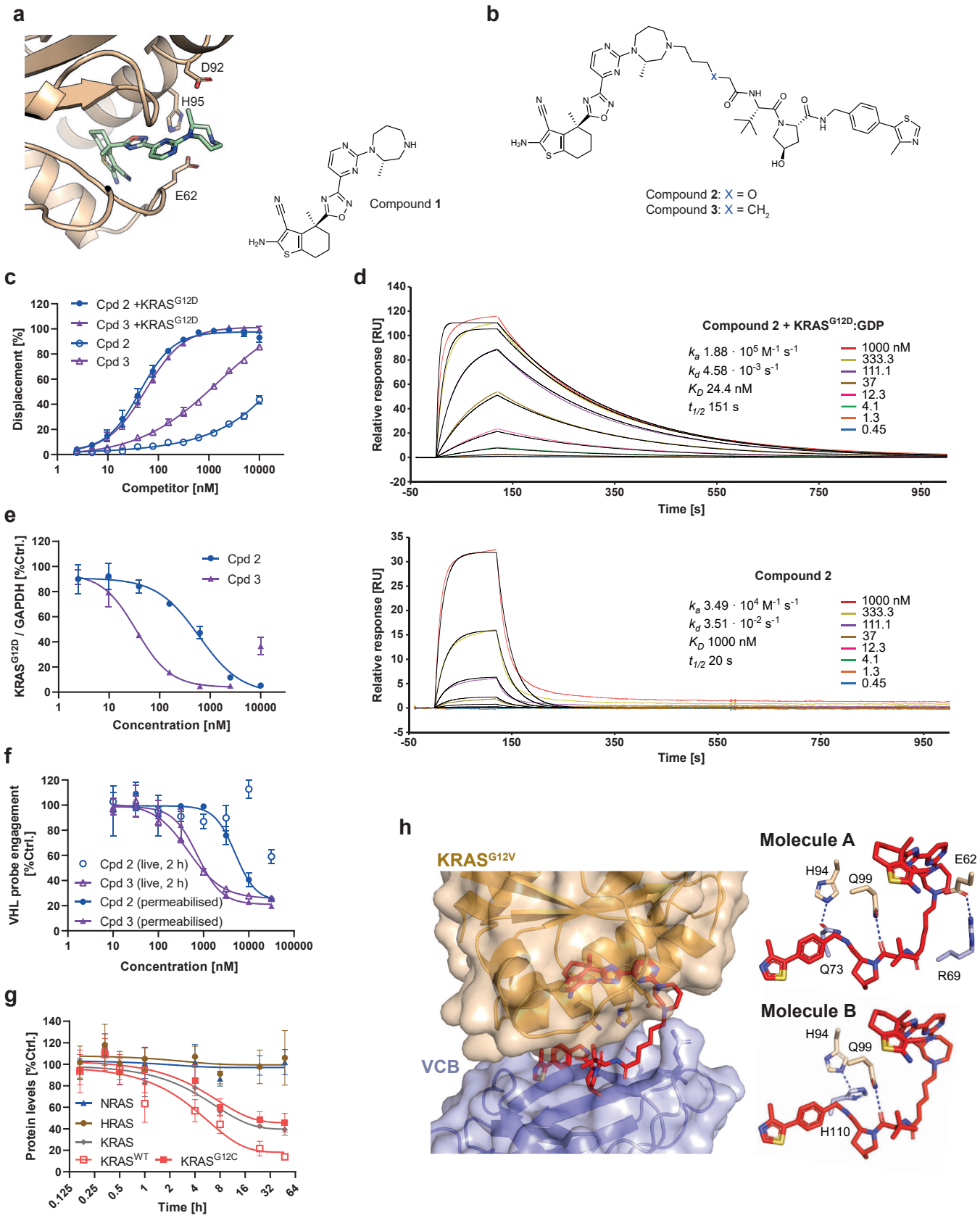
a
D92
H95
E62
Compound 1
b
Compound 2: X = O
Compound 3: X = CH2
c
Cpd 2 +KRASG12D
Cpd 3 +KRASG12D
Cpd 2
Cpd 3
Displacement [%]
Competitor [nM]
d
Compound 2 + KRASG12D:GDP
ka 1.88 · 10^5 M^-1 s^-1
kd 4.58 · 10^-3 s^-1
KD 24.4 nM
t1/2 151 s
1000 nM
333.3
111.1
37
12.3
4.1
1.3
0.45
Relative response [RU]
Time [s]
Compound 2
ka 3.49 · 10^4 M^-1 s^-1
kd 3.51 · 10^-2 s^-1
KD 1000 nM
t1/2 20 s
e
KRASG12D / GAPDH [%Ctrl.]
Concentration [nM]
f
VHL probe engagement [%Ctrl.]
Cpd 2 (live, 2 h)
Cpd 3 (live, 2 h)
Cpd 2 (permeabilised)
Cpd 3 (permeabilised)
g
Protein levels [%Ctrl.]
NRAS
HRAS
KRAS
KRASWT
KRASG12C
Time [h]
h
KRASG12V
VCB
Molecule A
H94
Q99
E62
Q73
R69
Molecule B
H110

Fig. 2

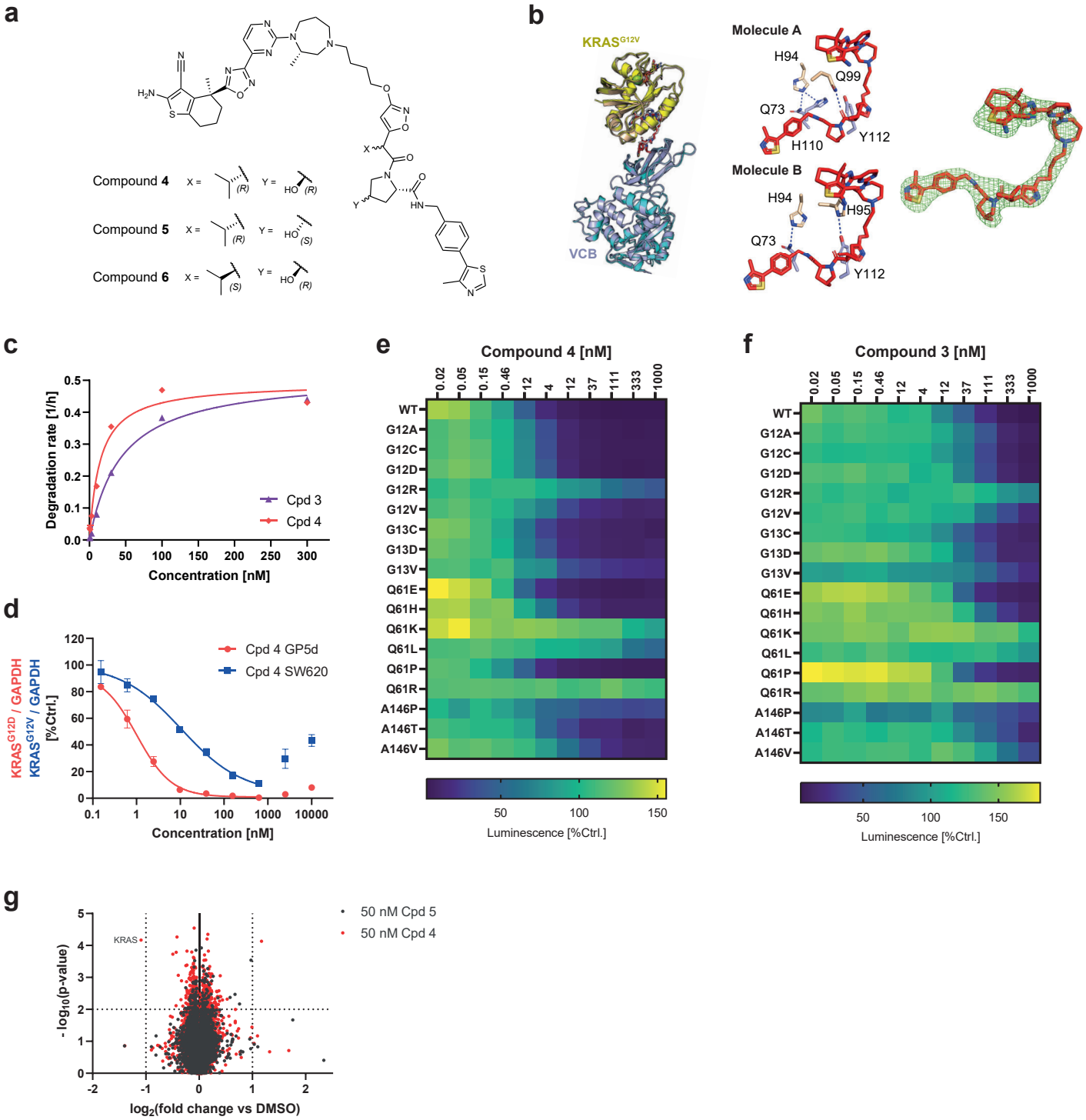
a
Compound 4
Compound 5
Compound 6
b
KRASG12V
VCB
Molecule A
H94
Q99
Q73
H110
Y112
Molecule B
H94
H95
Q73
Y112
c
Degradation rate [1/h]
Concentration [nM]
Cpd 3
Cpd 4
d
KRASG12D / GAPDH
KRASG12V / GAPDH
[%Ctrl.]
Cpd 4 GP5d
Cpd 4 SW620
Concentration [nM]
e
Compound 4 [nM]
0.02
0.05
0.15
0.46
12
4
12
37
111
333
1000
WT
G12A
G12C
G12D
G12R
G12V
G13C
G13D
G13V
Q61E
Q61H
Q61K
Q61L
Q61P
Q61R
A146P
A146T
A146V
Luminescence [%Ctrl.]
f
Compound 3 [nM]
Luminescence [%Ctrl.]
g
KRAS
50 nM Cpd 5
50 nM Cpd 4
- log10(p-value)
log2(fold change vs DMSO)

Figure 3

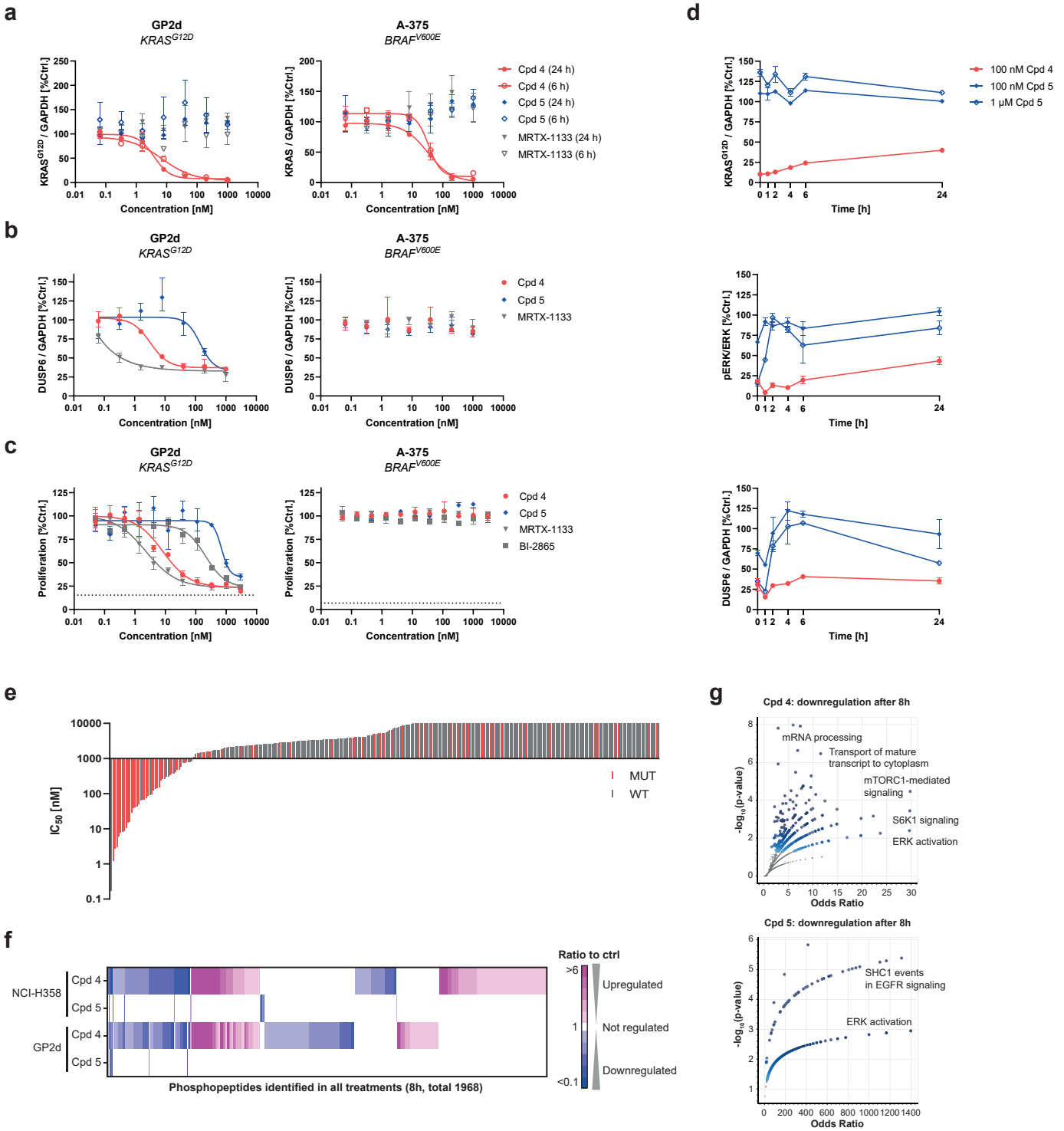
a
GP2d
KRASG12D
A-375
BRAFV600E
KRASG12D / GAPDH [%Ctrl.]
KRAS / GAPDH [%Ctrl.]
Concentration [nM]
Cpd 4 (24 h)
Cpd 4 (6 h)
Cpd 5 (24 h)
Cpd 5 (6 h)
MRTX-1133 (24 h)
MRTX-1133 (6 h)
b
DUSP6 / GAPDH [%Ctrl.]
Cpd 4
Cpd 5
MRTX-1133
c
Proliferation [%Ctrl.]
BI-2865
d
100 nM Cpd 4
100 nM Cpd 5
1 µM Cpd 5
Time [h]
pERK/ERK [%Ctrl.]
e
IC50 [nM]
MUT
WT
f
NCI-H358
GP2d
Cpd 4
Cpd 5
Phosphopeptides identified in all treatments (8h, total 1968)
Ratio to ctrl
>6
Upregulated
1
Not regulated
<0.1
Downregulated
g
Cpd 4: downregulation after 8h
mRNA processing
Transport of mature transcript to cytoplasm
mTORC1-mediated signaling
S6K1 signaling
ERK activation
-log10(p-value)
Odds Ratio
Cpd 5: downregulation after 8h
SHC1 events in EGFR signaling
ERK activation

Figure 4

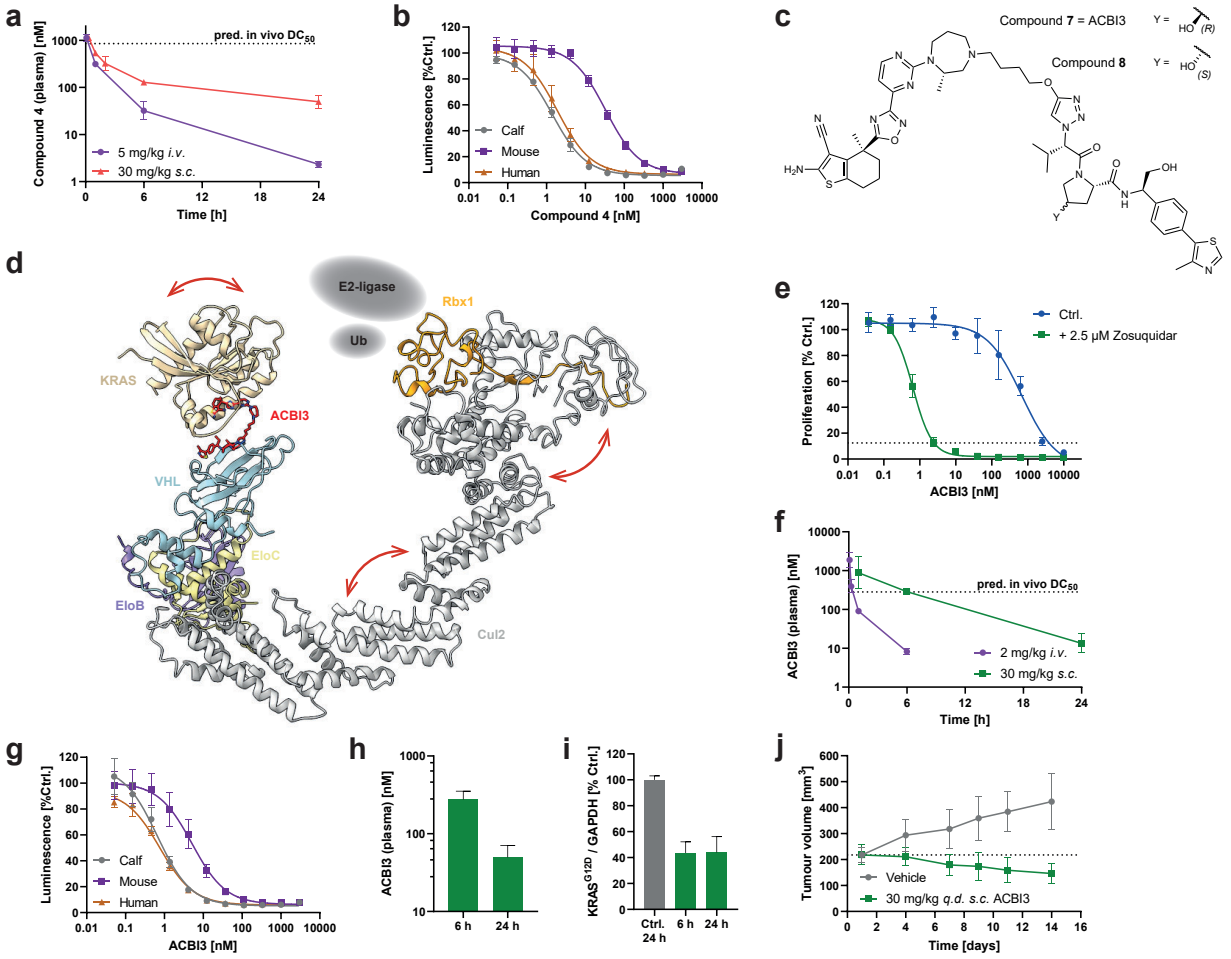
a
Compound 4 (plasma) [nM]
pred. in vivo DC50
5 mg/kg i.v.
30 mg/kg s.c.
Time [h]
b
Luminescence [%Ctrl.]
Calf
Mouse
Human
Compound 4 [nM]
c
Compound 7 = ACBI3
Compound 8
d
E2-ligase
Ub
Rbx1
KRAS
ACBI3
VHL
EloC
EloB
Cul2
e
Proliferation [% Ctrl.]
Ctrl.
+ 2.5 µM Zosuquidar
ACBI3 [nM]
f
ACBI3 (plasma) [nM]
pred. in vivo DC50
2 mg/kg i.v.
30 mg/kg s.c.
Time [h]
g
Luminescence [%Ctrl.]
Calf
Mouse
Human
ACBI3 [nM]
h
ACBI3 (plasma) [nM]
6 h
24 h
i
KRASG12D / GAPDH [% Ctrl.]
Ctrl. 24 h
6 h
24 h
j
Tumour volume [mm3]
Vehicle
30 mg/kg q.d. s.c. ACBI3
Time [days]

Extended Data Figure 1

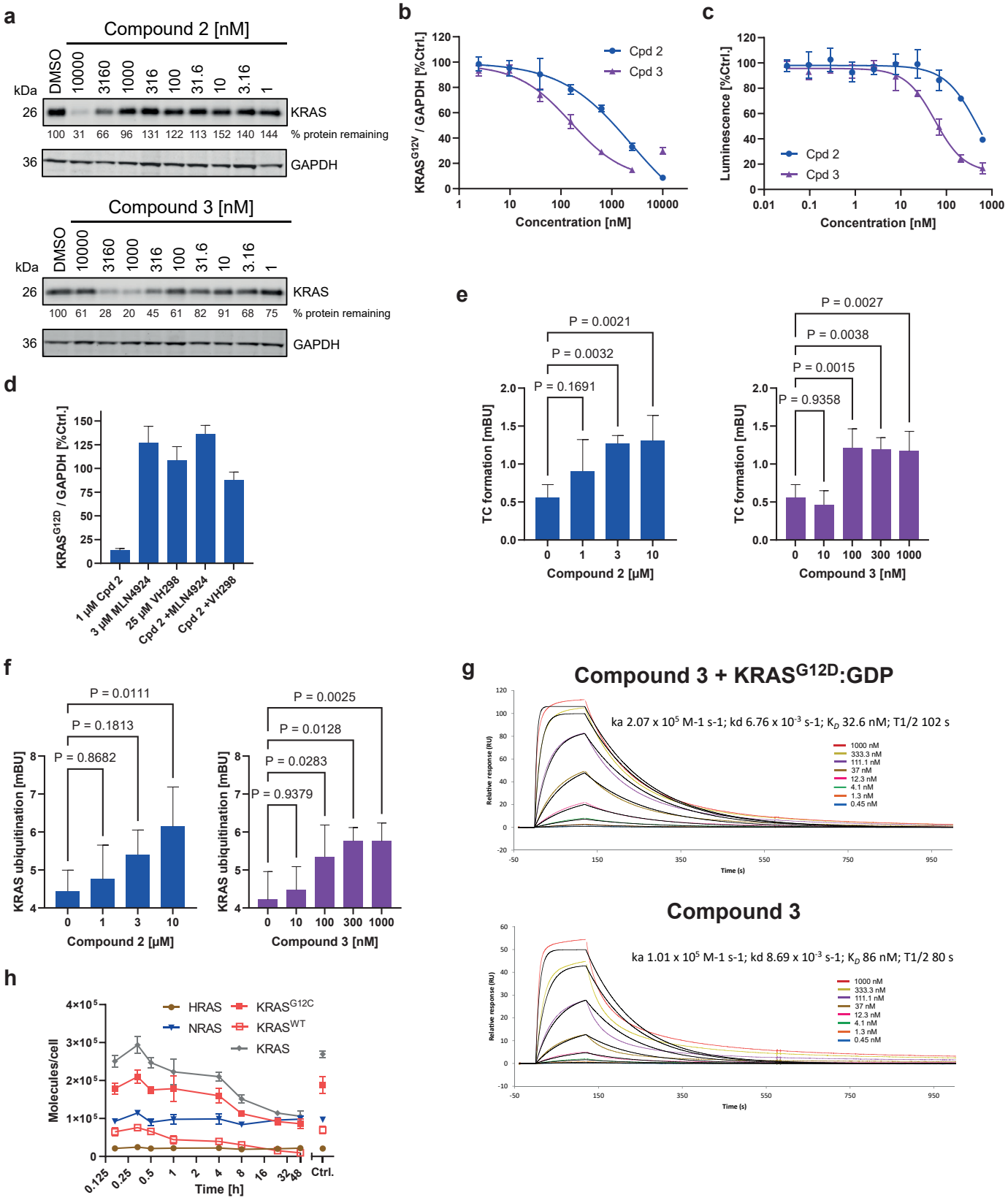

Extended Data Figure 2

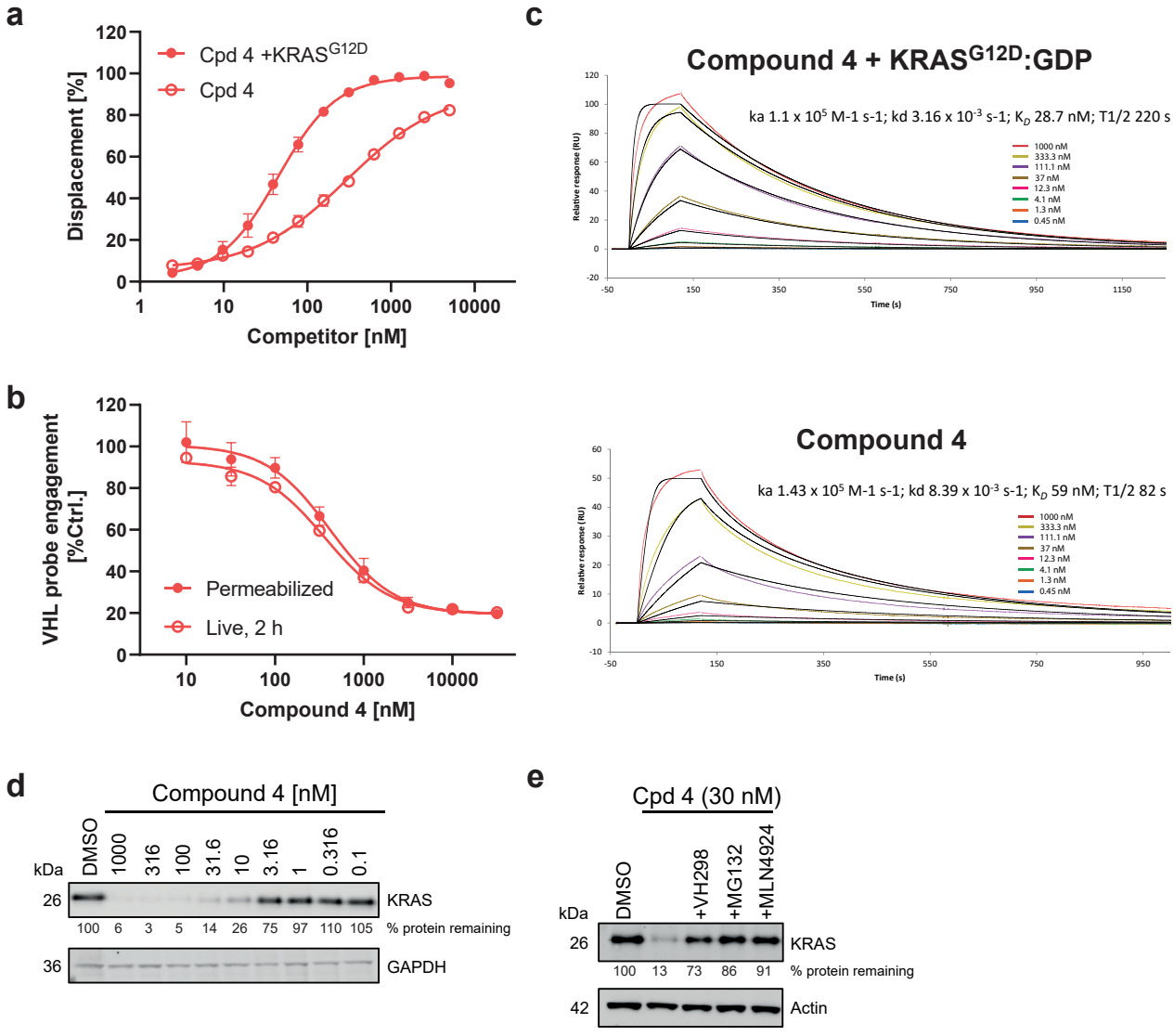

Extended Data Figure 3

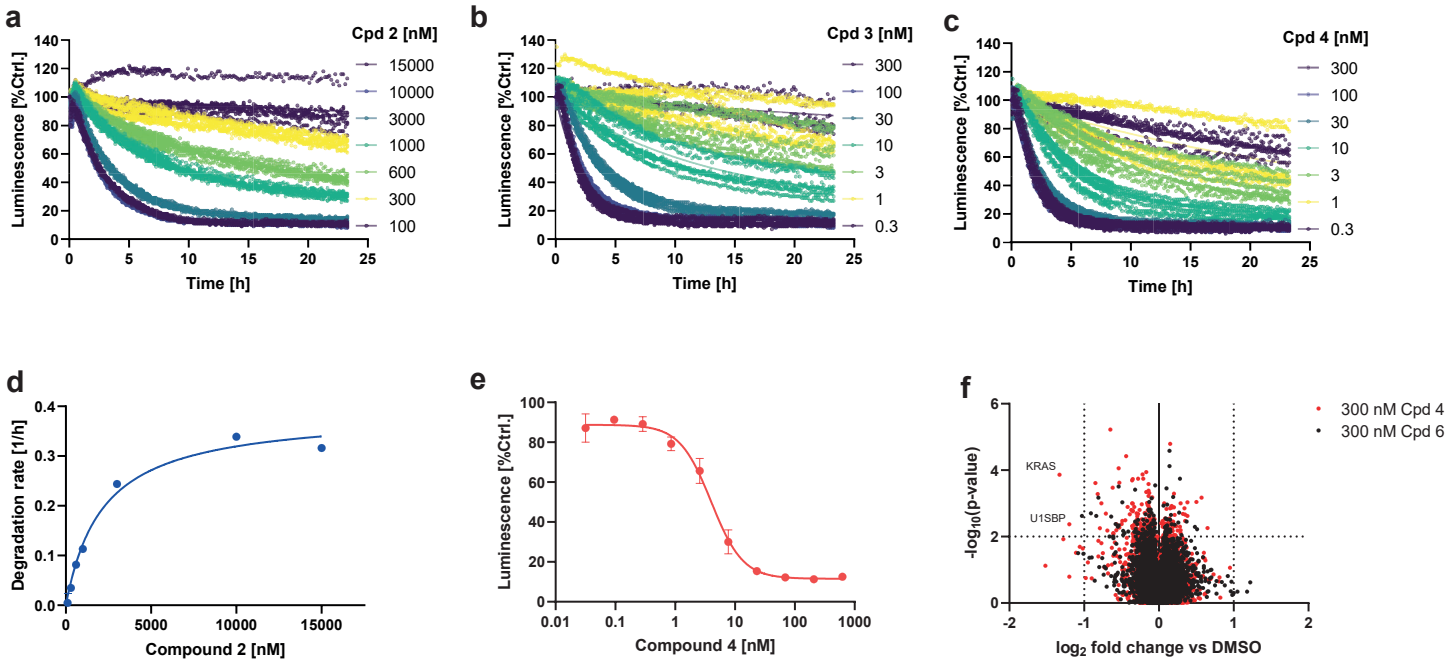

Extended Data Figure 4

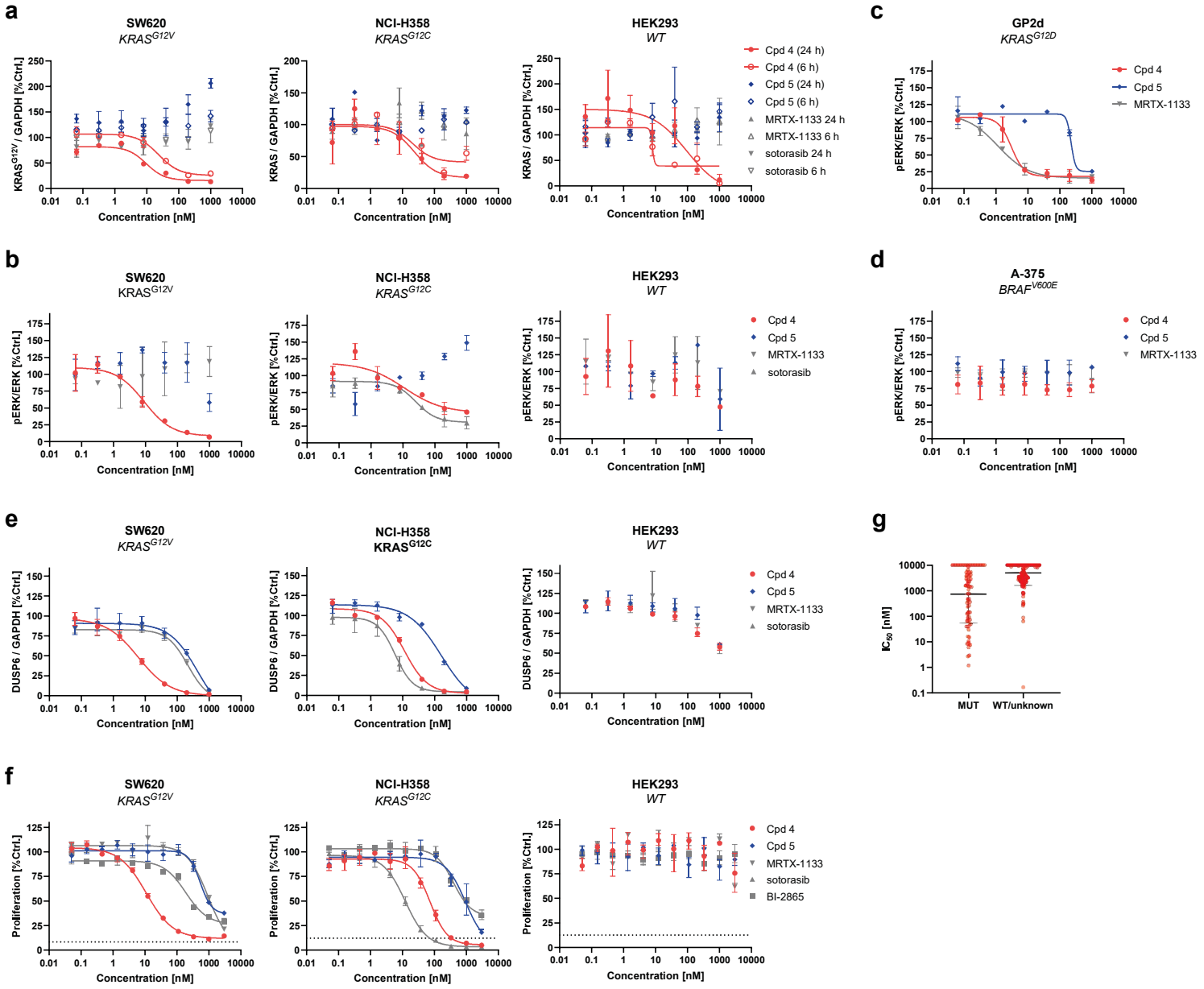

Extended Data Figure 5

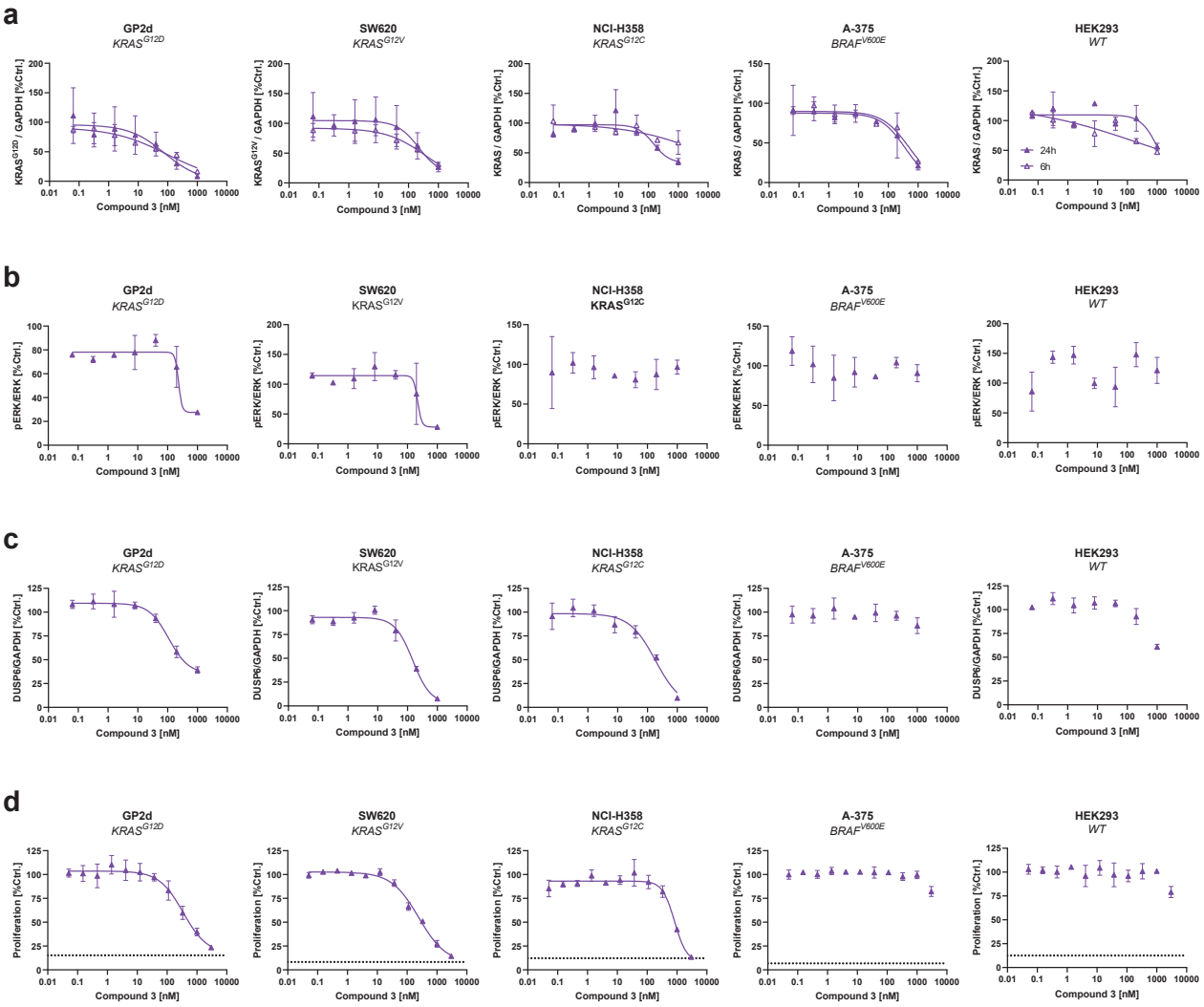

Extended Data Figure 6

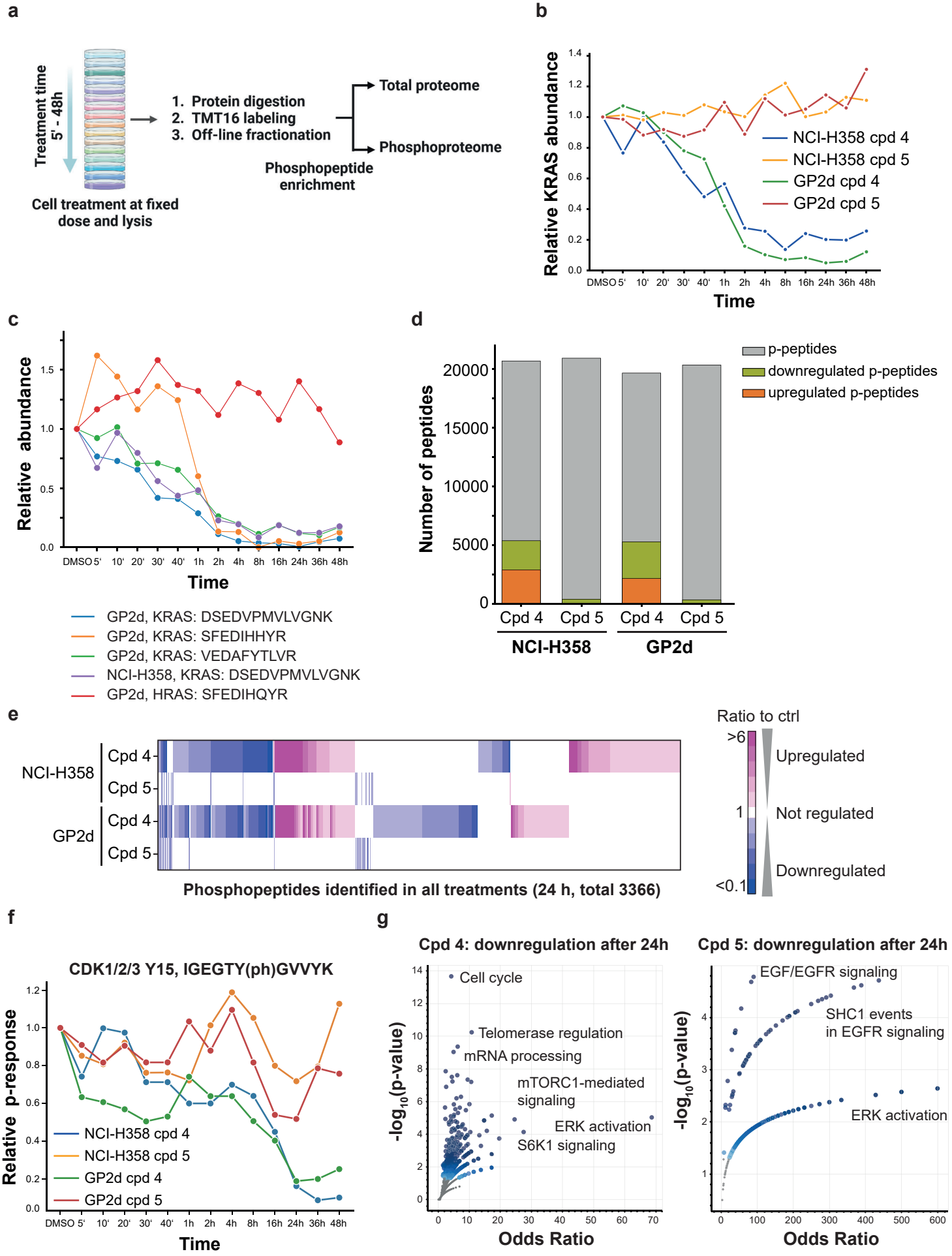

Extended Data Figure 7

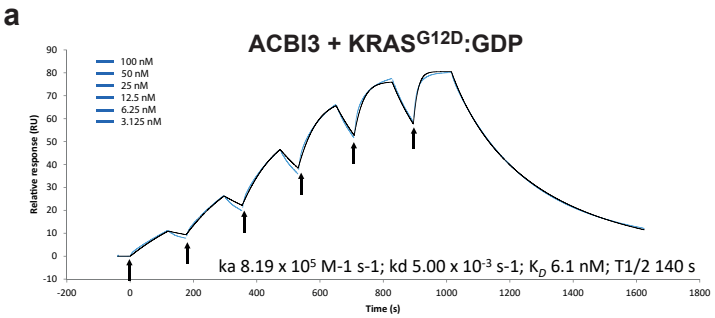

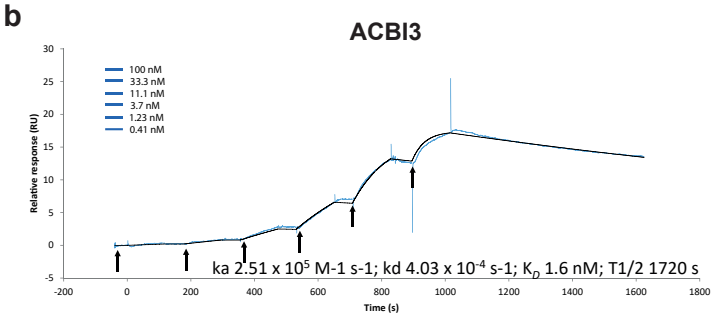

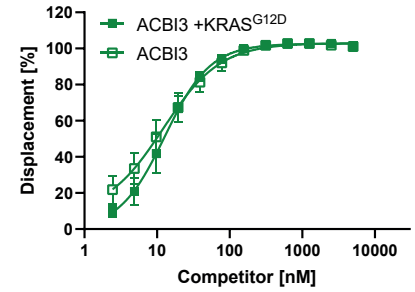

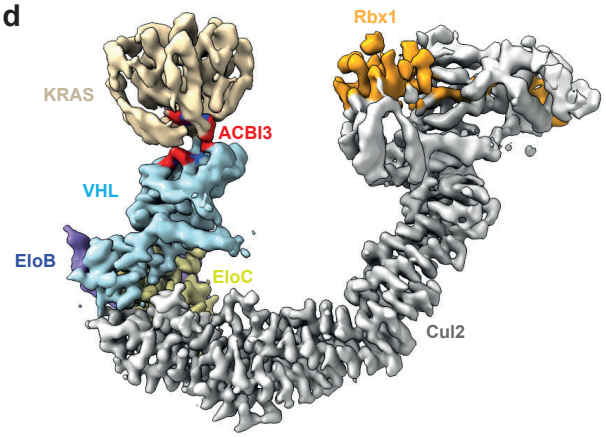

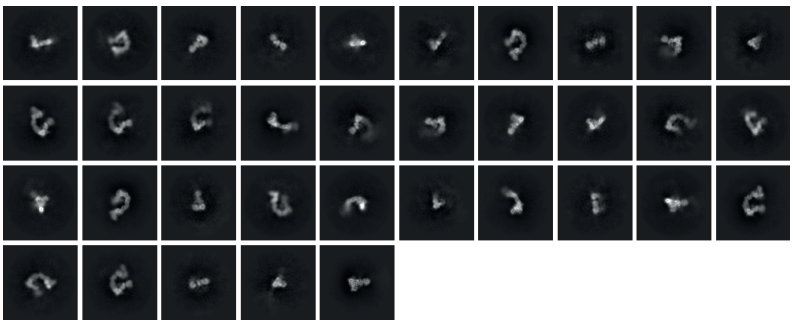

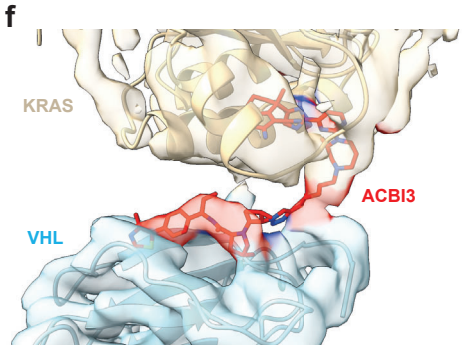

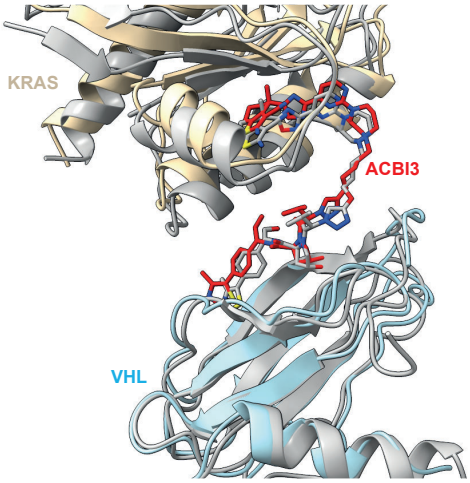

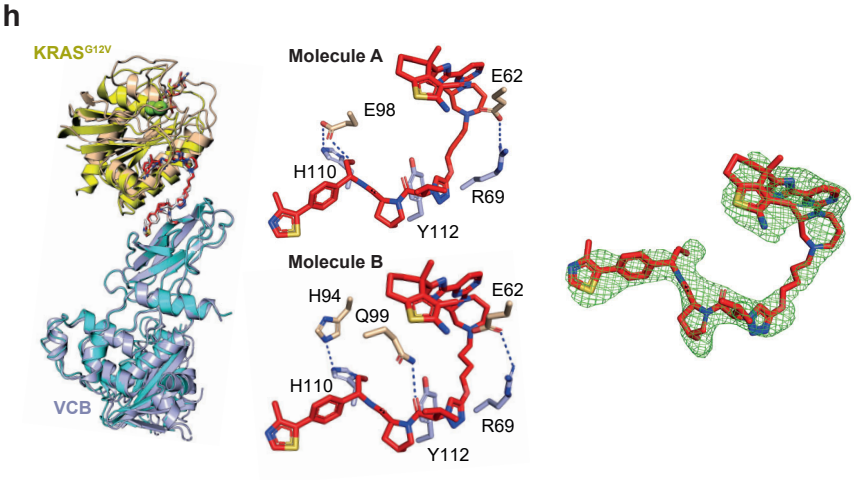

Extended Data Figure 8

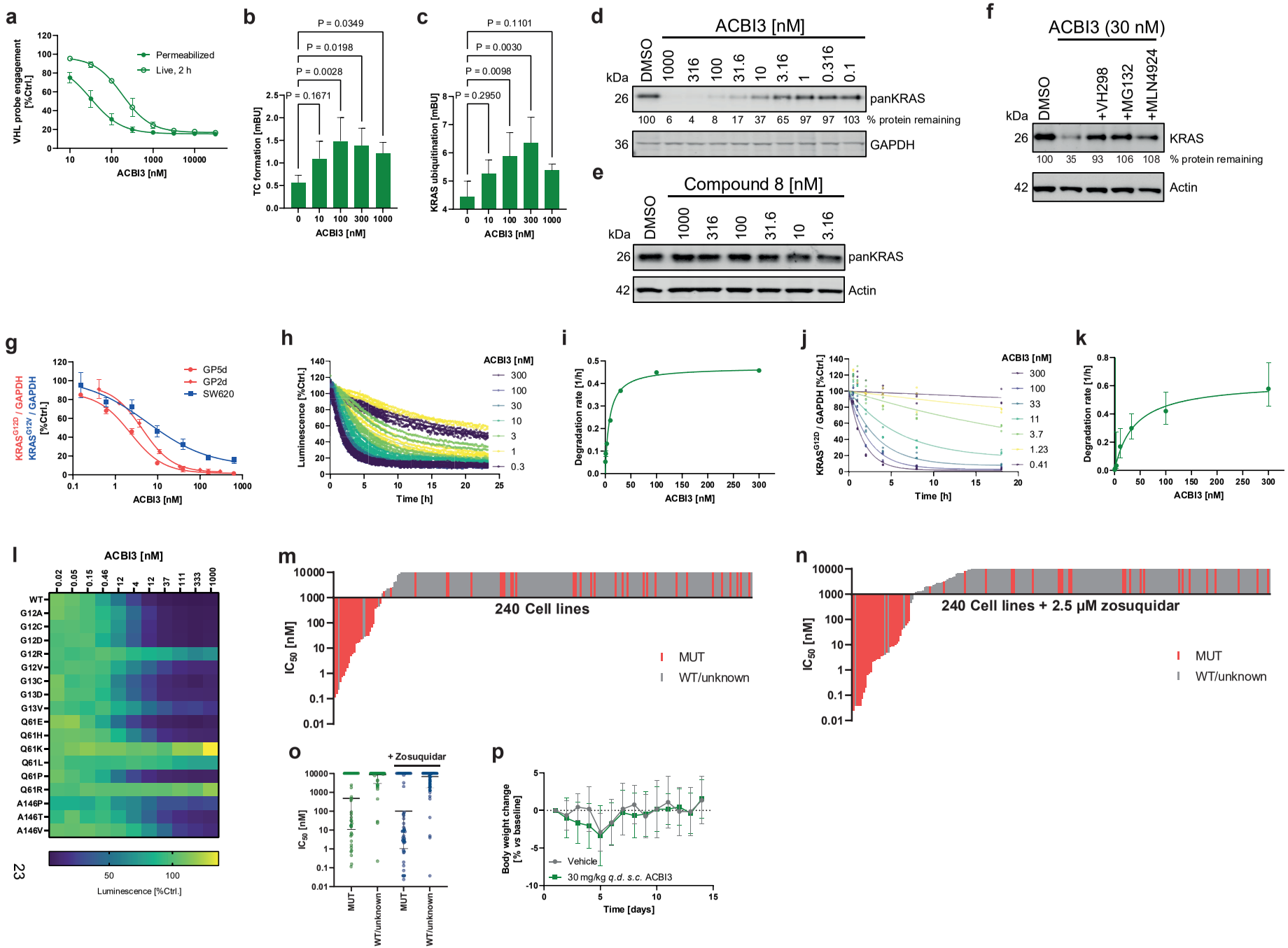

Extended Data Tables

Extended Data Table 1 – Data summary biophysical characterization

Binding affinities towards $KRAS^{G12D}$, $KRAS^{G12V}$, and VHL-ElonginC-ElonginB complex (VCB), as well as VCB ± $KRAS^{G12D}$ measuring cooperativities (alpha), ternary complex affinity and half-lives. Errors are ± standard deviation with repeats (n) specified in brackets. (alpha) is calculated as ratio between VCB K_D / VCB + $KRAS^{G12D}$ K_D values measured in the same run, respectively.

		Cpd 1	Cpd 2	Cpd 3	Cpd 4	Cpd 5	ACBI3
Surface Plasmon Resonance (SPR)	**VCB K_D [nM]**		737 ± 388 (n = 3)	80 ± 24 (n = 3)	50 ± 9 (n = 3)		1.1 ± 0.3 * (n = 2)
	VCB $t_{1/2}$ [s]		n.d.	67	111		2146 *
	VCB K_{on} [M^{-1} s^{-1}]		n.d.	1.36E+05	1.41E+05		3.36E+05 *
	VCB+$KRAS^{G12D}$ K_D [nM]		20 ± 5 (n = 3)	30 ± 6 (n = 3)	26 ± 5 (n = 3)		6 ± 1 * (n = 2)
	VCB+$KRAS^{G12D}$ $t_{1/2}$ [s]		159	103	230		138 *
	VCB+$KRAS^{G12D}$ K_{on} [M^{-1} s^{-1}]		2.24E+05	2.42E+05	1.26E+05		8.19E+05 *
	alpha [-]		36,9	2,7	1,9		0,2
	$KRAS^{G12D}$ GDP K_D [nM]	N.D.	240 ± 31 (n = 3)	13 ± 2 (n = 3)	11 ± 1 (n = 3)	25 ± 5 (n = 3)	5 ± 1 (n = 3)
	$KRAS^{G12V}$ GDP K_D [nM]	25± 12 (n = 4)	136 ± 1 (n = 3)	9 ± 1 (n = 3)	8 ± 0 (n = 3)	13 ± 5 (n = 3)	4 ± 1 (n = 3)
Fluorescence Polarization (FP)	**VCB K_D [nM]**		7187 ± 2552 (n = 3)	340 ± 128 (n = 3)	110 ± 38 (n = 3)	1350 ± 370 (n = 3)	5 ± 2.5 (n = 3)
	VCB+$KRAS^{G12D}$ K_D [nM]		15 ± 2 (n = 3)	20 ± 3 (n = 3)	16 ± 1 (n = 3)	670 ± 120 (n = 3)	4 ± 1 (n = 3)
	alpha [-]		479.1	17.0	6.9	2.0	1.3

* Values are derived from single cycle experiment kinetic fitting.

Extended Data Table 2 – Data summary in vitro degradation, pathway engagement and proliferation.

	Cell line / condition	Compound 2	Compound 3	Compound 4	Compound 5	MRTX1133	sotorasib	ACBI3	BI-2865
***DC_{50}* 6 h (95%CI) [nM]**	**GP2d ($KRAS^{G12D}$)**	n.d.	53.4 (4.1-812)	7.3 (3.7-14.1)	>1000	>1000	n.d.	n.d.	n.d.
	SW620 ($KRAS^{G12V}$)	n.d.	159 (40.9-725.6)	24 (13.1-43.6)	>1000	>1000	n.d.	n.d.	n.d.
	NCI-H358	n.d.	158.9 (0-infinity)	19.6 (3.3-99.1)	>1000	n.d.	>1000	n.d.	n.d.
	A375	n.d.	750.6 (162.3-infinity)	36.7 (17.7-75.2)	>1000	>1000	n.d.	n.d.	n.d.
	HEK293	n.d.	>1000	12.8 (1.9-212.6)	>1000	>1000	n.d.	n.d.	n.d.
***DC_{50}* 24 h (95%CI) [nM]**	**GP5d ($KRAS^{G12D}$)**	607.1 (387.3-764.3)	31.8 (22.7-43.4)	0.9 (0.7-1.1)	n.d.	n.d.	n.d.	2.1 (1.7-2.6)	n.d.
	GP5d (HiBit-$KRAS^{G12D}$)	493.6 (295.7-613.5)	68.1 (51.6-90)	1.4 (1.3-1.6)	n.d.	n.d.	n.d.	0.7 (0.5-0.8)	n.d.
	GP5d (HiBit-$KRAS^{G12D}$) 10% mouse serum	n.d.	n.d.	33.1 (28.2-38.8)	n.d.	n.d.	n.d.	5.1 (3.8-6.9)	n.d.
	GP5d (HiBit-$KRAS^{G12D}$) 10% human serum	n.d.	n.d.	1.9 (1.5-2.4)	n.d.	n.d.	n.d.	0.8 (0.6-0.9)	n.d.
	GP2d ($KRAS^{G12D}$)	n.d.	76.3 (4.3-1985)	3.6 (1.7-7.5)	>1000	>1000	n.d.	3.9 (3-4.9)	n.d.
	SW620 ($KRAS^{G12V}$)	1203 (757.1-1569)	278.1 (17.4-infinity)	12.6 (5.8-29)	>1000	>1000	n.d.	6.9 (3.7-12.9)	n.d.
	NCI-H358	n.d.	240.9 (34.7-infinity)	25.1 (2.4-295.2)	>1000	n.d.	>1000	n.d.	n.d.
	A375	n.d.	455.1 (61.6-infinity)	33.4 (15.1-58.4)	>1000	>1000	n.d.	n.d.	n.d.
	HEK293	n.d.	>1000	86.7 (6.1-977.2)	>1000	>1000	n.d.	n.d.	n.d.
***D_{max}* 24 h (95%CI) [%]**	**GP5d ($KRAS^{G12D}$)**	100 (93-100)	99 (94-100)	100 (98-100)	n.d.	n.d.	n.d.	99 (97-100)	n.d.
	GP5d (HiBit-$KRAS^{G12D}$)	100 (80-100)	95 (88-100)	94 (91-96)	n.d.	n.d.	n.d.	95 (92-97)	n.d.
	GP2d ($KRAS^{G12D}$)	n.d.	96 (57-100)	96 (85-100)	<15	<15	n.d.	99 (96-100)	n.d.
	SW620 ($KRAS^{G12V}$)	100 (90-100)	88 (83-96)	89 (79-100)	<15	<15	n.d.	83 (77-100)	n.d.
	NCI-H358	n.d.	81 (43-100)	86 (53-100)	<25	n.d.	<15	n.d.	n.d.
	A375	n.d.	76 (71-80)	100 (82-100)	<15	<15	n.d.	n.d.	n.d.
	HEK293	n.d.	48 (42-54)	100 (39-100)	<20	<15	n.d.	n.d.	n.d.
λ_{max} (95%CI) [h^{-1}]	**GP5d (HiBit-$KRAS^{G12D}$, live mode)**	0.4 (0.3-0.6)	0.6 (0.5-0.6)	0.5 (0.4-0.6)	n.d.	n.d.	n.d.	0.5 (0.4-0.5)	n.d.
***$Dmax_{50}$* (95%CI) [nM]**		3447 (1480-9658)	56 (46-69)	17 (9-33)	n.d.	n.d.	n.d.	8 (5-14)	n.d.
λ_{max}/ $Dmax_{50}$ [μM^{-1} h^{-1}]		0.1	11	29	n.d.	n.d.	n.d.	58	n.d.
***IC_{50}* pERK (95%CI) [nM]**	**GP2d**	n.d.	771.6 (210.9-1554)	3.1 (1.4-6.9)	1091.0 (206.0-infinity)	1.3 (0.5-2.9)	n.d.	n.d.	n.d.
	SW620	n.d.	708.4 (48.8-2225.0)	9.2 (3.4-25.7)	>1000	>1000	n.d.	n.d.	n.d.
	NCI-H358	n.d.	>1000	8.2 (1.0-112.1)	>1000	n.d.	29 (8.5-107.7)	n.d.	n.d.
	A375	n.d.	>1000	>1000	>1000	>1000	n.d.	n.d.	n.d.
	HEK293	n.d.	>1000	>1000	>1000	>1000	n.d.	n.d.	n.d.
***IC_{50}* DUSP6 (95%CI) [nM]**	**GP2d**	n.d.	128.9 (76.1-221)	3.3 (2-5.4)	245.3 (61.2-3760)	0.1 (0-0.3)	n.d.	n.d.	n.d.
	SW620	n.d.	205.3 (127.5-341.7)	6.2 (4.4-8.6)	428.7 (212.3-1110.0)	309.8 (195.0-522.0)	n.d.	n.d.	n.d.
	NCI-H358	n.d.	248.3 (124.2-527.9)	11.4 (8.9-14.6)	138.4 (97.1-197.7)	n.d.	5.6 (3.6-8.8)	n.d.	n.d.
	A375	n.d.	>1000	>1000	>1000	>1000	n.d.	n.d.	n.d.
	HEK293	n.d.	>1000	>1000	>1000	>1000	n.d.	n.d.	n.d.
***IC_{50}* Proliferation (95%CI) [nM]**	**GP2d**	n.d.	373.7 (233.6-607.3)	8.3 (5.5-12.8)	1738 (561.8-19428)	2.4 (1.7-3.4)	n.d.	n.d.	250.7 (141.7-449.1)
	SW620	n.d.	231.7 (187-287.5)	11.0 (9.6-12.6)	993.0 (602.2-1732.0)	1523.0 (1004.0-2458.0)	n.d.	n.d.	207.7 (144.6-297.7)
	NCI-H358	n.d.	983.2 (723.9-1331)	85.4 (61.7-118.4)	1755.0 (945.9-3931.0)	n.d.	12.3 (10.1-14.9)	n.d.	613.1 (416.1-922.8)
	A375	n.d.	>1000	>1000	>1000	>1000	n.d.	n.d.	>1000
	HEK293	n.d.	>1000	>1000	>1000	>1000	n.d.	n.d.	>1000

n.d. not determined

Extended Data Table 3 – Compound pharmacokinetics in in NMRI mice.

All data represent mean of 3 animals. Source data are provided as a Source Data file.

	Cpd 4		**ACBI3**	
Administration route	*i.v.*	*s.c.*	*i.v.*	*s.c.*
Formulation	HP-ß-CD	HP-ß-CD, Ringer's solution	HP-ß-CD	PEG-400, Transcutol, Kolliphor HS 15
Dose [mg/kg]	5	30	2	30
$AUC_{0\text{-}inf}$ [nmol/L h]	1890	5330	857	9040
Clearance [mL min^{-1} kg^{-1}]	45	–	39	–
V_{ss} [L/kg]	5,3	–	1,6	–
Mean residence time [h]	2,0	6,8	0,67	6,8
Bioavailability [%]	–	47	–	70

Extended Data Table 4 – Physicochemical properties and in vitro DMPK parameters.

Data represent mean values with errors stated as ± standard deviation from N assay repeats after removal of operator results.

				Cpd 2	Cpd 3	Cpd 4	ACBI3
Solubility	*N*			2	2	7	5
	Aqueous pH 4.5	[µg/mL]		5.0	9.0	< 1	4.0 ± 3
	Aqueous pH 6.8			10	10	< 1	< 1
	N			0	0	0	1
	10% HP-β-CD pH 7.2	[mg/mL]		–	–	–	2.6
Lipophilicity	*clogP*			5.3	5.7	5.5	4.9
Transport across human Caco-2 cells	Standard assay	*N*		1	2	3	2
		P_{ab}	[10^{-6} cm/s]	< 14	< 1.5	0.049	< 0.048
		P_{ba}		6.5	14 ± 0.7	14 ± 1	8.2 ± 0.4
		Efflux ratio		> 0.5	> 9.0	270	> 170
	Pre-incubation assay	*N*		0	0	1	1
		P_{ab}	[10^{-6} cm/s]	–	–	0.59	0.79
		P_{ba}				61	16
		Efflux ratio				100	20
	Pre-incubation assay with Pgp inhibition	*N*		0	0	1	1
		P_{ab}	[10^{-6} cm/s]	–	–	7.5	0.98
		P_{ba}				19	5
		Efflux ratio				2.5	5.1
Stability in liver microsomes	Mouse	*N*		1	2	7	5
		Clearance [% Q_H]		69	> 88	> 88	> 88
	Rat	*N*		1	2	7	5
		Clearance [% Q_H]		54	84 ± 2	> 88	84 ± 4
	Human	*N*		1	1	6	5
		Clearance [% Q_H]		82	> 88	> 88	> 88
Plasma protein binding	FCS (10%)	*N*		1	3	1	1
		f_u [%]		2.8	7.3 ± 2	3.5	11
	Mouse	*N*		0	1	1	1
		f_u [%]		–	< 0.2	< 0.07	< 0.04
	Rat	*N*		0	1	1	1
		f_u [%]		–	< 0.03	< 0.05	< 0.3
	Human	*N*		0	1	1	1
		f_u [%]		–	< 0.2	< 0.04	< 0.3

Extended Data Table 5 – Crystallographic data collection and refinement statistics

	$KRAS^{G12C}$-compound **1** (PDB: 8QUG)	$KRAS^{G12V}$:compound **3**:VCB (PDB: 8QW6)	$KRAS^{G12V}$:compound **4**:VCB (PDB: 8QW7)	$KRAS^{G12V}$:ACBI3:VCB (PDB: 8QVU)
Data collection				
Space group	$P\ 4_3\ 2_1\ 2$	P 1	$P\ 1\ 2_1\ 1$	$P\ 1\ 2_1\ 1$
Cell dimensions				
a, *b*, *c* (Å)	91.0, 91.0, 52.7	70.2, 72.3, 80.8	72.5, 125.9, 81.1	72.2, 120.9, 81.0
α, β, γ (°)	90, 90, 90	112.3, 100.6, 100.6	90, 111.6, 90	90, 111.6, 90
Resolution (Å)	64.4-1.6 (1.654-1.562) *	66.3-2.21 (2.46-2.21)	67.4-2.4 (2.70-2.41)	75.2-2.2 (2.54-2.2)
R_{meas}	0.043 (1.696)*	0.065 (0.577)	0.035	0.153 (1.417)
$I / \sigma I$	26.2 (1.4)*	7.4 (1.5)	13.2 (1.6)	8.0 (1.6)
Completeness (%)	95.3 (67.5)*	82.3 (54.3)	92.8 (64.1)	90.6 (60.6)
Redundancy	12.6	2.5	7.0	7.1
Refinement				
Resolution (Å)	40-1.6	46.4-2.2	64.67-2.4	55.86-2.7
No. reflections	26177	39189	30834	32178
R_{work} / R_{free}	19.1/22.2	25.50/29.49	24.59/27.26	24.16/28.04
No. atoms (non-hydrogen)				
Protein	1371	7869	7566	7720
Ligand	32	140	132	151
Water	204	48	24	66
B-factors				
Protein	35.7	47.78	56.85	61.32
Ligand	33.7	33.7	46.02	40.3
Water	50.0	35.3	46.97	35.64
R.m.s. deviations				
Bond lengths (Å)	0.010	0.025	0.016	0.008
Bond angles (°)	1.00	2.06	1.82	1.16

*Values in parentheses are for highest-resolution shell.

Extended Data Table 6 – Cryo-EM data collection, refinement and validation statistics

	KRAS-ACBI3-VHL-EloB-EloC-Cul2-Rbx1 complex (EMD-18657) (PDB 8QU8)
Data collection and processing	
Magnification	165.000x
Voltage (kV)	300
Electron exposure (e–/Å2)	40
Defocus range (μm)	-0.8 to -2.0
Pixel size (Å)	0.745
Symmetry imposed	C1
Initial particle images (no.)	2,414,422
Final particle images (no.)	217,000
Map resolution (Å)	3.5
FSC threshold	0.143
Refinement	
Initial model used (PDB code)	8QUG (KRAS), 5N4W (VHL/EloB/EloC/Cul2/Rbx1)
Model resolution (global, Å)	3.5
FSC threshold	0.143
Map sharpening	deepEMhancer
Model composition	
Non-hydrogen atoms	10855
Protein residues	1325
Ligand atoms	72
B factors (Å2)	
Protein	133
Ligand	173
R.m.s. deviations	
Bond lengths (Å)	0.003
Bond angles (°)	0.663
Validation	
MolProbity score	1.91
Clashscore	9.40
Poor rotamers (%)	0.17
Ramachandran plot	
Favored (%)	93.75
Allowed (%)	6.10
Disallowed (%)	0.15

Acknowledgements and Funding

We would like to acknowledge technical and experimental support by Sandra Doebel, Michael Galant, and Patrick Werni (molecular cloning, protein production and purification of KRAS proteins), Aldina Crnic, Corinna Melichar, Ana Orsolic (cellular biology assays), James Habineza, Sonja Porits, Katrin Gitschtaler (in vivo pharmacology), Nina Braun and Romy Schopper (Cellular assay support), Bernadette Sharps, Thomas Gerstberger and Niklas Baumann (Biochemical assay support), Klaus Rumpel (biophysics assay support), Ines Truebenbach, Ida Dinold, Philipp Toplak (formulation development), Angelika Hörschläger (targeted proteomics) - all from Boehringer-Ingelheim. We also acknowledge Abdel Atrih and Douglas Lamont from the University of Dundee FingerPrint Proteomics facility for support with mass spectrometry proteomics. We also thank European Synchrotron Radiation Facility and Diamond Light Source for beamtime (BAG proposal MX14980) and for support at beamlines I23-1 and I24 respectively. This work has received funding from Boehringer Ingelheim. Biophysics and drug discovery and proteomics/computing activities at Dundee were partially supported by Wellcome Trust strategic awards (100476/Z/12/Z, 094090/Z/10/Z and 097945/C/11/Z respectively).

Competing Interests

Johannes Popow, Andreas Gollner, Christiane Kofink, Gerhard Fischer, Melanie Wurm, Nikolai Mischerikow, Carina Hasenoehrl, Heribert Arnhof, Silvia Arce-Solano, Sammy Bell, Georg Boeck, Jale Karolyi-Oezguer, Theresa Klawatsch, Manfred Koegl, Roland Kousek, Barbara Kratochvil, Katrin Kropatsch, Arnel A. Lauber, Sabine Olt, Daniel Peter, Oliver Petermann, Vanessa Roessler, Peggy Stolt-Bergner, Patrick Strack, Eva Strauss, Jens Quant, Harald Weinstabl, Peter Ettmayer are current or former employees of Boehringer Ingelheim. A.C. is a scientific founder, shareholder and advisor of Amphista Therapeutics, a company that is developing targeted protein degradation therapeutic platforms. The Ciulli laboratory receives or has received sponsored research support from Almirall, Amgen, Amphista Therapeutics, Boehringer Ingelheim, Eisai, Merck KaaG, Nurix Therapeutics, Ono and Tocris-Biotechne.

Contributions

J.P., W.F., C.K. and A.G. contributed equally and will be putting their name first on the citation in their CVs. A.C. and P.E. co-conceived the study, designed and supervised experiments and co-wrote the paper. J.P. and W.F. designed, analysed and supervised experiments, prepared figures and co-wrote the paper. C.K. and A.G. designed compounds and synthetic routes and co-wrote the paper. E.D., A.B.F., J.G.-T., R.M., N.T., H.W. and S.Z. designed compounds and synthetic routes. J. K-O., T.K., O.P. synthesised key compounds. M.K. co-wrote the manuscript. G.F., S. A-S., D.P. and P. S-B. contributed to production and analysis of cryo-EM data. R.K. performed small molecule structure identification and analysis. B.K., P.P., C.H. and A.L. designed and performed phosphoproteomics studies. B.K. produced binary x-ray structures. A.W. and D.Z. crystallised ternary complexes KRAS:PROTAC:VCB and solved their co-crystal structures. K.K. and A.W. designed and performed biophysical assays. S.K., C.W., V.V., S.O. and V.R., designed, interpreted and performed cellular assays. R.M. and V.V. designed, analysed and performed proteomics studies. N.M. designed and interpreted targeted proteomics and co-wrote the manuscript and N.M. and H.A. designed in vivo PK and in vitro ADME studies. M.W., P.S., E.S., S.B. and G.B. designed and interpreted in vivo studies and co-wrote figures. J.Q. measured effects of pgp substrate properties on cancer cell line panel data.

Data Availability Statement

Atomic coordinates and structure factors for x-ray crystallographic and cryo electron microscopy structures have been deposited in the Protein Data Bank (and the EMDB) with accession codes

8QUG, 8QU8 (EMD-18657), 8QW6, 8QW7 and 8QVU. All raw data and search results for proteomics studies have been deposited to the ProteomeXchange Consortium with the dataset identifiers PXD046161, PXD045416 and PXD045460, respectively. Source data are provided with this manuscript.

Code availability Statement

All data were analysed using publicly available code.

References

1 Skoulidis, F. *et al.* Sotorasib for Lung Cancers with KRAS p.G12C Mutation. *N Engl J Med* **384**, 2371-2381 (2021). https://doi.org:10.1056/NEJMoa2103695

2 Herdeis, L., Gerlach, D., McConnell, D. B. & Kessler, D. Stopping the beating heart of cancer: KRAS reviewed. *Curr Opin Struct Biol* **71**, 136-147 (2021). https://doi.org:10.1016/j.sbi.2021.06.013

3 Huang, L., Guo, Z., Wang, F. & Fu, L. KRAS mutation: from undruggable to druggable in cancer. *Signal Transduct Target Ther* **6**, 386 (2021). https://doi.org:10.1038/s41392-021-00780-4

4 Ou, S. I. *et al.* First-in-Human Phase I/IB Dose-Finding Study of Adagrasib (MRTX849) in Patients With Advanced KRAS(G12C) Solid Tumors (KRYSTAL-1). *J Clin Oncol* **40**, 2530-2538 (2022). https://doi.org:10.1200/JCO.21.02752

5 Wang, X. *et al.* Identification of MRTX1133, a Noncovalent, Potent, and Selective KRAS(G12D) Inhibitor. *J Med Chem* **65**, 3123-3133 (2022). https://doi.org:10.1021/acs.jmedchem.1c01688

6 Kim, D. *et al.* Pan-KRAS inhibitor disables oncogenic signalling and tumour growth. *Nature* **619**, 160-166 (2023). https://doi.org:10.1038/s41586-023-06123-3

7 Farnaby, W., Koegl, M., McConnell, D. B. & Ciulli, A. Transforming targeted cancer therapy with PROTACs: A forward-looking perspective. *Curr Opin Pharmacol* **57**, 175-183 (2021). https://doi.org:10.1016/j.coph.2021.02.009

8 Chirnomas, D., Hornberger, K. R. & Crews, C. M. Protein degraders enter the clinic - a new approach to cancer therapy. *Nat Rev Clin Oncol* **20**, 265-278 (2023). https://doi.org:10.1038/s41571-023-00736-3

9 Zeng, M. *et al.* Exploring Targeted Degradation Strategy for Oncogenic KRAS(G12C). *Cell Chem Biol* **27**, 19-31 e16 (2020). https://doi.org:10.1016/j.chembiol.2019.12.006

10 Bond, M. J., Chu, L., Nalawansha, D. A., Li, K. & Crews, C. M. Targeted Degradation of Oncogenic KRAS(G12C) by VHL-Recruiting PROTACs. *ACS Cent Sci* **6**, 1367-1375 (2020). https://doi.org:10.1021/acscentsci.0c00411

11 Bondeson, D. P. *et al.* Catalytic in vivo protein knockdown by small-molecule PROTACs. *Nat Chem Biol* **11**, 611-617 (2015). https://doi.org:10.1038/nchembio.1858

12 Tolcher, A. P., W.; Wang, J.S.; Spira, A.; Janne, P.; Lee, H.; Gill, S.; LoRusso, P.; Herzberg, B.; Goldman, J.: Morgensztern, D.; Berlin, J.; Kasi, A.; Fujii, H.; Pelster, M. Trial in progress: A phase 1, first-in-human, open-label, multicenter, dose-escalation and dose-expansion study of ASP3082 in patients with previously treated advanced solid tumors and KRAS G12D mutations. *J Clin Oncol* **41**, Suppl 4 (2023). https://doi.org:10.1200/JCO.2023.41.4_suppl.TPS764

13 Galdeano, C. *et al.* Structure-guided design and optimization of small molecules targeting the protein-protein interaction between the von Hippel-Lindau (VHL) E3 ubiquitin ligase and the hypoxia inducible factor (HIF) alpha subunit with in vitro nanomolar affinities. *J Med Chem* **57**, 8657-8663 (2014). https://doi.org:10.1021/jm5011258

14 Gadd, M. S. *et al.* Structural basis of PROTAC cooperative recognition for selective protein degradation. *Nat Chem Biol* **13**, 514-521 (2017). https://doi.org:10.1038/nchembio.2329

15 Schwinn, M. K. *et al.* CRISPR-Mediated Tagging of Endogenous Proteins with a Luminescent Peptide. *ACS Chem Biol* **13**, 467-474 (2018). https://doi.org:10.1021/acschembio.7b00549
16 Soucy, T. A. *et al.* An inhibitor of NEDD8-activating enzyme as a new approach to treat cancer. *Nature* **458**, 732-736 (2009). https://doi.org:10.1038/nature07884
17 Frost, J. *et al.* Potent and selective chemical probe of hypoxic signalling downstream of HIF-alpha hydroxylation via VHL inhibition. *Nat Commun* **7**, 13312 (2016). https://doi.org:10.1038/ncomms13312
18 Roy, M. J. *et al.* SPR-Measured Dissociation Kinetics of PROTAC Ternary Complexes Influence Target Degradation Rate. *ACS Chem Biol* **14**, 361-368 (2019). https://doi.org:10.1021/acschembio.9b00092
19 Dragovich, P. S. *et al.* Antibody-Mediated Delivery of Chimeric BRD4 Degraders. Part 2: Improvement of In Vitro Antiproliferation Activity and In Vivo Antitumor Efficacy. *J Med Chem* **64**, 2576-2607 (2021). https://doi.org:10.1021/acs.jmedchem.0c01846
20 Imaide, S. *et al.* Trivalent PROTACs enhance protein degradation via combined avidity and cooperativity. *Nat Chem Biol* **17**, 1157-1167 (2021). https://doi.org:10.1038/s41589-021-00878-4
21 Buckley, D. L. *et al.* Targeting the von Hippel-Lindau E3 ubiquitin ligase using small molecules to disrupt the VHL/HIF-1alpha interaction. *J Am Chem Soc* **134**, 4465-4468 (2012). https://doi.org:10.1021/ja209924v
22 Canon, J. *et al.* The clinical KRAS(G12C) inhibitor AMG 510 drives anti-tumour immunity. *Nature* **575**, 217-223 (2019). https://doi.org:10.1038/s41586-019-1694-1
23 Hallin, J. *et al.* Anti-tumor efficacy of a potent and selective non-covalent KRAS(G12D) inhibitor. *Nat Med* **28**, 2171-2182 (2022). https://doi.org:10.1038/s41591-022-02007-7
24 Mares, A. *et al.* Extended pharmacodynamic responses observed upon PROTAC-mediated degradation of RIPK2. *Commun Biol* **3**, 140 (2020). https://doi.org:10.1038/s42003-020-0868-6
25 Slate, D. L. *et al.* RS-33295-198: a novel, potent modulator of P-glycoprotein-mediated multidrug resistance. *Anticancer Res* **15**, 811-814 (1995).
26 Shah, S. M., Jain, A. S., Kaushik, R., Nagarsenker, M. S. & Nerurkar, M. J. Preclinical formulations: insight, strategies, and practical considerations. *AAPS PharmSciTech* **15**, 1307-1323 (2014). https://doi.org:10.1208/s12249-014-0156-1
27 Viale, P. H. The American Cancer Society's Facts & Figures: 2020 Edition. *J Adv Pract Oncol* **11**, 135-136 (2020). https://doi.org:10.6004/jadpro.2020.11.2.1

Methods

Ethics Approval

The authors confirm that the research in this study complies with all relevant ethical regulations.

Chemical synthesis

Full details of synthetic procedures and NMR spectra of final compounds are provided as Supplementary Methods.

Protein Production

Wild-type and mutant versions of human proteins were used for all protein expression, as follows: VHL (UniProt accession number P40337), ElonginC (Q15369), ElonginB (Q15370) and KRAS G12D C118S (P01116, residues 1-169).

The VCB complex was expressed and purified as described previously[1]. Briefly, N-terminally His6-tagged VHL (54–213), ElonginC (17–112) and ElonginB (1–104) (Addgene ID 204500 & 204501) were co-expressed in *E. coli* and the complex isolated by Ni-affinity chromatography. The His6 tag was removed using TEV protease, and the complex was further purified by anion exchange and size-exclusion chromatography (SEC).

N-terminally His6-tagged KRAS G12D/G12V C118S was expressed and purified as described previously (doi: 10.1073/pnas.1904529116). In brief, the protein was overexpressed in *E. coli* in Terrific Broth (TB) supplemented with 0.2 mM IPTG for expression induction. Expression was performed overnight at 18 ^{o}C. The protein was then purified by Ni-affinity chromatography, followed by His6 tag removal using TEV protease, another round of Ni-affinity chromatography to remove His6-tag and the uncleaved protein, and SEC.

Protein Crystallography

VCB, compound **3** and KRAS G12V C118S GDP were mixed in a 1:1.1:1 stoichiometric ratio in 20 mM HEPES, pH 8.0, 100 mM sodium chloride, 1 mM TCEP, 2% DMSO, 1 mM GDP incubated for 30 min on ice. The complex was concentrated to 8 mg/mL. The drops were prepared by combining 200 nL of the ternary complex with 200 nL of well solution (200 mM lithium sulfate monohydrate, 100 mM BIS-TRIS propane pH 5.5, 25% w/v polyethylene glycol 3350) and crystallized at 4 °C using the sitting-drop vapor diffusion method. Crystals were grown for 27 days then cryoprotected by addition of ~500 nL well solution supplemented with 20% (v/v) glycerol to the crystallization drop followed by harvesting and flash cooling in liquid nitrogen.

VCB, compound **4** and KRAS G12V C118S GDP were mixed in a 1:5:5 stoichiometric ratio in 20 mM HEPES, pH 8.0, 100 mM sodium chloride, 1 mM TCEP, 2% DMSO, 1 mM GDP incubated for 30 min on ice before purification by size exclusion chromatography (SEC) to isolate the formed ternary complex. The complex was concentrated to 10 mg/mL. The drops were prepared by combining 200 nL of the ternary complex with 200 nL of well solution (200 mM sodium citrate, 100 mM BIS-TRIS propane pH 8.5, 20% w/v polyethylene glycol 3350) and crystallized at 4 °C using the sitting-drop vapor diffusion method. Crystals were grown for 5 days then cryoprotected by addition of ~500 nL well solution supplemented with 20% (v/v) glycerol to the crystallization drop followed by harvesting and flash cooling in liquid nitrogen.

VCB, ACBI-3 and KRAS G12V C118S GDP were mixed in a 1:1:1.5 stoichiometric ratio in 20 mM HEPES, pH 8.0, 100 mM sodium chloride, 1 mM TCEP, 2% DMSO, 1 mM GDP incubated for 30 min on ice prior SEC to isolate the formed ternary complex. The eluted complex was concentrated to a final concentration of approximately 5-10 mg/mL. The drops were prepared by combining 200 nL of the ternary complex with 200 nL of well solution and crystallized at 4 °C using the hanging-drop vapor diffusion method. Crystals were grown in 20% w/v PEG 8000, 0.2 M lithium chloride, 0.1 M Tris pH 8.0 for several days until they reached a suitable size. Harvested crystals were flash cooled in liquid nitrogen following gradual equilibration into cryo-protectant solution consisting of 30% (v/v) glycerol in 20% PEG 8000, 0.2 M lithium chloride, 0.1 M Tris, pH 8.0.

Diffraction data for the ternary complex crystals were collected at beamline X10SA at the Swiss Light Source, Switzerland at a wavelength of 1.0 Å. Images were processed using autoPROC[2], the phase problem solved using PHASER[3] using previously determined structures, the model built using Coot[4] and iteratively refined using Phenix[5]. The structures were deposited in the PDB with codes 8QW6, 8QW7 and 8QVU.

The binary crystal structure of KRAS-G12C-C118S (UniprotID P01116) with compound **1** was obtained through backsoaking. The hexagonally shaped source crystals were obtained by hanging drop co-crystallisation of 0.75 µL of 43 mg/mL KRAS-G12C-C118S with a mixture of 0.75 µL of 2 mM dimethyl-aminocyanothiophen in 0.1M sodium acetate pH 5.2, 1.55M ammonium sulfate. The crystals were transferred to a 1 µL drop containing 10 mM compound **1** in 0.1 M sodium acetate pH 5.2, 1.55 M ammonium sulfate and incubated for 48h. Subsequently, the crystals were cryocooled in liquid nitrogen, using 25% ethylene glycol as cryoprotectant.

Data were collected at beamline ID23-1 at the European Synchrotron Facility, France at a wavelength of 0.97 Å (compound **1**). Images were processed using autoPROC[2], the phase problem solved using PHASER[3] using a previously determined structure, the model built using Coot[4] and iteratively refined using autoBUSTER, CCP4[6] and Phenix[5]. The structure has been deposited in the PDB with code 8QUG (compound **1**). Ramachandran analysis showed 95.6% of residues in favoured regions, 4.24% in allowed regions and no outliers.

Cryo Electron Microscopy

The ternary complex was prepared by mixing 2.15 µL of 48 mg/mL KRAS-G12V-C118S solution, 5.35 µL of ACBI3 and 318 µL of 1.25 mg/mL VHL-ElonginB-ElonginC-Cullin2-Rbx1-complex obtained from Abcam, UK (catalogue no. ab271787, lot no. GR3409294-5), incubating at room temperature for 10 minutes, concentration of the sample to 70 µL using a 10MWCO Amicon Ultra concentrator followed by size exclusion chromatography (Superdex 200; running buffer 50 mM Tris pH=7.5, 100 mM NaCl, 0.5 mM TCEP, 2 mM $MgCl_2$). After elution, 4 µL of the heptameric complex peak were immediately applied to a plasma-cleaned (Pelco EasyGlow, 45 sec, 15 mA) Quantifoil 1.2/1.3, 200 mesh copper grid and vitrified in liquified ethane using an automated plunge freezer (Vitrobot Mk4, Thermofisher Scientific; blotting time 2 sec, humidity 95%, 4 °C).

Data were collected on a Titan Krios G4 equipped with a Falcon 4 camera (Thermofisher Scientific) and a Selectris energy filter at an electron acceleration voltage of 300 kV and a nominal magnification of 165.000x, corresponding to a pixel size of 0.745 Å/px. Images were acquired in counting mode using EPU datacollection software. Data were processed using the cryoSPARC v4 suite. Briefly, data were motion- and CTF-corrected (Patch Motion Correction, Patch CTF Estimation). 2,414,422 particles were automatically identified (blob picking followed by template picking) from 6907 images. Subsequently, 2D classification was carried out, followed by 3D-heterogenous

refinement and 3D variability analysis. The modes determined herein were used as initial latent input indices for 3D flex refinement with 217,000 particles, which was followed by deepemhancer for map sharpening.

Model building and refinement was based on the ternary crystal structure presented in this paper (PDB entry 8QVU) for KRAS, VHL, ElonginB and Elongin C, and PDB entry 5N4W for Cul2 and Rbx1[7]. Initial docking and figures were performed using ChimeraX[8], while subsequent model building and optimization was performed using Coot[4]. During realspace refinement with PHENIX[5], the KRAS- and Rbx1-chains were heavily restrained against their input X-ray-models, as densities in this region were low resolution and hence only sufficient to provide the approximate orientation of the proteins. The structure has been deposited in the PDB and EMDB with accession codes 8QU8 and EMD-18657 respectively.

Surface Plasmon Resonance Experiments

Surface plasmon resonance experiments were performed on Biacore 8K instruments (Cytiva). Streptavidin (Prospec) was immobilized at 25 °C on CM5 Chips (Cytiva) using 10 mM HBS-P+ buffer (pH 7.4) (Cytiva). The surface was activated using 400 mM 1-ethyl-3-(3-dimethylaminopropyl)-carbodiimide and 100 mM N-hydroxysuccinimide (Cytiva) (contact time 420 s, flow rate 10 mL min−1). Streptavidin was diluted to a final concentration of 1 mg mL−1 in 10 mM sodium acetate (pH 5.0) and injected for 600 s. The surface was subsequently deactivated by injecting 1 M ethanolamine for 420 s and conditioned by injecting 50 mM NaOH and 1 M NaCl. Dilution of the biotinylated target proteins and coupling was performed using a running buffer without DMSO. The two kRAS target proteins were prepared at 0.1 mg mL−1 and coupled to the chip to a density between 200 and 800 response units. All KRAS binary interaction experiments were performed at 25 °C in running buffer (20 mM Tris(hydroxymethyl)aminomethane, 150 mM potassium chloride, 2 mM magnesium chloride, 2 mM Tris(2-carboxyethyl) phosphine hydrochloride, 0.005% Tween20, 40 µM Guanosine 5'-diphosphate, pH 8.0, 1% DMSO). The compounds were diluted in running buffer and injected over the immobilized target proteins (concentration range, 3.33–1,000 nM). Sensorgrams from reference surfaces and blank injections were subtracted from the raw data before data analysis using Biacore Insight software. Affinity and binding kinetic parameters were determined by using a 1/1 interaction model, with a term for mass transport included.

For VCB immobilisation, sensor chips pre-coated with streptavidin (Cytiva) were used. Biotinylated Avi-tagged-VCB was prepared as previously described. Excess free biotin was removed by extensive dialysis (3-times) into buffer containing 20 mM HEPES pH 7.5, 200 mM NaCl and 0.25 mM TCEP. All interaction experiments involving VCB were done at 20 °C in running buffer (20 mM HEPES, pH 8.0, 150 mM potassium chloride, 2 mM magnesium chloride, 2 mM TCEP, 0.05% Tween20, 2% DMSO). The compounds were diluted in running buffer and injected over the immobilized target proteins (concentration range, 3.33–1,000 nM). For ternary complex measurements, experiments were run in the presence of 2 µM KRAS G12D-GDP during the injection phase. Data analysis was performed as described above.

Fluorescence Polarization Experiments

All FP measurements were taken using a PHERAstar FS (BMG LABTECH) with fluorescence excitation and emission wavelengths (λ) of 485 nm and 520 nm, respectively. FP competitive binding assays were performed in duplicate on 384-well plates (#3575, Corning) with a total well volume of 15 µL. Each well solution contained 5 nM of FAM-labelled HIF-1α peptide (FAM-DEALAHypYIPMDDDFQLRSF, KD = 3 nM as measured by a direct FP titration), 15 nM of VCB protein,

and decreasing concentrations of PROTACs (13-point serial 2-fold dilutions starting from 10 µM) or PROTAC:KRAS G12D-GDP (13-point serial 2-fold dilution starting from 10 µM of the PROTAC and constant concentration of KRAS G12D-GDP at 20 µM) in 100 mM HEPES pH 7.5, 100 mM NaCl, 1 mM TCEP with a final DMSO concentration of 2%. To obtain percentage of displacement, control wells containing peptide in the absence of protein (maximum displacement), or VCB and peptide with no compound (zero displacement) were also included. These values were then fitted by nonlinear regression using Prism (GraphPad, version 7.03) to determine average IC50 values and standard error of the mean (SEM) for each titration. A displacement binding model was used to back-calculate inhibition constants (KI) from the measured IC50 values, as described previously[9].

Cell Culture

Cell lines were obtained through ATCC or ECACC, verified for identity by satellite repeat analysis, tested for mycoplasm contamination at regular intervals, and cultured in the specified media in a humidified cell incubator at 37 °C and 5 % CO2, unless specified otherwise. Dulbecco's modified Eagle medium (DMEM) was obtained from Lonza (product code BE12-604F), Eagle's minimal essential medium (EMEM) from ATCC (product code 30–2003), Leibovitz's L15 medium from Themo Fisher (product code 11415064) and RPMI-1640 from Gibco (product code A10491). The following cell lines (product codes and culture media / conditions in parentheses) were used for the described experiments: GP2d (ECACC No. 95090714, DMEM plus 10 % FCS), GP5d (ECACC No. 95090715, DMEM plus 10% FCS), SW620 (ATCC No. CCL-227, Leibovitz´s L15 plus 10 % FCS, no CO2), NCI-H358 (ATCC No. CRL-5807 RPMI-1640 plus 10 % FCS), HEK293 (ATCC No. CRL-1573, EMEM plus 10 % FCS), MIA PaCa-2 (ATCC No. CRL-1420, DMEM plus 10 % FCS) and A375 (ATCC No. CRL-1619, DMEM plus 10 % FCS).

Cell Proliferation

Cells were seeded at 500 cells per well in 40 µL of growth medium in a white bottom opaque 384-well plate and allowed to grow overnight. To obtain starting densities, a set of cells seeded in parallel were lysed and measured using 40 µL CellTiter-Glo luminescent cell viability reagent (Promega product code G7570) per well as per the manufacturer's recommendation. The compounds were added to the cells at logarithmic dose series using a HP Digital Dispenser D300 (Tecan), normalizing for added DMSO. After compound addition, the cells were incubated for five days and the viability measured using the CellTiter-Glo reagent as described above. The results are stated as mean and standard deviation of triplicate experiments. IC_{50} values including 95% confidence intervals were computed using a 3-parametric logistic model restricting the bottom to be > 0.

High-throughput Proliferation Screen

High throughput proliferation profiling in presence or absence of the ABCB1 inhibitor zosuquidar (2.5 µM) was performed at Horizon Discovery. Briefly, the cells were seeded in 25 µl of growth media in black 384-well tissue culture plates at the density defined for the respective cell line and plates were placed at 37 °C, 5% CO2 for 24 h before treatment. At the time of treatment, a set of assay plates (which did not receive treatment) were collected and ATP concentrations were measured by using CellTiter-Glo v.2.0 (Promega) and luminescence reading on an Envision plate reader (Perkin Elmer). BI-1138 was transferred to assay plates using an Echo acoustic liquid handling system. Assay plates were incubated with the compound for 5 days and were then analysed by using CellTiter-Glo. All data points were collected by means of automated processes and were subject to quality control and analysed using Horizon's proprietary software. Horizon uses growth inhibition as a measure of

cell growth. The growth inhibition percentages were calculated by applying the following test and equation: if T < V0 then 100 (1 − (T − V0)/V0) and if T ≥ V0 then 100 (1 − (T − V0)/(V − V0)), where T is the signal measure for a test article, V is the untreated or vehicle-treated control measure and V0 is the untreated or vehicle-treated control measure at time zero (colloquially referred to as T0 plates). This formula was derived from the Growth Inhibition (GI) calculation used in the National Cancer Institute's NCI-60 high-throughput screen.

KRAS Degradation Assays via Detection of Split Nanoluciferase (Hibit)

To assess PROTAC-mediated degradation of HiBit-tagged KRAS constructs, cells were seeded at 25000 cells per well in culture medium into white bottom opaque 96 well plates (Perkin Elmer cat no. 5680). Plates were incubated at 37 °C, 5 % CO2 in a humidified incubator over night to allow the cells to adhere. Test compounds (10 mM stock in DMSO) were added at logarithmic dose series using the HP Digital Dispenser D300 (Tecan), normalizing for added DMSO. Plates were further incubated at 37°C for 18 hours. Following incubation, 100 µL per well Promega Nano-Glo HiBit lytic detection reagent mix (Promega Nano-Glo HiBit Lytic Detection System #N3050), prepared according to the manufacturer´s instructions in the kit, were added. To allow for adequate cell lysis, plates were incubated on an orbital shaker for 15 min and further incubated 30 min at room temperature. Upon completion of cell lysis, luminescence was measured using an Envision plate reader using the Ultrasensitive Luminescence Protocol for 96 well plates. Luminescence levels were normalized by the values obtained with DMSO-treated samples and plotted as percent of DMSO control. DC_{50} values were computed using a four parametric logistic model. Dmax values represent the maximal extent of degradation observed and are stated as percent of control treatments.

GP5d Cells With HiBit-tagged KRAS Locus

Genetic introduction of a split luciferase tag into the KRAS locus was conducted at Horizon Discovery (https://horizondiscovery.com). Briefly, a HiBit protein detection tag (amino acid sequence VSGWRLFKKIS) was introduced immediately downstream of the initiating Methionine codon of the endogenous KRAS locus (Ensembl gene ID ENSG00000133703.7) of GP5d cells (ECACC Cat. No. 95090715) by CRISPR-based genome engineering using a KRAS(G12D) mutant donor construct encoding the HiBit tag. This resulted in the heterozygous introduction of an N-terminal HiBit tagged version of KRAS(G12D) into the KRAS(WT) allele. Correct modification of the KRAS locus was assessed by PCR-based genotyping and Sanger sequencing of the isolated PCR products. The resulting cell line is referred to as GP5d-HiBit-KRAS(G12D).

Retroviral Transduction of HiBit-tagged KRAS Mutants

The therapeutically relevant mutant KRAS constructs (WT, A146P, A146T, A146V, G12A, G12C, G12D, G12R, G12V, G13C, G13D, G13V, Q61E, Q61H, Q61K, Q61L, Q61P, Q61R) were obtained by site directed mutagenesis using a KRAS4B WT cDNA construct as a template at Genscript (https://www.genscript.com). GP5d cells (ECACC Cat. No. 95090715) expressing transgenic murine Slc7a1 to allow for transduction ecotropic lentiviral particles (Takarabio Cat. No. 631278) were transduced with lentiviral vectors expressing mutant KRAS4B cDNA under control of a CMV promoter. Stably transduced cells were selected using a neomycin selectable marker encoded on the construct.

HiBit-based Degradation Assay at 10 % Mouse or Human Serum

GP5d cells expressing HiBit-tagged KRAS G12D were seeded at 25000 cells per well in 100 µL medium into white bottom opaque 96 well plates. Plates were incubated at 37 °C, 5 % CO2 in a

humidified incubator over night to let the cells adhere. The day of the assay the incubation medium was removed by suction and replaced with pre-warmed fresh DMEM medium containing 10 % serum from NMRI female mice (without preservatives added, sterile filtered, supplied by Envigo RMS S.r.l. Z.I.) or human serum (Sigma cat. No. S7023). Compounds (10 mM stock in DMSO) were added at logarithmic dose series using a HP Digital Dispenser D300 (Tecan), normalizing for added DMSO. Plates were further incubated at 37°C for 18 hours. Subsequently, media were removed by suction and replaced with 100 µL PBS at room temperature. The luminescence reaction was started by adding 100 µL per well Promega Nano-Glo HiBit lytic detection reagent mix, prepared according to the manufacturer´s instructions. Plates were agitated for 15 min on an orbital shaker and incubated for 30 min at room temperature. Luminescence was measured on an Envision plate reader using a Ultrasensitive Luminescence Protocol for 96 well plates. Luminescence was normalized to values obtained with DMSO-treated samples and are reported as percent of DMSO control. DC50 values, Dmax values and 95% confidence intervals were computed using a 3-parametric logistic model.

Kinetic Live Cell HiBiT Detection

LgBiT construct were diluted into Transfection Carrier DNA (Promega) at a mass ratio of 1:4 (mass/mass), after which FuGENE HD was added at a ratio of 1:3 (µg DNA: µL FuGENE HD). FuGENE HD complexes thus formed were combined with GP5d HiBiT G12D cells suspended at a density of 2.5 × 10^5 cells/mL, transferred to a tissue-culture treated flask, and incubated in a humidified, 37 °C/5% CO2 incubator for 20hr. Following transfection, cells were plated in white 96-well tissue culture plates at a density of 5 × 104 cells per well in 100 µL of growth medium and incubated overnight at 37 °C, 5% CO2. For continuous live cell detection out to 24 h, an equal volume of CO2-independent medium (Gibco) containing a 2× concentration of Endurazine (Promega) was added to each well. Plates were incubated at 37 °C, 5% CO2, for 2.5 h to allow luminescence to equilibrate before addition of each compound. Plate Lid was removed and replaced with a Breathe-Easy sealing membrane. Plates were read for a period of 24 h on the GloMax Discover (Promega) set to 37 °C.

Degradation rate were calculated by fitting only the initial degradation portion of each kinetic concentration curve to the equation: Y = (Y0 - Plateau) * exp(-K * X) + Plateau, where K= degradation rate in units of h–1.

VHL Nanoluciferase Target Engagement

Target engagement and intracellular availability for VHL ligands were assessed using the NanoBRET TE Intracellular E3 ligase assay (Promega). HEK293 cells were transfected with the VHL-NanoLuc fusion constructs using FuGENE HD (Promega) according to the manufacturer's protocol. Briefly, VHL- Nanoluc construct were diluted into Transfection Carrier DNA (Promega) at a mass ratio of 1:9 (mass/mass), after which FuGENE HD was added at a ratio of 1:3 (µg DNA: µL FuGENE HD). FuGENE HD complexes thus formed were combined with HEK293 cells suspended at a density of 2 × 105 cells/mL, transferred to a tissue-culture treated flask, and incubated in a humidified, 37 °C/5% CO2 incubator for 20 h. Following transfection, cells were washed, harvested by trypsinization, and resuspended in Opti-MEM. BRET assays were performed in white, 96-well non-binding surface plates (Corning CAT# 3600) at a density of 2 × 104 cells/well. All chemical inhibitors were prepared as concentrated stock solutions in DMSO (Sigma-Aldrich) and diluted in Opti-MEM (unless otherwise noted) to prepare working stocks.

For measurement of intracellular affinity for VHL ligands, live cells were equilibrated for 2 h with VHL Tracer and test compound prior to BRET measurements. VHL Tracer was prepared as a 100X intermediate stock at 100 µM in pure DMSO, and subsequently diluted to a working concentration of

20X in tracer dilution buffer (12.5 mM HEPES, 31.25% PEG-400, pH 7.5). VHL Tracer was added to live cells at a final concentration of 1 µM from the 20X working stock. To measure BRET, NanoBRET NanoGlo Substrate and Extracellular NanoLuc Inhibitor (Promega) were added according to the manufacturer's recommended protocol, and filtered luminescence was measured on a Pherastar equipped with 450 nm BP filter (donor) and 600 nm LP filter (acceptor), using 1 s integration time. Milli-BRET units (mBU) are calculated by multiplying the raw BRET values by 1000. Competitive displacement data were then plotted with GraphPad Prism software and IC_{50} values were determined using the [inhibitor] vs response - variable slope (four parameters) equation available in GraphPad Prism (Equation 1): Y = Bottom + (Top - Bottom) / (1 + (IC_{50} / X)^HillSlope)

For measurement of intrinsic affinity for VHL ligands, the NanoBRET TE assay was applied as described above, except that the cells were permeabilized by adding digitonin to a final concentration of 50 µg/mL, the final VHL tracer concentration used was 0.25 µM, the permeabilized cells were incubated with tracer and test compound for 10 min at room temperature, and the Extracellular NanoLuc Inhibitor was omitted from the NanoGlo substrate solution

Cellular NanoBRET Ubiquitylation and Ternary Complex Experiments

GP5d clonal cells (7 × 10E5) expressing the HiBiT-KRAS were transfected with FuGENE HD (Promega) and 1 µg of HaloTag-VHL, or HaloTag-UBB in 6-well plates. The following day, 5 × 104 transfected cells were replated into white 96-well tissue culture plates in the presence or absence of HaloTag NanoBRET 618 Ligand (Promega) and incubated overnight at 37 °C, 5% CO2. The following day, cells were treated with compound for 4 h. Following treatment time point, NanoBRET NanoGlo (Promega) were added according to the manufacturer's recommended protocol, and filtered luminescence was measured on a Pherastar with 450 nm BP filter (donor) and 600 nm LP filter (acceptor), using 1 s integration time. Background subtracted NanoBRET ratios expressed in milliBRET units were calculated from the equation: mBRET_ratio = ((acceptor_channel / donor_channel) – (acceptor_channel(no_ligand) / donor_channel(no_ligand)) * 1000.

Real-time Quantitative PCR

Cells were seeded at 10 000 cells in 200 µL culture medium per well in a 96-well plate. Cells were allowed to adhere overnight. Compound dilutions were added from DMSO stock solutions using a HP D300 Dispenser (Tecan) (final DMSO concentration 0.1%). Typically, cells were incubated at 37°C for 6 hours. Treated cells were processed using the FastLane Cell Multiplex Kit (Qiagen product code 216513). Threshold cycle numbers were determined using an AriaMx Real-time PCR System (Agilent Technologies) and GAPDH (Applied Biosystems Cat. No. 4326317E-1301046, VIC) and DUSP6 (Life Technologies Cat No. Hs00169257_m1, FAM) probes. Results were analyzed by relative quantification and are specified as percent of matched DMSO controls. IC_{50} values and 95% confidence intervals were computed using a 3-parametric logistic model restricting the bottom to be > 0.

Protein Detection by Capillary Electrophoresis

Cells (50 000) were seeded the day before treatment into 96-well clear-flat bottom plates and incubated overnight (37 °C, humidified tissue culture incubator, 5 % CO2). Compounds were added from DMSO stock solution using a digital dispenser and cells are incubated at 37 °C as specified (24 h for KRAS degradation, 6 h for determination of pERK levels). At the end of the incubation, medium was removed, cells washed with ice cold PBS, PBS removed and 50 µL Lysis Buffer (Sigma Product Code R0278) supplemented with 1:100 HALT Phosphatase-Protease Inhibitors (Thermo Scientific

Catalog number 78441) added to each well. Plates with lysis buffer were immediately transferred to -80 °C freezer for at least 2 h and then thawed on ice. Lysates were transferred to a 96 well V bottom plate and insoluble debris is pelleted by centrifugation for 20 minutes at 4000 rpm. 40 µL of the supernatant were transferred to a fresh Eppendorf PCR plate. Analysis of protein levels was conducted using the Wes System, ProteinSimple (https://www.bio-techne.com/) as specified by the manufacturer. Briefly, Wes Master Mix (12- 230 kDa WES Separation Module, 8 x 25 capillary cartridges, ProteinSimple #SM-W004) and molecular weight markers were prepared as specified in the manufacturer's recommendations. To detect primary antibodies, anti-rabbit (Protein Simple #DM-001) or anti mouse (Protein Simple #DM-002) detection modules were used. 7.2 µL lysate + 1.8 µL master mix were combined and heated to 95 °C for 5 min. The following antibodies were used and diluted as recommended in Antibody Diluent II: KRASG12D (Cell Signaling product code 14429, 1:100), KRASG12V (Cell Signaling product code 14412, 1:100), KRAS (Lifespan product code C175665, 1:100), Phospho-p44/42 MAPK (Cell Signaling product code 9101, 1:200), p44/42 MAPK (Cell Signaling product code 4695, 1:400), GAPDH (Abcam product code ab8245, 1:2000). Results were analyzed using the Compass Software. Capillaries with no signal were assumed to be experimental artifacts and were excluded from further analyses as indicated in the raw data. Protein levels were normalized to DMSO controls run in the same cartridge and specified in % of control. IC_{50} or DC_{50} and Dmax values including 95% confidence intervals were computed using a 3-parametric logistic model restricting the bottom to be > 0.

Western Blot

VH298, MG132 and ML4924 co-treatment. $5x10^5$ GP5d cells were seeded into 6-well plates 24 hours before treatment. Next day, several wells were treated with 30 nM of Compound **4** or ACBI3. Immediately after, VH298 (Selleckchem Cat. No. S8449), MG132 (Selleckchem Cat. No. S2619) and MLN4924 (Tocris Cat. No. 6499) were added to the wells at 10 µM final concentration and incubated for 4h. 0.1% (v/v) DMSO was added to the wells with single treatments to achieve the same concentration of DMSO in all wells.

Degradation experiments. 5×10^5 GP5d cells in 2 mL/well were seeded into 6 well plates 24 h before treatment. Cells were treated for 4 hours as indicated, washed with PBS and lysed with lysis buffer (1% Triton X-100, 150 mM NaCl, 1 mM EDTA, 50 mM Tris pH 7.4, protease inhibitor cocktail (Roche), 50 units/mL benzonase nuclease (Sigma). Lysates were cleared by centrifugation at 4 °C, at 15800 × *g* for 10 min and the supernatants stored at -20 °C. Protein concentration was determined by BCA assay (Pierce) and the absorbance at 562 nm measured by spectrophotometry on a plate reader (BMG Labtech PHERastar). Samples were separated by SDS-PAGE using 20 µg of protein per well of NuPAGE Novex 4-12% BIS-TRIS gels (Invitrogen) and transferred to 0.2 µm pore nitrocellulose membrane (Amersham) by wet transfer. Western blot images were obtained through detection of mouse anti panKRAS (1:1000, LsBio-C175665), rabbit anti-β-actin (1:2500, Cell Signaling Technology #4970S), mouse anti-β-actin (1:2500, Cell Signalling Technology #3700S) and rabbit anti-GAPDH (1:2500, Abcam ab9485) antibodies with donkey anti-rabbit IRDye 800CW secondary antibody (1:10000, LI-COR #926-32213) using a ChemiDoc MP imaging system (Bio-Rad). Western blots were quantified using Image Studio Lite (Licor, version 5.2) with normalisation to loading control and DMSO and further analysed using GraphPad Prism (version 9.2.0) and ImageJ (Fiji).

Pharmacokinetic Analyses

Compound concentrations in plasma aliquots were measured by quantitative HPLC-MS/MS using an internal standard. Calibration and quality control samples were prepared using blank plasma from untreated animals. Samples were precipitated with acetonitrile and injected into a HPLC system

(Agilent 1200). Separation was performed by gradients of 5 mmol/L ammonium acetate pH 4.0 and acetonitrile with 0.1% formic acid on a 2.1 mm by 50 mm XBridge BEH C18 reversed-phase column with 2.5 µm particles (Waters). The HPLC was interfaced by ESI operated in positive ionisation mode to a triple quadrupole mass spectrometer (5000 or 6500+ Triple Quad System, SCIEX) operated in multiple reaction monitoring mode. Chromatograms were analyzed with Analyst (SCIEX) and pharmacokinetic parameters were calculated by non-compartmental analysis using BI-proprietary software.

Solubility Testing

Compound solubility was determined by dilution of a 10 mmol/L compound solution in DMSO into buffer to a final concentration of 125 µg/mL. Dilution into a 1:1 mixture of acetonitrile and water was used as reference. After 24 h, the incubations were filtrated, and the filtrate was analyzed by LC-UV.

Microsomal Stability

The degradation kinetics of 1 µmol/l compound in 0.5 mg/mL liver microsomes were inferred in 100 mM Tris-HCl pH 7.5, 6.5 mM MgCl2 and 1 mM NADPH at 37 °C. Reactions were terminated by addition of acetonitrile and precipitates separated by centrifugation. Compound concentrations in supernatants were measured by HPLC-MS/MS and clearance was calculated from compound half-lives using the well-stirred liver model.

Plasma Protein Binding

Binding of compound to plasma proteins was determined by equilibrium dialysis of 3 µmol/L compound in plasma or serum against PBS through an 8 kDa molecular-weight cut-off cellulose membrane (RED device, Thermo Fisher) at 37 °C for 5 h. After incubation, aliquots from donor and acceptor compartments were precipitated and the concentrations in the supernatants were determined by quantitative LC-MS/MS. Calibration and quality control samples were prepared using blank plasma and internal standard. The fraction unbound was calculated as ratio of the compound concentration in the acceptor compartment to the concentration in the donor compartment.

Bidirectional Permeability in Caco-2 Cells

Bidirectional permeability of test compounds across a Caco-2 cell monolayer was measured as described[10]. Briefly, Caco-2 cells were seeded onto Transwell inserts (Corning, Wiesbaden, Germany) at a density of 160,000 cells/cm^2 and cultured in DMEM (high glucose) containing 10% FCS for 14-21 days. Cells were incubated with culture media containing 1 µM compound for 24 h. After the preincubation period, culture media were removed and fresh transport buffer (128 mM NaCl, 5.4 mM KCl, 1 mM $MgSO_4$, 1.8 mM $CaCl_2$, 4.2 mM $NaHCO_3$, 1.2 mM Na_2HPO_4, 0.41 mM NaH_2PO_4, 15 mM 2-[4-(2-hydroxyethyl)piperazin-1-yl]ethanesulfonic acid (HEPES), 20 mM glucose, pH 7.4, 0.25% bovine serum albumin) containing 1 µM test compound was added to the apical (apical to basal) or basal (basal to apical) compartment (donor compartment), transport buffer without test compound was added to the opposite compartment (receiver compartment). Samples were taken at different time points for up to 2 h. Test compound in the samples was quantified by LC-MS/MS. To elucidate the role of drug transporter P-gp in the transcellular transport, permeability measurement was performed in the absence and presence of 5 µM of the selective P-gp inhibitor zosuquidar. Apparent permeability coefficients (P_{ab}, P_{ba}) were calculated as $P_{ab} = Q_{ab} / (C_0 \times s \times t)$ and $P_{ba} = Q_{ba} / (C_0 \times s \times t)$ where Q is the amount of compound recovered in the receiver compartment after the incubation time t, C_0 the initial compound concentration given to the donor compartment, and s the

surface area of the Transwell inserts. Efflux ratio is calculated as the quotient of P_{ba} (mean of duplicate) to P_{ab} (mean of duplicate). The P-gp substrate apafant and one low permeable compound (BI-internal reference, $P_{ab} \approx 3 \times 10^{-7}$ cm/s, no efflux) were included in every assay plate. In addition, transepithelial electrical resistance (TEER) values were measured for each plate before the permeability assay. All three parameters (efflux of the reference substrates, P_{ab} values of the low permeable compound, and TEER values) were used to ensure the quality of the assays.

Animals, Biomarker and Xenograft experiments

In vivo experiments were performed at the AAALAC accredited animal facility of Boehringer Ingelheim RCV GmbH & CoKG. Female BomTac:NMRI-*Foxn1*^{nu} mice were obtained from Taconic Denmark at 6-8 weeks of age. After the arrival, mice were allowed to adjust to the housing conditions at least for 5 days before the start of the experiment. Food and water were provided ad libitum. Mice were group housed (3-10 mice per cage) in pathogen-free and controlled environmental conditions (21 ± 1.5°C temperature, 55 ± 10% humidity, and 12-h light-dark cycle; open cage housing), and handled according to the institutional, governmental and European Union guidelines (Austrian Animal Protection Laws, GV-SOLAS and FELASA guidelines).

Studies were approved by the internal ethics committee of Boehringer Ingelheim RCV GmbH & Co KG in the department of Cancer Pharmacology and Disease Positioning. Furthermore, all protocols were approved by the Austrian governmental committee (MA 60 Veterinary office; approval numbers GZ: MA 58-426431-2019-13, MA 58-458067-2021-17 and MA 58-546776-2022-13).

For pharmacokinetic (PK) studies mice (n=3 per group) were dosed with the respective degrader i.v. bolus at the indicated dose formulated with HP-ß-CD 25% or as an s.c. with the formulation and dose indicated by the respective experiment. Five plasma samples were collected from the vena saphena at defined timepoints.

To establish subcutaneous tumors for biomarker or xenograft experiments, mice were injected with 5 x 10^6 GP2d cells with 1:2 Matrigel : PBS with 5%FBS. Tumor diameters were measured with a caliper. The volume of each tumor [in mm^3] was calculated according to the formula "tumor volume = length * diameter^2 * π/6."

For the biomarker study mice were randomized (n=7 for the control and n=5 for each treatment groups) when tumor size reached between ~200 and 500 mm^3. Mice were treated with ACBI3 three consecutive days before tumors and plasma were collected at 6 and 24 hours after the last treatment. Fresh frozen tumors were lysed in ice cold Tris lysis buffer (50 mM NaCl, 20 mM Tris-HCl pH 7.5, 1 mM EDTA, 1 mM EGTA, 1% Triton-X-100), supplemented with phosphatase inhibitors (Sigma product codes P0044 and P5726). Lysates were cleared by centrifugation (10 min, 10000 x g) and analyzed by capillary electrophoresis as described herein.

For the Xenograft study mice were randomized into the treatment groups when tumor size reached ~220 mm^3. Group sizes were calculated based on historical GP2d Xenograft experiments. 10 mice per group were used for the study based on the power analysis performed with a sample size calculator (). 30 mg/kg ACBI3 formulated in PEG-400, Kolliphor HS 15 and Transcutol were dosed daily s.c. and control mice received this formulation at the same dosing schedule without compound added. TGI (tumor growth inhibition was calculated with the formular: TGI =100 x (1-[(treated final day– treated day 1) / (control final day– control day 1)]). To monitor side effects of treatment, mice were inspected daily for abnormalities and body weight was determined daily during treatment. Lesions at the skin at injection sites were detected in the context of ACBI3, which resulted in an early stop of the experiment. Two animals out of the treatment groups were euthanized at day 7 due to skin lesions

and one animals of the control groups was euthanized at day 9 due to skin lesion/irritation. ACBI3 is not recommended for further *in vivo* use.

Targeted proteomics assay for KRASG12C, KRASWT, HRAS and NRAS

Lysates of 50,000 cells per sample were precipitated using a methanol-chloroform method. Precipitates were digested with 5 µg Lys-C and 10 µg Trypsin in digestion buffer (5 mmol/L tris(2-carboxyethyl)phosphin hydrochloride, 10 mmol/L 2-chloro-acetamide, 1% (w/v) sodium deoxycholate, 50 mmol/L triethylammonium bicarbonate pH 8.5) containing stable isotope-labeled synthetic peptides with the following amino acid sequences: LVVVGAGGVGK(+8), LVVVGAC(carbamidomethyl)GVGK(+8), SFEDIHHYR(+10)EQIK, SFADINLYR(+10)EQIK, SFEDIHQYR(+10)EQIK (SpikeTides TQL, JPT). Digests were acidified and purified by C18 RP solid-phase extraction. Peptides were chromatographically separated on 200 cm µPAK C18 RP columns (PharmaFluidics) using a 60 min gradient of effectively 2 to 28% acetonitrile in 0.1% formic acid and water at 300 nL/min on a RSLCnano HPLC system (Thermo Scientific) interfaced by ESI to a Q-Exactive Plus mass spectrometer (Thermo Scientific). Eluting peptide ions were analyzed using parallel reaction monitoring with an isolation window of 0.4 Th, a resolving power of 35,000, an automatic gain control target of 1e5 and a maximum injection time of 120 ms. Included were $[M+2H]^{2+}$ or $[M+3H]^{3+}$ molecular ions of the targeted peptides. Data were analyzed with Skyline and processed with R. The number of wild-type KRAS molecules per cell was calculated as mean of LVV..G minus SFE..H – SFE..Q and SFA minus LVV..C molecules per cell, while the number of molecules per cell of the other RAS species where directly inferred from the individual peptides. KRAS 4A and 4B were not discriminated.

Multiplexed Relative Phospho-proteomics

NCI-H358 cells (4 10^6 per 10 cm dish seeded on the day before treatment) were treated with 500 nM of compound **4** or compound **5**, GP2d (5 10^6 per 10 cm dish seeded on the day before treatment) cells were treated with 100 nM of compound **4** or compound **5** for 5 min, 10 min, 20 min, 30 min, 40 min, 1 h, 2 h, 4 h, 8 h, 16 h, 24 h, 36 h, and 48 h. To correct for any potential treatment-unrelated abundance changes, the cells were treated with DMSO vehicle control for 1h, 24h and 48h (13 treatment time points and 3 controls, 16 conditions in total). After the treatment, cells were washed twice with 5 mL PBS and lysed in 200 µL lysis buffer (2 % SDS in 100 mM Tris-HCl, pH 7.5, 95 °C, 10 min). Lysate was then acidified to 1 % trifluoroacetic acid (Sigma Cat. No. 302031) for DNA hydrolysis, followed by neutralization with 4-methylmorpholine (Sigma Cat. No. 407704, 2 % final concentration), and stored at -20°C until further use.

Sample preparation was performed following the previously reported procedures[11]. The protein yield was determined by Thermo Pierce BCA protein assay. All steps were performed according to the manufacturer's protocol. 200 µg protein lysate per treatment condition was cleaned by protein aggregation capture on a Bravo Agilent pipetting system following the SP3 Protocol. Briefly, 200 µg protein lysate was mixed with 1500 µg (7.5:1 beads to lysate ratio, 1:1 mix of washed magnetic Sera-Mag™ A & B; Cytiva) for 10 min 1000 rpm RT on a thermoshaker. All volumes were adjusted to 120 µl using 10 mM Tris-HCl (pH 7.6). Proteins were precipitated by adding 100% ethanol to a final concentration of 70% and shaking for 10 min at 1250 rpm on the Bravo shaking unit. The supernatant was removed on the magnet. The lysate was washed 3 times with 80% Ethanol, with 5 min shaking intervals off the magnet and supernatant removal on the magnet. Finally, beads were washed with 100% acetonitrile to remove residual ethanol. Proteins were reduced and alkylated in 100 µl RA buffer (100 mM EPPS/NaOH, pH 8.5, 50 mM CAA, 10 mM TCEP) for 1h at 37 °C and 1200 rpm. Next, 2 µg of Trypsin was added and digestion was performed overnight at 37 °C and 1000 rpm. The peptides were recovered on the Bravo magnet. Beads were washed with 110 µl 2% TFA for 3

min at 1250 rpm on the Bravo shaking unit and the wash supernatant was pooled to the recovered peptides. To further remove magnetic beads from the digest, the recovery plate was further incubated on a magnetic rack for 1h at 4 °C.

The digest was desalted using HLB desalting plates (10 mg N-Vinylpyrrolidon-Divinylbenzol porous particles 30 µm). Plates were cleaned by 500 µl isopropanol, acetonitrile, and solvent B (0.1% TFA 70% acetonitrile), and equilibrated by 1000 µl solvent A (0.1% TFA in deionized water), each step was followed by a 1 min centrifugation at 500 rpm. The digest was loaded by gravity. After washing twice with 1000 µl solvent A, peptides were eluted by gravity in 200 µl Solvent B, and the residual volume was collected via a 1 min centrifugation at 1000 rpm. The cleaned peptides were dried down in the speed-vac and stored at -20°C.

The dried and cleaned peptides were reconstituted in 20 µl of 100 mM EPPS*NaOH (pH 8.5) buffer. TMT-16plex reagent (Thermo Scientific; LOT: VI310352) was reconstituted in water-free acetonitrile to a working concentration of 20 µg/µl. 5 µl of this TMT reagent solution was transferred to the peptides. The reaction was incubated on the thermoshaker (23°C, 400 rpm) for one hour, followed by quenching with 5 µl of 1.5% hydroxylamine (final concentration of 0.25%). The TMT channels were then pooled together and acidified with formic acid (FA) to a final concentration of 1%. The reaction wells were washed with 25 µl washing solution (2.5% FA in 30% acetonitrile) and added to the TMT pool. The TMT pools were dried down in the speed-vac and stored at -20°C.

The TMT-pooled peptides were cleaned by solid-phase extraction on 50 mg C18 Sep-PAK cartridges. Briefly, the cartridges were primed with 1000 µl of acetonitrile, followed by the 1000 µl washes of buffer B (0.1% FA in 50% acetonitrile), and 1000 µl of buffer A (0.1% FA in deionized water). The TMT peptides were reconstituted in 700 µl of buffer A (pH adjusted to 2), and loaded on the Sep-PAK cartridges by gravity. The columns were washed twice with 1000 µl of buffer A. TMT peptides were then eluted with 400 µl of buffer B, dried down in the speed-vac, and stored at -20°C.

TMT peptides were resolved with high pH reversed-phase (RP) fractionation on Thermo Scientific Vanquish HPLC equipped with a Waters XBridge BEH130 C18 3.5 µm 4.6 x 250 mm column. In brief, dried peptides were reconstituted in 200 µl of 25 mM ammonium bicarbonate, pH 8, and fractionated over a 60 min gradient from 7% to 45% acetonitrile in the presence of 2.5 mM ammonium bicarbonate. The gradient was followed by a 7 min ramp to 80% acetonitrile of the column wash. Fractions were collected from minutes 7 to 55 after injection. Each fraction consisted of 30 sec at a flow rate of 1000 µl/min. The 96 fractions were pooled into 48, and acidified with FA to a final concentration of 0.1%. The 10% of fractionated TMT peptides was separately dried down in the speed-vac for MS analysis of the total proteome.

Phosphorylated peptides were separated from the TMT-pool peptide mix by immobilized metal ion affinity chromatography (IMAC) enrichment on a AssayMAP® Fe(III)-NTA cartridges with the Bravo Agilent pipetting system following the Phosphopeptide Enrichment Protocol, included in the Agilent AssayMAP® Bravo® Protein Sample Prep Workbench v2.0 software suite. Briefly, the dried 48 TMT peptide fractions were reconstituted in 0.1% TFA 80% acetonitrile and combined into 12 fractions (final volume of 200 µl per fraction). The AssayMAP® Fe(III)-NTA cartridges were primed with 150 µl of 0.1% TFA in acetonitrile at 300 µl/min, and further equilibrated with 150 µl 0.1% TFA in 80% acetonitrile at 10 µl/min. The TMT-pool peptide mix was loaded on the cartridges at 5 µl/min, and the flow through was collected. The cartridges were further washed three times with 150 µl 0.1% TFA in 80% acetonitrile at 50 µl/min. Upon a stringent syringe wash with 200 µl 0.1% TFA in acetonitrile, the retained on the cartridges phosphorylated peptides were eluted with 60 µl of 1%

ammonium hydroxide NH_4OH at 5 µl/min. The eluates were acidified up to 0.1% FA, dried down in the speed-vac, and stored at -20°C for MS analysis of the phosphoproteome.

Total proteome-TMT peptides were measured with a Fusion Lumos Tribrid mass spectrometer (Thermo Scientific) that was coupled to a Vanquish microflow pump (Thermo Scientific). The sample was reconstituted in 20 µl 1% FA 2% acetonitrile, and 10 µl were directly injected onto the Acclaim PepMap 100 C18 column (2 µm particle size, 1 mm ID × 150 mm). Separation was performed on a 25 min gradient with a flow rate of 50 µl/min starting from 4% B, followed by the linear phase to 32% B. The system was finally washed with 95 µl 90% B and re-equilibrated at 1% B. Solvent A consisted of 0.1% FA and 3% DMSO in water. Solvent B consisted of 0.1% FA and 3% DMSO in acetonitrile.

The MS was operated in a fast, data-dependent MS3-mode. The spray voltage was set to 3.5 kV supported by sheath gas (32 units) and aux gas (5 units) with a vaporizer temperature of 125 °C. Every 1.2 s, a full-scan (MS1) was recorded from 360 to 1600 m/z with a resolution of 60k in the Orbitrap in profile mode. The MS1 AGC target was set to 4e5, and the maxIT was set to 50 ms. Based on the full scans, precursors were targeted for MSMS scans if the charge was between 2 and 6, and the intensity exceeded 1e4. The MS2 quadrupole isolation window was set to 0.6 Th. The TMT peptides were HCD fragmented with an NCE of 34%. The MS2 spectra were acquired in the ion trap in rapid mode. The MS2 AGC target was set to 3e4 charges, and the maxIT was set to 40 ms. Precursors that have been targeted for fragmentation were excluded for 50 s for all possible charge stages. TMT reporter ions were measured in a consecutive MS3 scan based on the previous MSMS scan. Thus, a new batch of precursor ions was isolated with an MS3 quadrupole isolation window of 1.2. The isolated precursor was then HCD-fragmented identically to the previous MS2 scan. The top 8 fragment ions of the MS2 scans were isolated in the ion trap in parallel (synchronous precursor selection). Only fragment ions within a range of 400 to 2000 Th were considered. The selected top10 fragment ions were then HCD fragmented with an NCE of 55%. The MS3 spectrum was acquired with 50k resolution from 100 to 1000 Th in the Orbitrap in centroid mode. The MS3 AGC target was set to 2e5 charges, and the maxIT was set to 86 ms.

Phospho-TMT peptides were measured with a Fusion Lumos Tribrid mass spectrometer (Thermo Scientific) that was coupled to a Dionex UltiMate 3000 RSLCnano System (Thermo Scientific). Each of the 12 peptide fractions was reconstituted in 20 µl of 50 mM sodium citrate buffer, 10 µl were then injected for the MS analysis. After injection, the sample was transferred onto a trap column (75 µm x 2 cm) that was packed with 5 µm C18 resin (Reprosil PUR AQ - Dr. Maisch). Peptides were washed with the trap washing solvent (5 µl/min, 10 min) before conveying them to an analytical column (75 µm x 48 cm) that was packed with 3 µm C18 resin (Reprosil PUR AQ - Dr. Maisch). Separation was performed on an 80 min gradient with a flow rate of 300 nl/min starting from 4% B, followed by the first linear phase to 22.5% B in 65 min, followed by the second linear phase to 32% B in 15 min. The system was finally washed with 80% B for 2 min and re-equilibrated at 2% B. Solvent A consisted of 0.1% FA and 5% DMSO in water. Solvent B consisted of 0.1% FA and 5% DMSO in acetonitrile.

The MS was operated in a sensitive, data-dependent MS3-mode. Peptides were ionized using a nano source with 2.1 kV spray voltage. Every 3 s, a full-scan (MS1) was recorded from 360 to 1800 m/z with a resolution of 60k in the Orbitrap in profile mode. The MS1 AGC target was set to 4e5, and the maxIT was set to 50 ms. Based on the full scans, precursors were targeted for MSMS scans if the charge was between 2 and 6, the isotope envelop was peptidic (MIPS), and the intensity exceeded 5e4. The MS2 quadrupole isolation window was set to 0.7 Th. Peptide fragmentation occurred in the linear ion trap by CID-targeting the precursor and the precursor-H_2PO_4 in parallel (multistage-activation) with a q-value of 0.25, 35% CE, and 10 ms activation time. The MS2 spectrum was acquired with 30k resolution and auto scan range in the Orbitrap in centroid mode. The MS2 AGC

target was set to 5e4 charges, and the maxIT was set to 60 ms. The maxIT or AGC target could be dynamically exceeded when the previous scan took longer than the calculated injection time (inject beyond mode). Precursors that have been targeted for fragmentation were excluded for 90 s for all possible charge stages. TMT reporter ions were measured in a consecutive MS3 scan based on the previous MSMS scan. Thus, a new batch of precursor ions was isolated with a charge stage-dependent MS3 quadrupole isolation window of 1.2 Th (z=2), 0.9 Th (z=3), 0.7 Th (z=4-6) to include the first isotope in the isolation while using the most narrow isolation window possible. The isolated precursor was then MSA-fragmented identically to the previous MS2 scan. The top 10 fragment ions of the MS2 scans were isolated in the ion trap in parallel (synchronous precursor selection). Only fragment ions were considered that were within a range of 400 to 2000 Th and laid outside the precursor exclusion range (precursor -50 Th, precursor + 5 Th). The selected top10 fragment ions were then HCD fragmented with an NCE of 55%. The MS3 spectrum was acquired with 50k resolution from 100 to 1000 Th in the Orbitrap in centroid mode. The MS3 AGC target was set to 1e5 charges, and the maxIT was set to 120 ms.

MaxQuant (version 2.1.3.0) with its built-in search engine Andromeda was used to identify and quantify phospho and total proteome TMT peptides. MSMS spectra were searched against the human Uniprot database supplemented with common contaminants. Unless stated otherwise, MaxQuant's default parameters were applied. These included for all searches: Trypsin/P as the proteolytic enzyme with up to three missed cleavage sites allowed; carbamidomethylation of cysteine as fixed modification, oxidation of methionine and N-terminal protein acetylation as variable modifications; precursor tolerance was set to ±4.5 ppm and fragment ion tolerance to ±20 ppm (FTMS). Phosphorylation on serine, threonine, and tyrosine was allowed as variable modification specifically for the phosphoproteome enrichment data. Andromeda score and delta score cut-offs for modified peptides were set to 40 and 6, respectively; peptide spectrum match (PSM) and protein false discover rate (FDR) employing a target-decoy approach using reversed protein sequences were set to 1%. Isotope impurities of the TMT batch were specified in the configuration of TMT modifications to allow MaxQuant the automated correction of TMT intensities.

The data plotted in the Fig. 3f and g and the Extended Data Figure 6d-g were extracted from MQ evidence files, where prior to plotting, all impurity-corrected TMT channels were median-based normalized[11]. Methionine oxidation was removed from the modified sequence, and all duplicated modified sequences were summed up. Next, ratios were calculated against the DMSO controls, where later time points were corrected for their respective DMSO controls of 24h and 48h. The phospho-responses were categorized for regulation by unsupervised K-means clustering algorithm on Z-score normalized phospho-response ratios (using the Euclidean distance after normalizing the sum of ratios across all TMT channels to 1). The obtained 7 clusters in each treatment were further filtered, and the phosphosites were considered as regulated following the criteria for downregulation: the p-response ratio must be < 0.5 after 8h (early) and/or 24h (late downregulation); and for upregulation: the ratio > 2 after 8h and/or 24h.

The protein groups and the evidence files from the total proteome datasets were processed as mentioned above and were used for plotting Extended Data Figure 6b and c. Extended data figure 6c was plotted using peptide abundances as mentioned above, whereas Extended data figure 6b represents the abundance of KRAS protein group across the treatment time points.

The gene set enrichment analysis of the median protein phosphorylation responses in both cell lines for the Fig. 3f was performed using EnrichR tool[12] with integrated NCATS BioPlanet pathway resource. The GO ontology enrichment visualization for Extended Data Figure 6g was performed using Proteomaps[13].

All raw data and search results have been deposited to the ProteomeXchange Consortium (http://www.proteomexchange.org/) via the MassIVE partner repository with the dataset identifier MSV000093122 (ProteomeXchange ID PXD046161). Reviewers can access the dataset at https://massive.ucsd.edu/ProteoSAFe/QueryPXD?id=PXD046161 using the following credentials: Login: MSV000093122_reviewer, Password: revieweronly.

Multiplexed relative proteomics (Degradation Specificity)

GP2d cells in DMEM were seeded at 5×10^6 cells on a 100 mm plate 24 h before treatment. Cells were treated in triplicate by addition of test compounds at 50 nM. After 8 h, the cells were washed twice with 10 mL of cold PBS and lysed in 4% (w/v) SDS in 100 mM Tris at pH 8.5. MiaPaca-2 cells in RPMI 1640 (Invitrogen) were seeded at 5×10^6 cells on a 100 mm plate 24 h before treatment. Cells were treated in triplicate by addition of test compounds at 100 nM. After 8 h, the cells were washed twice with 10 mL of cold PBS and lysed in 500 µL of 100 mM TEAB with 5% (w/v) SDS.

The lysates were pulse sonicated briefly and then centrifuged at 15,000 × g for 10 min. Samples were quantified using a micro-BCA protein assay kit (Thermo Fisher Scientific). 400 µg (Mia Paca-2) or 300 µg (GP2d) of each sample was reduced with DTT, alkalised with iodoacetamide and digested with trypsin using the modified S-TRAP mini (ProtiFi) protocol. Peptide quantification was done using Pierce™ Quantitative Fluorometric Peptide Assay and equal amount from each sample was labelled using TMTproTM 16plex Label Reagent Set Set (GP2d) or TMTproTM 10plex Label Reagent Set Set (Mia Paca-2) (Thermo Fisher Scientific) as per the manufacturer's instructions. The samples were then pooled and desalted using a 7 mm, 3 mL C18 SPE cartridge column (Empore, 3M). The pooled and desalted sample was fractionated using high pH reverse-phase chromatography on an XBridge peptide BEH column (130 Å, 3.5 µm, 2.1 × 150 mm, Waters) on an Ultimate 3000 HPLC system (Thermo Scientific/Dionex). Buffers A (10 mM ammonium formate in water, pH 9) and B (10 mM ammonium formate in 90% acetonitrile, pH 9) were used over a linear gradient of 2% to 100% buffer B over 80 min at a flow rate of 200 µL/min. 80 fractions were collected using a WPS-3000 FC auto-sampler (Thermo Scientific) before concatenation into 20 fractions based on the UV signal of each fraction. All the fractions were dried in a Genevac EZ-2 concentrator and resuspended in 1% formic acid for MS analysis.

The fractions were analyzed sequentially on a Q Exactive HF Hybrid Quadrupole-Orbitrap Mass Spectrometer (Thermo Scientific) coupled to an Dionex Ultimate 3000 RS (Thermo Scientific). Buffers A (0.1% formic acid in water) and B (0.1% formic acid in 80% acetonitrile) were used over a linear gradient from 5% to 35% buffer B over 125 min and then from 35% buffer B to 98% buffer B in 2 min at a constant flow rate of 300 nL/min. The column temperature was 50 °C. The mass spectrometer was operated in data dependent mode with a single MS survey scan from 335-1600 m/z followed by 15 sequential m/z dependent MS2 scans. The 15 most intense precursor ions were sequentially fragmented by higher energy collision dissociation (HCD). The MS1 isolation window was set to 0.7 m/z and the resolution set at 120,000. MS2 resolution was set at 60,000. The AGC targets for MS1 and MS2 were set at 3x106 ions and 1x105 ions, respectively. The normalized collision energy was set at 32%. The maximum ion injection times for MS1 and MS2 were set at 50 ms and 200 ms respectively. The mass accuracy was checked before the initiation of sample analysis.

Peptide and protein identification Raw MS data files for all 20 fractions were merged and searched against the Uniprot-sprot-Human-Canonical database by Maxquant software 2.0.3.0 for protein identification and TMT reporter ion quantitation. The Maxquant parameters were set as follows: enzyme used Trypsin/P; maximum number of missed cleavages equal to two; precursor mass tolerance equal to 10 p.p.m.; fragment mass tolerance equal to 20 p.p.m.; variable modifications:

oxidation (M), dioxidation (MW), acetyl (N-term), deamidation (NQ), Gln -> pyro-Glu (Q N-term); fixed modifications: carbamidomethyl (C). The data was filtered by applying a 1% false discovery rate followed by exclusion of proteins with less than two unique peptides. Quantified proteins were filtered if the absolute fold-change difference between the three DMSO replicates was ≥ 1.5. The mass spectrometry proteomics data generated in cell line Mia Paca-2 have been deposited to the ProteomeXchange Consortium via the PRIDE[14] partner repository with the dataset identifier PXD045416. Data generated in cell line GP2d can be found in the same repository with the dataset identifer PXD045460.

References

1 Farnaby, W. *et al.* BAF complex vulnerabilities in cancer demonstrated via structure-based PROTAC design. *Nat Chem Biol* **15**, 672-680 (2019). https://doi.org:10.1038/s41589-019-0294-6

2 Vonrhein, C. *et al.* Data processing and analysis with the autoPROC toolbox. *Acta Crystallogr D Biol Crystallogr* **67**, 293-302 (2011). https://doi.org:10.1107/S0907444911007773

3 McCoy, A. J. *et al.* Phaser crystallographic software. *J Appl Crystallogr* **40**, 658-674 (2007). https://doi.org:10.1107/S0021889807021206

4 Emsley, P., Lohkamp, B., Scott, W. G. & Cowtan, K. Features and development of Coot. *Acta Crystallogr D Biol Crystallogr* **66**, 486-501 (2010). https://doi.org:10.1107/S0907444910007493

5 Liebschner, D. *et al.* Macromolecular structure determination using X-rays, neutrons and electrons: recent developments in Phenix. *Acta Crystallogr D Struct Biol* **75**, 861-877 (2019). https://doi.org:10.1107/S2059798319011471

6 Agirre, J. *et al.* The CCP4 suite: integrative software for macromolecular crystallography. *Acta Crystallogr D Struct Biol* **79**, 449-461 (2023). https://doi.org:10.1107/S2059798323003595

7 Cardote, T. A. F., Gadd, M. S. & Ciulli, A. Crystal Structure of the Cul2-Rbx1-EloBC-VHL Ubiquitin Ligase Complex. *Structure* **25**, 901-911 e903 (2017). https://doi.org:10.1016/j.str.2017.04.009

8 Pettersen, E. F. *et al.* UCSF ChimeraX: Structure visualization for researchers, educators, and developers. *Protein Sci* **30**, 70-82 (2021). https://doi.org:10.1002/pro.3943

9 Testa, A., Hughes, S. J., Lucas, X., Wright, J. E. & Ciulli, A. Structure-Based Design of a Macrocyclic PROTAC. *Angew Chem Int Ed Engl* **59**, 1727-1734 (2020). https://doi.org:10.1002/anie.201914396

10 Cui, Y. *et al.* A Bidirectional Permeability Assay for beyond Rule of 5 Compounds. *Pharmaceutics* **13** (2021). https://doi.org:10.3390/pharmaceutics13081146

11 Zecha, J. *et al.* Decrypting drug actions and protein modifications by dose- and time-resolved proteomics. *Science* **380**, 93-101 (2023). https://doi.org:10.1126/science.ade3925

12 Chen, E. Y. *et al.* Enrichr: interactive and collaborative HTML5 gene list enrichment analysis tool. *BMC Bioinformatics* **14**, 128 (2013). https://doi.org:10.1186/1471-2105-14-128

13 Liebermeister, W. *et al.* Visual account of protein investment in cellular functions. *Proc Natl Acad Sci U S A* **111**, 8488-8493 (2014). https://doi.org:10.1073/pnas.1314810111

14 Rigden, D. J. & Fernandez, X. M. The 2022 Nucleic Acids Research database issue and the online molecular biology database collection. *Nucleic Acids Res* **50**, D1-D10 (2022). https://doi.org:10.1093/nar/gkab1195

Targeting cancer with small molecule panKRAS degraders – Supporting Information

Johannes Popow*[,1], William Farnaby*[,2,3], Andreas Gollner*[,1], Christiane Kofink*[,1], Gerhard Fischer[1], Melanie Wurm[1], David Zollman [2,3], Andre Wijaya [2,3], Nikolai Mischerikow[1], Carina Hasenoehrl[1], Polina Prokofeva[4], Heribert Arnhof[1], Silvia Arce-Solano[1], Sammy Bell[5], Georg Boeck[1], Emelyne Diers[3], Aileen B. Frost[2,3], Jake Goodwin-Tindall[3], Jale Karolyi-Oezguer[1], Shakil Khan[2,3], Theresa Klawatsch[1], Manfred Koegl[1], Roland Kousek[1], Barbara Kratochvil[1], Katrin Kropatsch[1], Arnel A. Lauber[1], Ross McLennan [2,3], Sabine Olt[1], Daniel Peter[1], Oliver Petermann[1], Vanessa Roessler[1], Peggy Stolt-Bergner[1], Patrick Strack[1], Eva Strauss[1], Nicole Trainor[3], Vesna Vetma[2,3], Claire Whitworth[3], Siying Zhong[3], Jens Quant[1], Harald Weinstabl[1], Bernhard Kuster[4], Peter Ettmayer[#,1], Alessio Ciulli[#,2,3]

1 Boehringer Ingelheim RCV GmbH & Co KG, Dr.-Boehringer-Gasse 5-11, 1221 Vienna, Austria.

2 Centre for Targeted Protein Degradation, School of Life Sciences, University of Dundee, 1 James Lindsay Place, DD1 5JJ, Dundee, UK.

3 Division of Biological Chemistry and Drug Discovery, School of Life Sciences, James Black Centre, University of Dundee, Dow Street, DD1 5EH Dundee, Scotland, U.K.

4 Proteomics and Bioanalytics, School of Life Sciences, Technical University of Munich, 85354 Freising, Germany.

5 Boehringer Ingelheim Pharmaceuticals Inc., 900 Ridgebury Road, Ridgefield, CT 06877, USA.

General information

Commercially available dry solvents were used from Sigma Aldrich. All reagents unless otherwise noted were commercially available and purchased from Sigma Aldrich, Combi Blocks, ABCR, Fluorochem, Activate or Enamine, at least 95% pure and used without further purification. All reactions were carried out in oven- or flame dried glassware under nitrogen atmosphere. Normal phase TLC was carried out on pre-coated silica plates (Kieselgel 60 F254, BDH) with visualization via UV light (UV 254 and/or 365 nm) and/or basic potassium permanganate solution. Isolute® phase separator columns from Biotage were used. Flash column chromatography was performed using either a Teledyne Isco Combiflash Rf or Rf200i or a Biotage Isolera One with prepacked Redisep RF normal phase disposable columns. Reverse phase chromatography was carried out using Biotage SNAP-C18 columns. Strong cation exchange (SCX) chromatography was carried out using Biotage Isolute SCX-2 columns. NMR Spectra were recorded on Bruker 400 MHz, 500 MHz or 600MHz spectrometers as specified. Chemical shifts are quoted in ppm and referenced to the residual solvent signals: ^{1}H NMR δ (ppm) = 7.26 ($CDCl_3$-*d*), ^{13}C NMR δ (ppm) = 77.2 ($CDCl_3$-*d*), ^{1}H NMR δ (ppm) = 2.50 (DMSO-d_6), ^{13}C NMR δ (ppm) = 39.5 (DMSO-d_6). Signal splitting patterns are described as singlet (s), doublet (d), triplet (t), quartet (q), quintet (quin.), multiplet (m), broad (br) or a combination thereof. Coupling constants (*J*) are measured in Hertz (Hz). Diastereomeric ratios (dr) were calculated using the ratios of NMR integrals.

Analytical MS Methods and instrumentation:

Method 1: HRMS data was recorded using a LTQ Orbitrap XL (Thermo Scientific) coupled with a Triversa Nanomate Nanospray ion source (ADVION Bioscience Inc.) The mass calibration was

performed using the Pierce LTQ Velos ESI positive ion calibration solution from Thermo Scientific (Product Nr. 88323).
MS parameters: The scan window was set to 50–400 amu with a maximum injection time of 500 ms and 1 microscan. Resolution of the Orbitrap was 60000 with a mass accuracy ≤ 5 ppm. The ion mode set to positive with a capillary temperature 200 °C and voltage of 60 eV. The tube lens potential was set to 110 eV. 12 NanoESI voltage was 1.45 kV and the N_2 gas pressure set to 0.45 psi. Total sample volume was 5 µL and the acquisition time was 0.4 sec, with 10 scans of averaging per spectrum Sample dilution: 10 mM DMSO stock solution was diluted 1:200 in 50% MeOH +0.01% formic acid.

Method 2: Agilent Technologies 1200 series HPLC connected to an Agilent Technologies 6130 quadrupole LC/MS with an Agilent diode array detector. **Method 2a** was run under the following conditions: Waters Xbridge C18 column, 2.5 µm particle size, 2.1 x 20 mm. Run time 2.1 minutes, flow 1 mL/min, column temperature 60 °C and 5 µL injections. Solvent A (20mM NH_4HCO_3/NH_4OH pH 9), solvent B (MS grade acetonitrile). Start 10% B, gradient 10% - 95% B from 0.0 - 1.5 min, 95% B from 1.5 - 2.0 min, gradient 95% - 10% B from 2.0 – 2.1 min. Purity was determined via UV detection with a bandwidth of 170 nm in the range from 230-400 nm. **Method 2b** used a Waters XBridge column (50 mm × 2.1 mm, 3.5 µm particle size) and the compounds were eluted with a gradient 5−95% acetonitrile/water + 0.1% formic acid ("acidic method").

Preparative purification methods and instrumentation:
Method 3: Preparative HPLC was performed on a Gilson system with Waters C18 columns (50 mm x 150 mm; 10 µm particle size) and a gradient of 10% to 95% acetonitrile in water over 8 minutes and a flow rate of 150 mL/min, with a SunFire column and 0.1% formic acid (**Method 3a**) or a XBridge column and 0.5% ammonium bicarbonate/ammonia buffer pH 9 (**Method 3b**) in the aqueous phase.
Method 4: Preparative HPLC was performed on a Waters Prep 150 LC system with a Waters XBridge C18 column (100 mm x 19 mm; 5 µm particle size) and a gradient of 5% to 95% acetonitrile in water over 10 minutes and a flow rate of 25 mL/min, with 0.1% formic acid (**Method 4a**) or ammonia (**Method 4b**) in the aqueous phase.
Method A: Chrial purification
Chiral separations were performed on a Agilent 1100/1200 system using a Chiralpak; Part. No. 85394; IE, 5 µm; 150 x 2.1 mm column. Solvents used were n-Heptan / EtOH + 0,1% DEA, 0-70% isocratic flow. Detection signal was UV 315 nm, (bandwidth 170, reference off) and the spectrum range: 190 – 400 nm; slit: 4 nm. Peak width > 0.0031 min (0.063 s response time, 80Hz), 0,5 µL standard injection and 1.2 mL/min flow at 45°C column temperature.
Stop time: 5 min

Abbreviations used: aq. for aqueous, BH_3-DMS for borane-dimethylsulfide complex, Boc for *N*-*tert*-butyloxycarbonyl, Boc_2O for di-*tert*-butyl dicarbonate, DCE for 1,2-dichloroethane, DCM for dichloromethane, DEA for diethylamine, DMA for *N*,*N*-dimethylacetamide, DMF for *N*,*N*-dimethylformamide, DIPEA for *N*,*N*-diisopropylethylamine, DMSO for dimethylsulfoxide, Et_3N for triethylamine, EtOAc for ethyl acetate, HATU for 1-[bis(dimethylamino)methylene]-1*H*-1,2,3-triazolo[4,5-*b*]pyridinium 3-oxideHexafluorophosphate, KOAc for potassium acetate, MeOH for methanol, MsCl for methanesulfonyl chloride, PTSA for *p*-toluene sulfonic acid monohydrate, sat. for saturated, $SOCl_2$ for thionyl chloride, THF for tetrahydrofuran.

Synthesis of pan KRAS binders

Synthesis of KRAS binder Compound 1:

Intermediate **Int-6**:

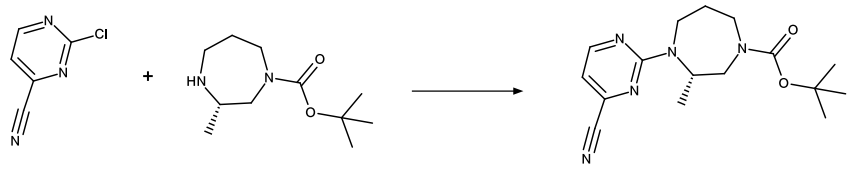

Int-1

To a solution of (S)-tert-butyl-3-methyl-1,4-diazepane-1-carboxylate (846 mg, 3.948 mmol, 1.0 eq.) and 2-chloropyrimidine-4-carbonitrile (529 mg, 3.791 mmol, 1.0 eq) in DMSO (4 ml) is added TEA (1.1 ml, 7.896 mmol, 2.0 eq.) at rt. The reaction mixture is stirred at 80 °C for 1 h. After complete conversion the reaction mixture is cooled to rt and water and EtOAc is added. The phases are separated. The organic layer is washed with water, dried over sodium sulfate, then filtered and concentrated under reduced pressure to the get crude product which is purified by NP chromatography (0-20%, EtOAc/Heptane) to obtain intermediate **Int-1** (754 mg, 2.376 mmol, 63 % yield).

^{1}H NMR (DMSO-d_6) δ: 8.63 (br d, J=4.6 Hz, 1H), 7.08-7.13 (m, 1H), 5.07-5.17 (m, 0.19H rotamer), 5.01 (br d, J=5.3 Hz, 0.84H rotamer), 4.13 (br d, J=14.4 Hz, 0.56H rotamer), 4.05 (br d, J=14.2 Hz, 0.49H rotamer), 3.64-3.94 (m, 2H), 2.75-3.12 (m, 2H), 1.46-1.80 (m, 2H), 1.27 (br s, 5.71H rotamer), 1.16 (s, 3.18H rotamer), 1.05 (s, 3H)

Integrals may not add up to whole numbers due to overlapping rotamers or rotamers resonating under residual DMSO-d6 or HDO peaks

^{13}C NMR (DMSO-d_6) δ: 160.8, 160.6, 160.4, 153.9, 153.7, 140.5, 116.3, 112.1, 112.0, 78.5, 78.4, 52.2, 48.6, 48.3, 47.7, 47.6, 27.8, 27.7, 27.6, 26.1, 26.0, 15.0

More carbon peaks detected than present in the structure due to presence of rotamers

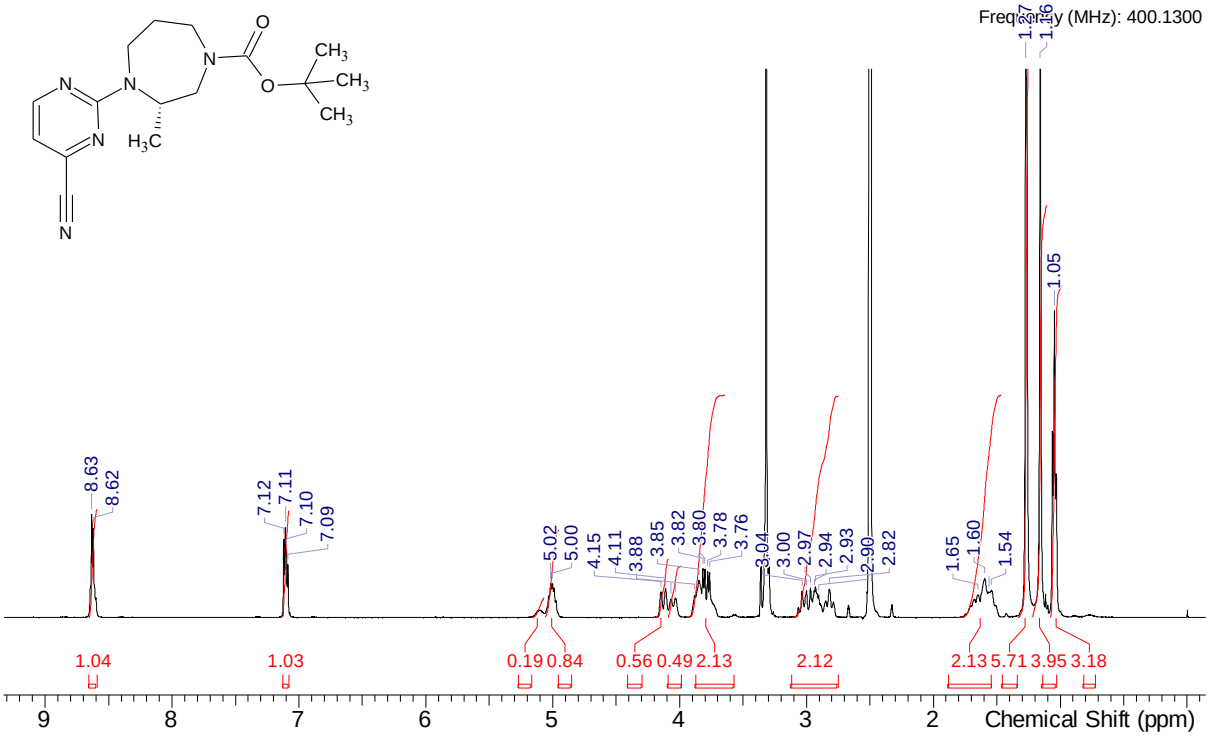

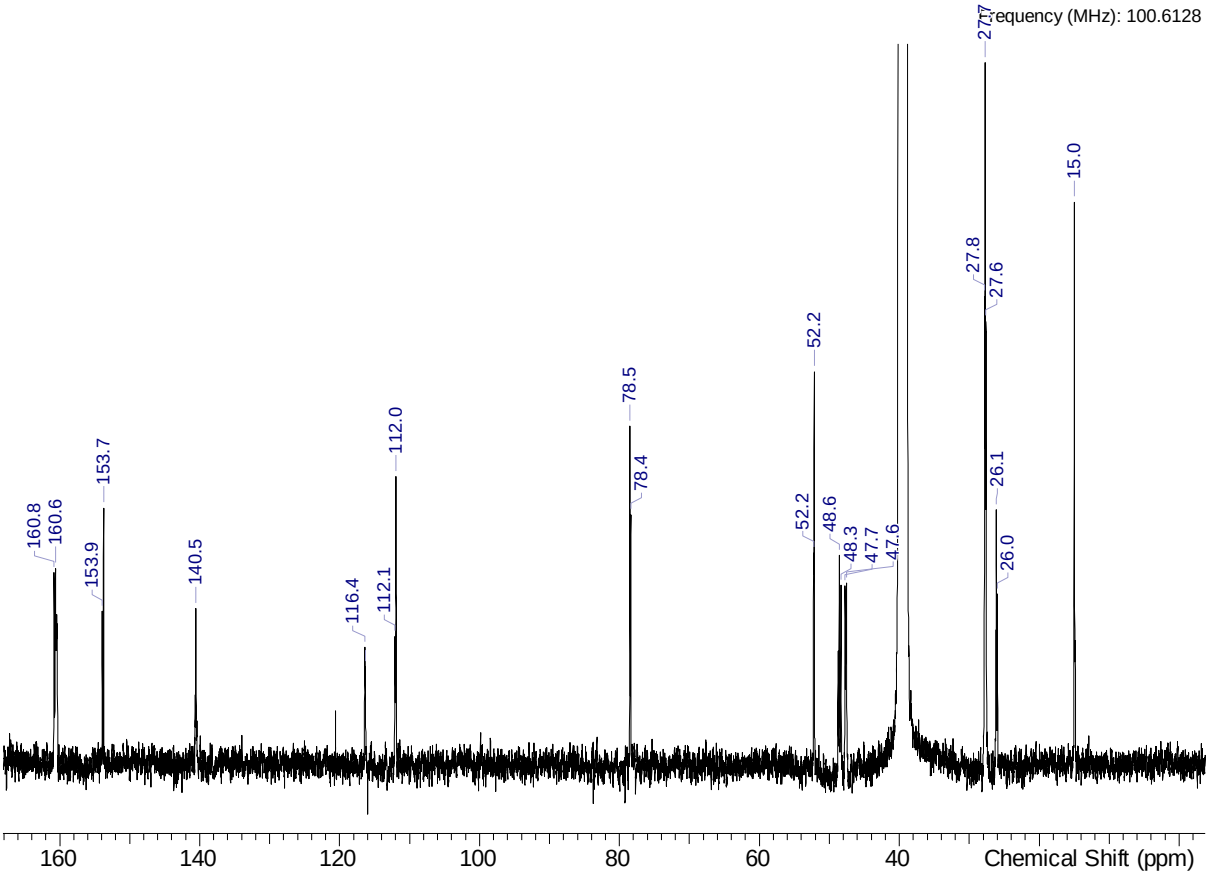

HRMS (*m/z*): $[M+H]^+$ calcd. for C16H23N5O2 , 318.19245; found, 318.19245

Intermediate **Int-2**:

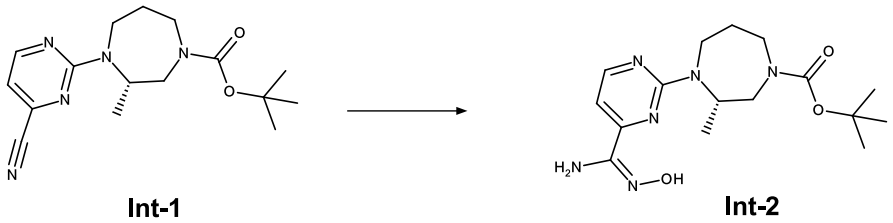

To a solution of **Int-1** (33.85 g, 106.65 mmol, 1.0 eq) in EtOH (270 ml) is added hydroxylamine solution 50 % in water (13.05 ml, 213.30 mmol, 2.0 eq) at rt. The reaction mixture is stirred at 60 °C for 1 h. After complete conversion the reaction mixture is concentrated under reduced pressure to afford **Int-2** (33.8 g, 102.7 mmol, 96 % yield) which is used for the next step without further purification.

^{1}H NMR (DMSO-d_6) δ: 10.06-10.21 (m, 1H), 8.29 (d, J=5.1 Hz, 1H), 6.90 (br dd, J=12.9, 4.8 Hz, 1H), 5.75 (br d, J=9.9 Hz, 2H), 5.10 (br d, J=14.2 Hz, 1H), 4.25 (br dd, J=57.4, 13.6 Hz, 1H), 3.63-3.92 (m, 2H), 3.25 (br t, J=13.3 Hz, 1H), 2.75-3.08 (m, 2H), 1.44-1.84 (m, 2H), 1.25 (br d, J=8.6 Hz, 5H), 1.15 (s, 3H), 1.10-1.31 (m, 1H), 1.05 (br d, J=3.3 Hz, 3H)

^{13}C NMR (DMSO-d_6) δ: 160.3, 157.8, 157.5, 154.0, 153.8, 148.7, 148.4, 103.5, 78.4, 52.6, 48.0, 27.7, 26.5, 15.3

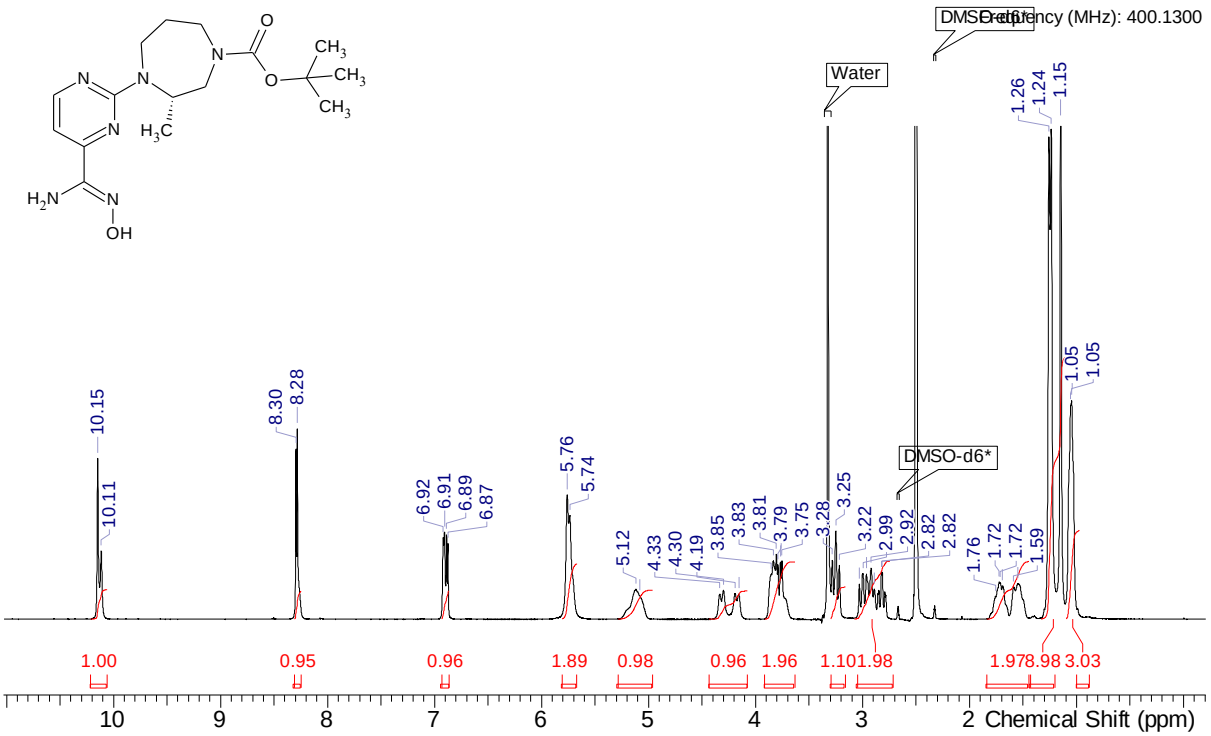

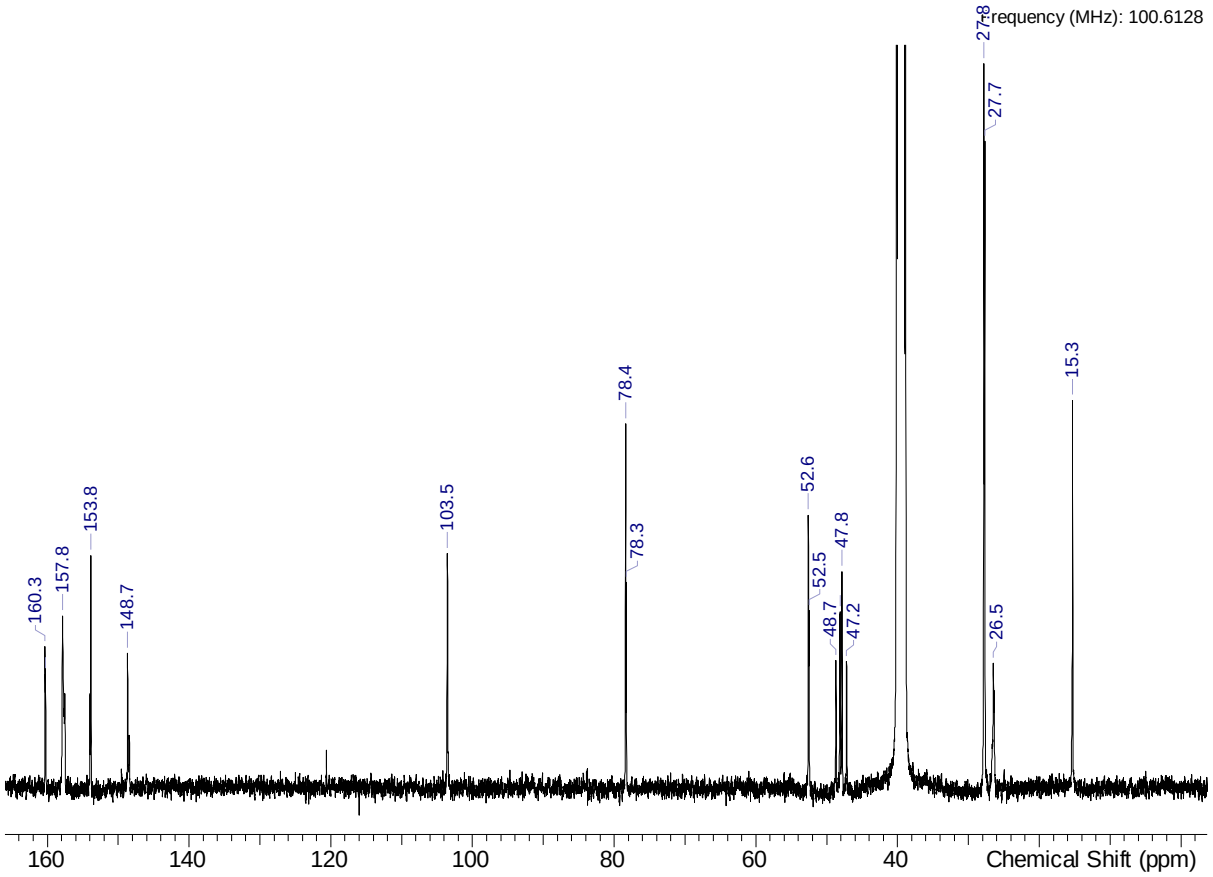

HRMS (*m/z*): $[M+H]^+$ calcd. for C16H26N6O3 , 351.21371; found, 351.21371

Intermediate **Int-4**:

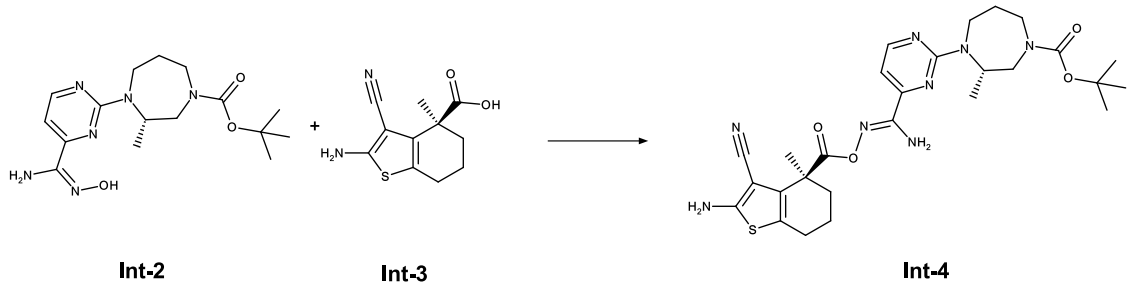

To a stirred solution of **Int-2** (2.53 g, 10.70 mmol, 1.0 eq.) in DMSO (10 ml) are added TEA (2.17 g, 21.40 mmol, 2.0 eq.) and HATU (4.27 g, 11.24 mmol, 1.10 eq.) at rt. The mixture is stirred for 15 min at rt. **Int-3** (3.75 g, 10.70 mmol, 1.0 eq) is added at rt and stirred overnight. After complete conversion the reaction mixture is diluted with water and EtOAc. The phases are separated. The organic layer is washed with water, dried over sodium sulfate, filtered, and concentrated under reduced pressure to get the crude product. This crude material is purified by normal phase column chromatography (0-5%, DCM/MeOH, 15 ml 7N NH3 / l solvent) to afford **Int-4** (4.59 g, 8.071 mmol, 75 % yield).

^{1}H NMR (DMSO-d_6) δ: 8.30-8.52 (m, 1H), 6.89-7.08 (m, 3H), 5.41-6.84 (m, 2H), 5.00-5.26 (m, 1H), 4.28-4.50 (m, 0.48H rotamer), 4.18 (br d, J=14.7 Hz, 0.36H rotamer), 3.60-3.94 (m, 2H), 3.15-3.31 (m, 2H), 2.97 (br dd, J=22.8, 12.9 Hz, 2H), 2.41-2.47 (m, 1H), 2.12-2.21 (m, 1H), 1.74 (br d, J=8.1 Hz, 4H), 1.60 (s, 4H), 1.26 (br s, 5H rotamer), 1.15 (s, 4H rotamer), 1.05 (br s, 3H)

Integrals may not add up to whole numbers due to overlapping rotamers or rotamers resonating under residual DMSO-d6 or HDO peaks

^{13}C NMR (DMSO-d_6) δ: 171.9, 163.9, 160.9, 159.5, 156.4, 156.2, 154.3, 154.0, 153.6, 132.9, 132.9, 121.1, 119.6, 117.6, 117.5, 105.4, 105.3, 82.7, 78.9, 78.8, 53.0, 52.9, 49.2, 48.8, 48.3, 47.8, 44.8, 36.1, 28.3, 28.2, 24.4, 24.3, 20.4, 15.9, 15.7

More carbon peaks detected than present in the structure due to presence of rotamers

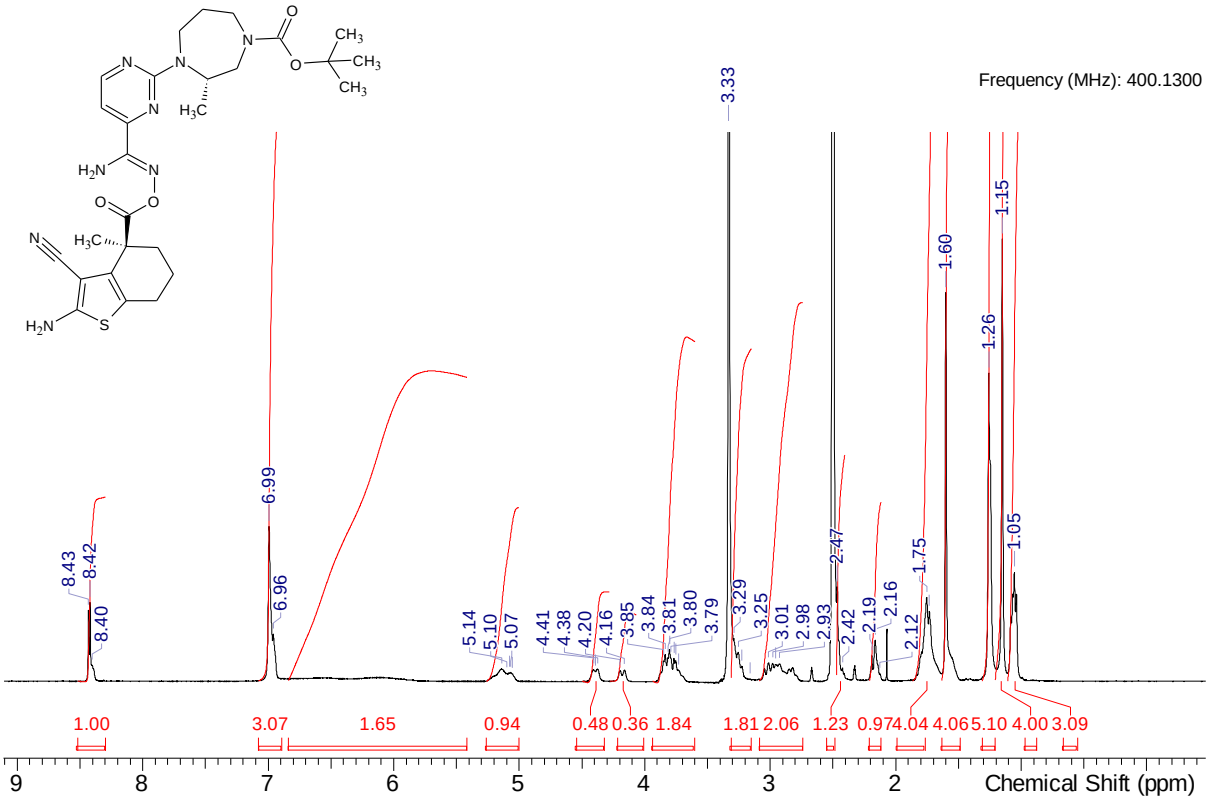

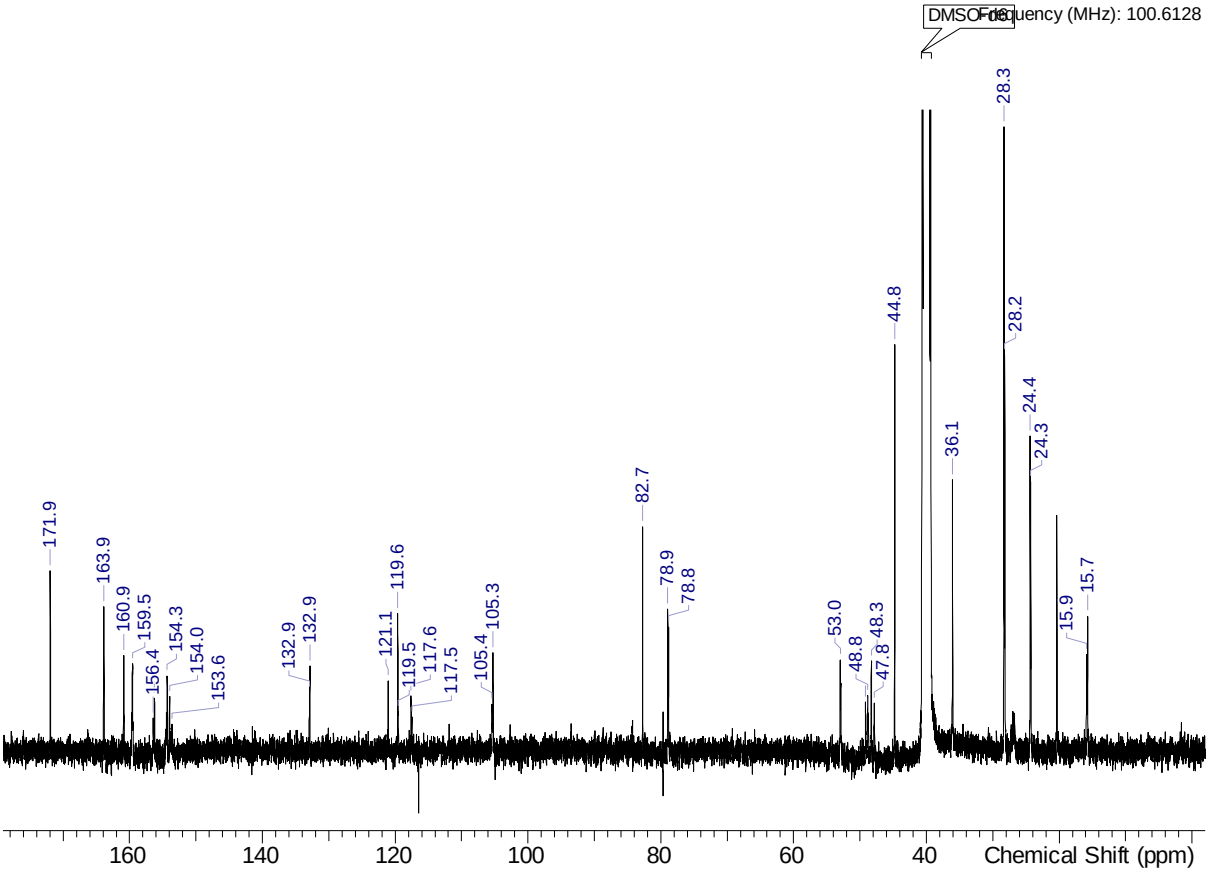

HRMS (*m/z*): $[M+H]^+$ calcd. for C27H36N8O4S , 569.26530; found, 469.21271 (-Boc)

Intermediate **Int-5**:

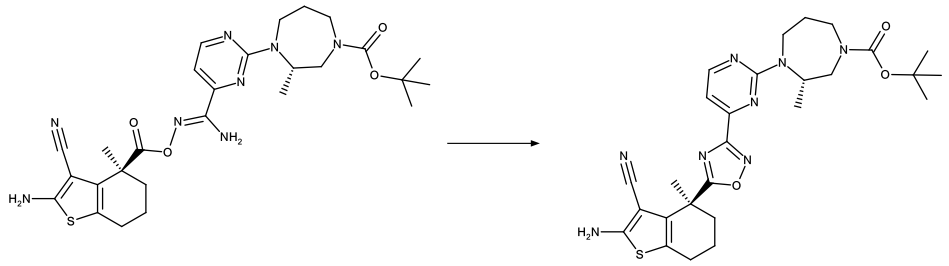

Int-4 **Int-5**

To a stirred solution of **Int-4** (300 mg, 0.528 mmol, 1.0 eq) in THF (3 mL) is added DBU (160 mg, 1.06 mmol, 2.0 eq) at rt. The reaction mixture is stirred at 70 °C overnight. After complete conversion the reaction mixture is concentrated under reduced pressure to get the crude product. The crude product is purified by normal phase column chromatography (0-2%, DCM/MeOH, 15 ml 7N NH3 / l solvent) to afford **Int-5** (231 mg, 0.419 mmol, 79 % yield.

^{1}H NMR (DMSO-d_6) δ: 8.55 (br d, J=4.4 Hz, 1H), 7.12 (br d, J=5.0 Hz, 1H), 7.08 (s, 2H), 5.22-5.38 (m, 0.45H rotamer), 5.11 (br d, J=5.0 Hz, 0.52H rotamer), 4.07-4.36 (m, 1H), 3.65-3.92 (m, 2H), 2.69-3.11 (m, 2H), 2.52-2.57 (m, 2H), 2.01-2.25 (m, 2H), 1.84 (br s, 3H), 1.79 (s, 3H), 1.63-1.76 (m, 1H), 1.47-1.63 (m, 1H), 1.27 (br s, 2H rotamer), 1.17 (br d, J=11.3 Hz, 7H rotamer), 1.06 (br d, J=6.3 Hz, 3H)

Integrals may not add up to whole numbers due to overlapping rotamers or rotamers resonating under residual DMSO-d6 or HDO peaks

^{13}C NMR (DMSO-d_6) δ: 184.9, 167.6, 167.5, 164.2, 161.3, 160.5, 154.5, 154.3, 154.0, 131.8, 120.1, 120.0, 116.2, 116.1, 108.1, 107.9, 81.8, 79.0, 79.0, 78.9, 53.1, 52.8, 49.0, 48.4, 48.2, 37.4, 37.2, 28.3, 28.2, 28.0, 26.8, 26.6, 25.2, 24.0, 19.9, 15.9, 15.7

More carbon peaks detected than present in the structure due to presence of rotamers

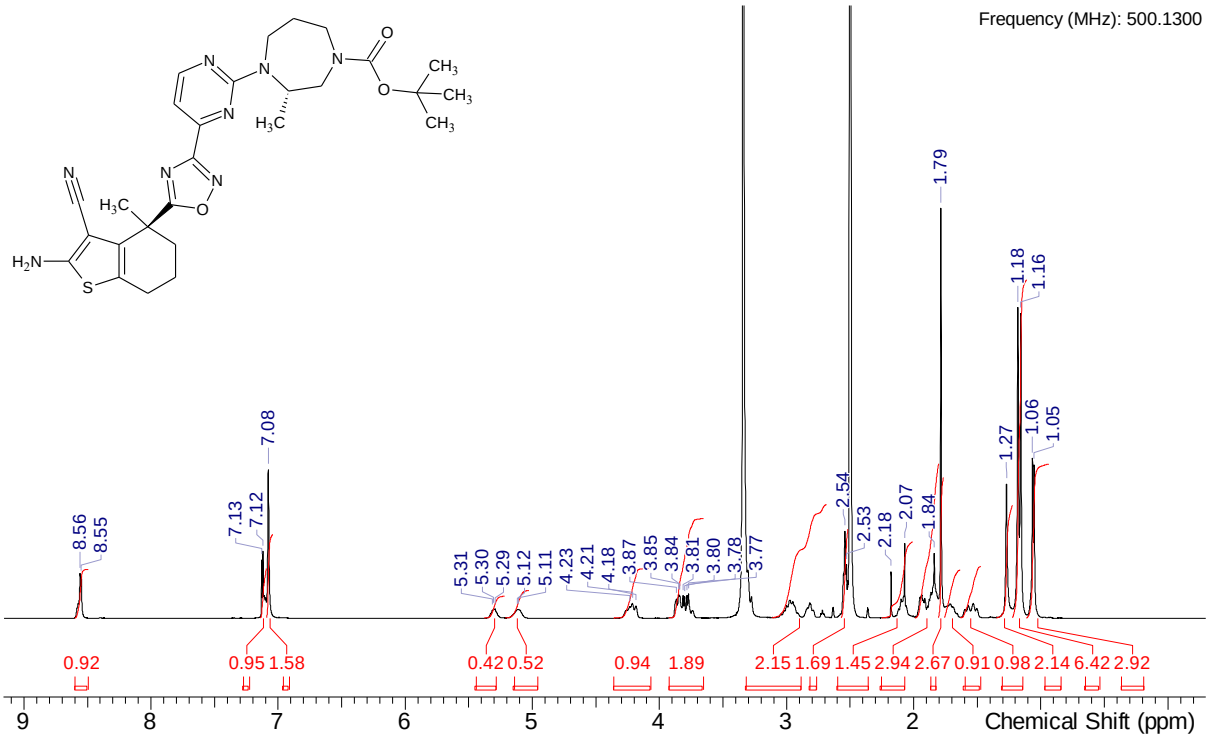

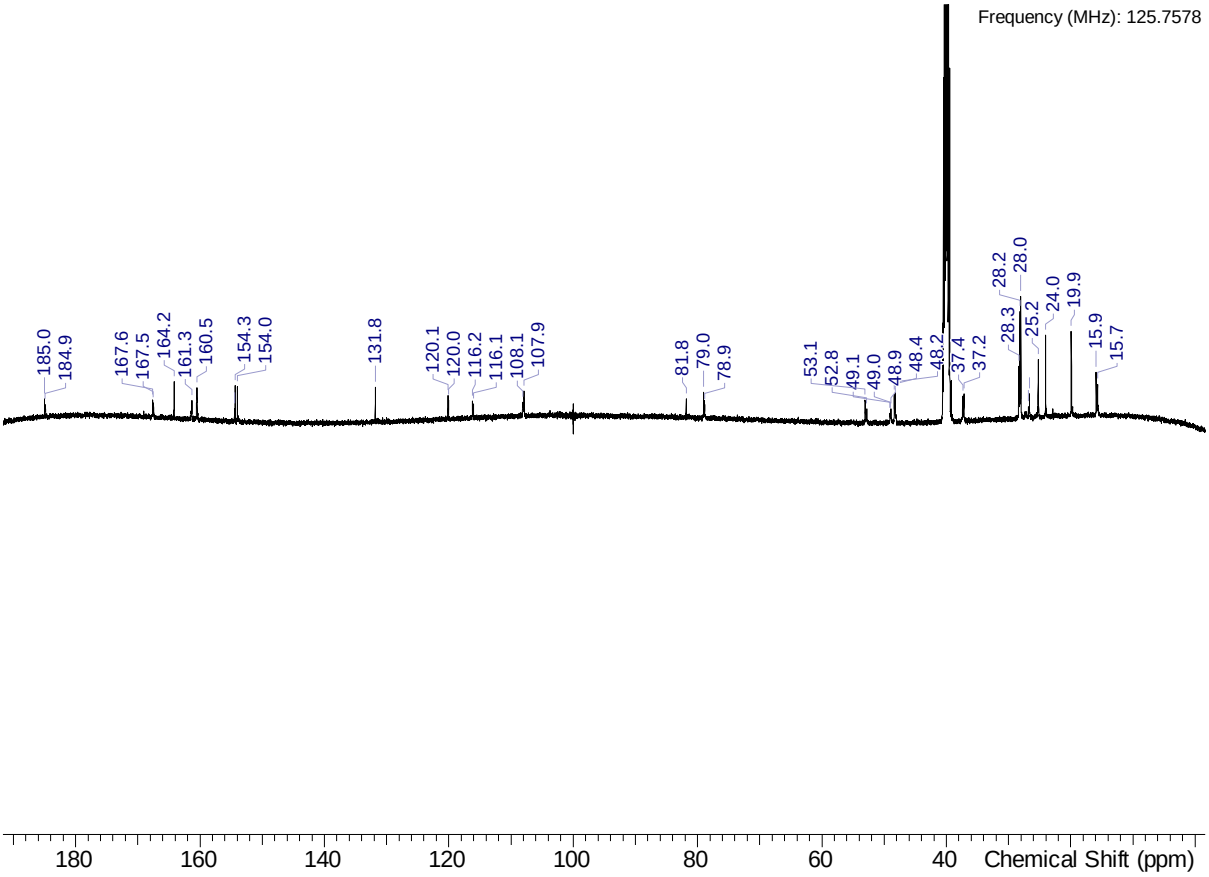

The spike observed at 99.5 ppm is an artefact from the carrier frequency.

HRMS (*m/z*): $[M+H]^+$ calcd. for C27H34N8O3S , 551.25473; found, 551.25421

Compound **1**:

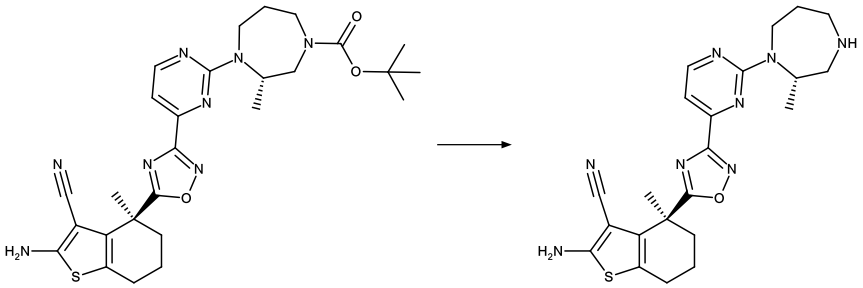

Int-5 **1**

To a stirred solution of **Int-5** (19.01 g, 34.52 mmol, 1.0 eq.) in MeOH (350 mL) is added conc. HCl (32.88 mL, 345.21 mmol, 10.0 eq.) at rt. The reaction mixture is stirred at 50 °C for 2 h. After complete conversion the reaction mixture is concentrated under reduced pressure and diluted with water. The aqueous phase is extracted with DCM. The combined organic layers are dried over sodium sulfate, filtered and concentrated under reduced pressure to afford crude **1** (14.54 g, 32.27 mmol, 94 % yield) which can be used for the next step without further purification.

^{1}H NMR (DMSO-d_6) δ: 8.56 (d, J=4.7 Hz, 1H), 7.11 (br d, J=4.1 Hz, 1H), 7.07 (s, 2H), 4.57-4.78 (m, 1H), 4.17-4.39 (m, 1H), 3.12-3.29 (m, 3H), 2.98 (br d, J=11.7 Hz, 1H), 2.54 (br d, J=5.0 Hz, 4H), 2.03-2.13 (m, 1H), 1.80-1.99 (m, 3H), 1.78 (s, 3H), 1.62 (br s, 2H), 0.97-1.08 (m, 3H) 1H under DMSO

^{13}C NMR (DMSO-d_6) δ: 184.5, 167.2, 163.8, 161.1, 160.1, 153.5, 131.4, 119.8, 115.8, 107.4, 81.4, 54.9, 54.6, 51.7, 50.1, 36.8, 29.3, 24.8, 23.6, 19.5, 15.7, 1C under DMSO

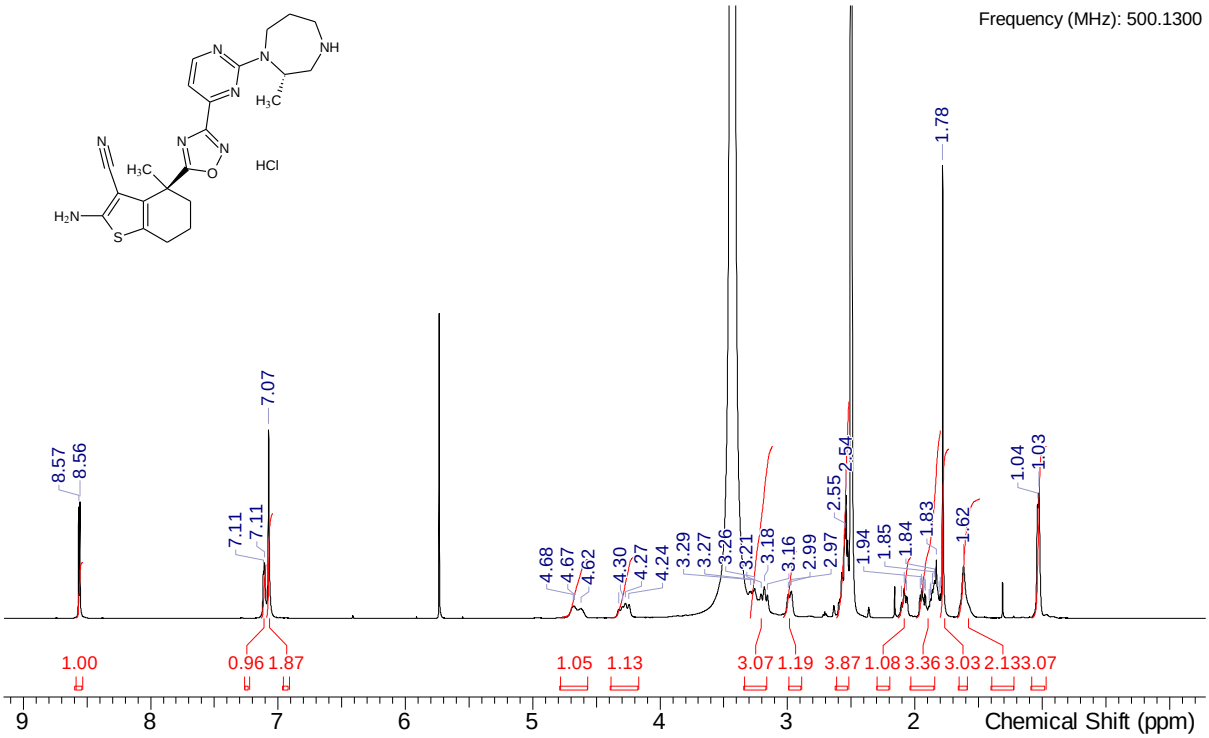

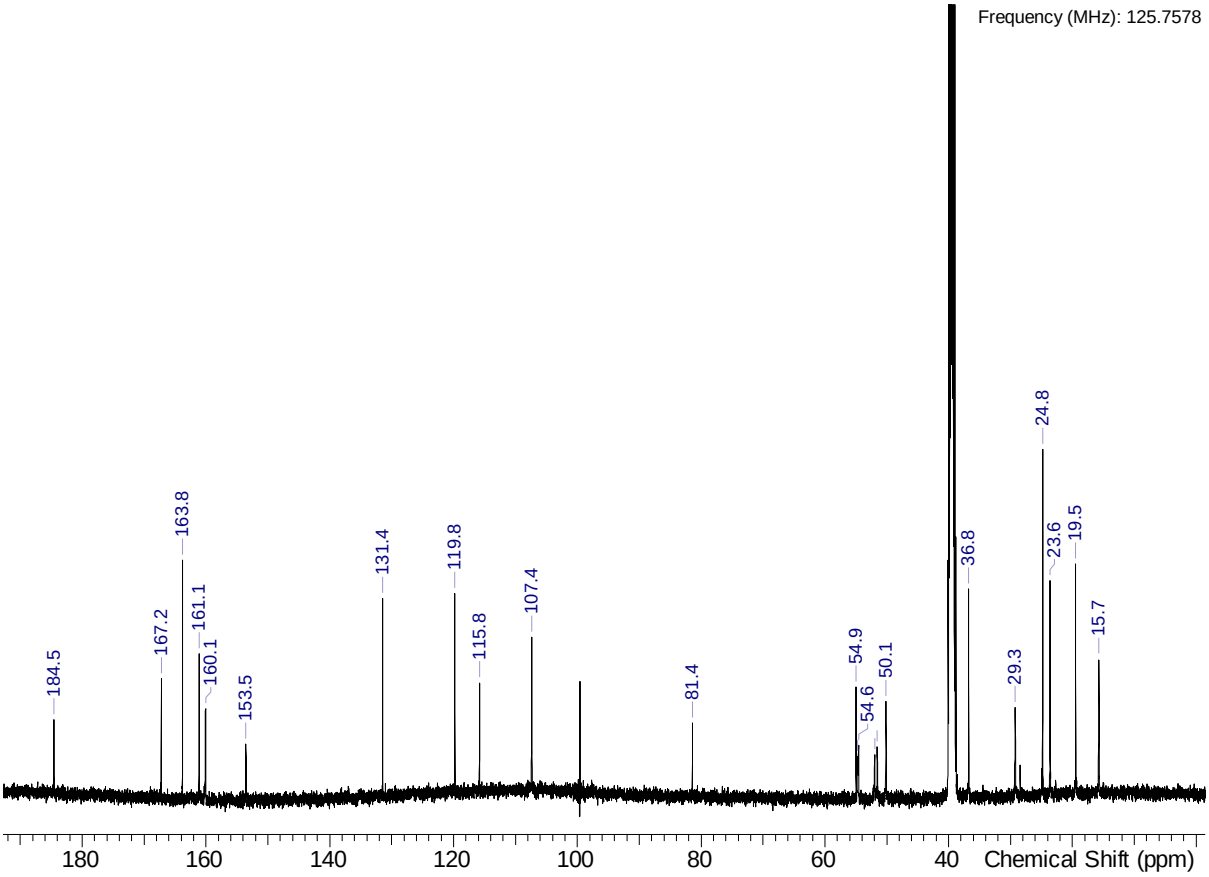

HRMS (*m/z*): $[M+H]^+$ calcd. for C22H26N8OS , 451.20231; found, 451.20224

Compound **S-1**:

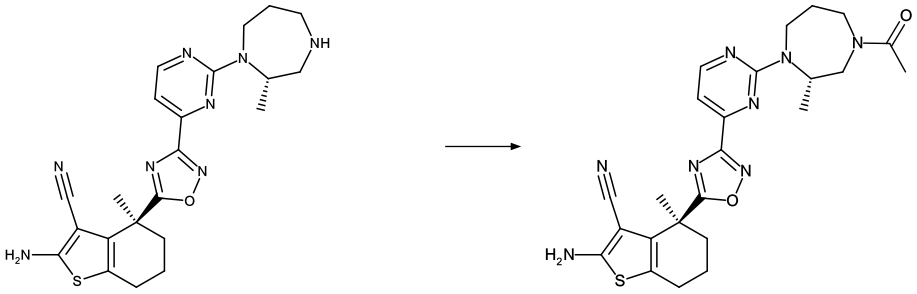

1 **S-1**

To a stirred solution of **1** (30 mg, 0.067 mmol, 1.0 eq.) in NMP (1 mL) was added acetic acid (0.011 mL, 0.200 mmol, 3.0 eq.) at 0°C was added HATU (37 mg, 0.093 mmol, 1.4 eq.) and DIPEA (0.058 mL, 0.333 mmol, 5.0 eq.). The mixture was stirred for 15 min and afterwards diluted with water and acetonitrile, purified by RP chromatography (Method 3b) to obtain **S-1** (28 mg, 0.057 mmol, 85 % yield).

^{1}H NMR (DMSO-d_6) δ: 8.57 (d, J=5.0 Hz, 0.41H rotamer), 8.56 (d, J=4.7 Hz, 0.61H rotamer), 7.14 (d, J=5.0 Hz, 0.52H rotamer), 7.13 (br d, J=5.0 Hz, 0.53H rotamer), 7.08 (s, 2H), 5.00-5.25 (m, 0.44H rotamer), 4.81-4.99 (m, 0.6H rotamer), 4.10-4.45 (m, 2H), 3.96-4.09 (m, 0.44H rotamer), 3.79 (br d, J=13.9 Hz, 0.59H rotamer), 3.35-3.41 (m, 1H), 2.95 (br dd, J=13.4, 12.1 Hz, 0.61H rotamer), 2.73 (br s, 0.47H rotamer), 2.52-2.60 (m, 2H), 2.04-2.14 (m, 1H), 1.75-1.99 (range, 9H rotamer), 1.71 (br s, 2H), 1.13 (br s, 1.3H rotamer), 1.06 (br s, 1.77H rotamer)

Integrals may not add up to whole numbers due to overlapping rotamers or rotamers resonating under residual DMSO-d6 or HDO peaks

^{13}C NMR (DMSO-d_6) δ: 184.5, 168.9, 168.8, 168.5, 167.0, 167.0, 163.7, 163.7, 160.9, 160.3, 160.0, 153.5, 131.3, 119.6, 115.7, 107.8, 107.6, 81.3, 81.3, 53.4, 51.0, 49.9, 49.0, 48.3, 48.1, 46.4, 36.7, 28.5, 28.2, 26.0, 25.7, 24.7, 23.5, 21.0, 20.5, 19.4, 15.6, 15.4, 15.3, 15.1

More carbon peaks detected than present in the structure due to presence of rotamers

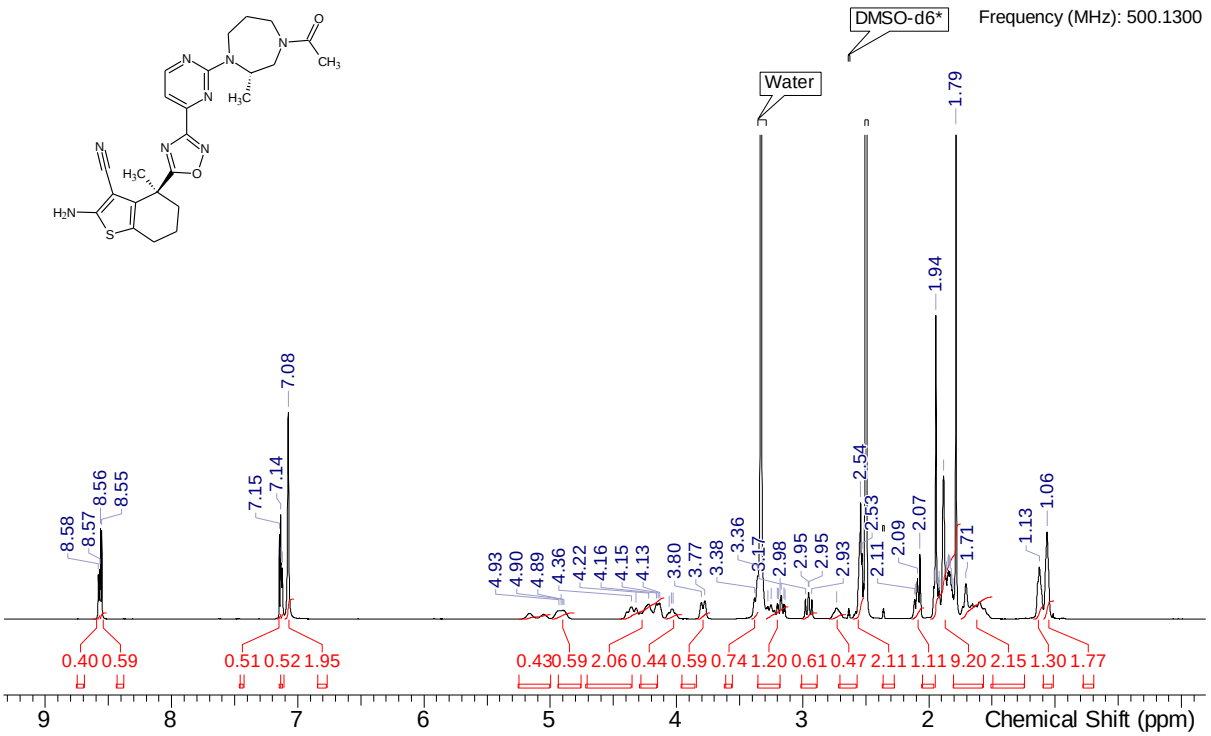

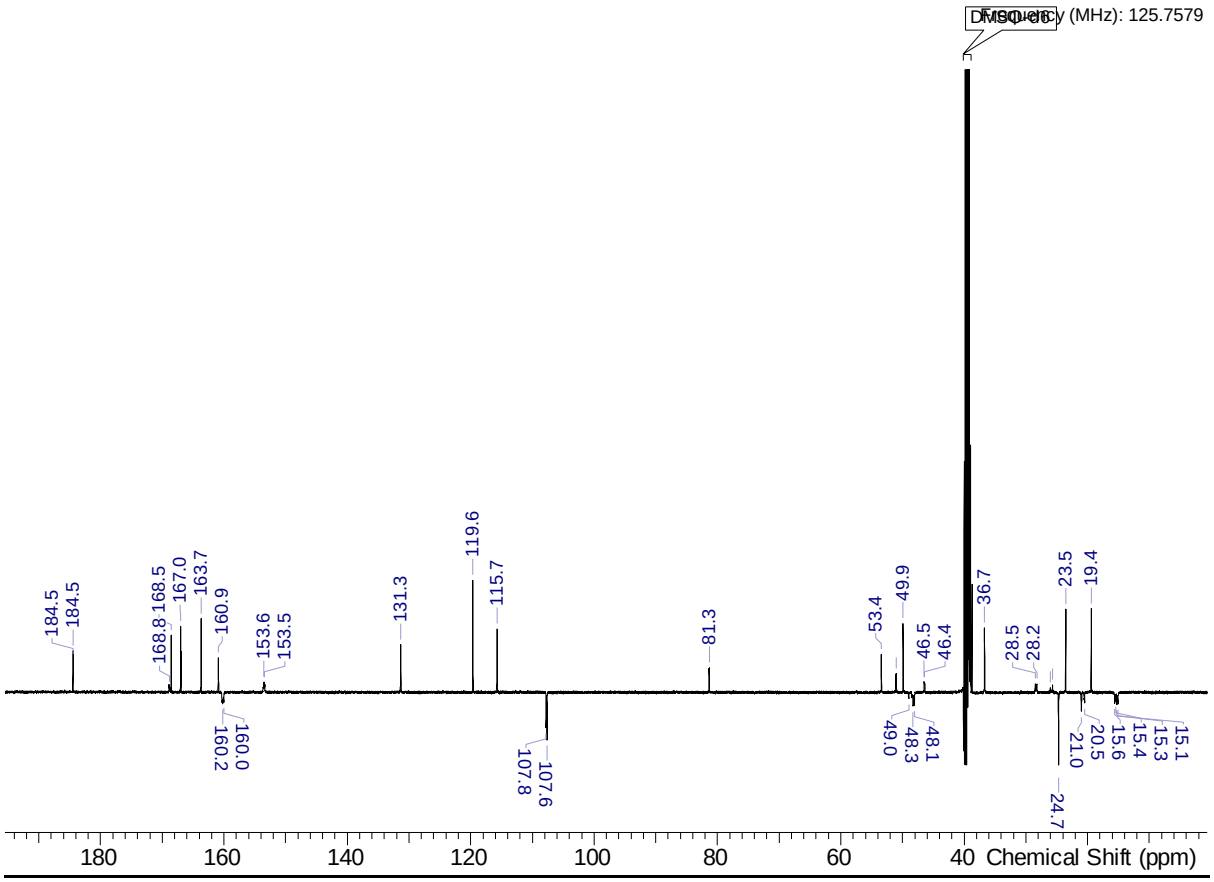

HRMS (*m/z*): $[M+H]^+$ calcd. for C24H28N8O2S , 493.21287; found, 493.21304

Synthesis of PROTAC compounds

Synthesis of compound 2

Intermediate **Int-6**:

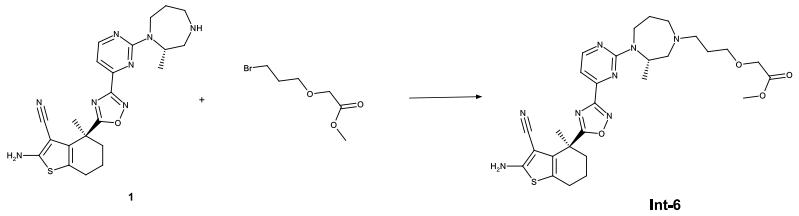

To a solution of **1** (450 mg, 0.899 mmol, 90%, 1.0 eq.) in acetonitrile (5 mL) was added 2-(3-bromopropoxy)acetate (399 mg, 1.798 mmol, 95%, 2.0 eq.) and DIPEA (408 mg, 3.146 mmol, 3.5 eq.). The mixture was heated to 50°C and stirred at this temperature for 16 h. The mixture is cooled to RT, filtered and purified by RP HPLC (Method 3b) and lyophilized to obtain **Int-6** (338 mg, 0.582 mmol, 65% yield).

^{1}H NMR (DMSO-d_6) δ: 8.56 (d, J=4.6 Hz, 1H), 7.04-7.13 (m, 3H), 4.70 (dt, J=11.3, 5.9 Hz, 1H), 4.29 (br t, J=16.3 Hz, 1H), 4.02 (br d, J=7.1 Hz, 2H), 3.60 (br d, J=6.3 Hz, 3H), 3.41 (t, J=6.3 Hz, 2H), 3.13-3.28 (m, 1H), 3.00 (br d, J=14.2 Hz, 1H), 2.81 (br d, J=11.9 Hz, 1H), 2.52-2.59 (m, 3H), 2.39-2.48 (m, 2H), 2.03-2.16 (m, 1H), 1.75-2.00 (m, 6H), 1.49-1.75 (m, 4H), 1.02 (br s, 3H) 1H under DMSO

^{13}C NMR (DMSO-d_6) δ: 184.4, 170.7, 167.1, 163.7, 160.7, 160.1, 160.0, 153.5, 153.5, 131.3, 119.6, 115.7, 107.2, 81.4, 69.0, 67.4, 59.7, 59.3, 56.3, 52.6, 52.0, 51.2, 50.0, 36.7, 27.7, 27.5, 27.3, 24.7, 23.6, 19.4, 15.7, 15.6 1C under DMSO, 1 carbon only observed in HSQC

More carbon peaks detected than present in the structure due to presence of rotamers

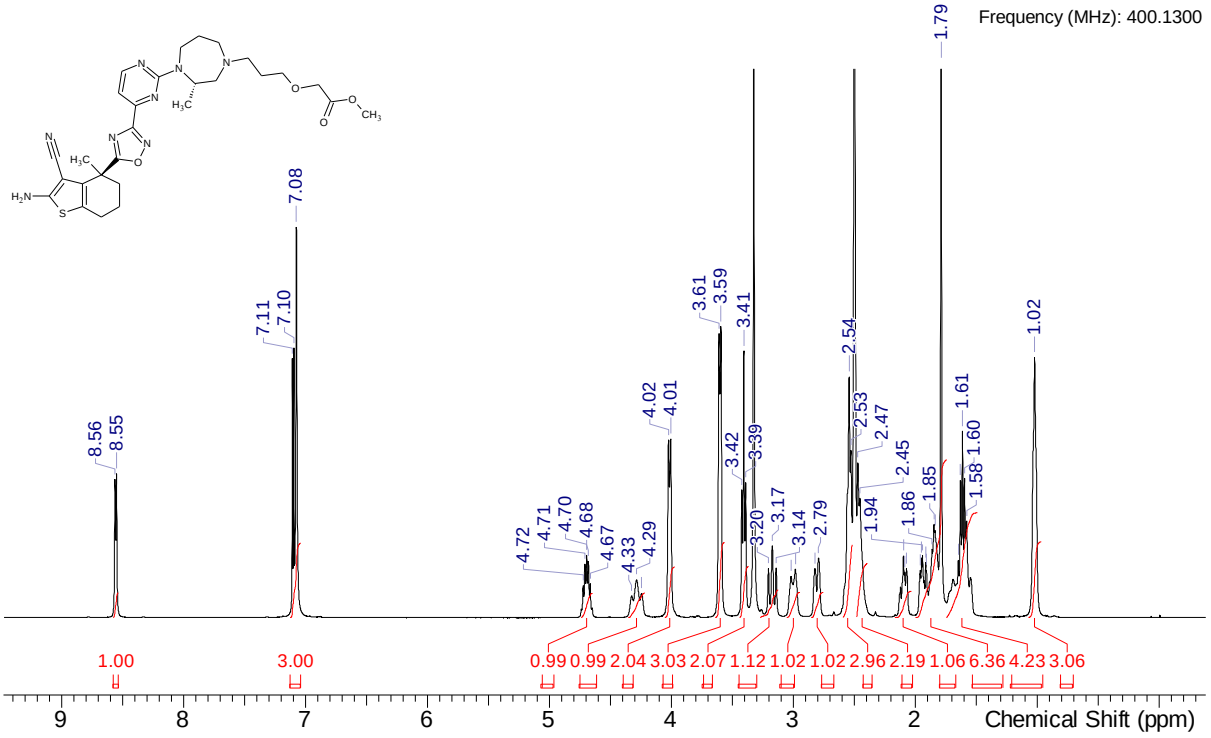

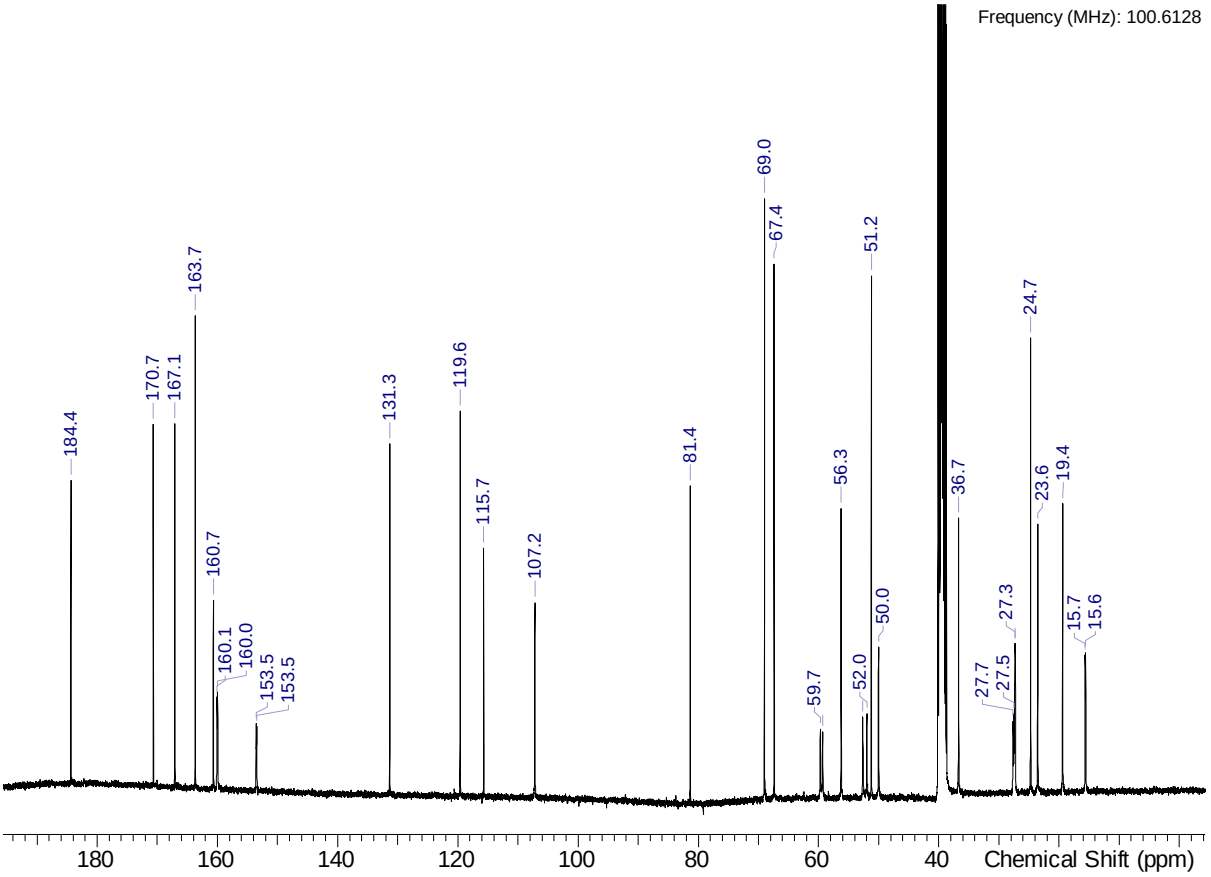

HRMS (*m/z*): $[M+H]^+$ calcd. for C28H36N8O4S , 581.26530; found, 581.26593

Intermediate **Int-7**:

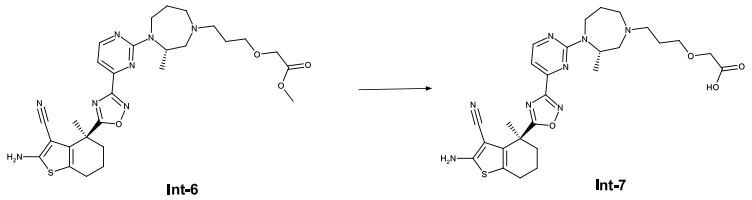

To a solution of **Int-6** (300 mg, 0.517 mmol, 1.0 eq.) in MeOH (5 mL) is added aqueous NaOH solution (2 mL, 2 M) and the mixture is stirred at 50°C for 1 h. The mixture is cooled to RT and the volatiles are removed under reduced pressure. The residue is taken up in a mixture of acetonitrile and water, purified by RP HPLC (Method 3b) and lyophilized to obtain **Int-7** (251 mg, 0.443 mmol, 86% yield).

^{1}H NMR (DMSO-d_6) δ: 8.55 (d, J=4.8 Hz, 1H), 7.10 (br s, 1H), 7.08 (s, 2H), 4.86 (br s, 1H), 4.34 (br s, 1H), 3.42-3.96 (m, 4H), 3.30 (br d, J=11.7 Hz, 3H), 3.01 (br d, J=11.2 Hz, 1H), 2.65-2.93 (m, 4H), 2.52-2.60 (m, 2H), 2.02-2.24 (m, 1H), 1.81-2.00 (m, 5H), 1.79 (s, 3H), 1.57-1.74 (m, 2H), 1.00-1.13 (m, 3H)

^{13}C NMR (DMSO-d_6) δ: 184.4, 172.5, 167.1, 163.7, 160.5, 160.0, 153.4, 131.3, 119.7, 115.8, 107.6, 81.4, 68.7, 57.3, 56.9, 56.5, 54.2, 53.3, 48.2, 38.7, 25.7, 25.6, 24.7, 23.6, 19.4, 1C under DMSO

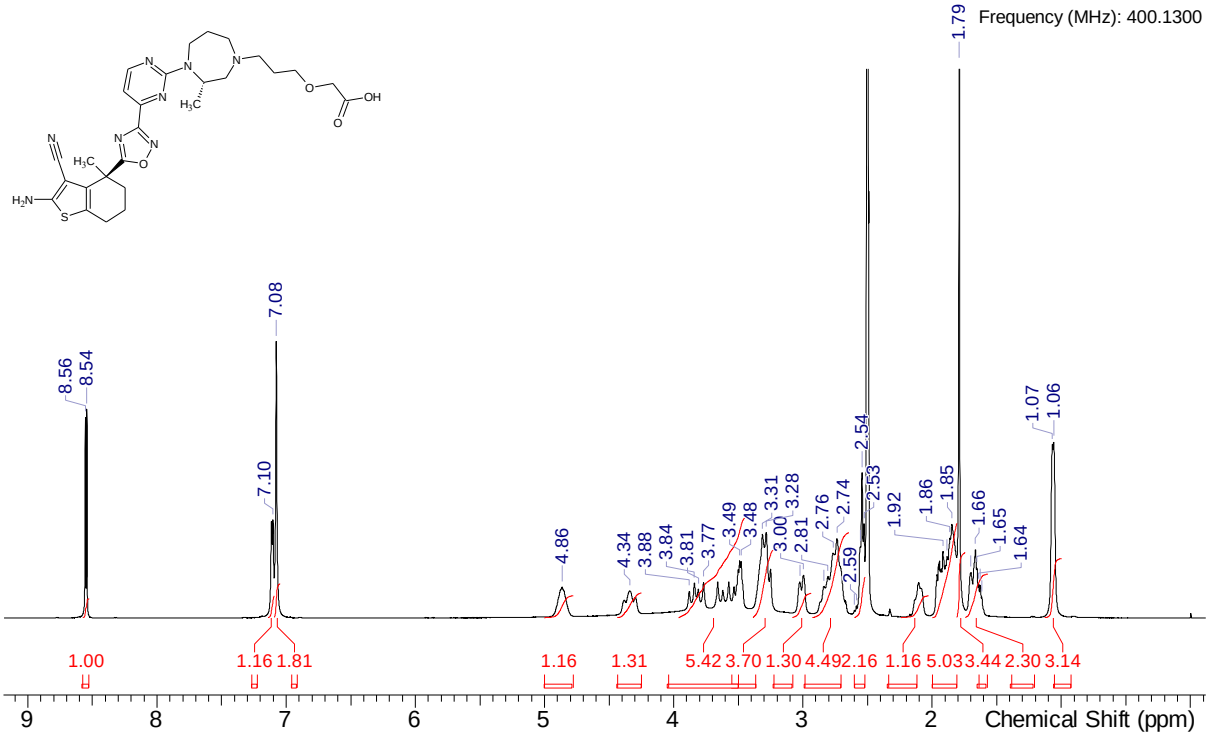

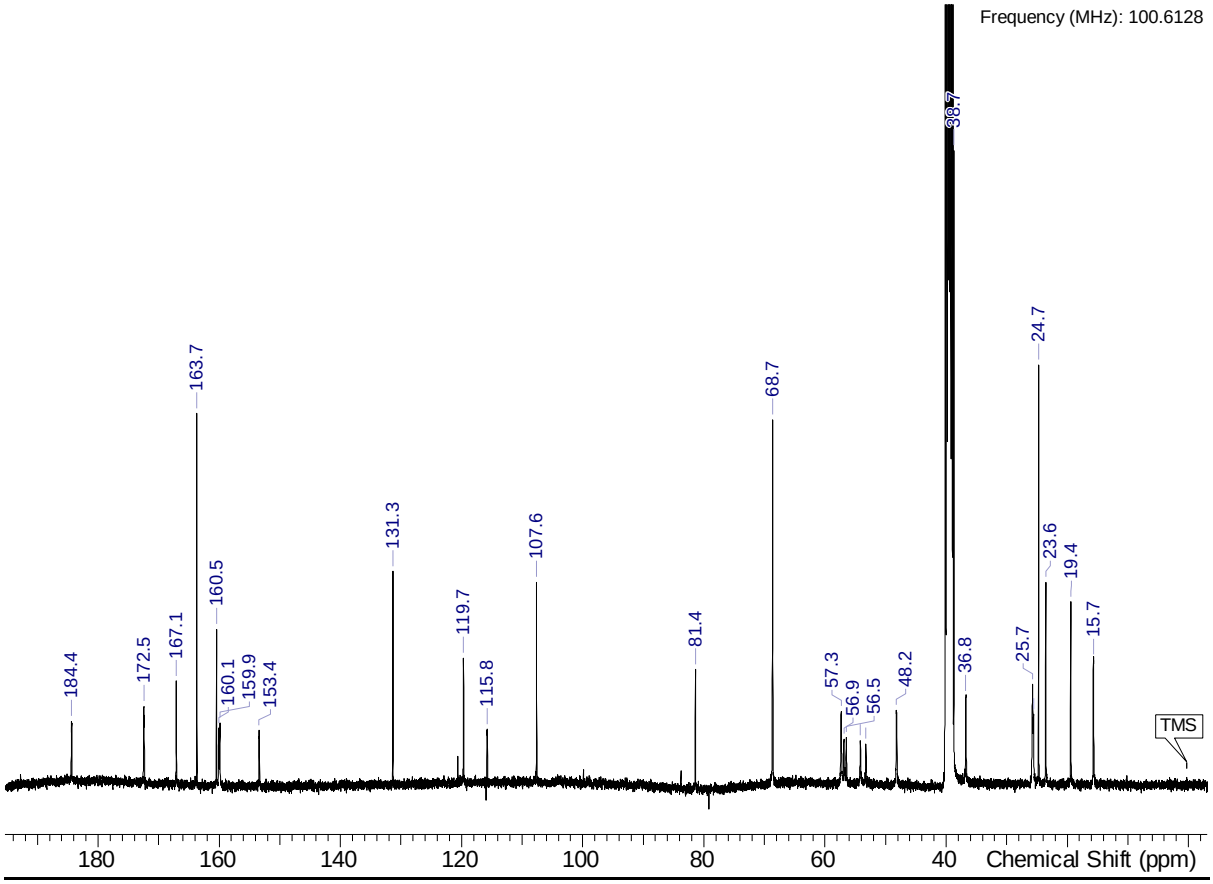

HRMS (*m/z*): $[M+H]^+$ calcd. for C27H34N8O4S , 567.24965; found, 567.24951

Compound **2**:

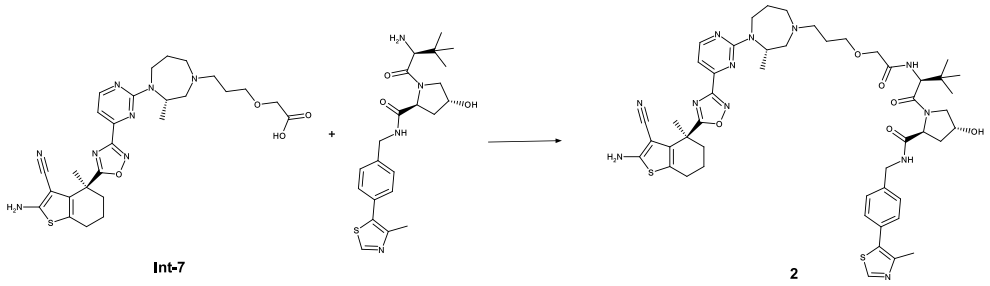

To a solution of **Int-7** in DMF (3.0 mL) is added HATU (227 mg, 0.598 mmol, 1.4 eq.), (2S,4R)-1-[(2S)-2-amino-3,3-dimethylbutanoyl]-4-hydroxy-N-{[4-(4-methyl-1,3-thiazol-5-yl)phenyl]methyl}pyrrolidine -2-carboxamide hydrochloride (248 mg, 0.532 mmol, 1.2 eq.) and DIPEA (172 mg, 1.33 mmol, 3.0 eq.). The reaction mixture is stirred at room temperature for 2 h. The reaction mixture is concentrated under reduced pressure. The residue is purified by chromatography to give **2**. The mixture is filtered, diluted with water and acetonitrile, purified by RP HPLC (Method 3b) and lyophilized to obtain **2** (347 mg, 0.354 mmol, 80% yield).

^{1}H NMR (DMSO-d_6) δ: 8.95-8.99 (m, 1H), 8.67 (br s, 0.14H rotamer), 8.60 (t, J=6.0 Hz, 1H), 8.52-8.56 (m, 1H), 7.39 (d, J=1.5 Hz, 4H), 7.32 (br d, J=7.9 Hz, 1H), 7.09 (d, J=4.8 Hz, 1H), 7.07 (s, 2H), 5.15 (d, J=3.3 Hz, 1H), 5.00 (d, J=2.3 Hz, 0.07H rotamer), 4.62-4.73 (m, 1H), 4.54 (br d, J=9.6 Hz, 1H), 4.15-4.48 (m, 6H), 3.86 (br s, 1.84H rotamer), 3.83 (br s, 0.18H rotamer), 3.56-3.70 (m, 2H), 3.44 (br t, J=6.2 Hz, 3H), 3.13 (br t, J=12.7 Hz, 1H), 3.00 (br d, J=10.1 Hz, 1H), 2.81 (br d, J=10.9 Hz, 1H), 2.52-2.60 (m, 4H), 2.45 (br s, 0.61H rotamer), 2.43 (s, 2.97H rotamer), 2.01-2.16 (m, 2H), 1.90 (br s, 4H), 1.78 (s, 3H), 1.66 (br s, 3H), 1.47-1.56 (m, 1H), 1.00 (br s, 3H), 0.88-0.97 (m, 9H)

1.77H rotamer)

Integrals may not add up to whole numbers due to overlapping rotamers or rotamers resonating under residual DMSO-d6 or HDO peaks

^{13}C NMR (DMSO-d_6) δ: 184.4, 171.8, 169.1, 168.5, 167.1, 163.7, 160.7, 160.1, 160.0, 153.5, 153.5, 151.4, 147.7, 139.4, 131.3, 131.1, 129.7, 128.9, 128.7, 128.1, 127.5, 119.6, 115.7, 107.2, 81.4, 69.4, 69.1, 68.9, 59.8, 59.4, 58.7, 56.6, 56.3, 55.6, 52.9, 52.1, 50.0, 41.7, 37.9, 36.7, 35.8, 27.7, 27.5, 27.3, 27.2, 26.2, 26.1, 24.7, 23.6, 19.4, 15.9, 15.6, 15.6

More carbon peaks detected than present in the structure due to presence of rotamers

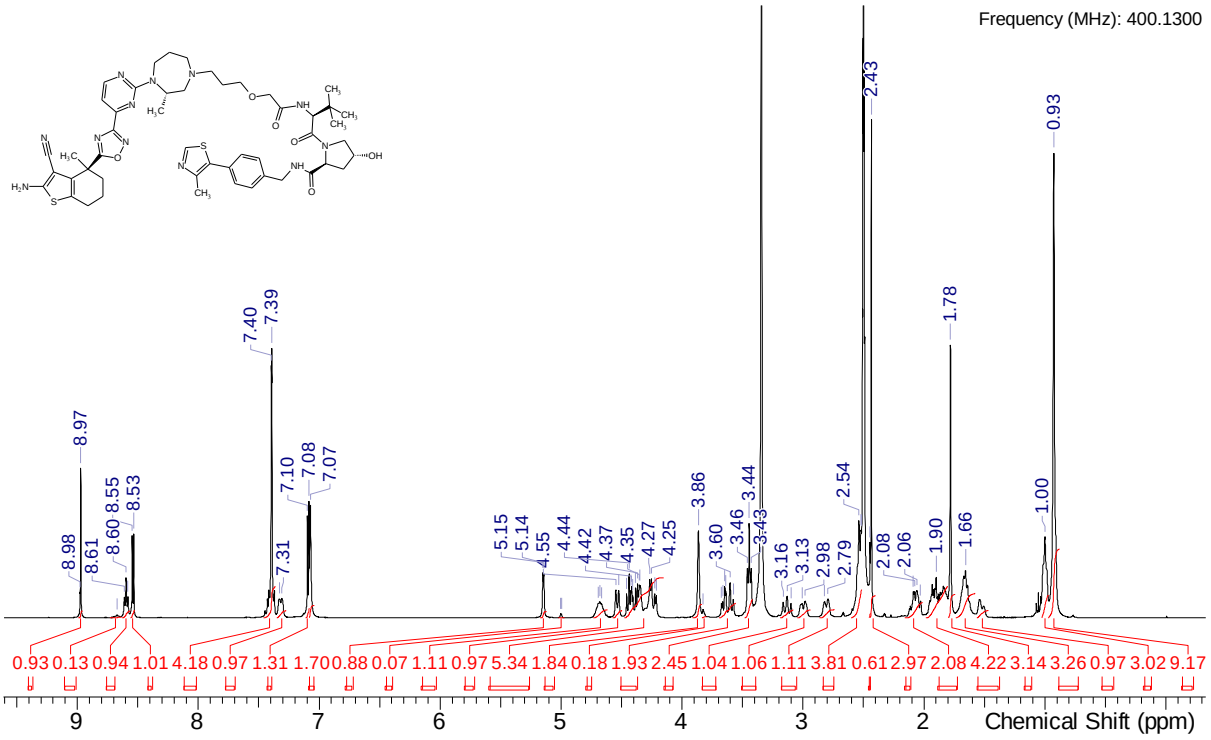

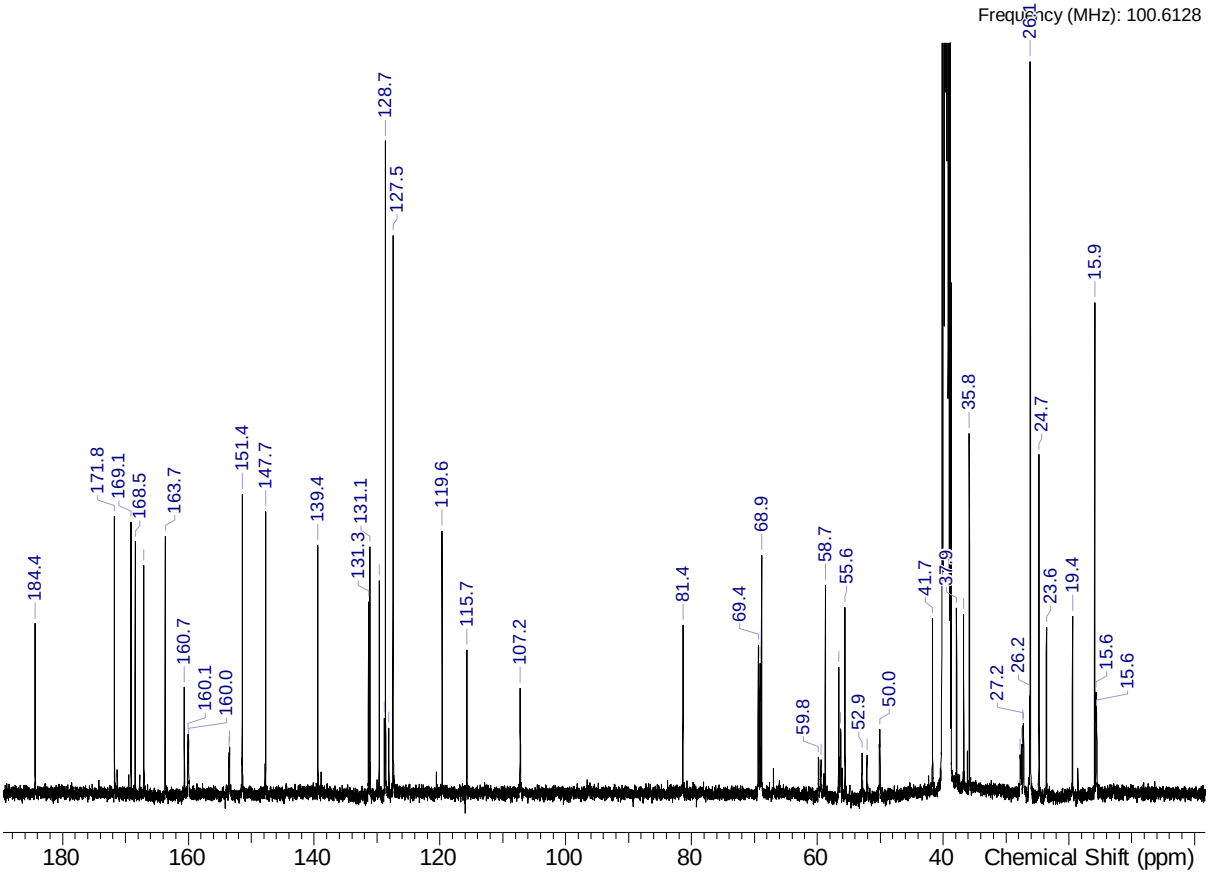

HRMS (*m/z*): $[M+H]^+$ calcd. for C49H62N12O6S2 , 979.44295; found, 979.44348

Synthesis of compound 3

Intermediate **Int-8**:

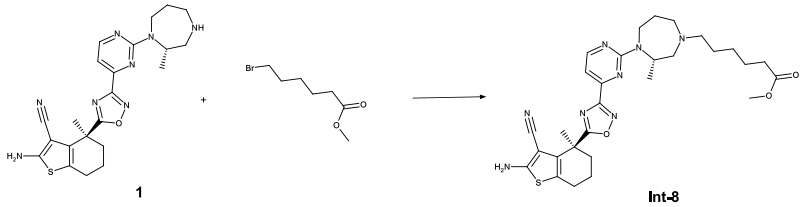

To a solution of **1** (450 mg, 0.899 mmol, 1.0 eq.) is added methyl 6-bromohexanoate (383 mg, 1.798 mmol, 2.0 eq.) and DIPEA (408 mg, 3.146 mmol, 3.5 eq.) and the mixture was stirred at 50 °C over night. The mixture is cooled to RT, filtered and purified by RP HPLC (Method 3b) and lyophilized to obtain **Int-8** (332 mg, 0.574 mmol, 64% yield).

^{1}H NMR (DMSO-d_6) δ: 8.55 (d, J=4.8 Hz, 1H), 7.10 (d, J=4.8 Hz, 1H), 7.08 (s, 2H), 4.69 (dt, J=11.3, 5.9 Hz, 1H), 4.28 (br t, J=16.7 Hz, 1H), 3.54 (br d, J=5.6 Hz, 3H), 3.16 (br t, J=12.7 Hz, 1H), 2.99 (br d, J=13.9 Hz, 1H), 2.80 (br d, J=11.7 Hz, 1H), 2.52-2.59 (m, 3H), 2.01-2.46 (m, 6H), 1.80-2.01 (m, 3H), 1.79 (s, 3H), 1.32-1.74 (m, 6H), 1.19 (br d, J=6.8 Hz, 2H), 1.02 (br s, 3H)

^{13}C NMR (DMSO-d_6) δ: 184.4, 173.3, 167.1, 163.7, 160.7, 160.0, 159.9, 153.5, 153.5, 131.3, 119.6, 115.7, 107.2, 81.4, 59.7, 59.3, 56.3, 55.7, 54.9, 51.1, 50.1, 50.0, 38.7, 36.7, 33.2, 27.7, 27.5, 26.7, 26.6, 26.2, 24.7, 24.3, 23.6, 19.4, 15.7, 15.6

More carbon peaks detected than present in the structure due to presence of rotamers

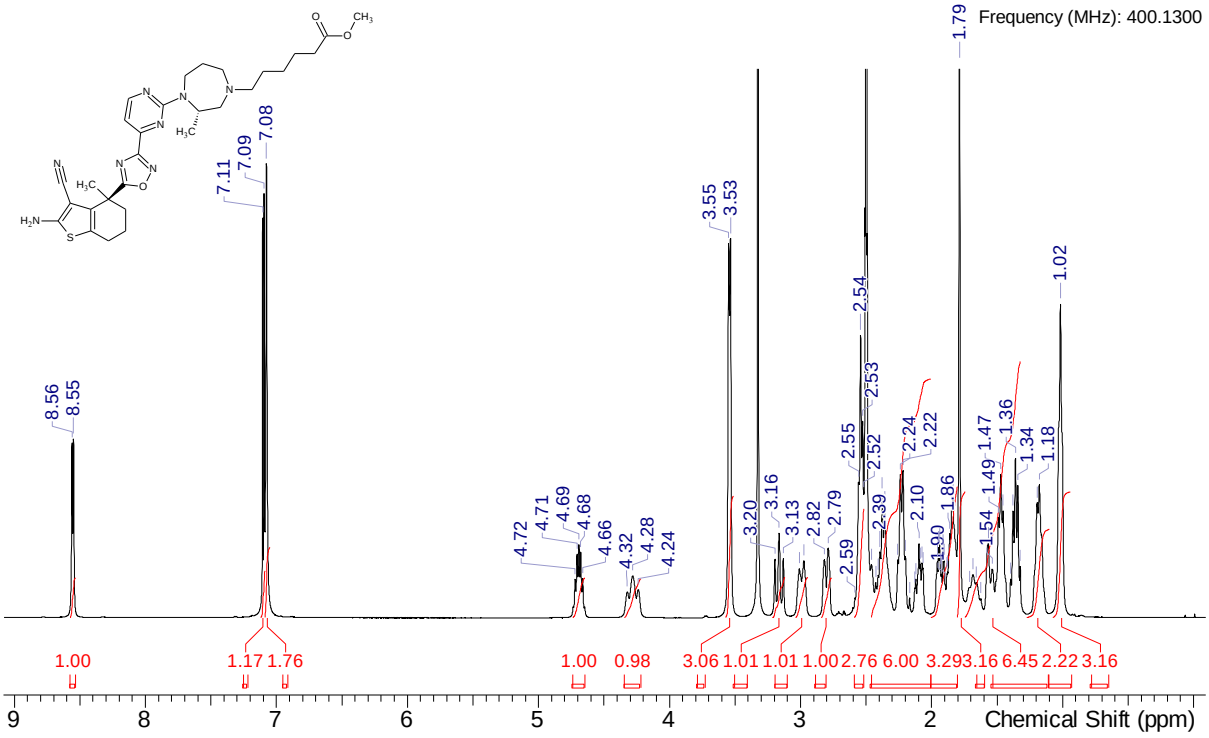

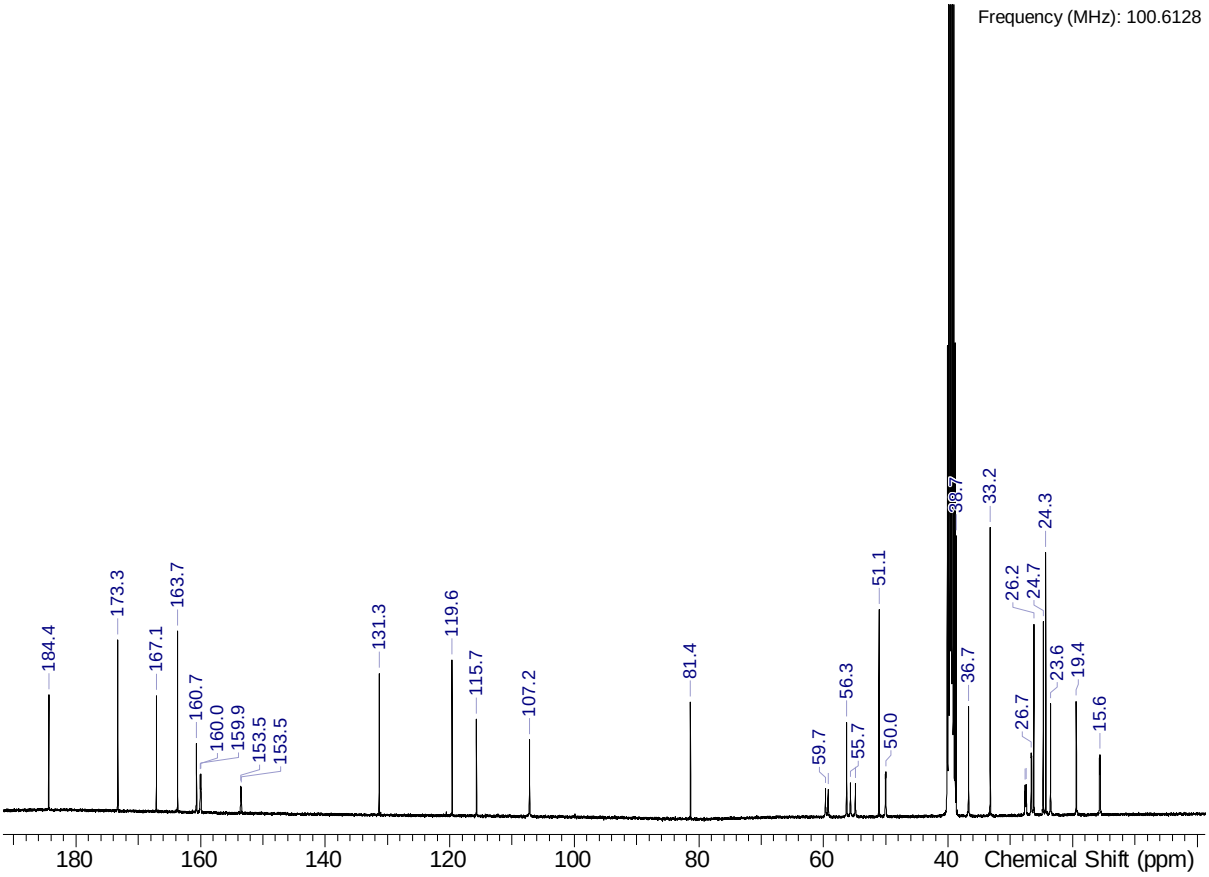

HRMS (*m/z*): $[M+H]^+$ calcd. for C29H38N8O3S , 579.28603; found, 579.28595

Compound **3**:

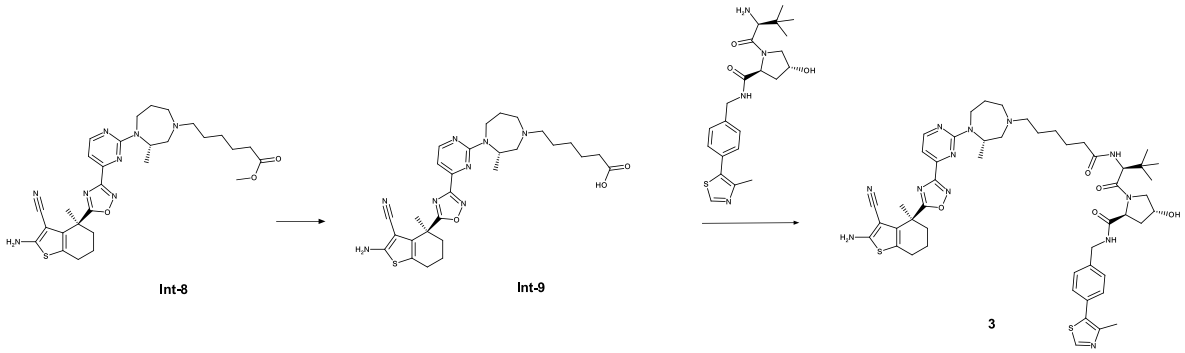

To a solution of **Int-8** (43 mg, 0.073 mmol, 1.0 eq.) in THF (2.0 mL) and water (2 mL) is added LiOH H_2O (15 mg, 0.36 mmol) and the reaction mixture is stirred at room temperature overnight. The reaction mixture is neutralized using 4M HCl in water, and concentrated under reduced pressure. The crude acid intermediate **Int-9** is taken up in DMF (2.0 mL). HATU (50 mg, 0.13 mmol, 1.8 eq.), HOAt (18 mg, 0.13 mmol, 1.8 qe.), (2S,4R)-1-[(2S)-2-amino-3,3-dimethylbutanoyl]-4-hydroxy-N-{[4-(4-methyl-1,3-thiazol-5-yl)phenyl]methyl}pyrrolidine -2-carboxamide hydrochloride (43 mg, 0.073 mmol, 1.8 eq.) and DIPEA (35 µL, 0.21 mmol, 2.9 eq.) are added. The reaction mixture is stirred at room temperature overnight. The reaction mixture is concentrated under reduced pressure. The residue is purified by RP chromatography (Method 3b) to give **3**.

^{1}H NMR (DMSO-d_6) δ: 8.56 (br d, J=4.1 Hz, 1H), 7.10 (d, J=4.8 Hz, 1H), 7.08 (s, 2H), 4.70 (dt, J=11.3, 5.9 Hz, 1H), 4.29 (br t, J=16.7 Hz, 1H), 3.11-3.23 (m, 2H), 2.95-3.06 (m, 1H), 2.81 (br d, J=11.7 Hz, 1H), 2.54 (br d, J=6.1 Hz, 3H), 2.38 (br d, J=6.8 Hz, 3H), 2.04-2.23 (m, 3H), 1.85 (br d, J=4.1 Hz, 3H), 1.79 (s, 3H), 1.41 (dt, J=33.8, 7.1 Hz, 6H), 1.13-1.26 (m, 2H), 1.02 (br s, 3H)

^{13}C NMR (DMSO-d_6) δ: 184.4, 174.6, 167.1, 163.7, 160.7, 160.1, 160.0, 153.5, 153.5, 131.3, 119.6, 115.7, 107.2, 81.3, 59.7, 59.2, 56.3, 55.8, 54.9, 50.1, 50.0, 38.7, 36.7, 33.8, 27.7, 27.5, 26.7, 26.6, 26.4, 24.7, 24.4, 23.5, 19.4, 15.7, 15.6, 1C under DMSO

More carbon peaks detected than present in the structure due to presence of rotamers

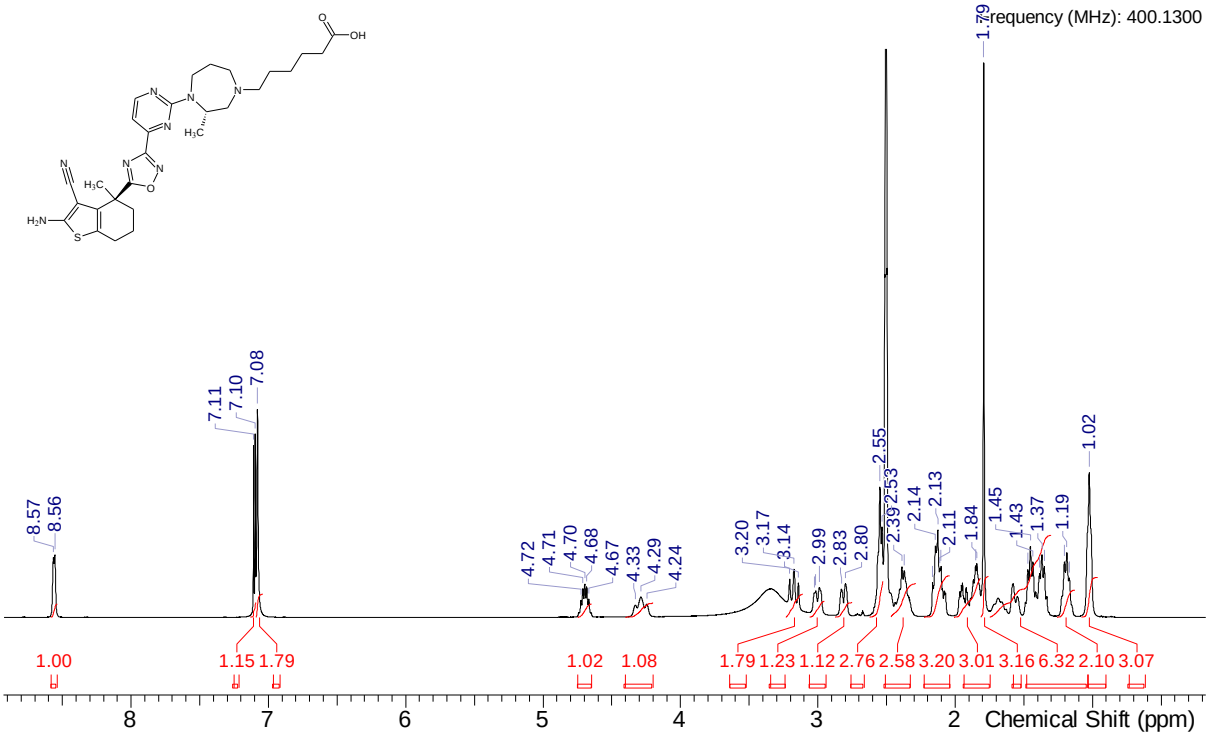

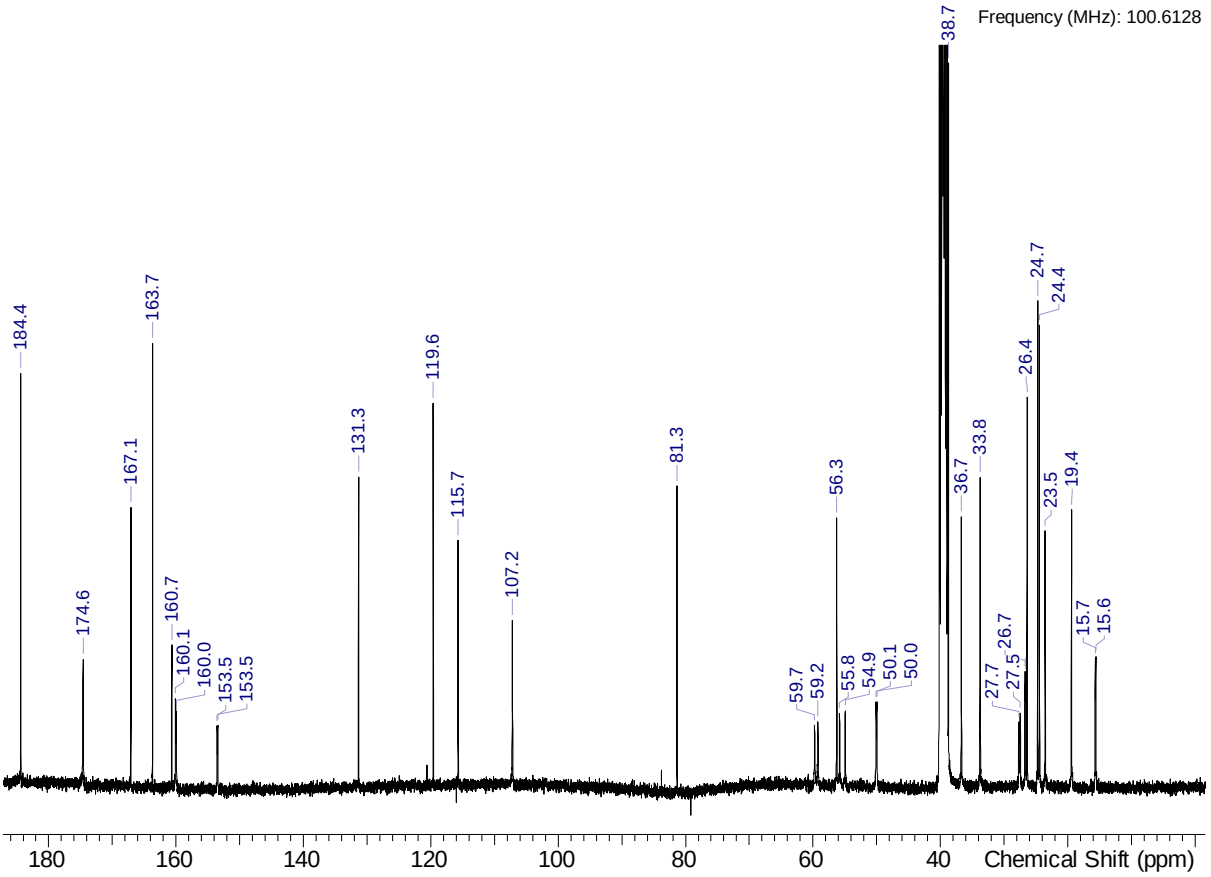

HRMS (*m/z*): $[M+H]^+$ calcd. for C28H36N8O3S , 565.27038; found, 565.27045

^{1}H NMR (DMSO-d_6) δ: 8.98 (s, 1H), 8.50-8.61 (m, 2H), 7.80 (br t, J=7.2 Hz, 1H), 7.40-7.43 (m, 2H), 7.36-7.39 (m, 2H), 7.10 (d, J=4.8 Hz, 1H), 7.08 (s, 2H), 5.11 (d, J=3.3 Hz, 1H), 4.62-4.74 (m, 1H), 4.52 (br d, J=9.4 Hz, 1H), 4.38-4.48 (m, 2H), 4.34 (br s, 1H), 4.17-4.31 (m, 2H), 3.58-3.70 (m, 2H), 3.16 (br t, J=12.5 Hz, 1H), 2.99 (dd, J=14.2, 5.6 Hz, 1H), 2.81 (br d, J=11.7 Hz, 1H), 2.52-2.60 (m, 3H), 2.44 (s, 3H), 2.30-2.41 (m, 2H), 2.22 (br s, 1H), 1.97-2.16 (range, 3H), 1.79-1.96 (range, 4H), 1.78 (s, 3H), 1.61-1.72 (m, 1H), 1.52-1.60 (range, 1H), 1.30-1.52 (range, 4H), 1.10-1.24 (m, 2H), 1.02 (br t, J=7.0 Hz, 3H), 0.91 (s, 9H), 1H under DMSO

^{13}C NMR (DMSO-d_6) δ: 184.4, 172.1, 171.9, 169.7, 167.1, 163.7, 160.7, 160.1, 160.0, 153.5, 153.5, 151.4, 147.7, 139.5, 131.3, 131.1, 129.6, 128.6, 128.0, 127.4, 119.6, 115.7, 107.2, 81.3, 68.8, 59.9, 59.4, 58.7, 56.3, 56.3, 56.1, 55.2, 50.2, 50.0, 41.6, 37.9, 36.7, 35.2, 34.8, 27.7, 27.5, 26.7, 26.6, 26.4, 26.3, 25.3, 24.7, 23.6, 19.4, 15.9, 15.7, 15.6;

More carbon peaks detected than present in the structure due to presence of rotamers, 1C under DMSO

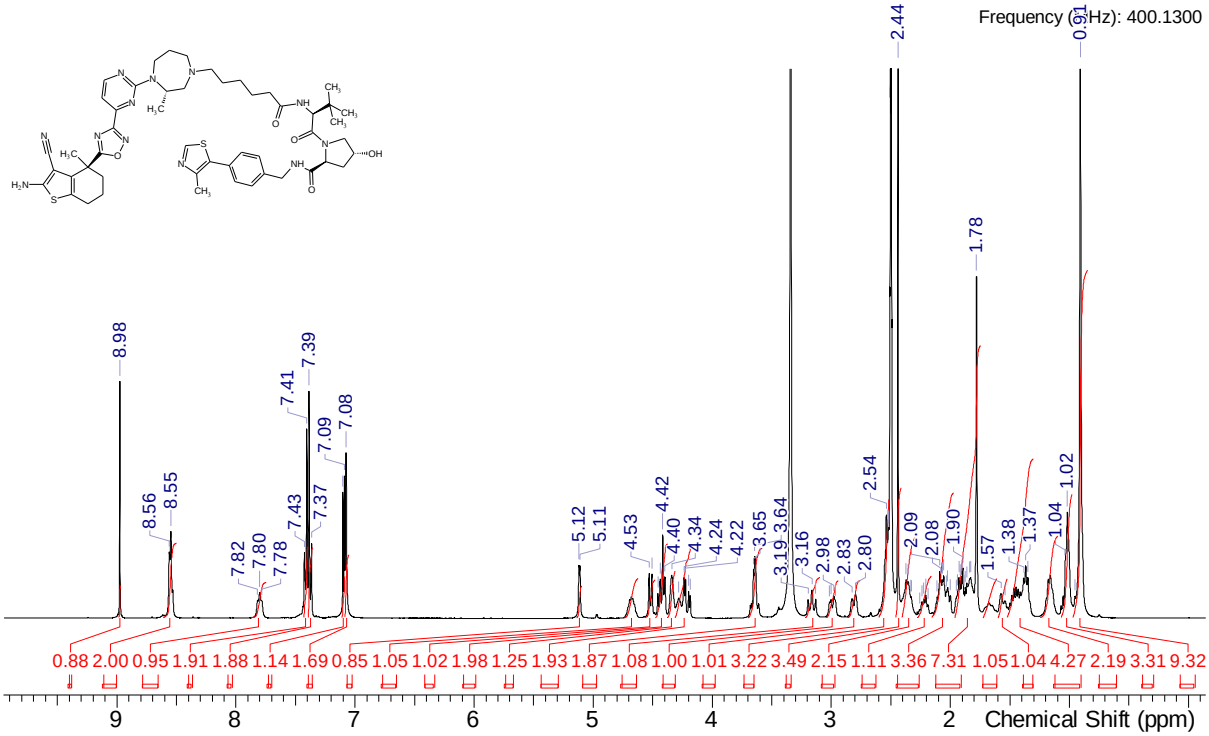

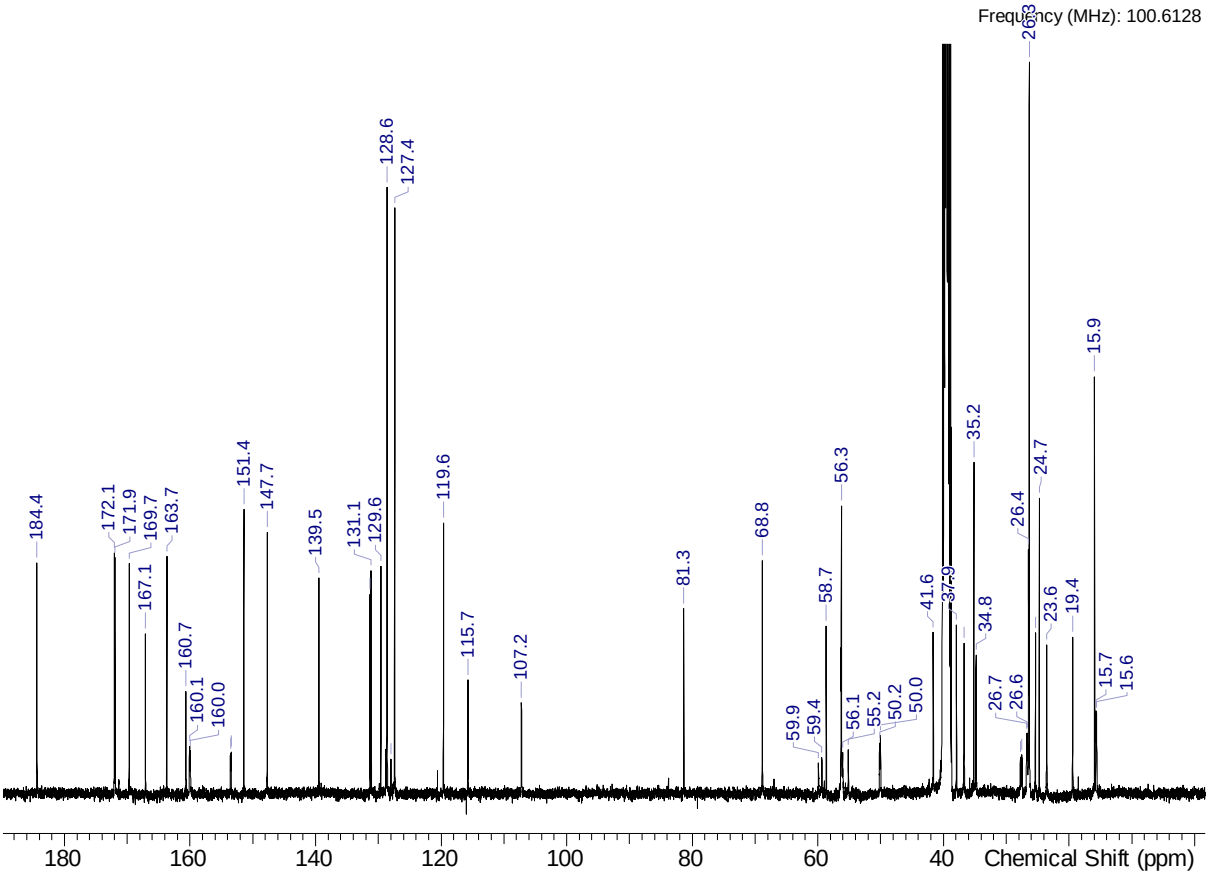

HRMS (*m/z*): $[M+H]^+$ calcd. for C50H64N12O5S2 , 977.46368; found, 977.46423

Synthesis of compound 4 and 6

Intermediate **Int-10**:

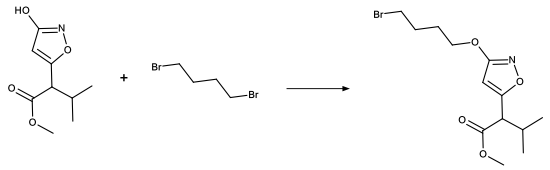

Int-10

To a stirred solution of methyl 2-(3-hydroxy-1,2-oxazol-5-yl)-3-methylbutanoate (11.00 g, 0.055 mol, 1.0 eq.) in DMF (75.0 mL) is added potassium carbonate (22.86 g, 0.166 mol, 3.0 eq.) at 0 °C. 1,3-Dibromobutane (11.92 g, 0.055 mol, 1.0 eq.) is added dropwise and the reaction mixture is stirred at 0 °C for 9 hours. After complete conversion the reaction mixture is quenched with water and extracted with EtOAc. The organic layer is washed with ice water, dried over sodium sulfate and concentrated under reduced pressure to give the crude product. The obtained crude compound is purified by column chromatography (hexane/EtOAc, 0-10%) to yield **Int-10** (5.01 g, 0.015 mmol, 27% yield) as a racemic mixture.

^{1}H NMR (DMSO-d_6) δ: 6.19 (s, 1H), 4.18 (t, J=6.3 Hz, 2H), 3.68 (d, J=8.8 Hz, 1H), 3.65-3.66 (m, 3H), 3.58 (t, J=6.6 Hz, 2H), 2.28 (s, 1H), 1.87-1.96 (m, 2H), 1.79-1.87 (m, 2H), 0.92 (d, J=6.6 Hz, 3H), 0.84 (d, J=6.6 Hz, 3H)

^{13}C NMR (DMSO-d_6) δ: 171.3, 169.9, 169.7, 94.3, 68.8, 52.3, 51.0, 34.7, 29.9, 28.8, 27.2, 20.3, 19.6

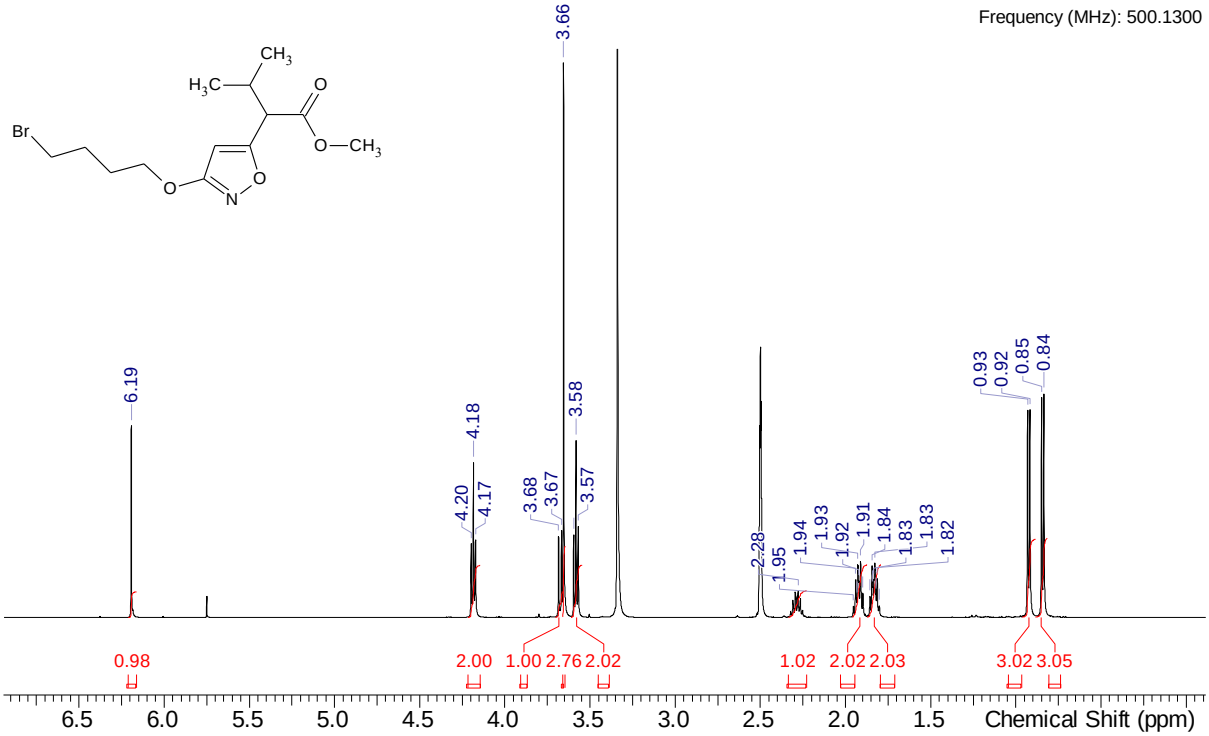

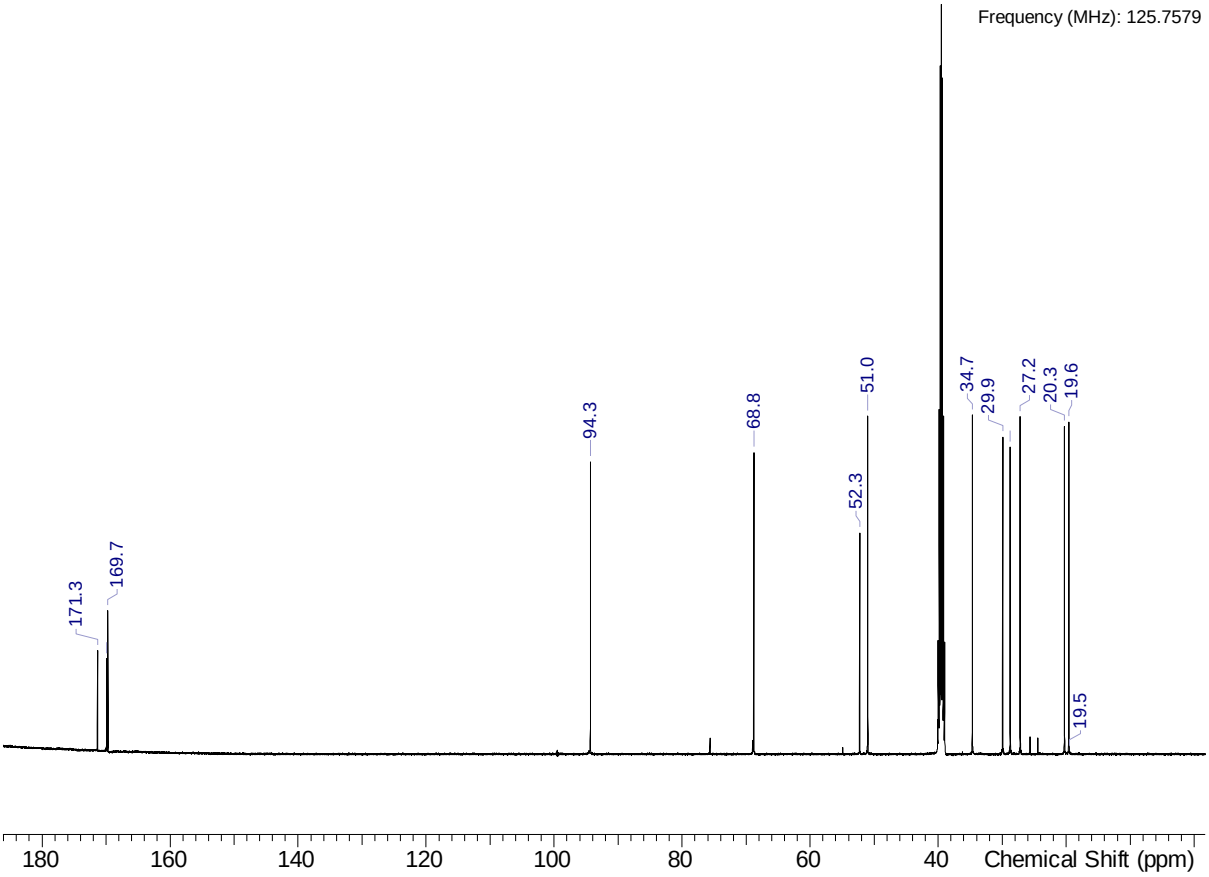

HRMS (*m/z*): $[M+H]^+$ calcd. for C13H20BrNO4 , 334.06485; found, 334.06482

Intermediate **Int-11**:

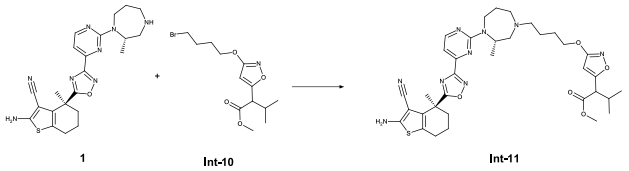

To a stirred solution of **1** (1.50 g, 3.22 mmol, 1.0 eq.) and I**nt-10** (1.16 g, 3.48 mmol, 1.1 eq) in acetonitrile (15.0 mL) is added potassium carbonate (0.89 g, 6.45 mmol, 2.0 eq) and the mixture is stirred at 60 °C under argon for 22 h. The reaction mixture is allowed to cool to rt, filtered and the solid is washed with acetonitrile. The combined solution is concentrated under reduced pressure and purified by normal phase chromatography (DCM / MeOH, 0-10%) to give **Int-11** (1.73, 2.46 mmol, 76 % yield) as a mixture of two diastereomers.

^{1}H NMR (DMSO-d_6) δ: 8.56 (d, J=5.0 Hz, 1H), 7.03-7.14 (m, 3H), 6.16 (br d, J=4.4 Hz, 1H), 4.71 (dt, J=11.3, 5.9 Hz, 1H), 4.22-4.39 (m, 1H), 4.12 (br s, 2H), 3.66 (s, 4H), 3.19 (br t, J=12.8 Hz, 1H), 2.95-3.09 (m, 1H), 2.83 (br d, J=11.7 Hz, 1H), 2.52-2.62 (m, 3H), 2.38 (br s, 3H), 2.28 (br d, J=8.2 Hz, 1H), 2.06-2.16 (m, 1H), 1.82-2.00 (m, 3H), 1.79 (s, 3H), 1.42-1.76 (m, 6H), 1.03 (br t, J=6.9 Hz, 3H), 0.93 (d, J=6.6 Hz, 1H), 0.84 (d, J=6.6 Hz, 3H), 2 H under DMSO

^{13}C NMR (DMSO-d_6) δ: 184.4, 171.4, 169.9, 169.6, 167.1, 163.7, 160.7, 160.1, 160.0, 153.5, 153.5, 131.3, 119.6, 115.7, 107.2, 94.3, 81.3, 69.6, 59.7, 59.2, 56.2, 55.3, 54.5, 52.2, 51.0, 50.0, 38.7, 36.7, 29.9, 27.7, 27.5, 26.3, 24.7, 23.5, 23.3, 23.2, 20.3, 19.6, 19.4, 15.7, 15.6

More carbon peaks detected than present in the structure due to presence of rotamers, 1C under DMSO

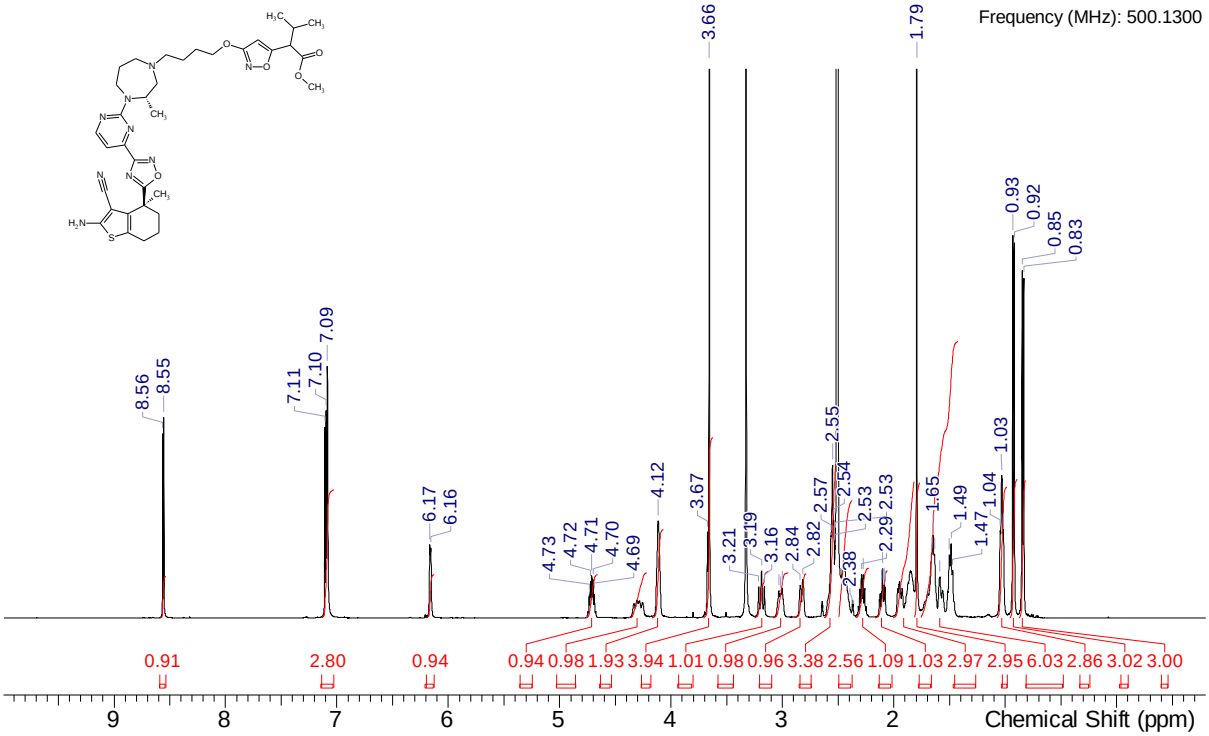

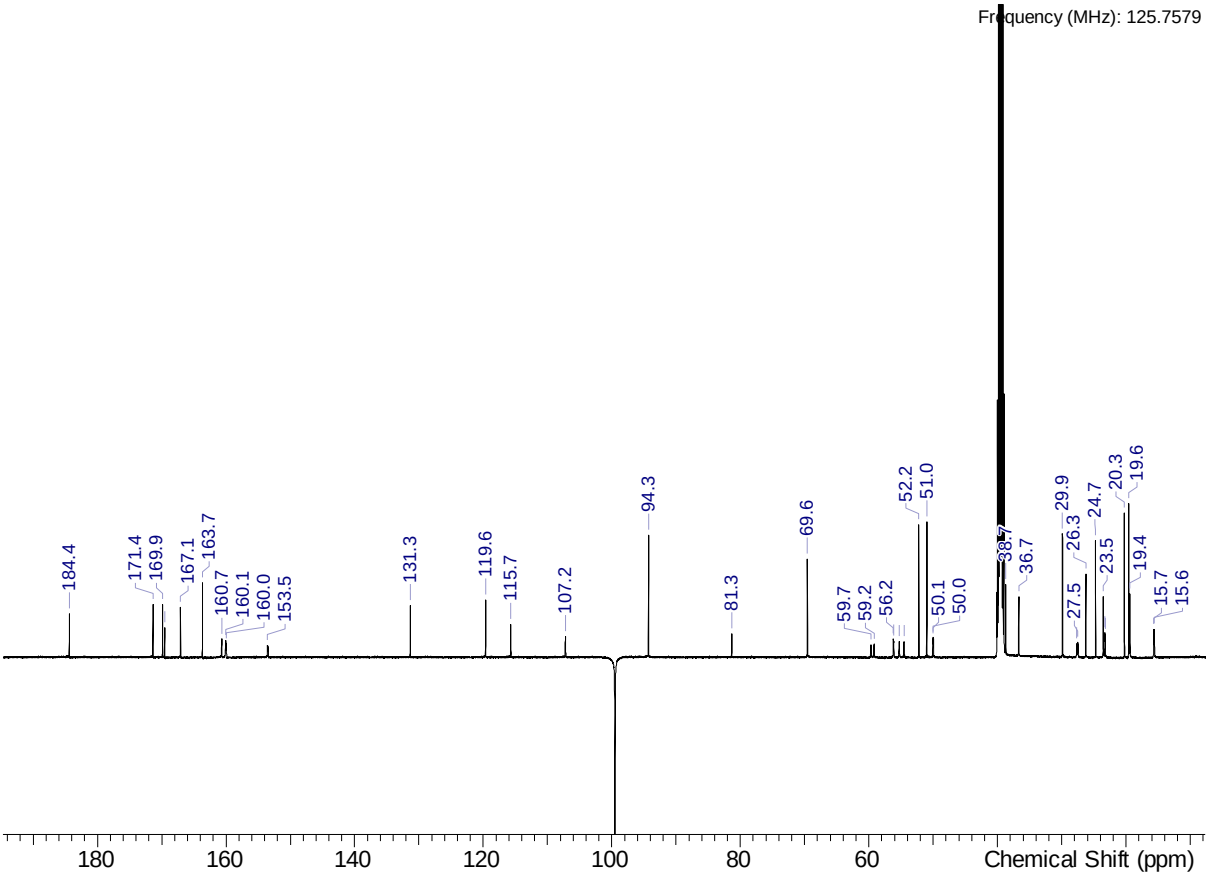

The spike observed at 99.5 ppm is an artefact from the carrier frequency.

HRMS (*m/z*): $[M+H]^+$ calcd. for C35H45N9O5S , 704.33371; found, 704.33331

Intermediate **Int-12**:

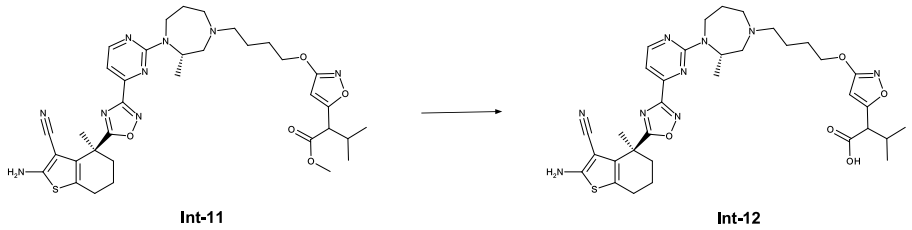

To a stirred solution of **Int-11** (1.30 g, 1.85 mmol, 1.0 eq.) in methanol (13.0 ml) is added sodium hydroxide solution (2 M in water, 1.85 ml, 3.70 mmol, 2.0 eq) and the reaction mixture is stirred at 45 °C for 1 h. After complete conversion the reaction mixture is concentrated under reduced pressure. The crude product is purified by RP chromatography (Method 3a) yielding **Int-12** (1.10 g, 1.60 mmol, 86%) as a mixture of two diastereomers.

^{1}H NMR (DMSO-d_6) δ: 11.47 (br s, 0.31H rotamer), 9.93 (br d, J=2.8 Hz, 0.25H rotamer), 9.72 (br s, 0.39H rotamer), 8.64 (br d, J=4.7 Hz, 1H), 7.19-7.30 (m, 1.04H rotamer), 6.14 (s, 0.66H rotamer), 5.98-6.11 (m, 0.3H rotamer), 4.97 (br s, 0.29H rotamer), 4.89 (br d, J=5.7 Hz, 0.75H rotamer), 4.30-4.51 (range, 1.32H rotamer), 4.19 (br t, J=6.0 Hz, 2H), 4.08 (br d, J=3.2 Hz, 1H), 3.51 (br d, J=8.8 Hz, 6H), 3.17-3.31 (m, 3H), 2.79-2.94 (m, 0.68H rotamer), 2.67-2.68 (m, 1H), 2.52-2.57 (m, 2H), 2.19-2.28 (m, 1H), 2.18 (s, 1H), 2.01-2.14 (m, 1H), 1.80-2.01 (range, 7H), 1.78 (s, 3H), 1.74 (br s, 1H), 1.58-1.69 (m, 1H), 1.13 (br s, 3H rotamer), 0.95 (br d, J=6.6 Hz, 1H), 0.78-0.87 (m, 3H)

Integrals may not add up to whole numbers due to overlapping rotamers or rotamers resonating under residual DMSO-d6 or HDO peaks

^{13}C NMR (DMSO-d_6) δ: 184.6, 171.3, 170.8, 170.6, 167.0, 163.8, 160.5, 160.1, 153.8, 153.6, 131.3, 131.3, 119.7, 119.6, 115.8, 115.7, 108.4, 94.0, 69.0, 57.8, 55.4, 53.1, 51.6, 47.6, 38.8, 38.2, 36.8, 36.7, 29.7, 25.7, 24.7, 23.6, 20.5, 19.6, 19.5, 19.4, 15.5, 15.4, 15.2

More carbon peaks detected than present in the structure due to presence of rotamers, 1C under DMSO

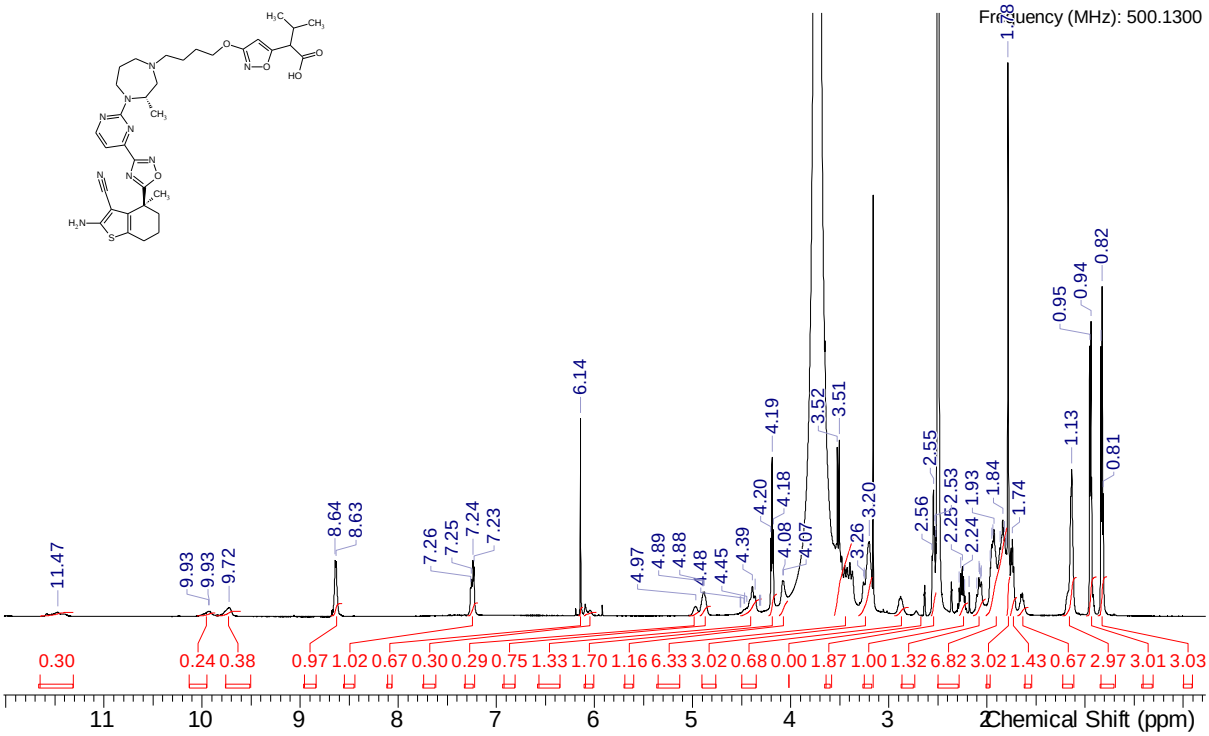

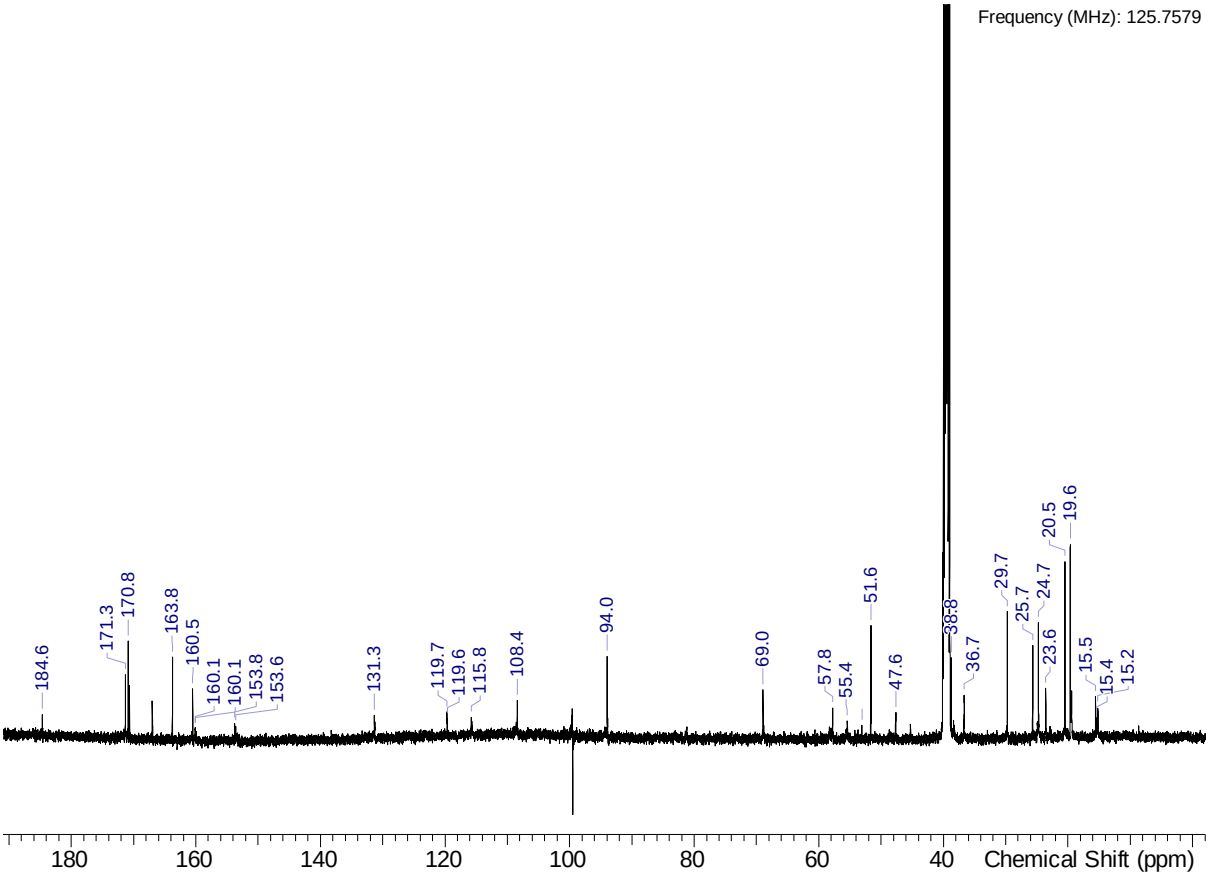

The spike observed at 99.5 ppm is an artefact from the carrier frequency.

HRMS (*m/z*): $[M+H]^+$ calcd. for C34H43N9O5S , 690.31806; found, 690.31806

Compound **4** and **6**:

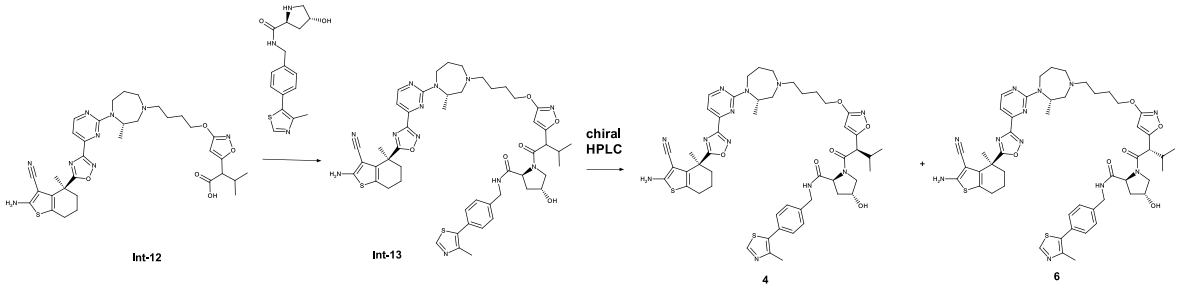

To a stirred solution of **Int-12** (490 mg, 0.71 mmol, 1.0 eq.), (2S,4R)-4-hydroxy-N-{[4-(4-methyl-1,3-thiazol-5-yl)phenyl]methyl}pyrrolidine-2-carboxamide (326 mg, 0.923 mmol, 1.1 eq.) and HATU (330 mg, 0.85 mmol, 1.2 eq.) in DMSO (4.9 ml) is added DIPEA (1.24 mL, 7.10 mmol, 10.0 eq) and the reaction mixture is stirred at rt for 15 min. After complete conversion the reaction mixture is quenched with water, diluted with acetonitrile and purified by RP chromatography (Method 3b) to obtain **Int-13** (426 mg, 0.431, 61 %) as a mixture of two diastereomers. The mixture **Int-13** (330 mg, 0.334 mmol) is separated by preparative chiral HPLC (Method A) to obtain **4** (136 mg, 0.137 mmol) and less active diastereomer **6** (146 mg, 0.148 mmol).

^{1}H NMR (DMSO-d_6) δ: 8.98 (s, 0.5H rotamer), 8.95-8.97 (m, 0.5H rotamer), 8.82 (s, 0.1H rotamer), 8.54 (s, 1.5H rotamer), 8.40-8.48 (m, 0.5H rotamer), 7.35-7.48 (m, 3H), 7.31 (s, 1H), 7.03-7.13 (m, 3H), 6.04 (br dd, J=15.9, 4.6 Hz, 1H), 5.65 (br d, J=4.4 Hz, 0.1H rotamer), 5.12 (dd, J=10.7, 3.5 Hz, 1H), 5.04 (d, J=2.8 Hz, 0.1H rotamer), 4.97 (d, J=3.2 Hz, 0.1H rotamer), 4.61-4.79 (range, 1H), 4.42 (br t, J=7.7 Hz, 0.5H rotamer), 4.17-4.39 (m, 4.5H rotamer), 3.99-4.14 (m, 2H), 3.71-3.83 (m, 0.9H rotamer), 3.65 (br d, J=9.5 Hz, 0.4H rotamer), 3.51-3.62 (m, J=5.0 Hz, 1H), 3.39-3.50 (m, 1H), 3.09-3.24 (m, 1H), 2.99 (br d, J=3.8 Hz, 1H), 2.80 (br s, 1H), 2.52-2.60 (range, 3H), 2.45 (s, 1H rotamer), 2.44 (s, 1.5H rotamer), 2.43 (br s, 0.8H rotamer), 2.41 (s, 0.7H rotamer), 2.39 (br d, J=7.9 Hz, 1H rotamer), 2.35-2.38 (m, 0.54H rotamer), 2.18-2.29 (m, 1H), 1.98-2.14 (m, 2H), 1.80-1.97 (m, 4H), 1.78 (s, 3H), 1.52-1.73 (m, 4H), 1.35-1.51 (m, 2H), 0.97-1.05 (m, 3H), 0.96 (d, J=6.6 Hz, 1.5H rotamer), 0.94 (br d, J=6.6 Hz, 1.5H rotamer), 0.82 (d, J=6.9 Hz, 1.5H rotamer), 0.78 (br d, J=6.6 Hz, 1.5H rotamer), 0.65 (d, J=6.6 Hz, 0.5H rotamer), 0.56 (d, J=6.6 Hz, 0.5H rotamer)

Integrals may not add up to whole numbers due to overlapping rotamers or rotamers resonating under residual DMSO-d6 or HDO peaks

^{13}C NMR (DMSO-d_6) δ: 184.4, 171.6, 171.6, 171.4, 171.3, 171.3, 167.7, 167.4, 167.1, 163.7, 160.7, 160.1, 160.0, 151.5, 151.4, 147.8, 147.8, 139.4, 139.3, 131.4, 131.1, 129.8, 129.7, 129.0, 128.9, 128.8, 128.7, 128.1, 127.9, 127.5, 127.4, 119.6, 115.7, 107.2, 93.6, 93.5, 93.2, 81.3, 69.5, 69.4, 68.7, 68.6, 59.7, 58.9, 56.2, 55.8, 55.4, 55.3, 54.5, 50.0, 49.3, 41.6, 41.5, 38.0, 37.9, 36.7, 31.1, 30.8, 27.7, 27.5, 26.3, 24.7, 23.6, 23.2, 20.7, 20.5, 19.9, 19.6, 19.4, 15.9, 15.7, 15.6

More carbon peaks detected than present in the structure due to presence of rotamers

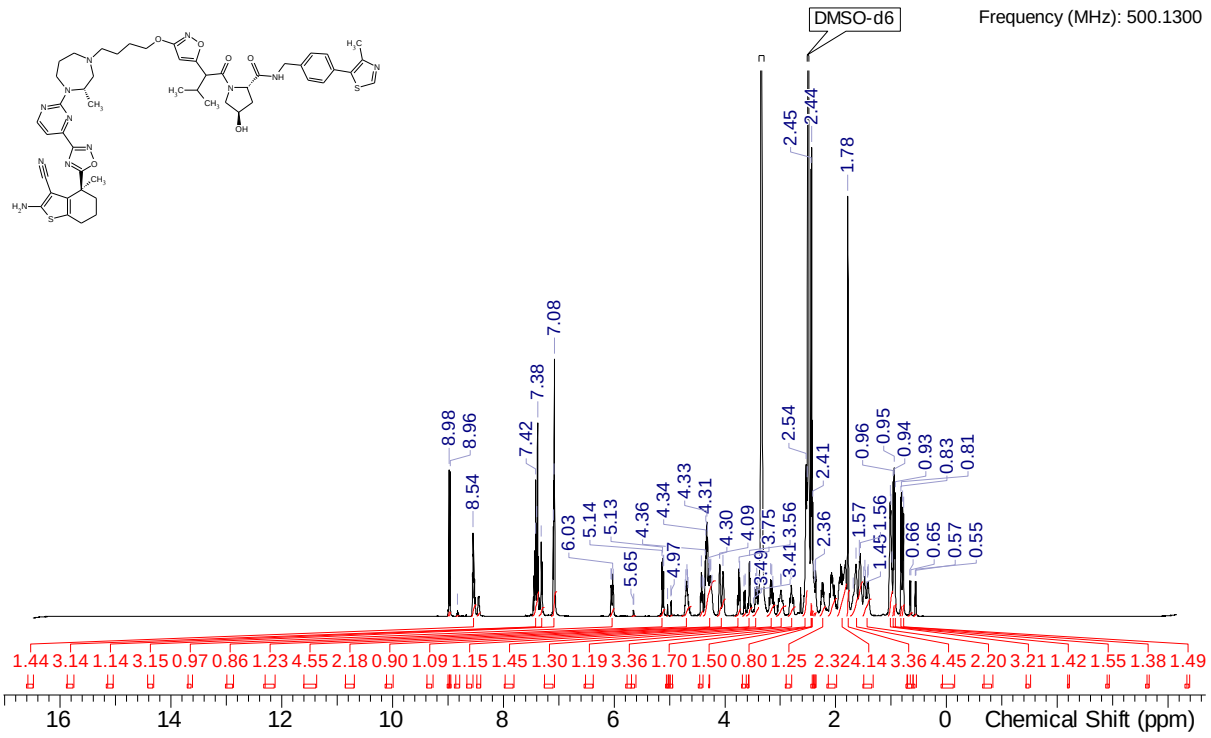

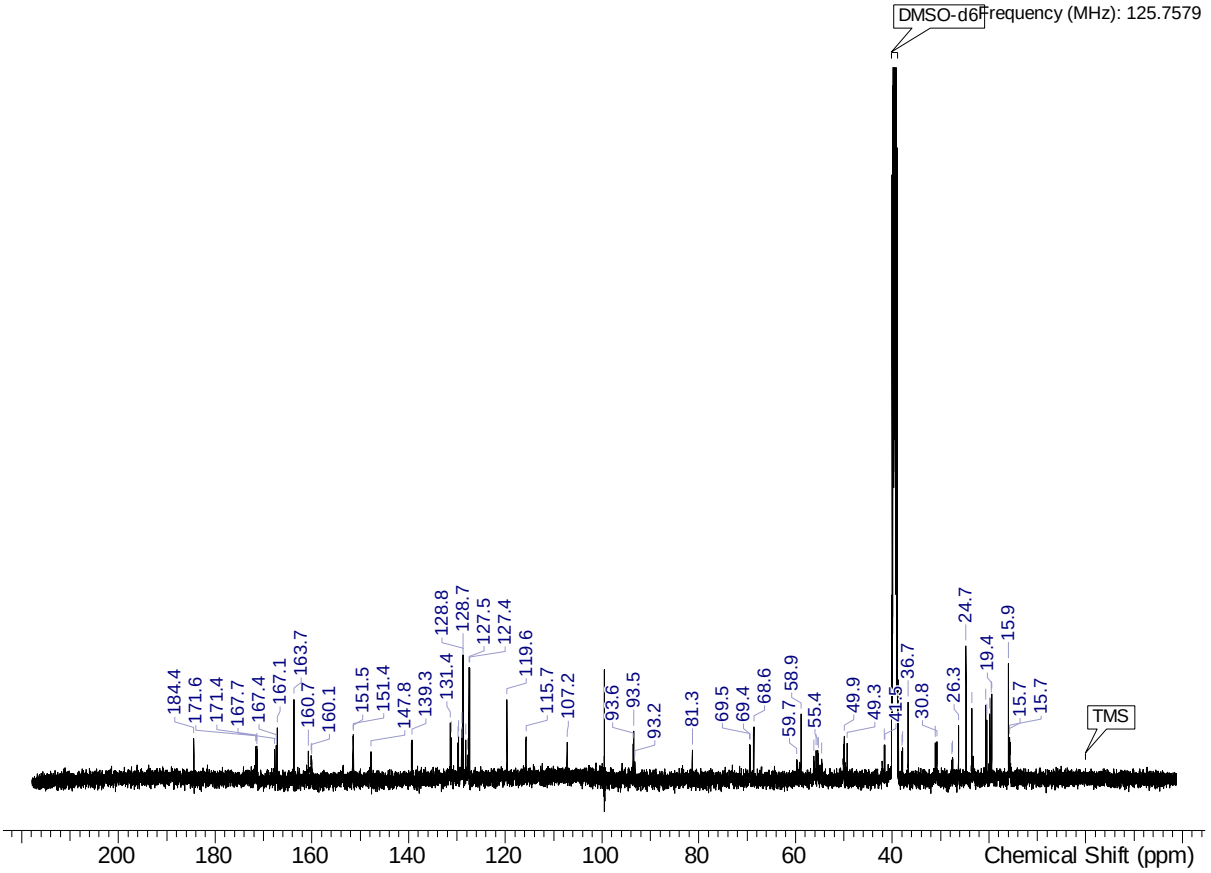

HRMS (*m/z*): $[M+H]^+$ calcd. for C50H60N12O6S2 , 989.42730; found, 989.4267

^{1}H NMR (DMSO-d_6) δ: 8.95-9.01 (m, 1H), 8.52-8.56 (m, 1H), 8.44 (br d, J=5.0 Hz, 0.8H rotamer), 7.45 (s, 0.4H rotamer), 7.37-7.43 (range, 2H rotamer), 7.31 (d, J=7.9 Hz, 1.6H rotamer), 7.02-7.14 (m, 3H), 6.02 (br d, J=5.4 Hz, 1H), 4.68 (br s, 2H), 4.43 (br t, J=7.7 Hz, 1H), 4.20-4.37 (m, 4H), 4.09 (br s, 0.4H rotamer), 4.04 (br d, J=3.5 Hz, 1.6H rotamer), 3.74 (d, J=8.5 Hz, 0.8H rotamer), 3.55 (br d, J=4.7 Hz, 2H), 3.09-3.21 (m, 1H), 2.92-3.06 (m, 1H), 2.74-2.86 (m, 1H), 2.52-2.59 (m, 3H), 2.42-2.47 (m, 3H rotamer), 2.32-2.42 (m, 2H), 1.97-2.29 (range, 4H), 1.81-1.96 (range, 4H), 1.78 (s, 3H), 1.36-1.74 (range, 6H), 0.98-1.05 (m, 3H), 0.96 (d, J=6.6 Hz, 2.4H rotamer), 0.82 (d, J=6.6 Hz, 2.4H rotamer), 0.63-0.69 (m, 0.6H rotamer), 0.52-0.59 (m, 0.6H rotamer)

^{13}C NMR (DMSO-d_6) δ: 184.4, 171.8, 171.5, 171.3, 171.2, 170.6, 167.6, 167.3, 167.1, 163.7, 160.6, 160.1, 159.9, 153.5, 153.4, 151.6, 151.4, 147.8, 147.7, 139.3, 139.0, 131.3, 131.1, 131.0, 130.2, 129.7, 129.2, 129.0, 128.7, 128.2, 128.1, 127.3, 119.6, 115.7, 107.2, 93.6, 93.5, 81.3, 69.5, 69.4, 68.7, 67.0, 59.7, 59.2, 58.8, 58.6, 56.2, 56.0, 55.4, 55.3, 54.8, 54.6, 50.1, 50.0, 49.6, 49.3, 42.0, 41.5, 38.7, 37.9, 36.7, 30.8, 29.8, 27.7, 27.5, 26.3, 24.7, 23.5, 23.3, 23.1, 20.7, 20.7, 19.5, 19.5, 19.4, 15.9, 15.8, 15.7, 15.6

More carbon peaks detected than present in the structure due to presence of rotamers

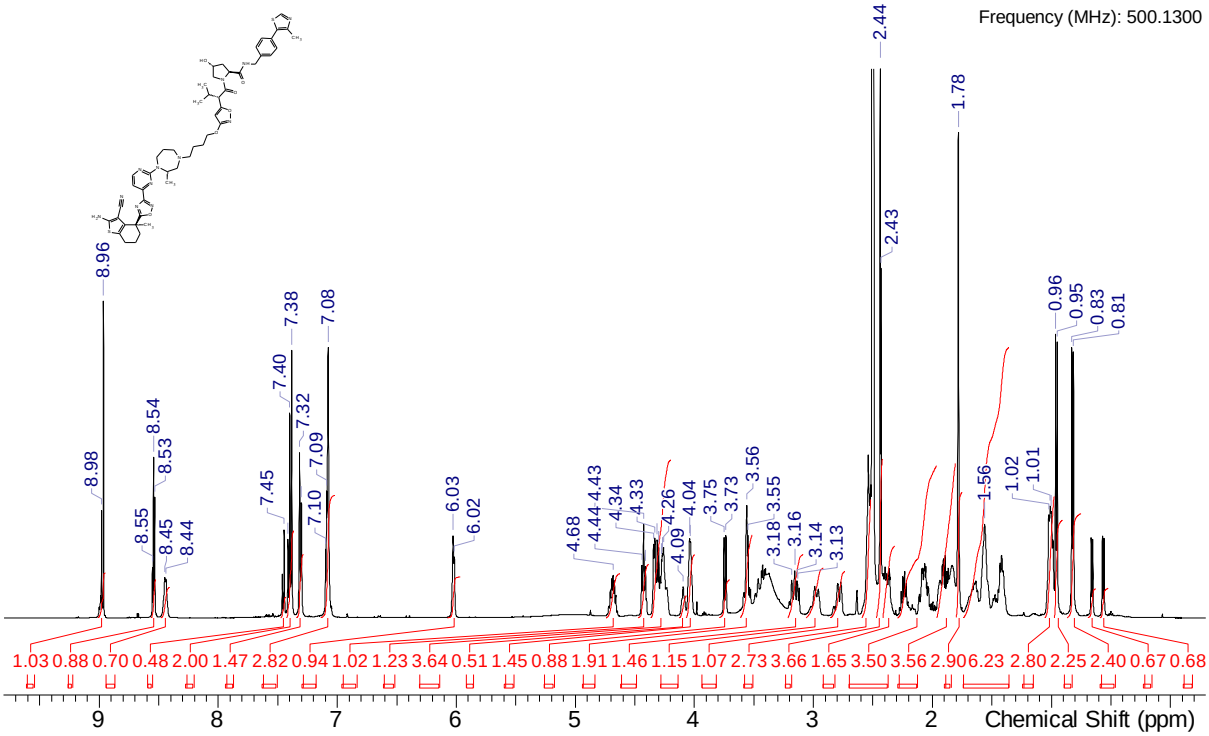

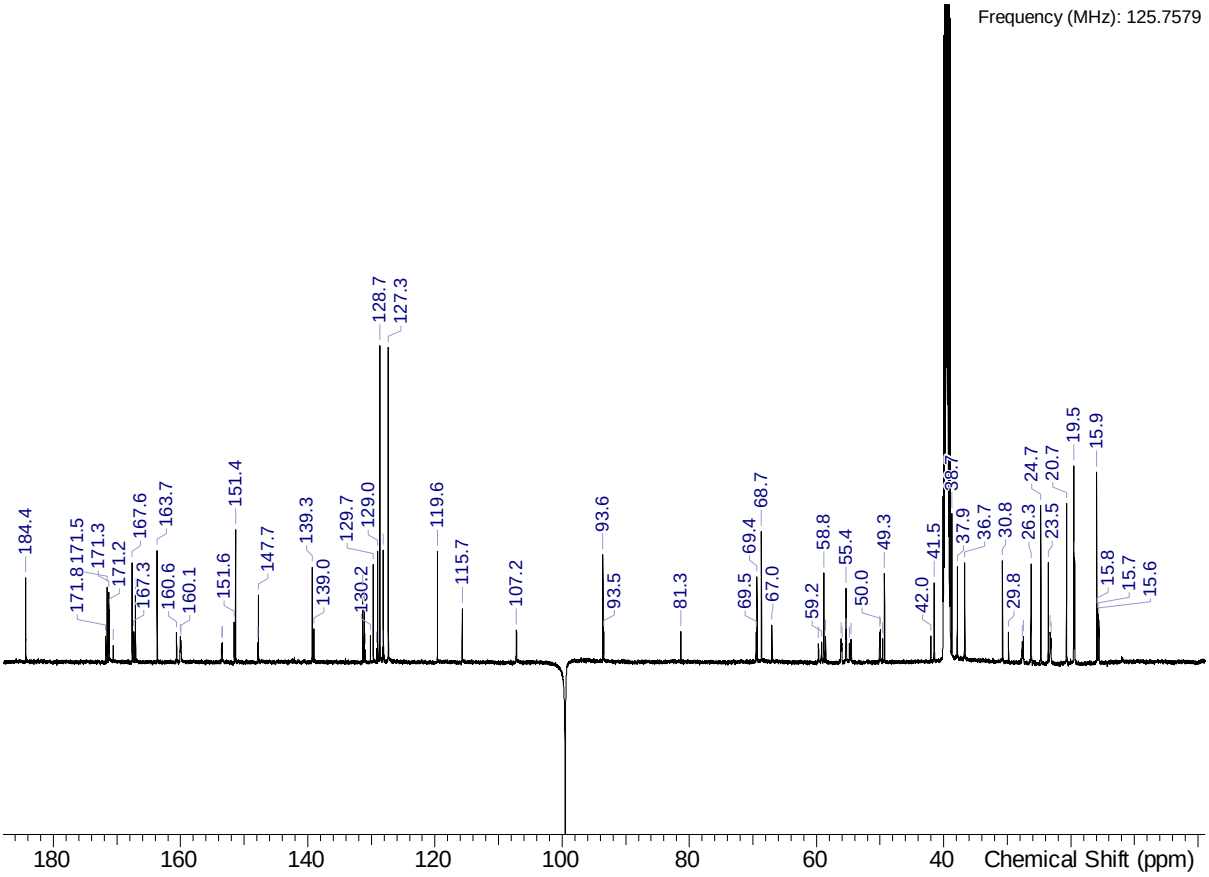

The spike observed at 99.5 ppm is an artefact from the carrier frequency.

^{1}H NMR (DMSO-d_6) δ: 8.98 (s, 0.85H rotamer), 8.97 (s, 0.15H rotamer), 8.82 (s, 0.15H rotamer), 8.55 (d, J=4.4 Hz, 1H), 8.51 (t, J=6.0 Hz, 1H), 7.40-7.46 (m, 2H), 7.36-7.39 (m, 1.7H rotamer), 7.34 (d, J=8.2 Hz, 0.3H rotamer), 7.05-7.12 (m, 3H), 6.03-6.08 (m, 0.85H rotamer), 5.66 (br s, 0.15H rotamer), 5.10 (d, J=3.8 Hz, 0.85H rotamer), 5.02 (d, J=2.8 Hz, 0.15H rotamer), 4.67-4.75 (m, 0.85H rotamer), 4.64 (s, 0.15H rotamer), 4.18-4.40 (m, 5H), 4.10 (br s, 1.7H rotamer), 3.99-4.06 (m, 0.3H rotamer), 3.76 (dd, J=10.6, 4.3 Hz, 0.85H rotamer), 3.65 (br d, J=9.8 Hz, 0.85H rotamer), 3.54-3.61 (m, 0.3H rotamer), 3.44 (br d, J=10.7 Hz, 0.85H rotamer), 3.35-3.41 (m, 0.3H rotamer), 3.18 (br t, J=12.6 Hz, 1H), 2.94-3.07 (m, 1H), 2.82 (br d, J=12.0 Hz, 1H), 2.54 (br s, 4H), 2.41-2.46 (m, 4H), 2.16-2.30 (m, 1H), 1.81-2.14 (range, 6H), 1.78 (s, 3H), 1.37-1.74 (range, 7H), 1.02 (br s, 3H), 0.94 (d, J=6.3 Hz, 3H), 0.79 (br d, J=6.6 Hz, 3H)

^{13}C NMR (DMSO-d_6) δ: 184.4, 171.6, 171.5, 171.4, 171.2, 171.1, 171.0, 168.3, 167.4, 167.1, 163.7, 160.6, 160.1, 160.0, 153.5, 153.4, 151.4, 147.8, 147.8, 139.4, 138.9, 131.3, 131.1, 131.0, 130.1, 129.8, 128.9, 128.8, 127.8, 127.5, 119.6, 115.7, 107.2, 93.5, 93.1, 81.3, 69.5, 69.3, 68.6, 67.0, 59.7, 59.2, 59.1, 58.8, 56.2, 56.1, 55.7, 55.3, 54.9, 54.5, 50.0, 50.0, 49.9, 49.3, 42.1, 41.6, 38.7, 38.0, 36.7, 32.0, 31.1, 27.7, 27.5, 26.3, 24.7, 23.5, 23.3, 23.2, 20.4, 20.1, 20.0, 19.8, 19.4, 15.9, 15.9, 15.7, 15.6

More carbon peaks detected than present in the structure due to presence of rotamers

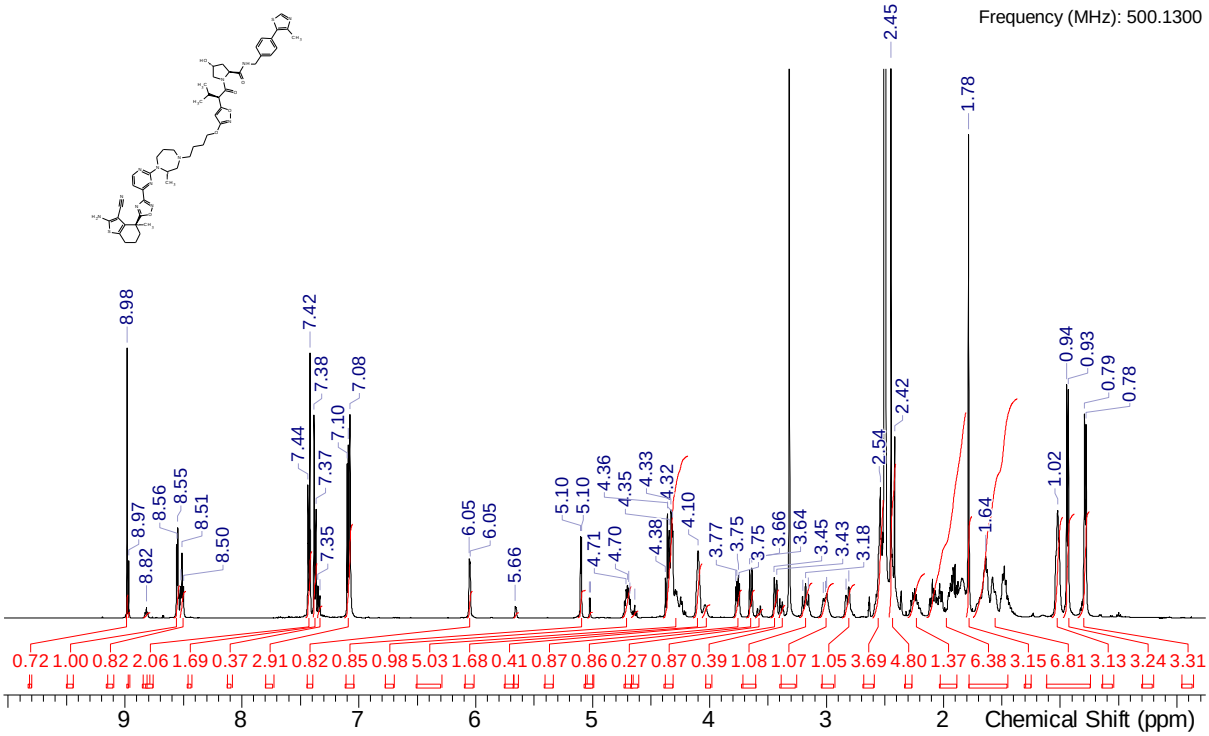

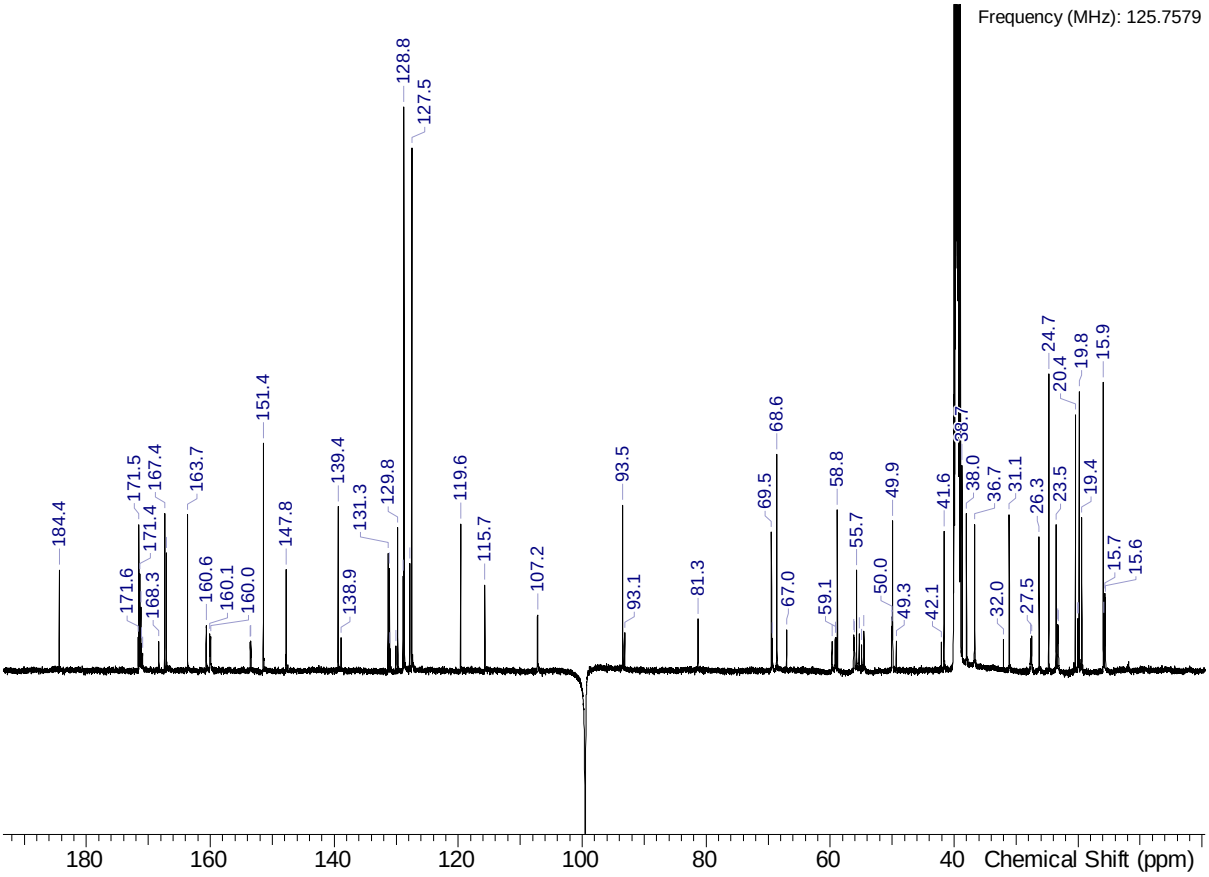

The spike observed at 99.5 ppm is an artefact from the carrier frequency.

HRMS (*m/z*): $[M+H]^+$ calcd. for C50H60N12O6S2 , 989.42730; found, 979.42767

Synthesis of cis VHL negative control compound 5

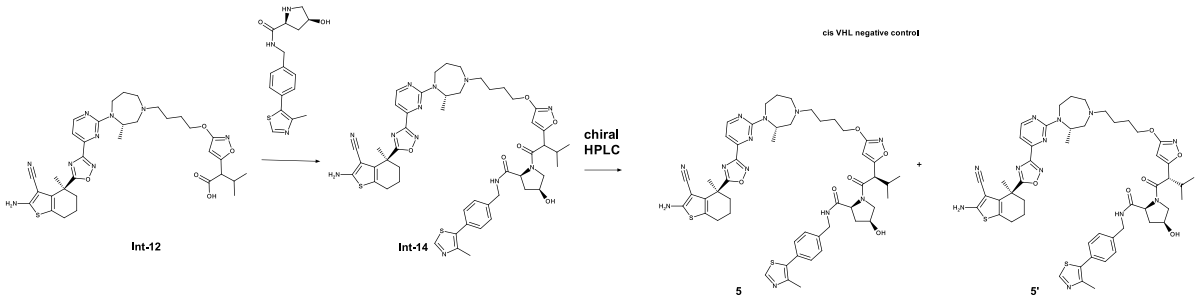

To a stirred solution of **Int-12** (166 mg, 0.24 mmol, 1.0 eq.), (2S,4S)-4-hydroxy-N-{[4-(4-methyl-1,3-thiazol-5-yl)phenyl]methyl}pyrrolidine-2-carboxamide (115 mg, 0.361 mmol, 1.5 eq.) and HATU (112 mg, 0.29 mmol, 1.2 eq.) in a 1:1 mixture of DMSO and acetonitrile (3 ml) is added TEA (174 mL, 1.20 mmol, 5.0 eq) and the reaction mixture is stirred at rt for 30 min. After complete conversion the reaction mixture is quenched with water, diluted with acetonitrile and purified by RP chromatography (Method 3b) to obtain a mixture of diastereomers **Int-14** (160 mg, 0.182, combined 67 % yield). The mixture is separated by preparative chiral HPLC (Method A) to obtain negative control compound **5** (46 mg, 0.045 mmol) and **5'** (61 mg, 0.062 mmol).

^{1}H NMR (DMSO-d_6) δ: 8.98 (s, 0.85H rotamer), 8.96 (s, 0.15H rotamer), 8.68-8.74 (m, 0.15H rotamer), 8.66-8.68 (m, 0.15H rotamer), 8.62 (br t, J=5.8 Hz, 0.85H rotamer), 8.50-8.57 (m, 1H rotamer), 7.29-7.47 (m, 4H), 7.01-7.15 (m, 3H), 6.06 (br d, J=5.7 Hz, 0.85H rotamer), 5.74 (br d, J=3.8 Hz, 0.15H rotamer), 5.43 (br s, 1H), 5.13-5.28 (m, 0.15H rotamer), 4.85-5.03 (m, 0.15H rotamer), 4.65-4.76 (m, 1H), 4.59-4.65 (m, 0.15H rotamer), 4.15-4.46 (range, 5H), 3.98-4.13 (range, 2H), 3.63-3.80 (m, 2H), 3.56 (br dd, J=10.1, 4.1 Hz, 1H), 3.45-3.50 (m, 0.15H rotamer), 3.17 (br t, J=12.6 Hz, 1H), 2.92-3.07 (m, 1H), 2.81 (br d, J=11.7 Hz, 1H), 2.53 (br s, 2H), 2.41-2.46 (m, 4H), 2.22-2.37 (m, 2H), 2.02-2.13 (m, 1H), 1.93 (br s, 1H), 1.83 (br d, J=3.2 Hz, 2H), 1.78 (s, 3H), 1.71-1.76 (m, 1H), 1.51-1.70 (range, 4H), 1.48 (br d, J=7.6 Hz, 2H), 1.19-1.27 (m, 2H), 1.01 (br d, J=6.3 Hz, 3H), 0.94 (br d, J=6.3 Hz, 2.55H rotamer), 0.87-0.91 (m, 0.45H rotamer), 0.81-0.87 (m, 0.45H rotamer), 0.79 (br d, J=6.6 Hz, 2.45H rotamer)

^{13}C NMR (DMSO-d_6) δ: 184.4, 172.3, 171.8, 171.4, 171.2, 171.0, 168.4, 167.6, 167.1, 163.7, 160.7, 160.1, 160.0, 153.5, 153.5, 151.5, 147.8, 139.1, 138.8, 131.3, 131.1, 131.0, 130.0, 129.8, 128.8, 128.8, 128.7, 127.8, 127.5, 127.4, 119.6, 115.7, 107.2, 107.2, 93.6, 93.2, 81.3, 69.5, 69.3, 69.0, 67.5, 59.7, 59.3, 59.2, 58.9, 56.2, 56.1, 55.4, 55.3, 54.8, 54.5, 50.0, 50.0, 49.7, 49.2, 42.2, 41.8, 38.7, 37.2, 36.7, 32.0, 31.5, 31.3, 30.8, 30.3, 29.4, 29.0, 28.7, 27.7, 27.5, 26.3, 24.7, 23.5, 23.3, 23.2, 22.1, 21.4, 20.4, 20.1, 19.9, 19.8, 19.7, 19.5, 19.4, 15.9, 15.7, 15.6,

More carbon peaks detected than present in the structure due to presence of rotamers

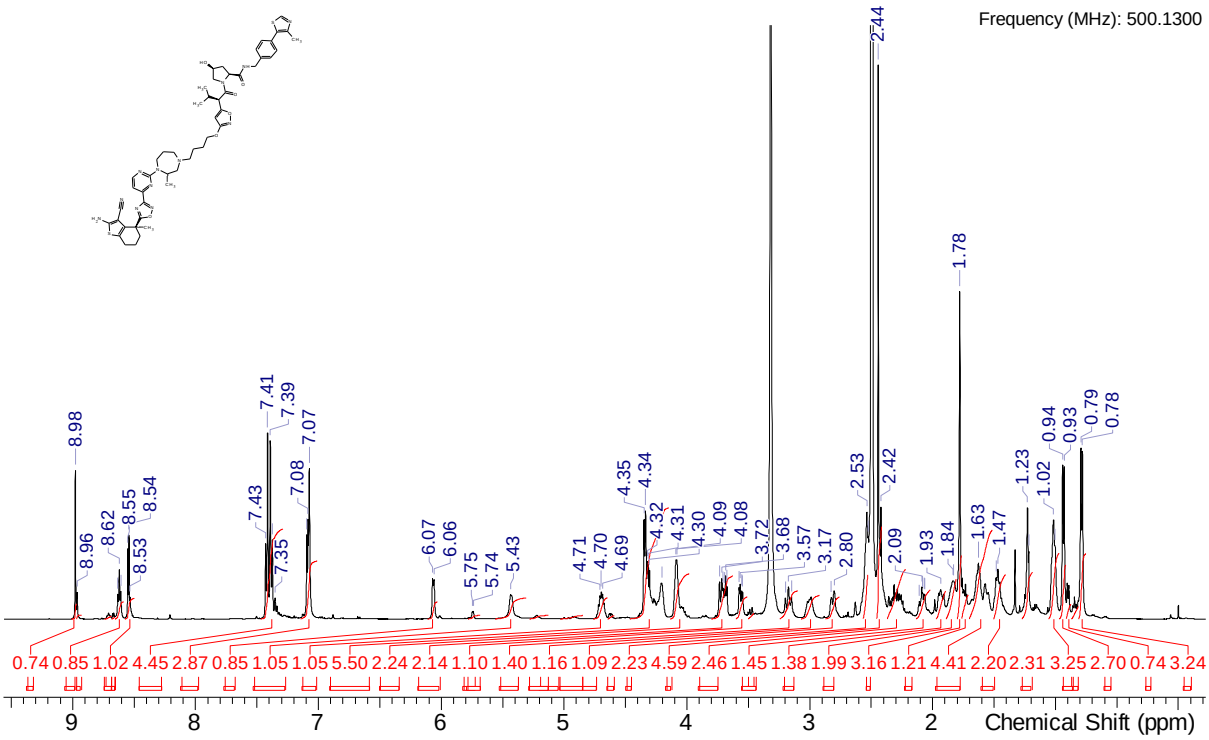

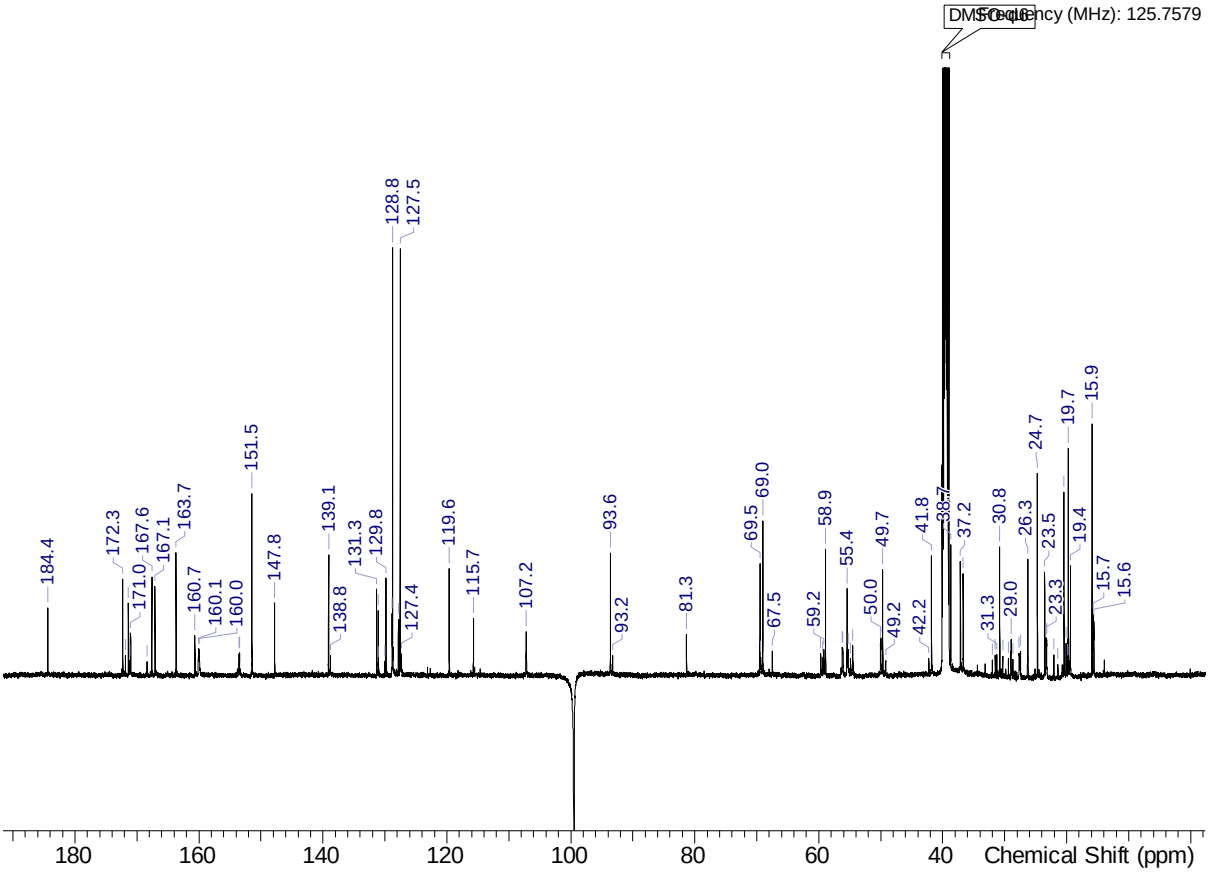

The spike observed at 99.5 ppm is an artefact from the carrier frequency.

^{1}H NMR (DMSO-d_6) δ: 8.98 (s, 0.25H rotamer), 8.96 (s, 0.75H rotamer), 8.53 (d, J=4.7 Hz, 1H), 8.48 (br d, J=5.7 Hz, 0.75H rotamer), 7.26-7.51 (m, 4H), 7.02-7.15 (m, 3H), 6.05 (br d, J=6.0 Hz, 0.25H rotamer), 6.01 (br d, J=3.2 Hz, 0.75H rotamer), 5.37 (br d, J=6.6 Hz, 0.75H rotamer), 5.20 (br d, J=5.4 Hz, 0.25H rotamer), 4.68 (br s, 1H), 4.19-4.43 (range, 5H), 3.96-4.18 (m, 2H), 3.85 (br dd, J=10.4, 5.4 Hz, 1H), 3.76 (d, J=8.8 Hz, 0.75H rotamer), 3.61 (br dd, J=12.0, 5.0 Hz, 0.25H rotamer), 3.10-3.23 (m, 1H), 2.97 (br d, J=14.5 Hz, 1H), 2.74-2.85 (m, 1H), 2.51-2.57 (m, 3H), 2.43 (s, 4H), 2.36 (br s, 3H), 2.23 (br d, J=8.2 Hz, 1H), 2.07 (br d, J=10.1 Hz, 1H), 1.94 (br d, J=9.1 Hz, 1H), 1.83 (br s, 2H), 1.76-1.80 (m, 3H), 1.36-1.73 (range, 7H), 1.20-1.25 (m, 1H), 0.96-1.05 (m, 3H), 0.93 (d, J=6.6 Hz, 2.25H rotamer), 0.81 (d, J=6.6 Hz, 2.25H rotamer), 0.69 (br d, J=6.6 Hz, 0.75H rotamer), 0.60 (br d, J=6.9 Hz, 0.75H rotamer)

^{13}C NMR (DMSO-d_6) δ: 184.4, 172.1, 172.1, 171.4, 171.3, 171.1, 167.8, 167.5, 167.1, 163.7, 160.7, 160.6, 160.1, 159.9, 153.5, 153.4, 151.5, 151.4, 147.8, 147.7, 139.0, 138.9, 131.3, 131.1, 131.0, 130.1, 129.7, 128.9, 128.9, 128.8, 128.7, 128.1, 127.4, 127.3, 119.6, 115.7, 107.2, 93.5, 81.3, 69.5, 69.4, 69.1, 67.4, 59.7, 59.2, 58.9, 56.2, 56.0, 55.3, 55.1, 54.6, 50.1, 50.0, 49.7, 49.3, 42.2, 41.7, 38.7, 37.0, 36.7, 30.6, 29.9, 27.7, 27.5, 26.3, 24.7, 23.5, 23.2, 23.1, 20.7, 20.6, 19.5, 19.4, 15.9, 15.9, 15.7, 15.6,

More carbon peaks detected than present in the structure due to presence of rotamers

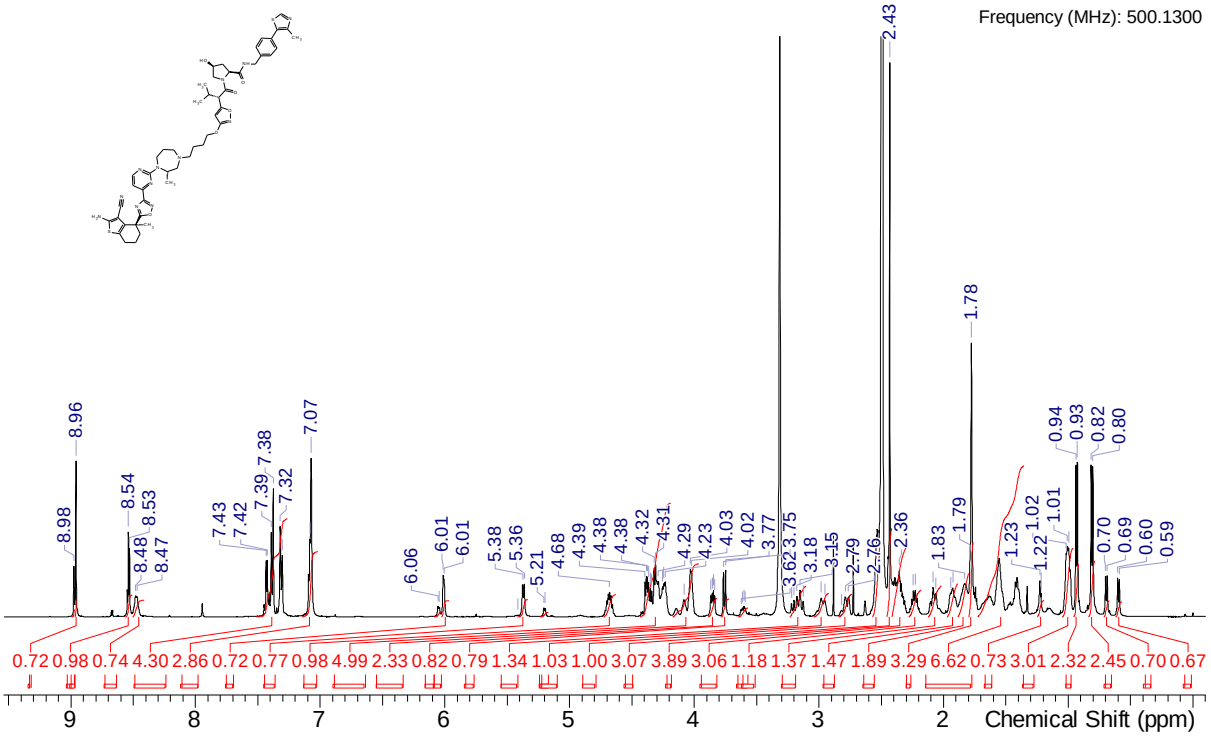

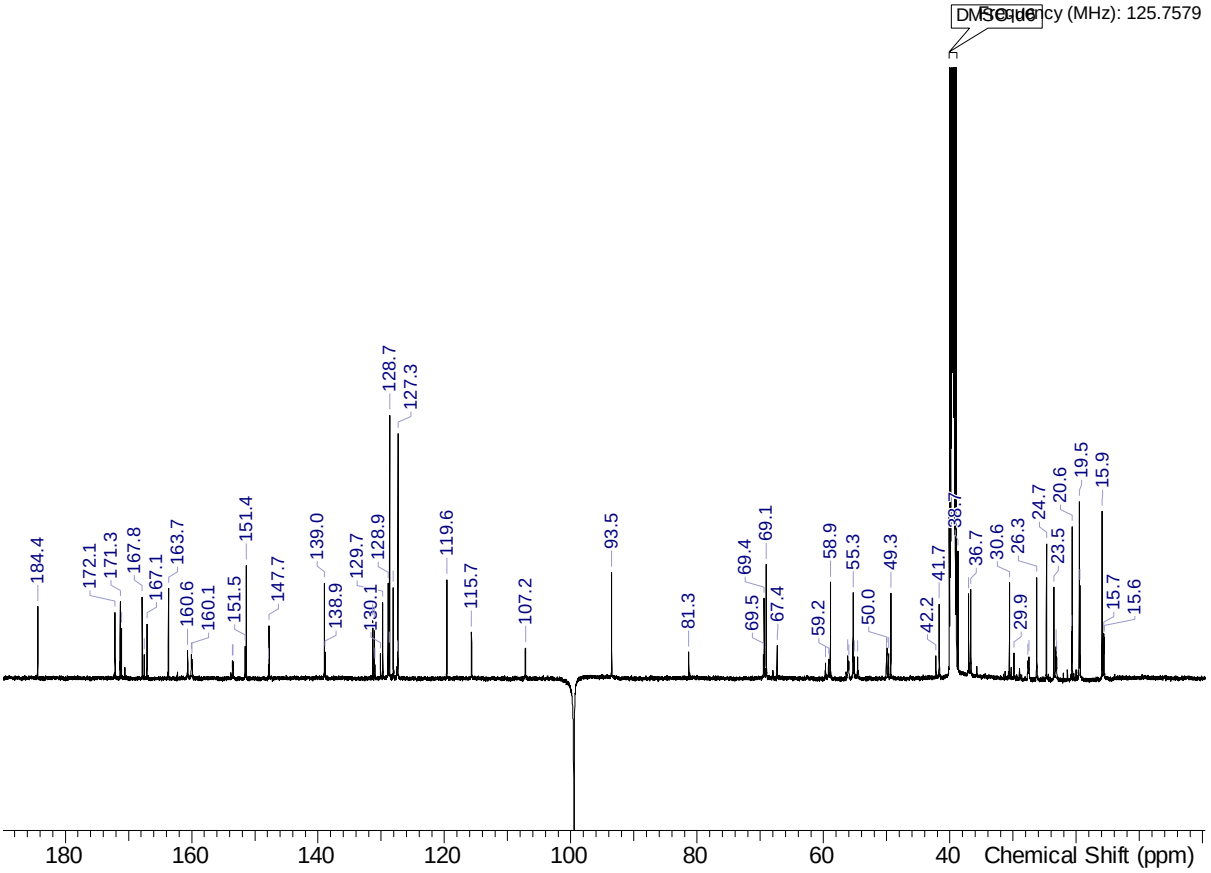

The spike observed at 99.5 ppm is an artefact from the carrier frequency.

Synthesis of Compound 7 (ACBI3):

Intermediate **Int-15**:

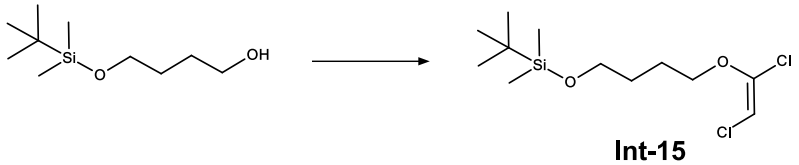

Int-15

To a stirred solution of 4-[(tert-butyldimethylsilyl)oxy]butan-1-ol (20.00 g, 0.10 mol, 1.0 eq.) in THF (200 ml) is added sodium hydride (2.81 g, 0.12 mol, 1.2 eq.) at 0 °C and stirred at rt for 1 h. To the reaction mixture is cooled to 0 °C and trichloroethylene (15.38 g, 0.12 mol, 1.2 eq.) is added at 0 °C. The reaction mixture is warmed to rt and stirred for 48 h. The reaction mixture is quenched with ice cold water and the aqueous solution extracted with EtOAc (3 times). The combined organic layer is washed with water and brine, dried over sodium sulfate, filtered and concentrated under reduced pressure to afford the crude product which is purified by normal phase chromatography yielding **Int-15** (20.00 g, 0.067 mol, 68% yield).

^{1}H NMR (DMSO-d_6) δ: 6.07 (s, 1H), 4.04 (t, J=6.3 Hz, 2H), 3.61 (t, J=6.2 Hz, 2H), 1.62-1.72 (m, 2H), 1.57 (dd, J=8.6, 5.6 Hz, 2H), 0.86 (s, 9H), 0.01-0.05 (m, 6H)

^{13}C NMR (DMSO-d_6) δ: 142.9, 97.8, 71.8, 62.0, 28.4, 25.8, 25.1, 17.9, -5.3

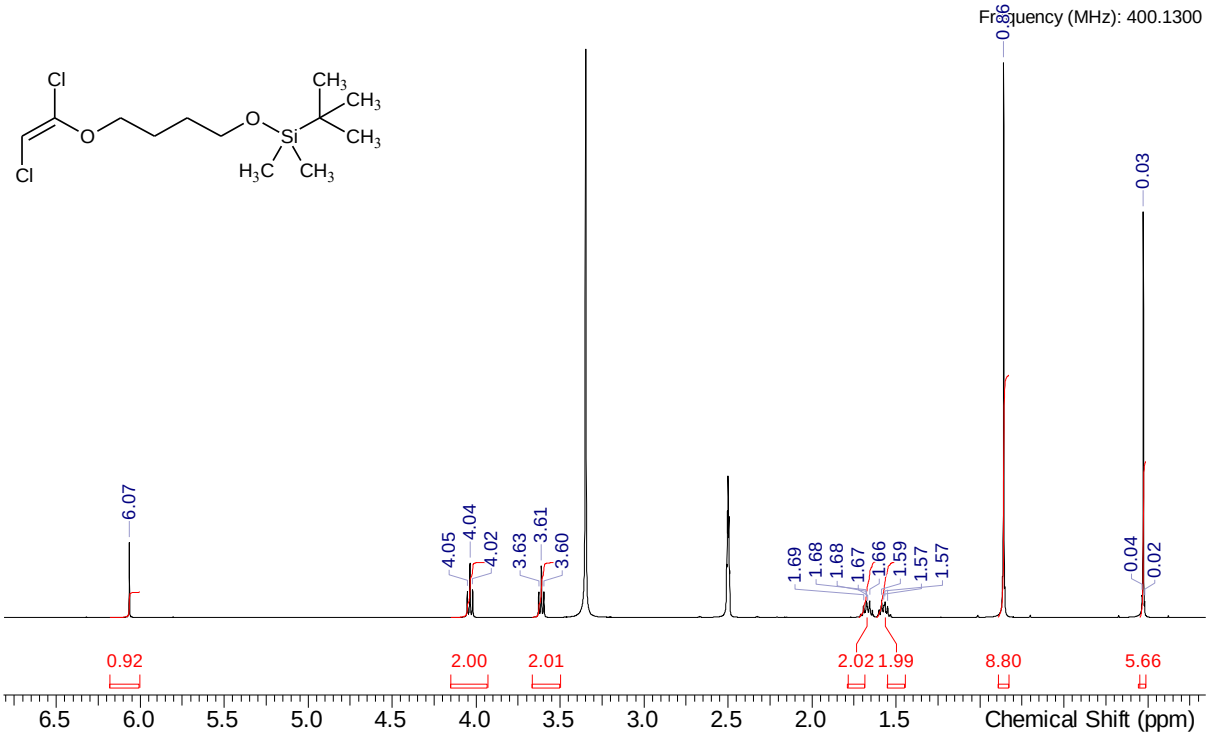
Frequency (MHz): 400.1300
Cl
Cl
O
O
Si
CH3
CH3
CH3
H3C
CH3
6.07
4.05
4.04
4.02
3.63
3.61
3.60
1.69
1.68
1.68
1.67
1.66
1.59
1.57
1.57
0.86
0.04
0.02
0.03
0.92
2.00
2.01
2.02
1.99
8.80
5.66
6.5
6.0
5.5
5.0
4.5
4.0
3.5
3.0
2.5
2.0
1.5
Chemical Shift (ppm)

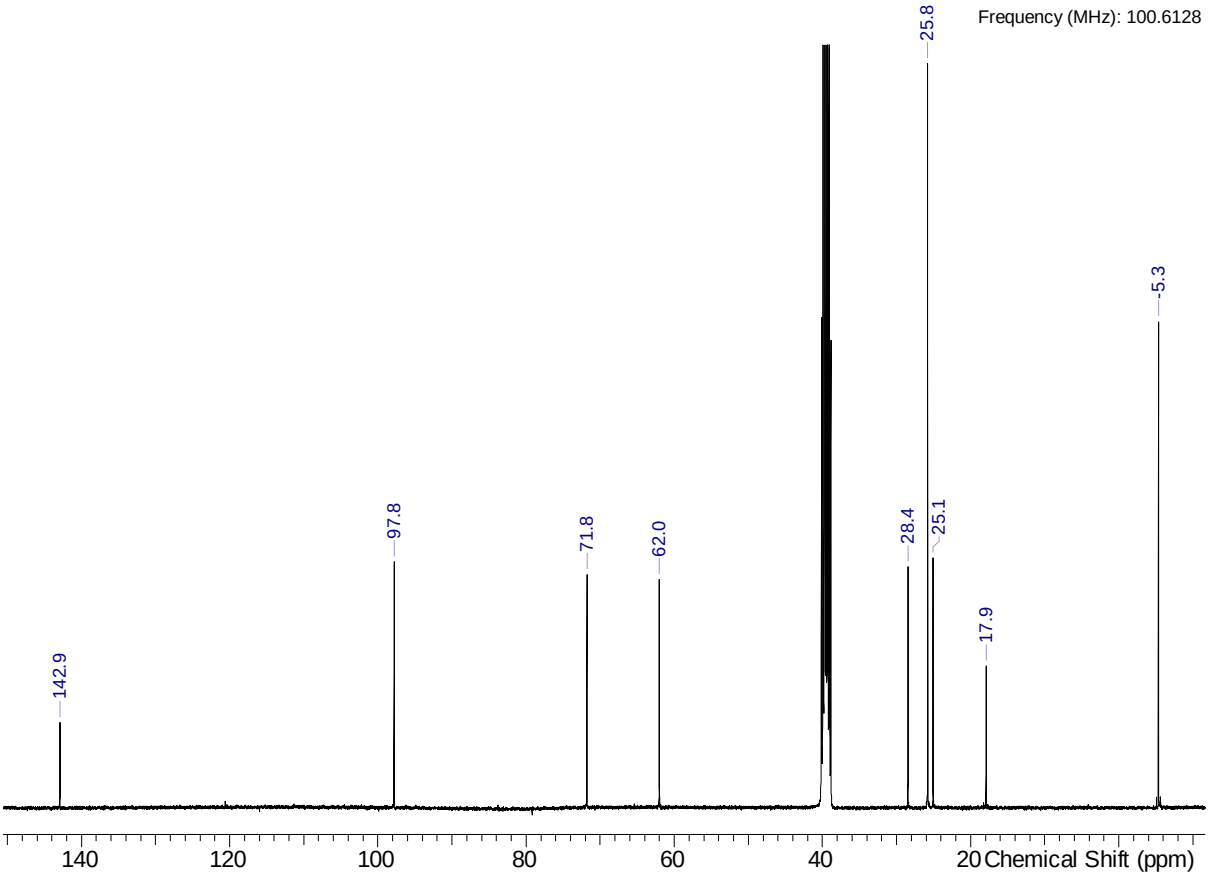
Frequency (MHz): 100.6128
142.9
97.8
71.8
62.0
28.4
25.8
25.1
17.9
-5.3
140
120
100
80
60
40
20
Chemical Shift (ppm)

Intermediate **Int-16**:

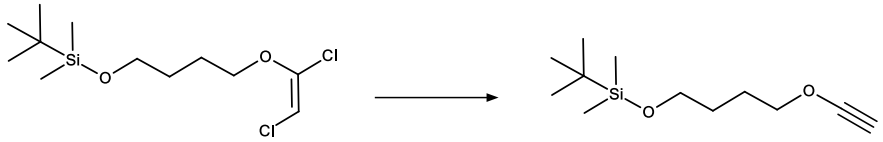

Int-15 **Int-16**

To a stirred solution of intermediate **Int-15** (10.00 g, 0.033 mol, 1.0 eq.) in THF (200 ml) is added n-butyllithium solution (33 mL, 0. mol, 2.5 eq, 2.5 M in hexanes) at -78 °C and stirred at -40 °C for 2 h. After complete conversion the mixture is quenched with saturated ammonium chloride solution and diluted with ice cold water. The aqueous solution extracted with EtOAc (3 x). The combined organic layer is washed with water and brine, dried over sodium sulfate, filtered, and concentrated under reduced pressure to afford the crude product. The crude product is purified by column chromatography yielding intermediate **Int-16** (6.98 g, 0.031 mmol, 92% yield).

^{1}H NMR (DMSO-d_6) δ: 4.10 (t, J=6.6 Hz, 2H), 3.60 (t, J=6.2 Hz, 2H), 2.33 (s, 1H), 1.72 (dd, J=8.6, 6.3 Hz, 2H), 1.43-1.57 (m, 2H), 0.83-0.88 (m, 9H), 0.01-0.04 (m, 6H)

^{13}C NMR (DMSO-d_6) δ: 90.9, 78.4, 61.9, 28.4, 28.0, 25.8, 24.8, 17.9, -5.4

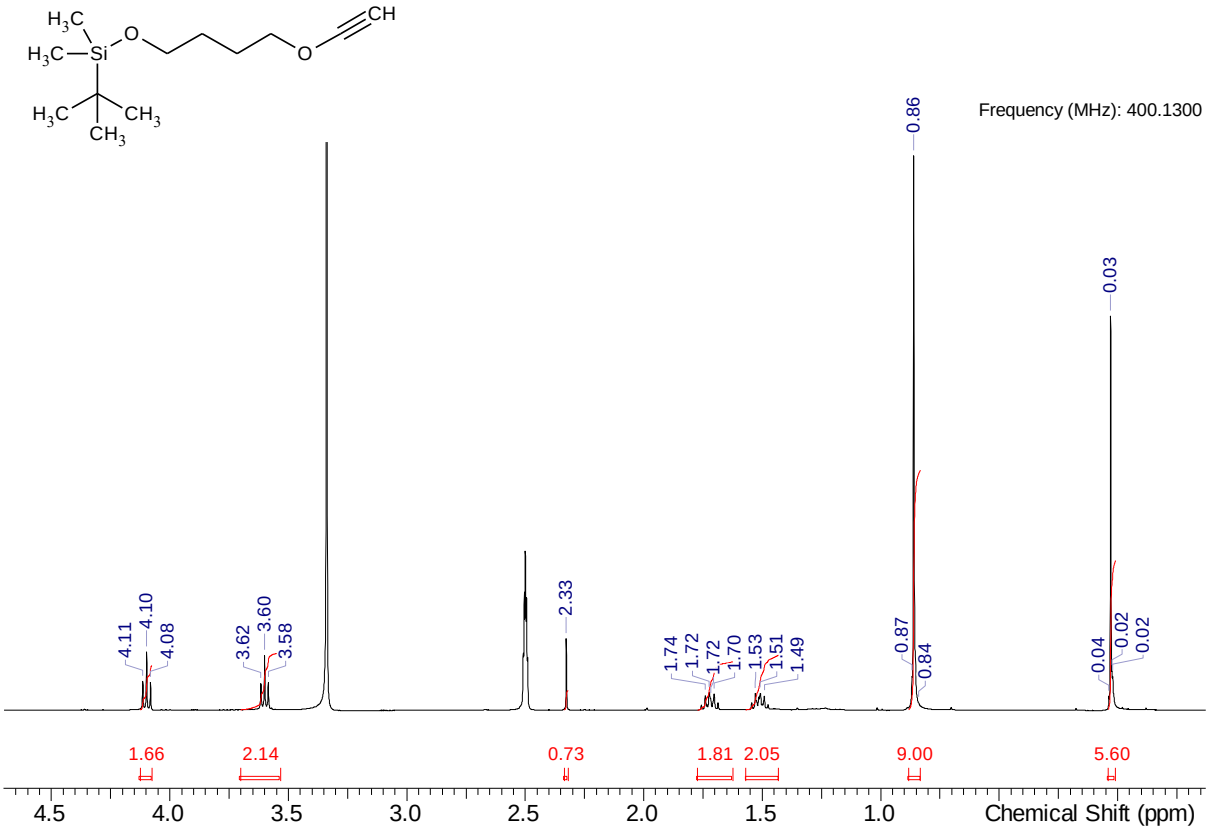
Frequency (MHz): 400.1300
0.86
0.03
4.11
4.10
4.08
3.62
3.60
3.58
2.33
1.74
1.72
1.72
1.70
1.53
1.51
1.49
0.87
0.84
0.04
0.02
0.02
1.66
2.14
0.73
1.81
2.05
9.00
5.60
4.5
4.0
3.5
3.0
2.5
2.0
1.5
1.0
Chemical Shift (ppm)

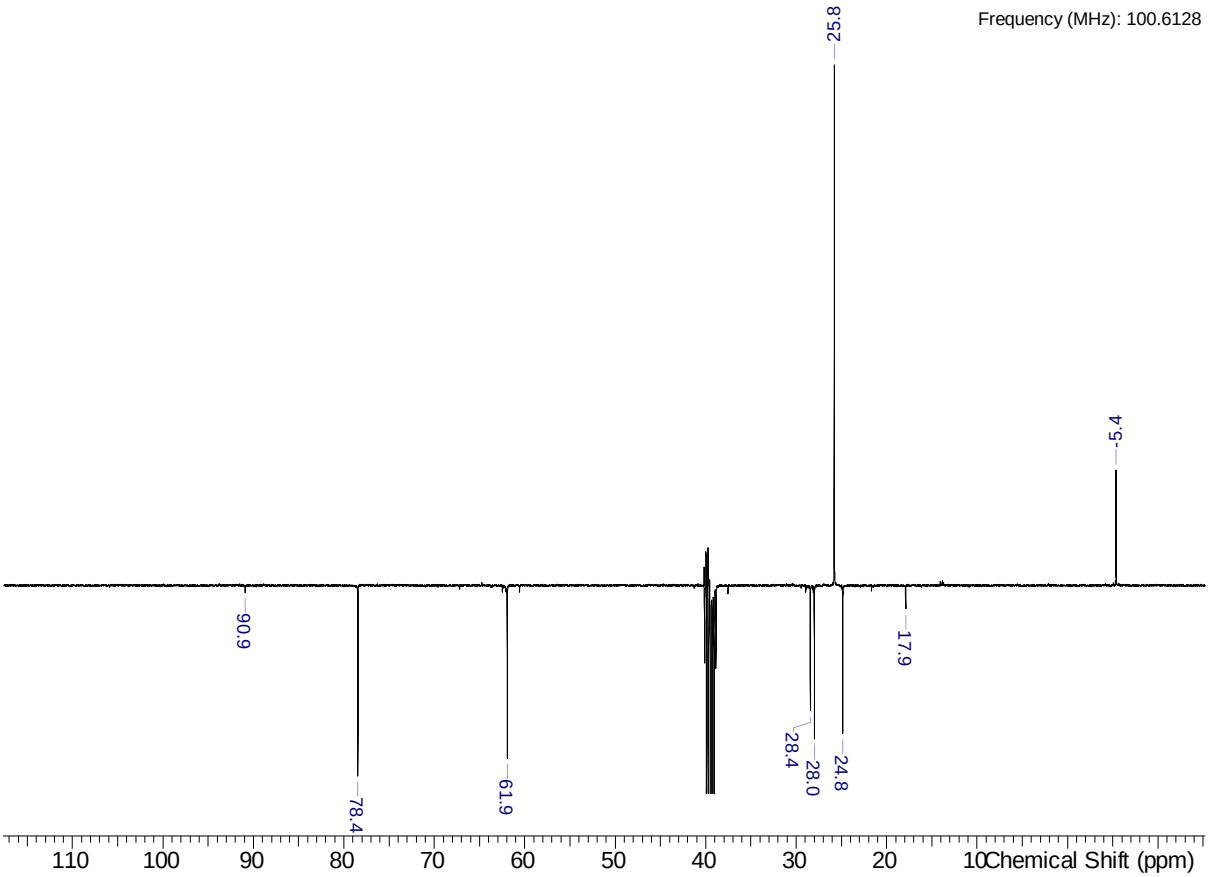
Frequency (MHz): 100.6128
25.8
-5.4
90.9
78.4
61.9
28.4
28.0
24.8
17.9
110
100
90
80
70
60
50
40
30
20
10
Chemical Shift (ppm)

Intermediate **Int-18**:

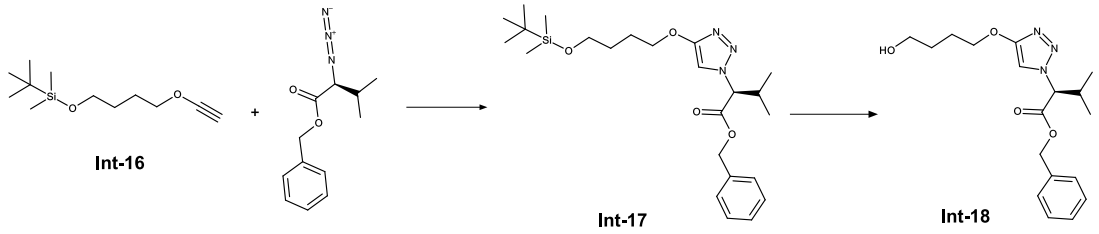

To a stirred solution of intermediate **Int-16** (39.95 g, 174.91 mmol, 2.0 eq.) in EtOAc (200 ml) and water (200 ml) is added methyl (2R)-2-azido-3-methylbutanoate (20.40 g, 87.45 mmol, 1.0 eq.), sodium L-ascorbate (17.3 g, 87.37 mmol, 1 eq) and copper(II) sulfate pentahydrate (6.99 g, 43.96 mmol, 0.5 eq) at 20 °C. The reaction is stirred for 3 h at 20 °C. To the reaction mixture is added water (200 ml) and EtOAc the phases are separated. The organic layer is washed with brine and dried over sodium sulfate, filtered, and concentrated under reduced pressure to afford the crude product **Int-17** as yellow oil which is directly used in the next step without further purification.

^{1}H NMR (DMSO-d_6) δ: 7.76 (s, 1H), 7.30-7.40 (m, 5H), 5.12-5.26 (m, 3H), 4.08 (td, J=6.6, 1.6 Hz, 2H), 3.62 (t, J=6.3 Hz, 2H), 2.52-2.58 (m, 1H), 1.73 (dd, J=8.8, 6.3 Hz, 2H), 1.52-1.62 (m, 2H), 0.92 (d, J=6.6 Hz, 3H), 0.86 (s, 9H), 0.77 (d, J=6.6 Hz, 3H), 0.03 (s, 6H)

^{13}C NMR (DMSO-d_6) δ: 168.0, 160.3, 135.2, 128.4, 128.3, 128.1, 106.8, 70.1, 68.5, 66.9, 62.1, 30.4, 28.6, 25.8, 25.3, 18.7, 18.3, -5.3, 1 carbons only observed in HSQC

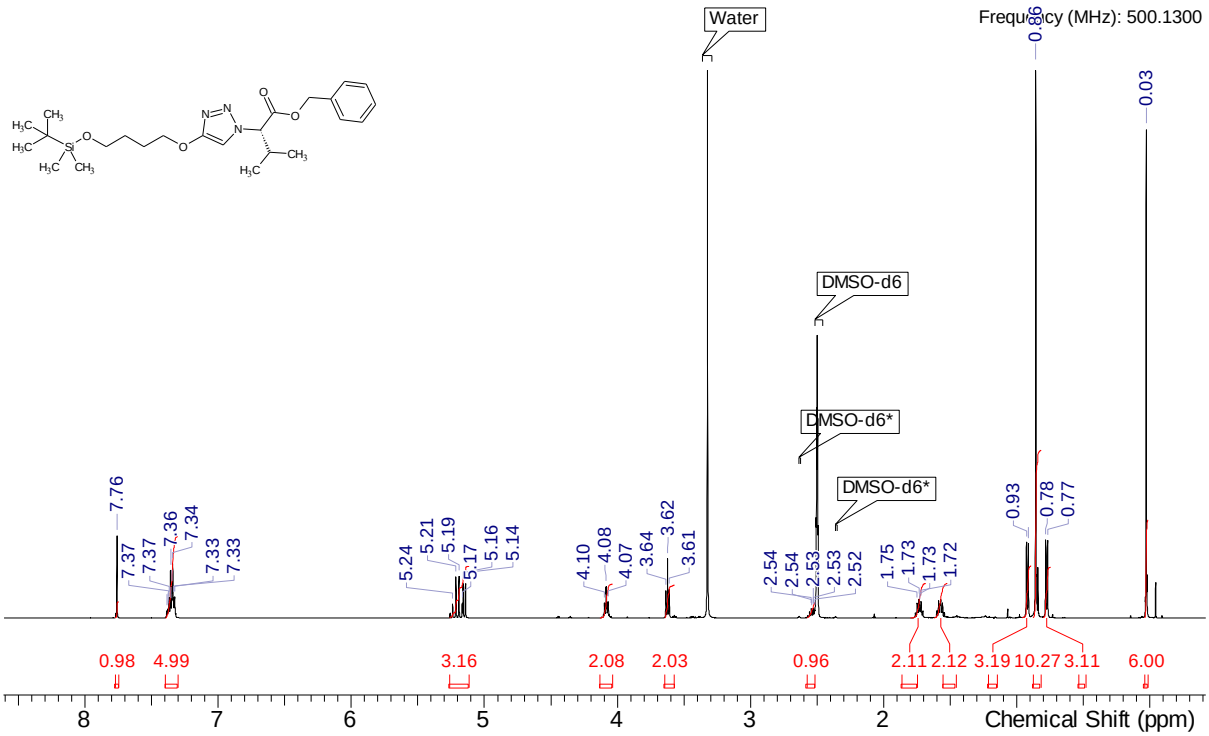

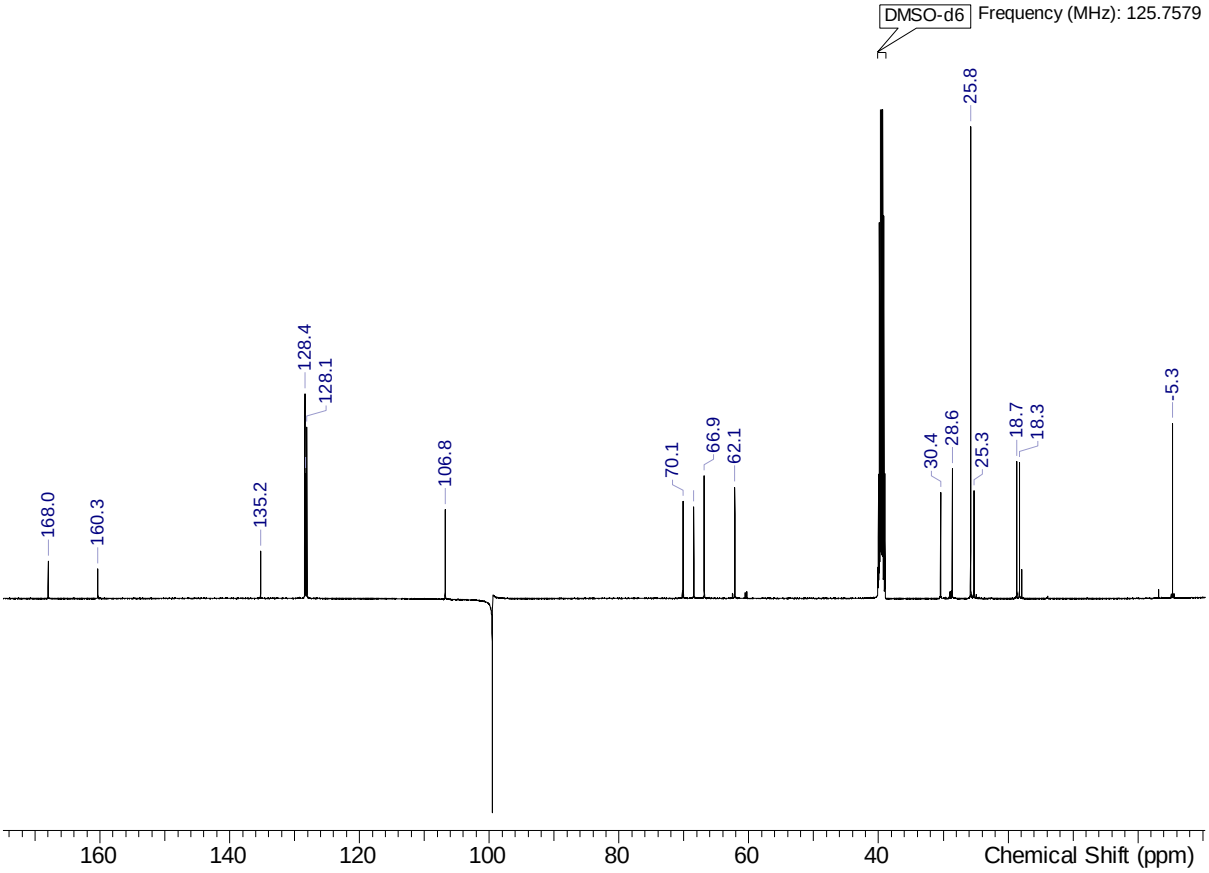

The spike observed at 99.5 ppm is an artefact from the carrier frequency.

HRMS (*m/z*): $[M+H]^+$ calcd. for C24H39N3O4Si , 348.19153; found, 347.18425 (-C6H14Si)

To the stirred solution of the obtained crude mixture in in THF (150 mL) at 10 °C is added HF-pyridine (38.6 g, 389.88 mmol) and the mixture is stirred at 10-20 °C for 2 h. To the mixture is added aqueous $NaHCO_3$ solution (1 M, 1.5 L) and the pH is adjusted to pH 7-8. The phases are separated, and the aqueous phase is extracted with ethyl acetate and the combined organic layers are dried aver Na_2SO_4. The crude product is purified by column chromatography (Petrol ether/EtOAC, 0-10%) to obtain intermediate **Int-18** (23.0 g, 66.20 mmol, 76 % yield over two steps).

^{1}H NMR (DMSO-d_6) δ: 7.77 (s, 1H), 7.28-7.42 (m, 5H), 5.20 (d, J=11.7 Hz, 2H), 5.15 (d, J=8.5 Hz, 1H), 4.45 (br s, 1H), 3.99-4.11 (m, 2H), 3.43 (t, J=6.5 Hz, 2H), 2.54 (m, 1H), 1.68-1.76 (m, 2H), 1.53 (dd, J=8.5, 6.3 Hz, 2H), 0.92 (d, J=6.6 Hz, 3H), 0.78 (d, J=6.6 Hz, 3H)

^{13}C NMR (DMSO-d_6) δ: 168.0, 160.4, 135.3, 128.5, 128.3, 128.1, 106.8, 70.2, 68.5, 66.9, 60.3, 30.4, 28.8, 25.4, 18.7, 18.3

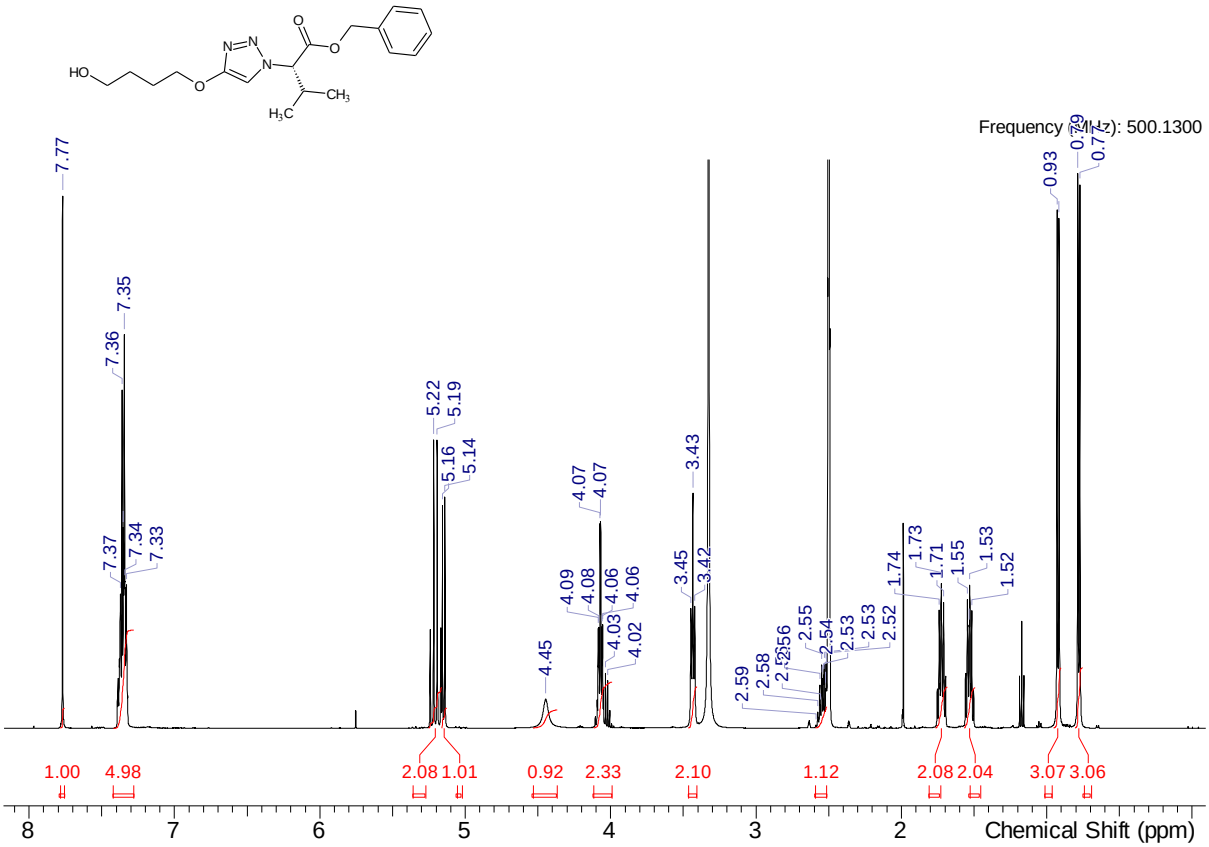

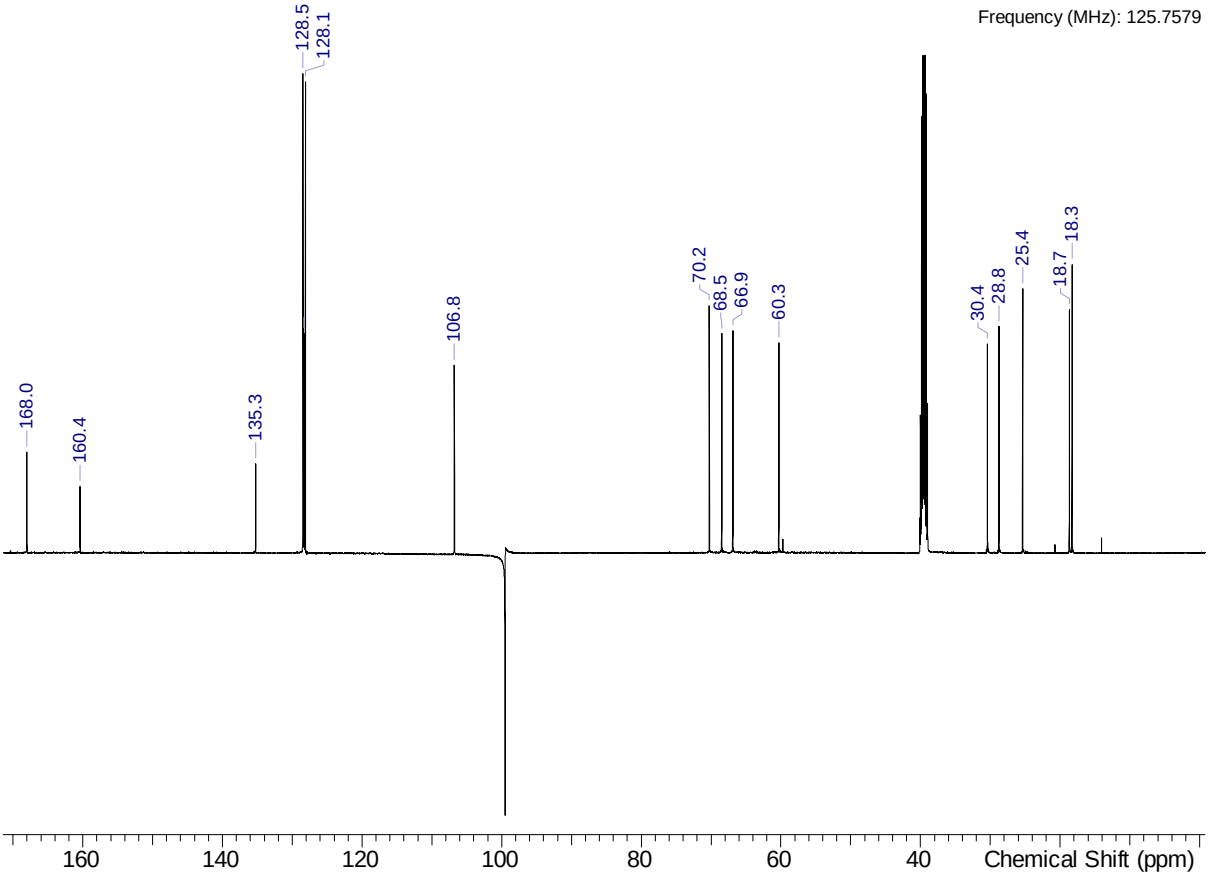

The spike observed at 99.5 ppm is an artefact from the carrier frequency.

HRMS (*m/z*): $[M+H]^+$ calcd. for C18H25N3O4 , 348.19178; found, 348.1911

Intermediate **Int-19**:

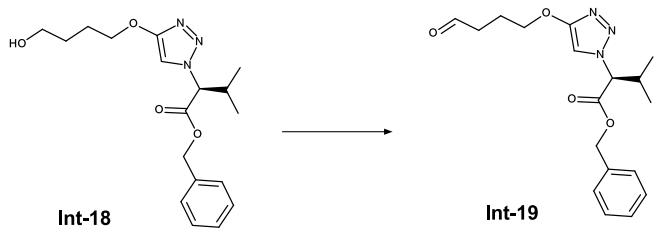

To a stirred solution of intermediate **Int-18** (1.50 g, 4.272 mmol, 1.0 eq) in DCM (30 mL) is added Dess-Martin periodinane (1.81 g, 4.272 mmol, 1.0 eq) and stirred at rt for 2.5 h. To the mixture is added saturated aqueous $NaHCO_3$ solution and the mixture is stirred for 10 min. The mixture is diluted with DCM and the phases are separated. The organic phase is concentrated under reduced pressure and the crude product is purified by column chromatography (Hexane/EtOAc, 0-40%) to obtain **Int-19** (1.2 g, 3.47 mmol, 81 % yield).

^{1}H NMR (DMSO-d_6) δ: 9.70 (t, J=1.1 Hz, 1H), 7.78 (s, 1H), 7.31-7.40 (m, 5H), 5.10-5.30 (m, 3H), 4.08 (t, J=6.6 Hz, 2H), 2.52-2.62 (m, 3H), 1.96 (quin, J=6.8 Hz, 2H), 0.92 (d, J=6.8 Hz, 3H), 0.78 (d, J=6.6 Hz, 3H)

^{13}C NMR (DMSO-d_6) δ: 202.9, 168.0, 160.2, 135.3, 128.5, 128.4, 128.2, 107.0, 69.5, 68.5, 66.9, 30.4, 21.5, 18.7, 18.3, 1C under DMSO

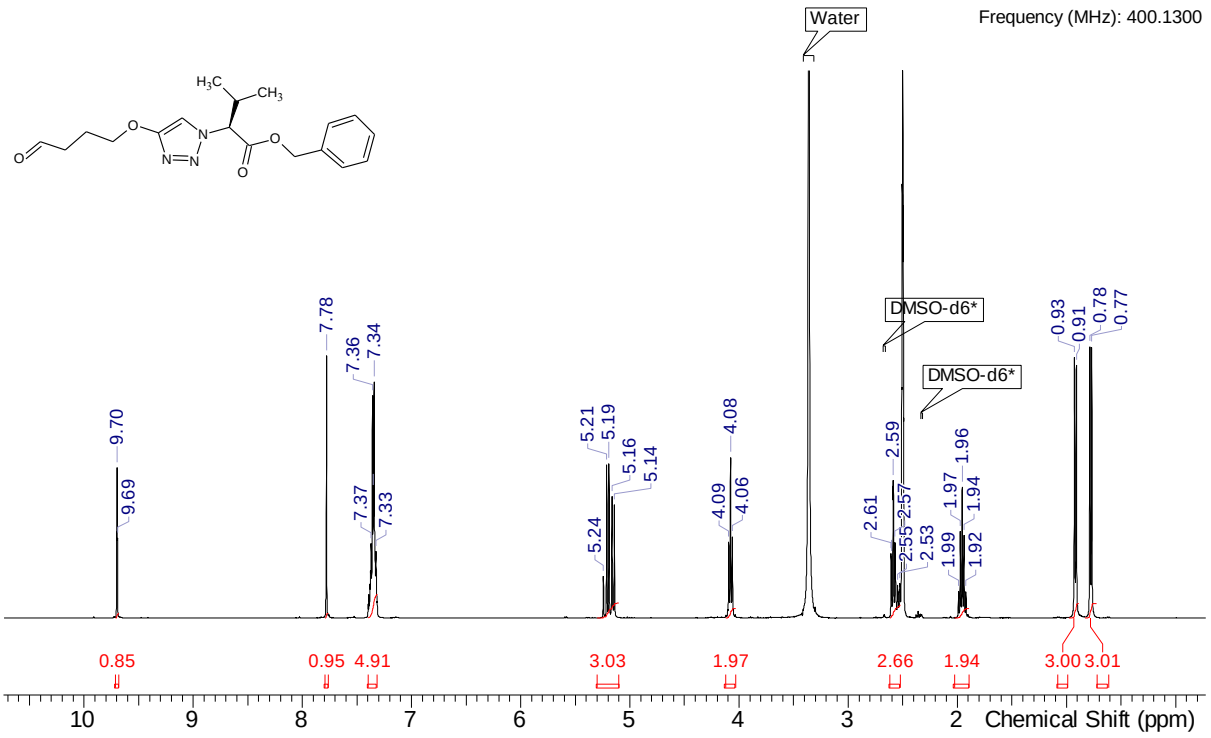

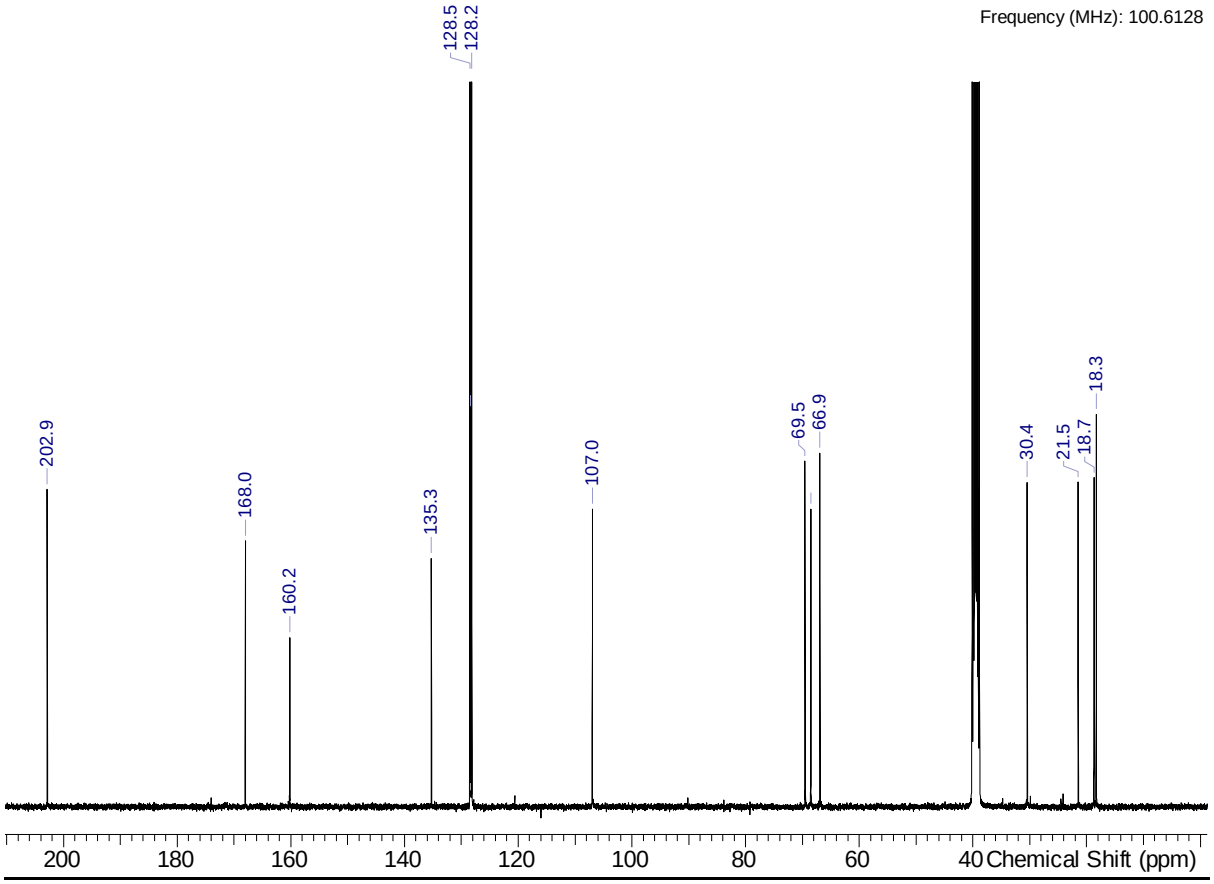

HRMS (*m/z*): $[M+H]^+$ calcd. for C18H23N3O4 , 346.17613; found, 346.17587

Intermediate **Int-20**:

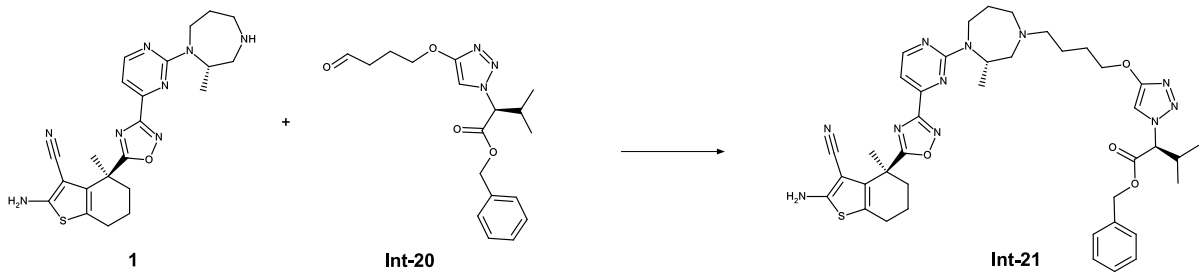

To a stirred solution of **1** (200 mg, 0.444 mmol, 1.0 eq.) and sodium triacetoxy borohydride (235 mg, 1,110 mmol, 2.5 eq.) in DMF (3 mL) at RT is slowly added a solution of **Int-20** (153 mg, 0.444 mmol, 1.0 eq.) in DMF (1 mL). The reaction is stirred for 30 min before it is quenched by addition of water. The solvents are removed under reduced pressure and the crude product is purified by chromatography (Method 3a) to obtain **Int-21** (1.33 g, 1.71 mmol, 84 % yield).

^{1}H NMR (DMSO-d_6) δ: 8.55 (d, J=4.7 Hz, 1H), 7.74 (s, 1H), 7.30-7.39 (m, 5H), 7.09 (s, 1H), 7.08 (s, 2H), 5.19 (d, J=11.0 Hz, 2H), 5.13 (br d, J=8.8 Hz, 1H), 4.65-4.75 (m, 1H), 4.21-4.37 (m, 1H), 4.03 (br s, 2H), 3.18 (br t, J=12.6 Hz, 1H), 3.01 (br d, J=13.9 Hz, 1H), 2.82 (br d, J=11.7 Hz, 1H), 2.51-2.59 (m, 4H), 2.37-2.46 (m, 2H), 2.01-2.19 (m, 1H), 1.80-1.98 (m, 3H), 1.78 (s, 3H), 1.44-1.74 (m, 6H), 1.02 (br s, 3H), 0.91 (d, J=6.6 Hz, 3H), 0.77 (q, J=6.6 Hz, 3H), 1H under DMSO

^{13}C NMR (DMSO-d_6) δ: 184.4, 168.0, 167.1, 163.7, 160.4, 160.1, 160.0, 153.6, 153.5, 135.2, 131.3, 128.5, 128.3, 128.1, 119.6, 115.7, 107.2, 106.8, 81.3, 70.2, 68.5, 66.9, 59.7, 59.2, 56.2, 56.1, 55.3, 54.6, 50.1, 50.0, 38.7, 36.7, 30.4, 27.7, 27.5, 26.4, 24.7, 23.6, 23.4, 23.3, 19.4, 18.7, 18.3, 15.7, 15.6

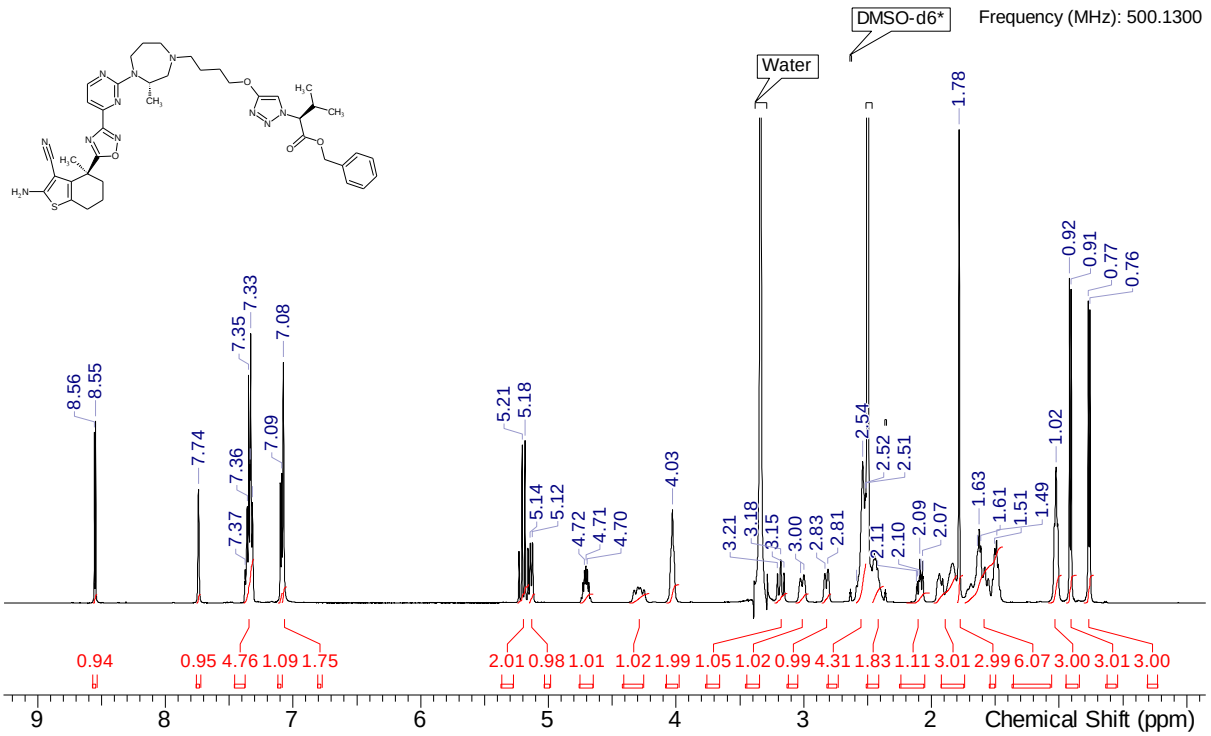

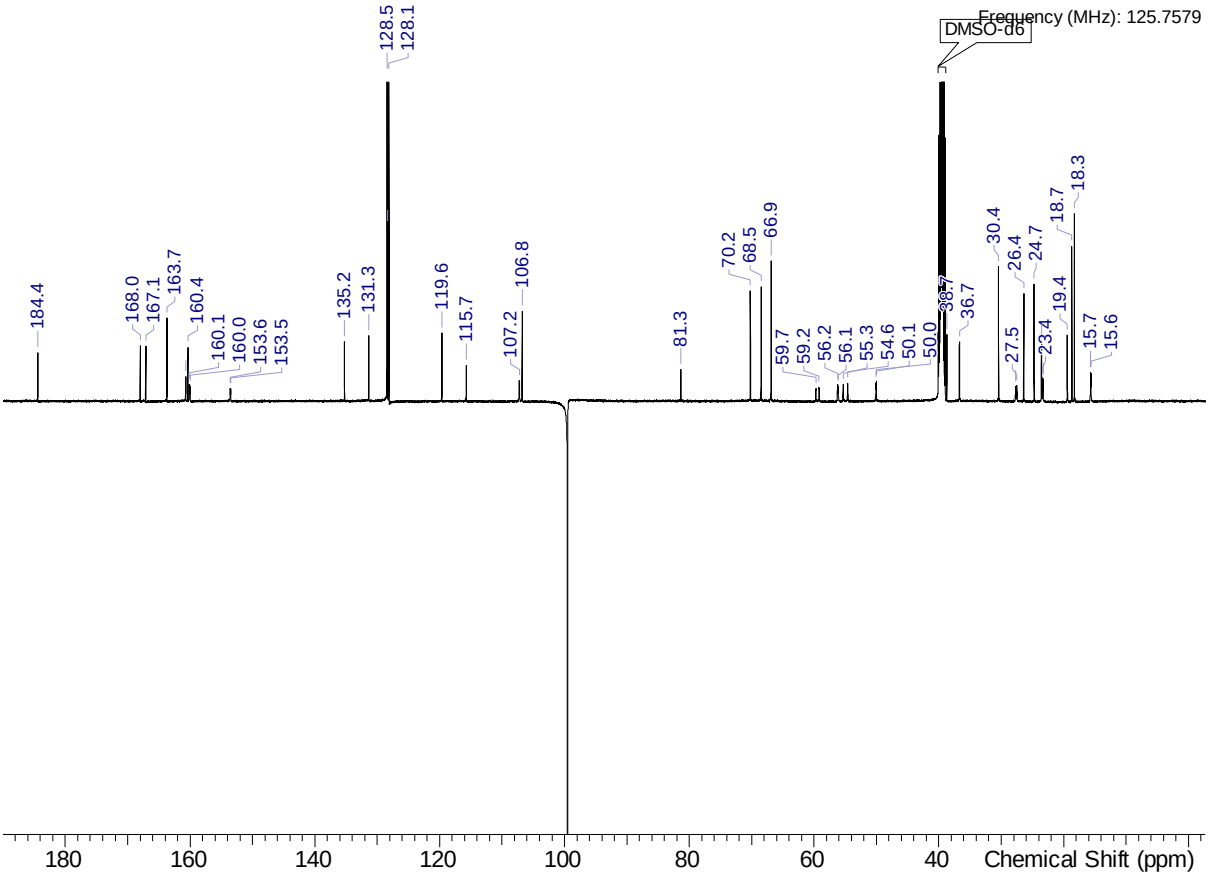

The spike observed at 99.5 ppm is an artefact from the carrier frequency.

HRMS (*m/z*): $[M+H]^+$ calcd. for C40H49N11O4S , 780.37625; found, 780.37671

Intermediate **Int-22**:

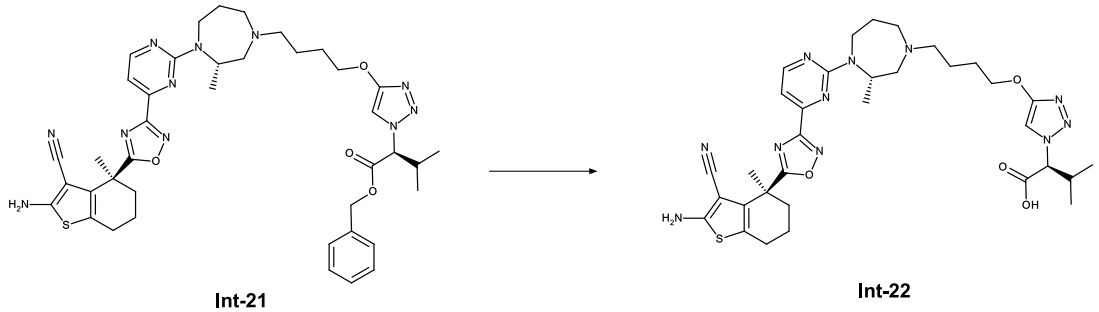

Int-21 **Int-22**

To a solution of intermediate **Int-21** (1.33 g, 1.705 mmol, 1.0 eq.) in MeOH (25 mL) in a hydrogenation reactor is added Pd/C (10%, 350.00 mg). The reaction mixture stirred under a pressure of 8 bar H_2 for 8 h. After complete conversion the reaction mixture is filtered, and the solvent is removed under reduced pressure to give intermediate **Int-22** (1.12 g, 1.624 mmol, 95 % yield) which was used without further purification.

^{1}H NMR (DMSO-d_6) δ: 8.51 (d, J=4.8 Hz, 1H), 7.57 (s, 1H), 6.96-7.19 (m, 3H), 4.71 (br d, J=7.1 Hz, 2H), 4.17-4.39 (m, 1H), 3.97 (br t, J=6.0 Hz, 3H), 2.66-2.96 (m, 3H), 2.50-2.65 (m, 3H), 2.23-2.38 (m, 2H), 1.95-2.08 (m, 1H), 1.45-1.95 (m, 14H), 0.92-1.06 (m, 3H), 0.84 (d, J=6.6 Hz, 3H), 0.67 (d, J=6.8 Hz, 3H)

^{13}C NMR (DMSO-d_6) δ: 184.4, 169.6, 167.1, 163.7, 160.6, 160.1, 153.5, 131.3, 120.6, 119.6, 115.7, 107.5, 106.5, 81.3, 70.1, 69.9, 58.7, 56.0, 55.8, 49.3, 38.7, 36.7, 30.5, 26.8, 26.3, 24.7, 23.5, 19.4, 19.1, 18.4, 15.6, 15.5, 1C under DMSO

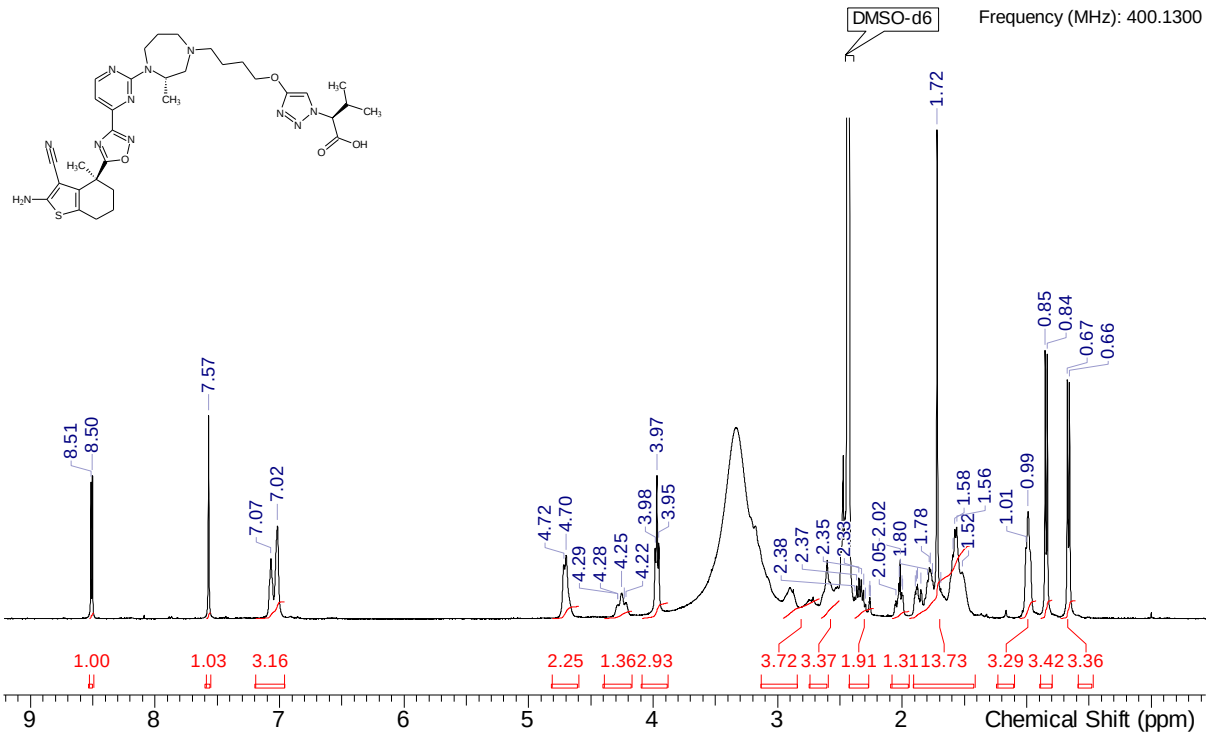

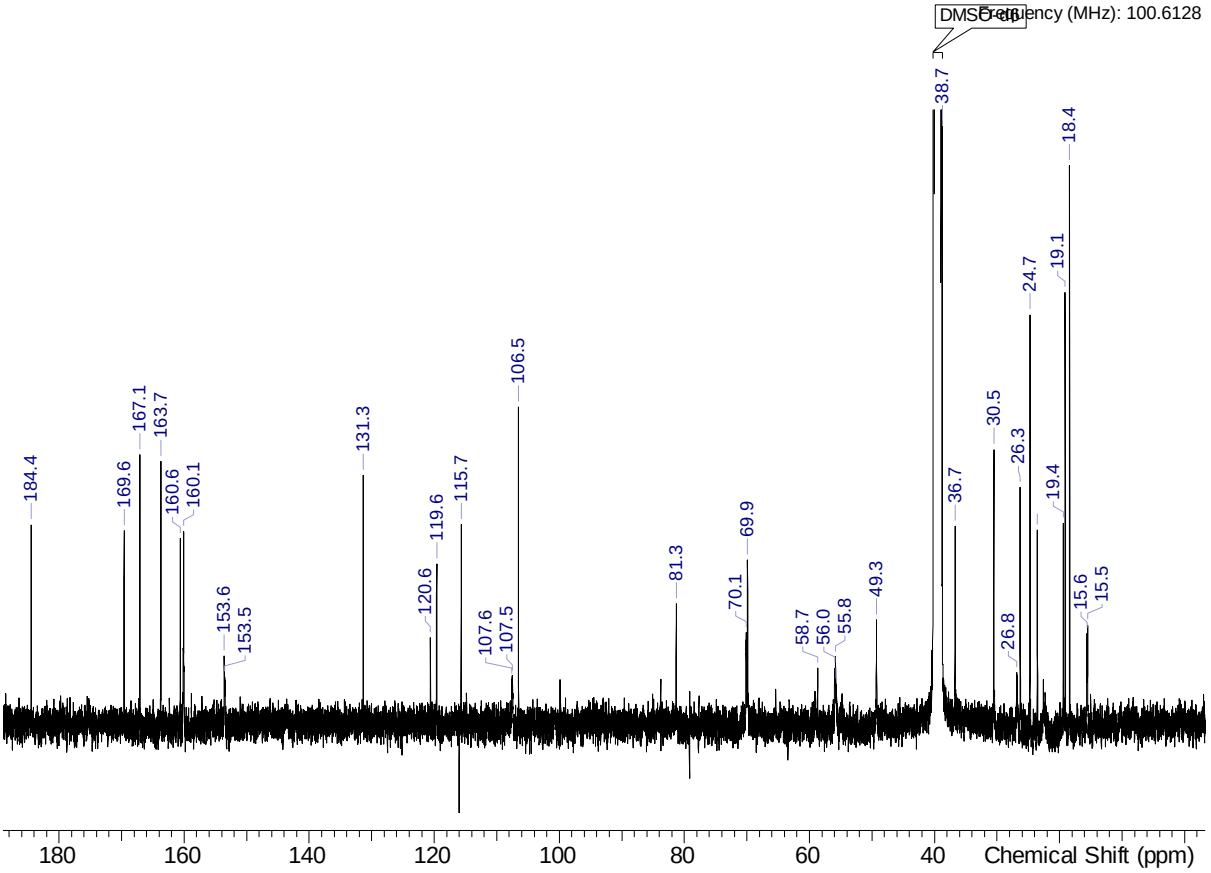

HRMS (*m/z*): $[M+H]^+$ calcd. for C33H43N11O4S , 689.32202; found, 689.32904

ACBI3:

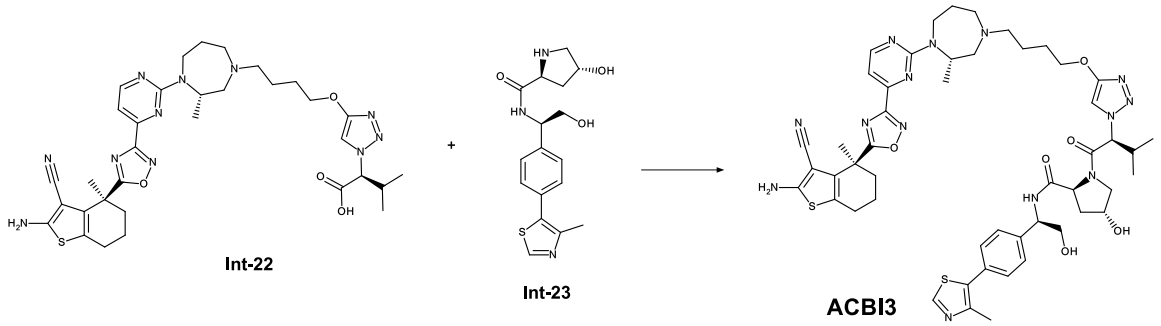

To a stirred solution of intermediate **Int-22** (69 mg, 0.10 mmol, 1.0 eq.), amine **Int-23** (55 mg, 0.13 mmol, 1.3 eq.) in a mixture of DCM (1 mL) and acetonitrile (0.35 mL) is added triethylamine (83.8 µl, 0.60 mmol, 6.0 eq.) at rt and the mixture is stirred for 5 min before propane phosphonic acid anhydride (119.0 µl, 50% solution in ethyl acetate, 0.200 mmol, 2.0 eq.) is added and the mixture is stirred for another 20 min. The mixture is diluted with DCM and saturated aqueous $NaHCO_3$ solution is added before it is stirred for 5 min. The phased are separated and the organic layer is concentrated under reduced pressure and the residue is purified by RP HPLC (Method 3b) and lyophilized to obtain **ACBI3** (63 mg, 0.062 mmol, 62 % yield).

^{1}H NMR (DMSO-d_6) δ: 8.98 (s, 1H), 8.52-8.59 (m, 1H), 8.47 (d, J=7.9 Hz, 1H), 7.65 (s, 1H), 7.41-7.49 (m, 2H), 7.37 (d, J=8.2 Hz, 2H), 7.04-7.14 (m, 3H), 5.14 (br s, 2H), 4.85 (br s, 2H), 4.65-4.76 (m, 1H), 4.44 (s, 1H), 4.21-4.37 (m, 2H), 3.97-4.10 (m, 2H), 3.75 (br d, J=6.6 Hz, 1H), 3.53-3.67 (m, 3H), 3.12-3.24 (m, 1H), 2.95-3.08 (m, 1H), 2.79-2.89 (m, 1H), 2.52-2.58 (m, 3H), 2.45-2.47 (m, 3H), 2.35-2.43 (m, 2H), 2.01-2.13 (m, 2H), 1.82-1.99 (m, 3H), 1.79 (s, 5H), 1.44-1.74 (m, 7H), 1.02 (br d, J=6.6 Hz, 6H), 0.66 (br d, J=6.3 Hz, 3H)

^{13}C NMR (DMSO-d_6) δ: 184.4, 170.5, 167.1, 166.1, 163.7, 160.7, 160.5, 160.1, 160.0, 153.6, 153.5, 151.5, 147.7, 141.2, 131.4, 131.1, 129.9, 128.7, 128.6, 127.5, 127.4, 119.6, 115.7, 107.2, 105.6, 81.3, 70.1, 68.6, 67.1, 64.5, 58.8, 56.1, 55.4, 54.7, 50.1, 50.0, 37.8, 36.7, 31.6, 27.7, 27.5, 26.4, 24.7, 23.6, 23.4, 23.2, 19.4, 18.3, 18.1, 16.0, 15.7, 15.6, 1C under DMSO

More carbon peaks detected than present in the structure due to presence of rotamers

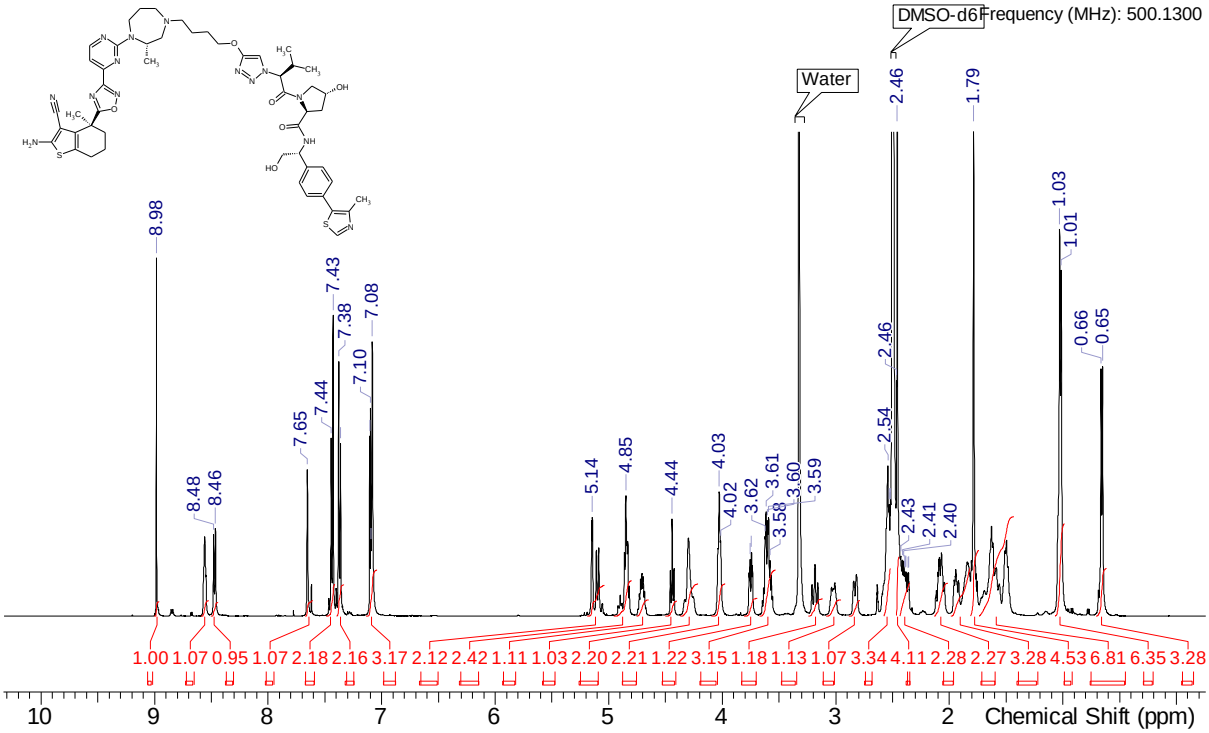

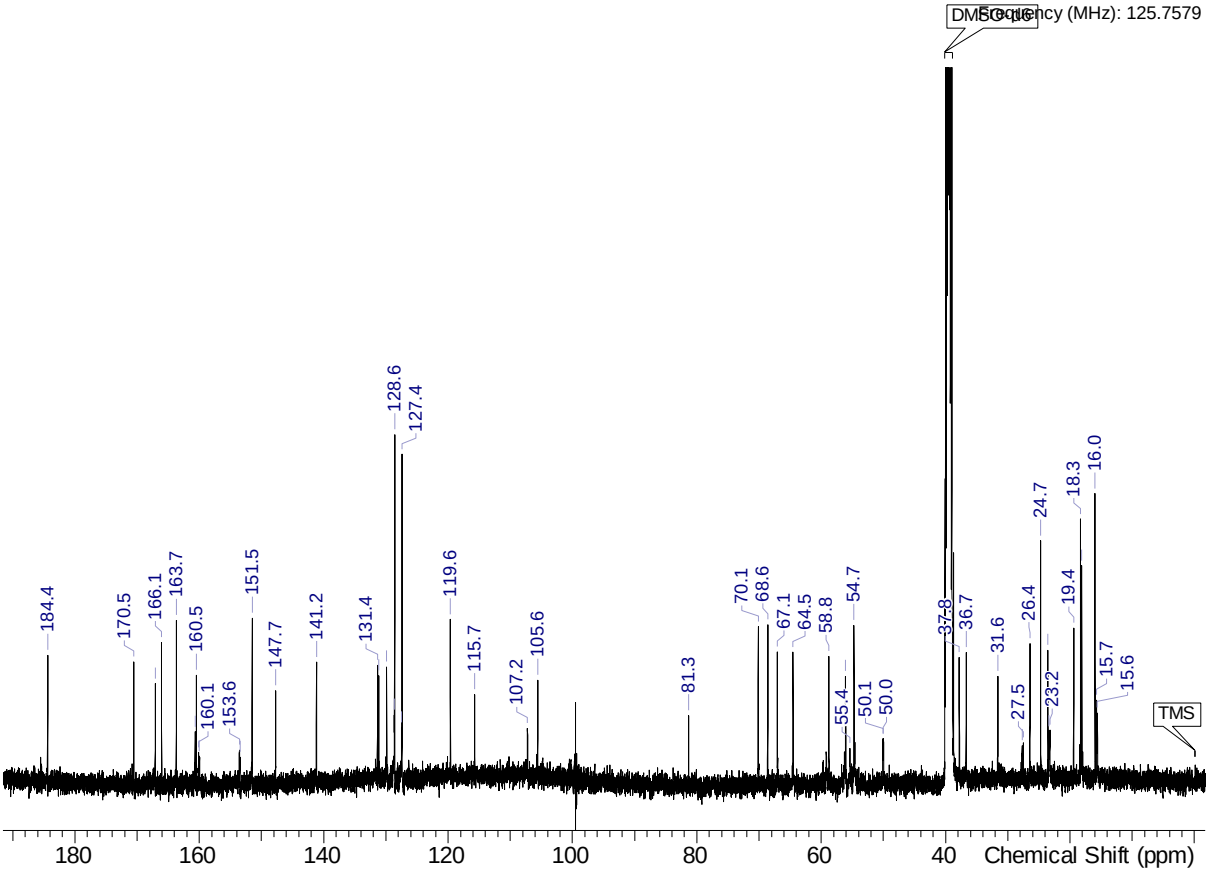

The spike observed at 99.5 ppm is an artefact from the carrier frequency.

HRMS (*m/z*): $[M+H]^+$ calcd. for C50H62N14O6S2 , 1019.44909; found, 1019.44867

Synthesis of the negative control compound 8 (cis-ACBI3)

Intermediate **Int-24**:

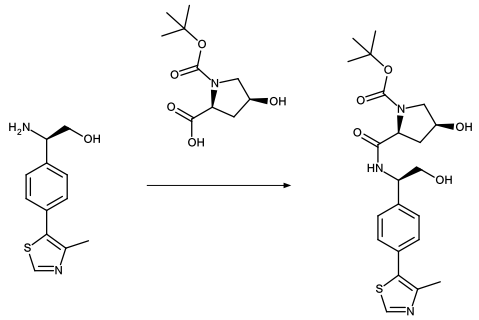

Int-24

To a stirred solution of (2S,4S)-1-[(tert-butoxy)carbonyl]-4-hydroxypyrrolidine-2-carboxylic acid (70 mg, 0.284 mmol, 1.0 eq.) in DMSO (1 mL) is added (2R)-2-amino-2-[4-(4-methyl-1,3-thiazol-5-yl)phenyl]ethan-1-ol (93 mg, 0.303 mmol, 81%, 1.1 eq.), HATU (173 mg, 0.440 mmol, 1.5 eq. and DIPEA (0.256 mL, 1.468 mmol, 5.0 eq.) and the mixture is stirred at RT for 20 min. The mixture is diluted with water and acetonitrile and purified by RP HPLC (Method 3a) and lyophilized to obtain **Int-24** (84 mg, 0.188 mmol, 63% yield).

^{1}H NMR (DMSO-d_6) δ: 8.98 (s, 1H), 8.30 (br d, J=7.9 Hz, 0.66H rotamer), 8.24 (br d, J=7.6 Hz, 0.35H rotamer), 7.38-7.46 (m, 4H), 5.19 (br d, J=5.6 Hz, 0.34H rotamer), 5.16 (br d, J=6.1 Hz, 0.67H rotamer), 4.77-4.92 (m, 2H), 4.11-4.21 (m, 2H), 3.64 (br d, J=3.5 Hz, 2H), 3.49 (dd, J=10.6, 5.3 Hz, 1H), 3.14-3.26 (m, 1H), 2.45 (s, 3H), 2.24-2.39 (m, 1H), 1.63-1.77 (m, 1H), 1.42 (br s, 3.17H rotamer), 1.32 (s, 5.84H rotamer)

Integrals may not add up to whole numbers due to overlapping rotamers or rotamers resonating under residual DMSO-d6 or HDO peaks

^{13}C NMR (DMSO-d_6) δ: 172.5, 172.2, 153.9, 153.4, 151.5, 147.7, 141.0, 131.1, 129.9, 128.6, 127.5, 127.4, 78.9, 78.8, 68.8, 68.0, 64.4, 64.1, 58.9, 54.9, 54.4, 37.7, 28.0, 28.0, 15.9

More carbon peaks detected than present in the structure due to presence of rotamers

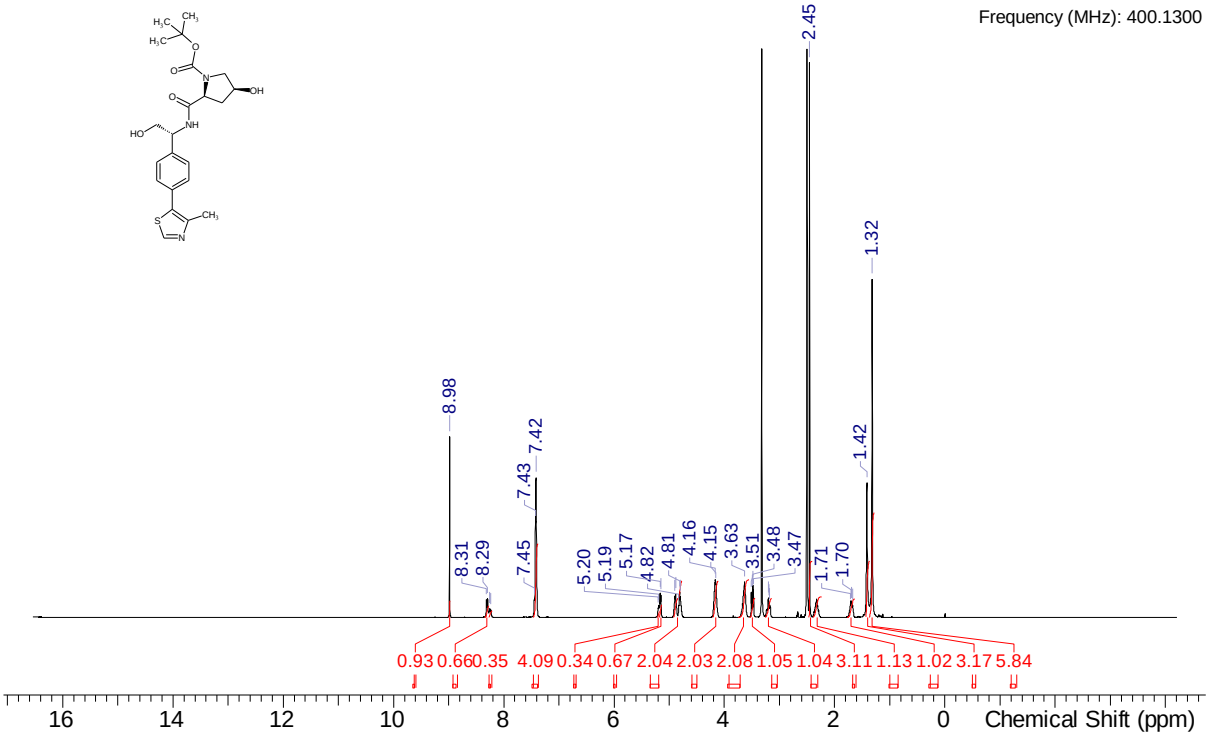

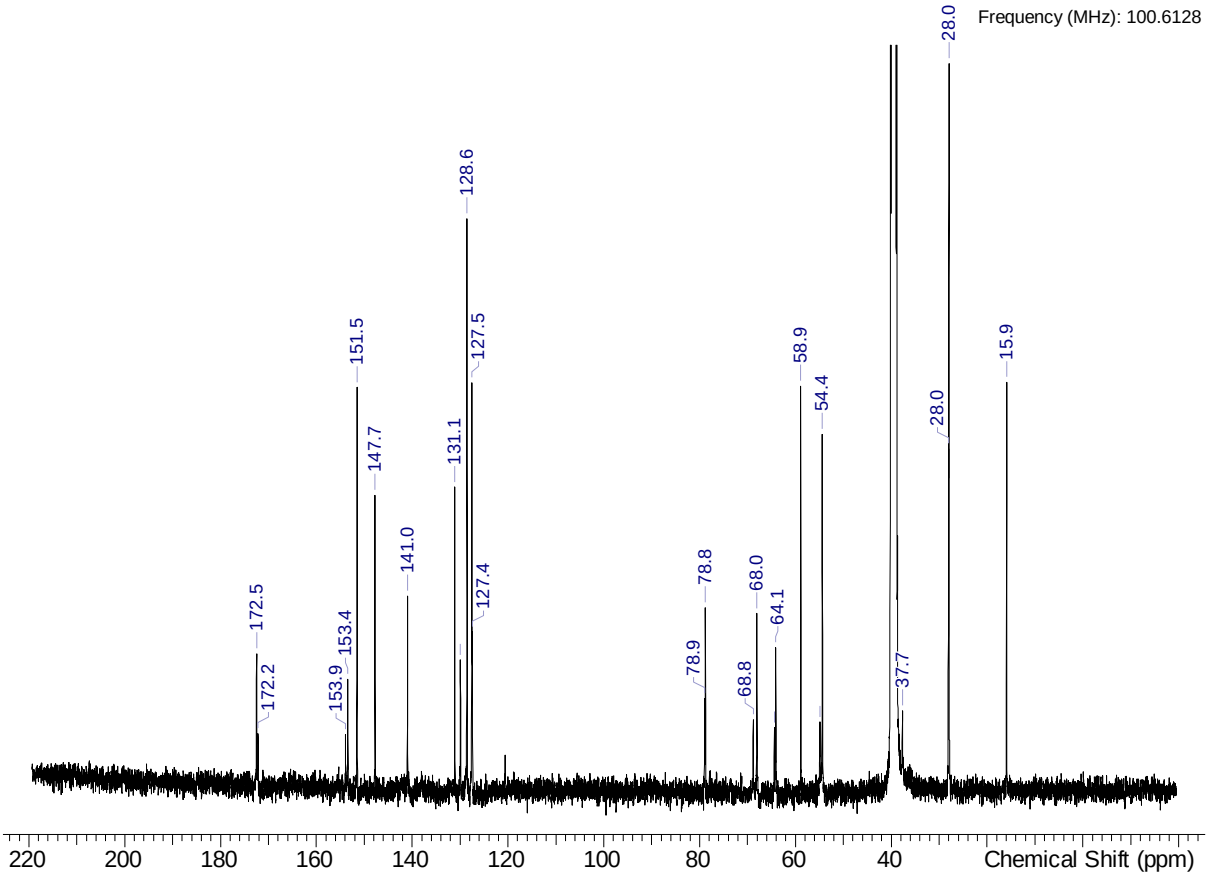

HRMS (*m/z*): $[M+H]^+$ calcd. for C22H29N3O5S , 448.19007; found, 448.1904

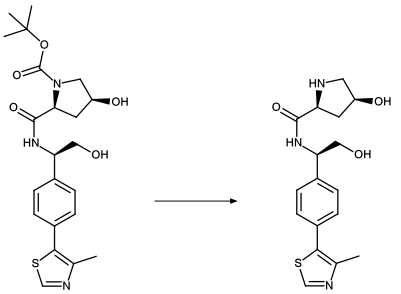

To a stirred solution of **Int-24** (60 mg, 0.134 mmol, 1.0 eq.)in methanol (0.3 mL) is added a HCl solution in dioxane (0.101 mL, 0.402 mmol, 4 M, 3.0 eq.) at RT. The mixture is heated to 45°C and stirred for 90 min. The mixture is cooled the RT and the all volatiles are evaporated under reduced pressure to obtain the curde product **Int-25** (51 mg, 0.134 mmol, 100% yield) as HCl salt which is used in the next step without further purification. An analytical sample of the free base was obtained by RP HPLC Method 3a) purification and lyophilization.

^{1}H NMR (DMSO-d_6) δ: 8.98 (s, 1H), 8.46 (br d, J=8.4 Hz, 1H), 7.33-7.54 (m, 4H), 4.81-5.23 (m, 2H), 4.73 (br s, 0.75H rotamer), 4.19 (br s, 0.25H rotamer), 4.13 (br s, 1H), 3.63 (br d, J=5.6 Hz, 2H), 3.47-3.58 (m, 1H), 3.19 (br s, 0.25H rotamer), 2.92 (dd, J=10.9, 5.3 Hz, 0.75H rotamer), 2.69 (dd, J=11.0, 3.9 Hz, 0.75H rotamer), 2.45 (s, 3H), 2.16 (br s, 1H), 1.79 (br d, J=11.4 Hz, 0.26H rotamer), 1.62 (dt, J=12.8, 5.0 Hz, 0.75H rotamer), one interchangeable missing

Integrals may not add up to whole numbers due to overlapping rotamers or rotamers resonating under residual DMSO-d6 or HDO peaks

^{13}C NMR (DMSO-d_6) δ: 174.0, 151.5, 147.7, 141.1, 140.9, 131.1, 131.1, 129.9, 129.8, 128.6, 128.6, 127.4, 71.1, 64.6, 64.4, 59.3, 54.6, 54.5, 54.0, 15.9

More carbon peaks detected than present in the structure due to presence of rotamers

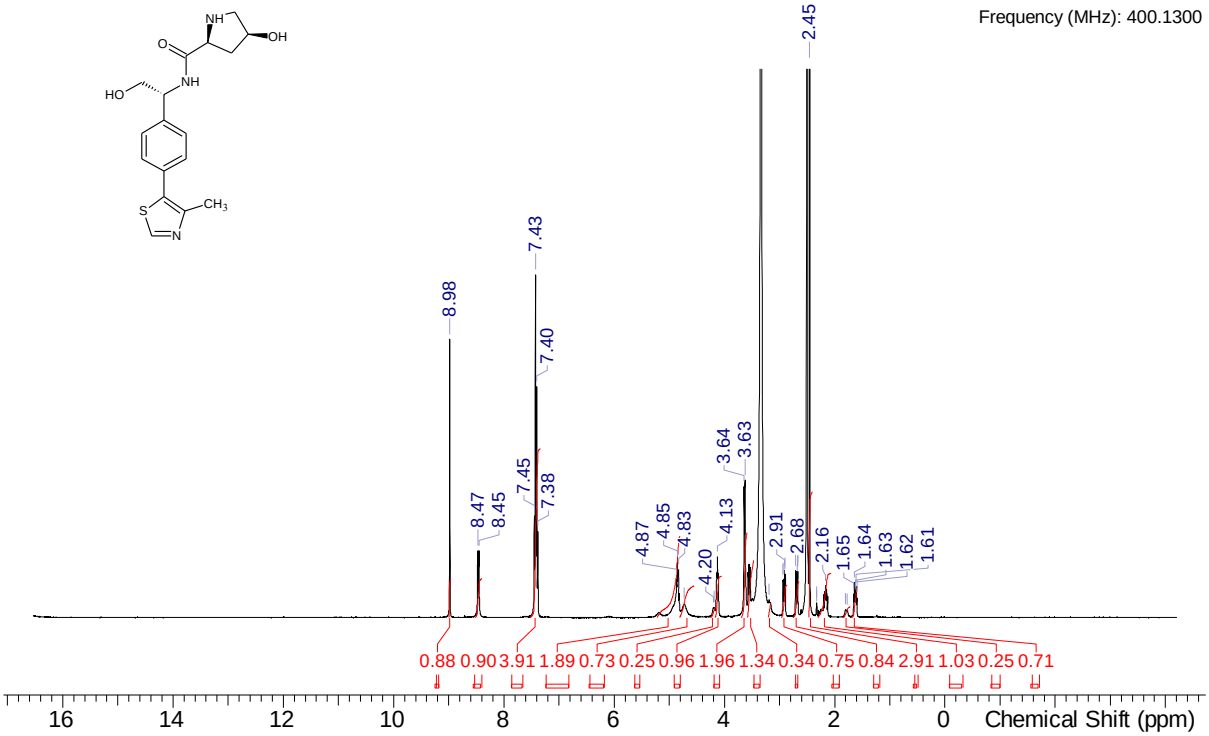

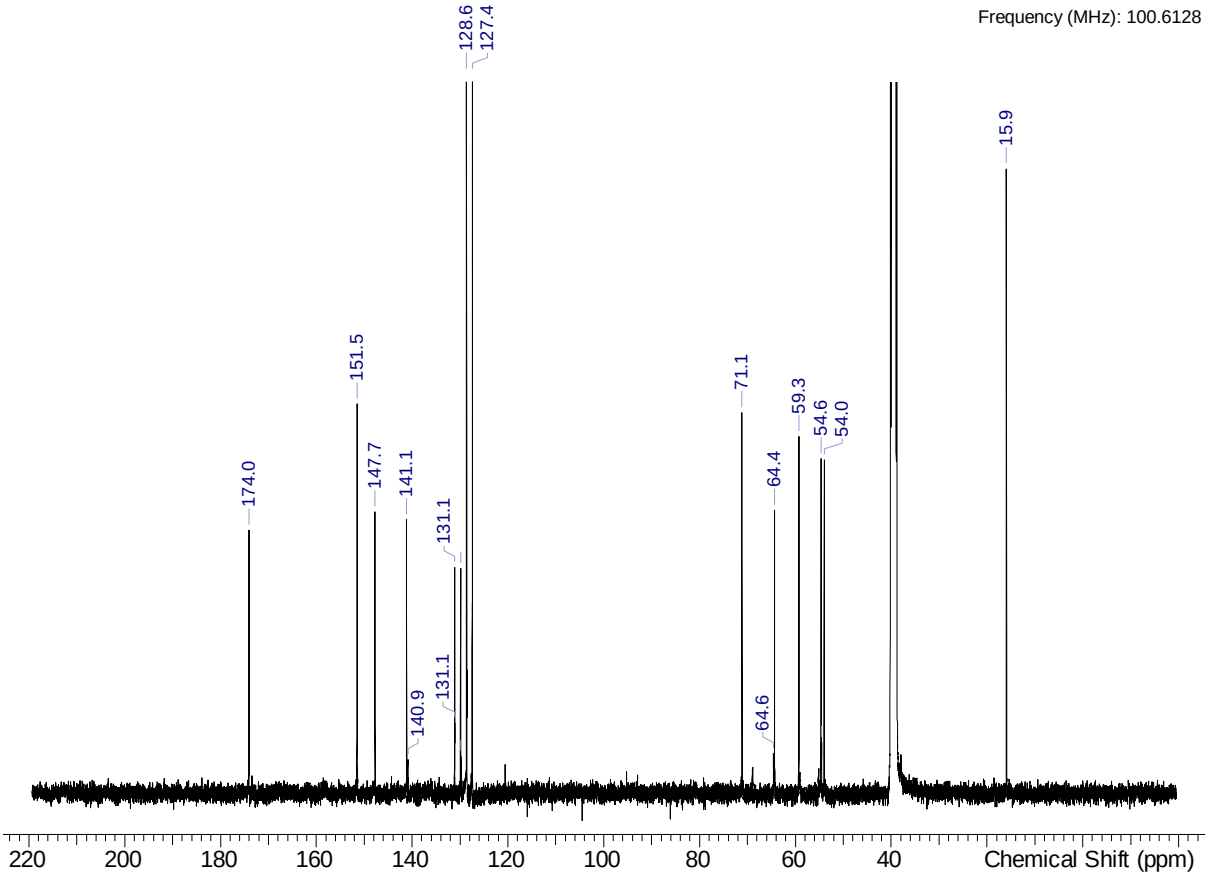

HRMS (*m/z*): $[M+H]^+$ calcd. for C17H21N3O3S , 348.13788; found, 348.13788

Compound **8** (cis ACBI3)

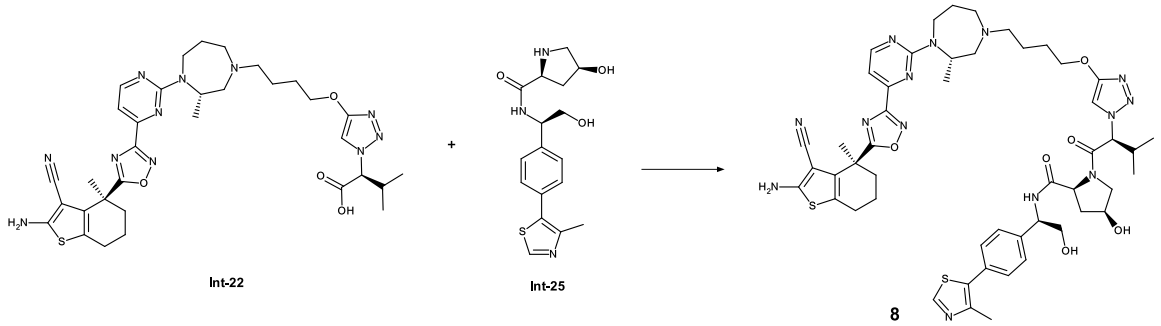

To a stirred solution of **Int-22** (35 mg, 0.051 mmol, 1.0 eq.), **Int-25** (50 mg, 0.130 mmol, 2.6 eq.) in NMP (1 ml) at 0°C is added HATU (28 mg, 0.071 mmol, 1.4 eq.) and DIPEA (0.044 mL, 0.254 mmol, 5.0 eq) and the reaction mixture is stirred at 0°C for 15 min. To the mixture is added water and acetonitrile and purified by RP chromatography (Method 4b) to obtain compound **8** (79 mg, 0.040 mmol, 79 %)

^{1}H NMR (DMSO-d_6) δ: 8.92 (s, 1H), 8.90 (s, 0.1H rotamer), 8.64 (d, J=7.6 Hz, 0.1H rotamer), 8.49 (d, J=4.6 Hz, 1H), 8.40 (d, J=7.6 Hz, 1H), 7.60 (s, 1H), 7.54 (d, J=18.5 Hz, 0.2H rotamer), 7.26-7.42 (m, 4H), 7.18-7.24 (m, 0.17H rotamer), 6.92-7.13 (m, 3H), 5.23 (d, J=6.8 Hz, 0.79H rotamer), 5.18-5.21 (m, 0.1H rotamer), 5.13 (s, 0.18H rotamer), 5.10 (br d, J=10.1 Hz, 1H), 4.89-4.94 (m, 0.1H rotamer), 4.79 (s, 2H), 4.55-4.70 (m, 1H), 4.09-4.38 (m, 3H), 3.95 (br s, 2H), 3.77 (br s, 1H), 3.63-3.72 (m, 0.24H rotamer), 3.41-3.62 (m, 3H), 3.12 (br s, 1H), 2.87-3.03 (m, 1H), 2.77 (br d, J=9.1 Hz, 1H), 2.47 (br s, 3H), 2.26-2.41 (m, 7H), 1.96-2.12 (m, 1H), 1.84 (s, 3H), 1.72 (s, 3H), 1.38-1.68 (m, 7H), 0.96 (br d, J=6.3 Hz, 6H), 0.87-0.92 (m, 0.52H rotamer), 0.61 (br d, J=6.6 Hz, 3H)

^{13}C NMR (DMSO-d_6) δ: 184.4, 171.1, 167.1, 166.2, 163.7, 160.7, 160.4, 160.1, 160.0, 153.5, 151.5, 147.8, 140.9, 131.3, 131.1, 129.9, 128.6, 127.4, 120.6, 119.6, 115.7, 107.2, 105.7, 81.3, 70.1, 68.8, 66.9, 64.4, 58.8, 56.2, 56.1, 55.1, 54.7, 50.0, 37.0, 36.7, 31.3, 26.4, 24.7, 23.6, 19.4, 18.2, 18.2, 16.0, 15.7, 15.6, 15.6, 1 C under DMSO

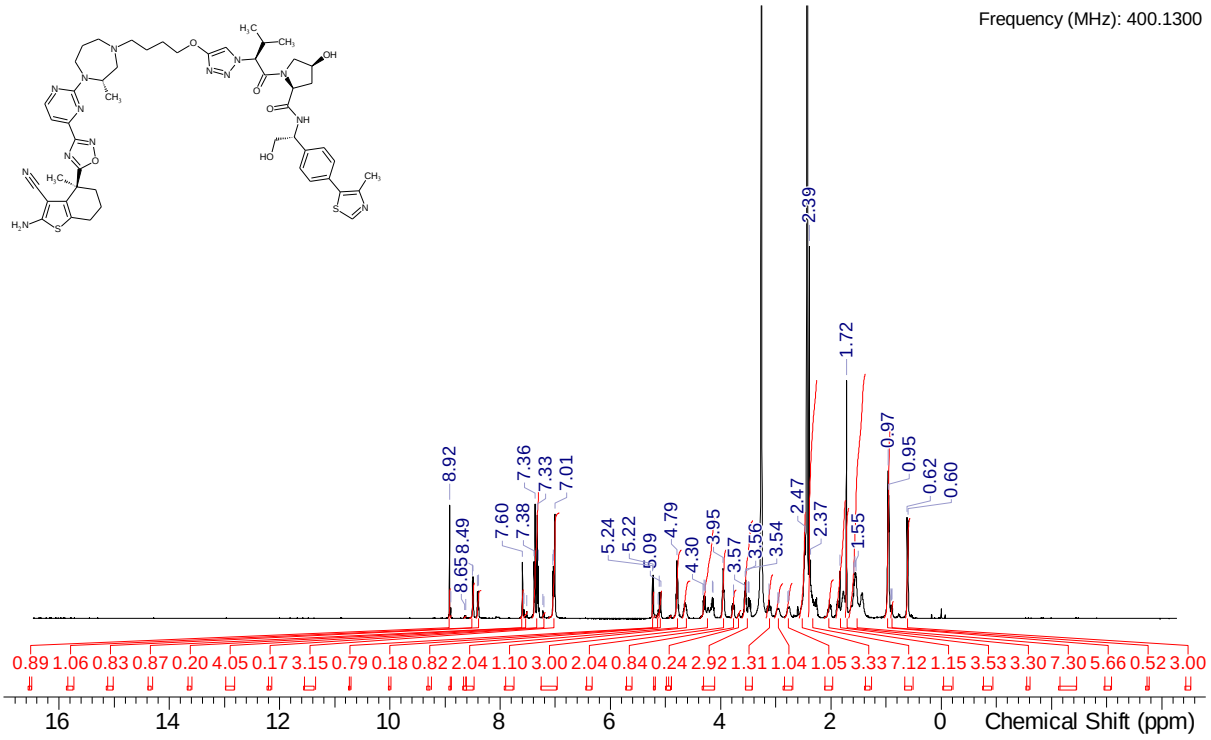

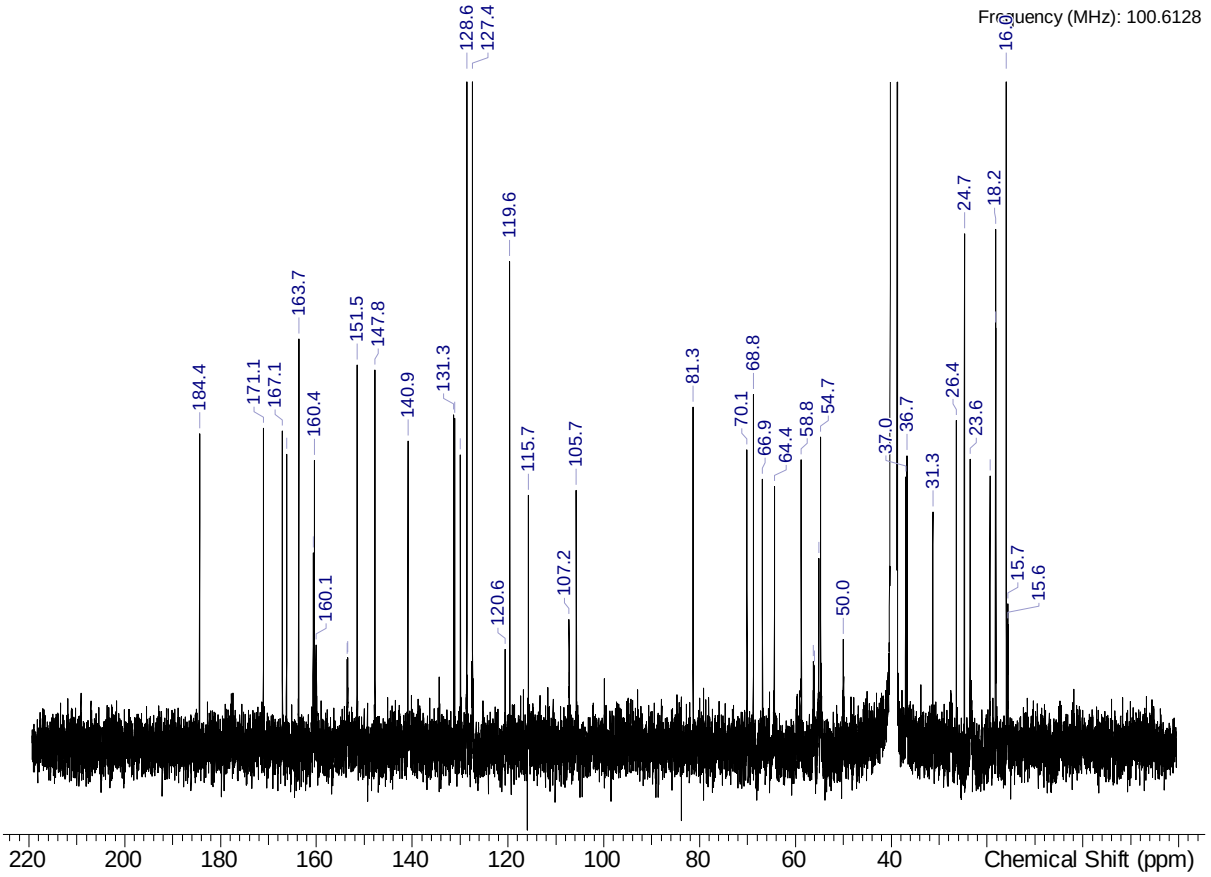

HRMS (*m/z*): $[M+H]^+$ calcd. for C50H62N14O6S2 , 1019.44909; found, 1019.44897